ELECTROHYDRODYNAMIC SOLIDIFICATION OF PHASE CHANGE MATERIALS

ECTROHYDRODYNAMIC SOLIDIFICATION OF PHASE CHANGE MATERIALS

BY ERIC THOMPSON B.ENG

A Thesis Submitted to the School of Graduate Studies in Partial Fulfilment of the Requirements for the Degree Master of Applied Science

McMaster University

McMaster University MASTER OF APPLIED SCIENCE (2017) Hamilton, Ontario (Mechanical Engineering)

Title: Electrohydrodynamic solidification of phase change materials

AUTHOR: Eric Thompson B. ENG (McMaster University)

SUPERVISOR: Professor J.S. Cotton

Number of Pages: xvii, 196

Abstract

In this investigation an electric field was applied to a phase change thermal storage system while it was discharging energy. The phase change material used was octadecane. Octadecane is a high purity dielectric material that has a melting temperature close to room temperature. The material was forced to solidify using a heat exchanger mount below the phase change material, cold water flowed through the heat exchanger to ensure it maintained a constant temperature below the melting temperature of the phase change material. By applying -8kV to 9 electrodes – positioned in the phase change material – and by using the heat exchanger as an electrical ground – an electric field was generated in the phase change material. The electric field caused unbalanced body forces in the fluid which generated electro-convection in the fluid. The system was designed such that electro-convection is the only source of convection in the system to isolate the effects of electro-convection, allowing for the underlying physics of electro-convection to be studied easier.

To understand the effects of applying electro-convection, a case where there is no applied voltage on the electrodes was compared to a case where there was -8 kV applied to the electrodes. Experiments showed that the effect of applying electro-convection depends on the initial temperature; however, it was found that the improvement after two hours was less than 10%. For a wall temperature of 8.5℃ and an initial temperature of 50℃ - the melting temperate of octadecane is 28℃- then the maximum enhancement of the energy extracted is 50%, but two hours after the start of the test the enhancement approached zero. For a wall temperature of 8.5℃ and an initial temperature of 30℃, the maximum enhancement is 10% and similarly fall to zero after a few hours of application.

A simple analytical model was developed. The experimental and numerical results showed that at the early stages of energy discharge the electro-convection case had a large improvement compared to a pure conduction case, however as time progresses this improvement decreases. The explanation for the trend is that adding convection only increases the rate that energy is taken out of the liquid, thus the maximum improvement is bounded by the amount of sensible energy in the liquid phase change material, once this sensible energy is removed applying electrohydrodynamics is no longer beneficial.

Acknowledgements

I would like to thank my supervisor Dr Cotton for his guidance throughout this project. I would also like to thank Dr Vick Lakhain for his help. It was an honour to work with both of you.

I would also like to thank the mechanical engineering technicians: Ron Lodewyks, John Colenbrander, Michael Lee, Mark Mackenzie and Dan Wright. Each of you provided me with well-needed advice during the design and construction of my experimental apparatus and I greatly appreciate your help. I would also like to thank the mechanical engineering staff: Florence Rosato, Leslie Kocsis and LiLy Sazz-Fayter. I would especially like to thank Florence for her help in guiding me through the bureaucratic nightmare of McMaster's School of graduate studies.

I would also like to thank OGS and NSERC for providing financial assistance. Without your help, I would not have had the opportunity to do graduate studies.

I would like to thank all my friends at McMaster University and in the TMRL Your help in complete (and distraction from) this project is greatly appreciated.

I would like to thank my family. To my parents and brothers thank you for making this all possible.

Finally, I would especially like to thank Meghan Rakowski for weathering the storm that comes with the chaotic schedule of a graduate student.

Table of Contents

Table of Figures

1 Introduction

Thermal energy storage systems provide a means for storing thermal energy so that it can be discharged at a later time. Thermal energy storage systems work for thermal energy in a similar manner to how an electrical batteries function in an electrical system. Excess thermal energy – from a process such as solar thermal collectors or waste heat recovery systems – is stored in a thermal energy storage system over time so that the energy can be used at when and where it is required. Thermal storage systems have many interesting applications for the energy sector, for example, residential heating demand is typically satisfied by on-demand burning of fossil fuels. Whereas electrical power plants, produce a large amount of heat that is ejected to the environment. From an electric power generation perspective, the heat being transferred to the environment is low quality because it is at a low temperature. Thus, it has a low Carnot efficiency for a heat engine. However, the temperature is high enough that it could be used for space heating. Thus, a thermal storage system that could store the excess thermal energy from the power plant and transport it to a residential neighbourhood, then the amount of fossil fuels that would be required for heating would be reduced and so would the total amount of energy consumption.

There are many methods of storing thermal energy; thermal energy can be stored in the sensible form, in the latent form or in thermochemical reactions. When the thermal energy is stored by increasing the temperature of a material, the thermal energy is stored in the sensible form. When the thermal energy is stored by causing a material to undergo a change of phase, the thermal energy is stored in the latent form and when the thermal energy is used to cause a material to undergo a chemical reaction the thermal energy is stored in a thermochemical reaction. Each of these methods has their own advantages and disadvantages. The appeal of latent heat thermal storage systems is that they have a high storage density, which means they can store a large amount of energy for a given volume, and therefore a system can be designed that stores the same amount of energy as a sensible energy storage system while being significantly smaller in size. The smaller size can be advantageous for applications where space is a constraint. Certain materials also have a very narrow melting temperature range, which allows for a large amount of energy to be stored for applications where the temperature range is fairly small. Thus, the motivation for studying latent heat thermal storage systems is the high storage density and the small operating temperatures that they provide.

Organic phase change materials are one method of storing thermal energy in latent heat thermal storage systems. The energy is stored in the phase change material in two forms, there is a sensible energy component and a latent energy component. The latent heat of fusion of organic phase change materials is large, so these materials can store a large amount of energy relative to other methods of storing thermal energy. The problem with these materials is the rate that energy can be added and removed from these systems is very small due to the low thermal conductivity of these materials. To mitigate this problem many researchers have looked at methods of enhancing the rate of charging and discharging energy. Electrohydrodynamics is one method of enhancing the charging rate of thermal storage systems that use organic phase change materials. Electrohydrodynamics is a phenomenon where fluid motion is induced using an electric field and can be used to enhance the heat transfer rates when a dielectric fluid is used as a working fluid. The other effect of Electrohydrodynamics is solid extraction which is a process where solid particles are pulled in to the liquid material (Nakhla et al., 2015).

The focus of this investigation is to study the use of electrohydrodynamics as a method of enhancing the discharge rate of thermal energy from a thermal storage system that uses organic phase change materials. Specifically, this study focuses on trying to understand the mechanisms behind how applying electrohydrodynamics affects the rate that energy is discharged from these systems. This investigation approached this problem experimentally and supported this experimental approach numerically and analytically. If electrohydrodynamics increases the rate of thermal energy discharged from a latent heat thermal storage system, these systems could become more competitive relative to the current method of thermal storage which is storing the energy in the sensible form. This could allow for more efficient energy usage because thermal storage can be used to capture thermal energy that would otherwise be rejected to the environment. As a result, any process that has an excess of thermal energy could be made more cost efficient by capturing this thermal. The purpose of studying the electrohydrodynamic phenomenon in phase change materials experimentally is that there are several possible effects of applying electric fields to the solidification of a material that are not fully understood and there are no existing models that can be implemented analytically or numerically to compensate for these effects. These will be explained in the literature review section of this thesis. However, the numerical and analytical models presented in this thesis are used to attempt to capture the major contributors to the change in energy discharge rate when electrohydrodynamics are applied.

In this thesis, the first chapter will discuss the motivation for thermal storage, as well as the types of thermal storage and methods for enhancing the rates of heat transfer in thermal storage systems. The experimental apparatus will be described in the second chapter. The experimental apparatus is explained in chapter three. The fourth chapter shows the analytical and numerical approach that I have taken to predict the effects of electrohydrodynamics. In the numerical section, the electric field distribution was analysed using Comsol software, the effect of convection is then explored analytically using a Neumann Solution and numerically, using an explicit finite difference discretization method. The experimental results are outlined in the fifth chapter. A comparison of the experimental and numerical results are is also presented in chapter five. Chapter six highlights the major conclusions of the investigation.

1.1 Objectives

The primary focus of this investigation is to investigate the solidification of organic phase change materials used in latent heat thermal storage systems. The study is primarily focused on understanding how applying electrohydrodynamics affects the rate of thermal energy discharge. Nakhla et al. (2015) have already investigated how applying electrohydrodynamics affects the energy charging rate, so this will not be investigated here. The goal is not to design a system that uses electrohydrodynamics to enhance the performance of the system but is rather to understand how applying electrohydrodynamics affects the rate of heat transfer and the rate of energy discharge from the system. The research objectives of this project are twofold:

- Generate a theoretical prediction for the effect of applying electrohydrodynamics
- Generate experimental results to show the actual effect of applying electrohydrodynamics

2 Literature Review

2.1 Motivation for using thermal storage systems

Thermal energy storage systems allow excess thermal energy, from processes such as solar thermal collectors and waste heat recovery systems, to be stored over time. This concept is similar to how an electrical battery allows electrical energy to be stored over time. Thermal Storage provides a solution for applications: (Zalba et al. 2003)

- when there is a time delay between the production of thermal energy and the demand for that thermal energy
- when the supply of thermal energy needs to be reliable
- when thermal inertia or thermal protection is desired

One possible application is for situations when there is a delay between production and demand for thermal energy is solar collectors. In solar collectors, thermal energy is only produced during the daylight hours; however, energy is demanded throughout the entire day and night. Thus, if a thermal storage system was implemented, then the excess energy which the solar collector produces could be stored so that it can be used at times when the demand for thermal energy exceeds the production. This scenario is represented in Figure 2-1 as the region marked by two cross-hatched regions.

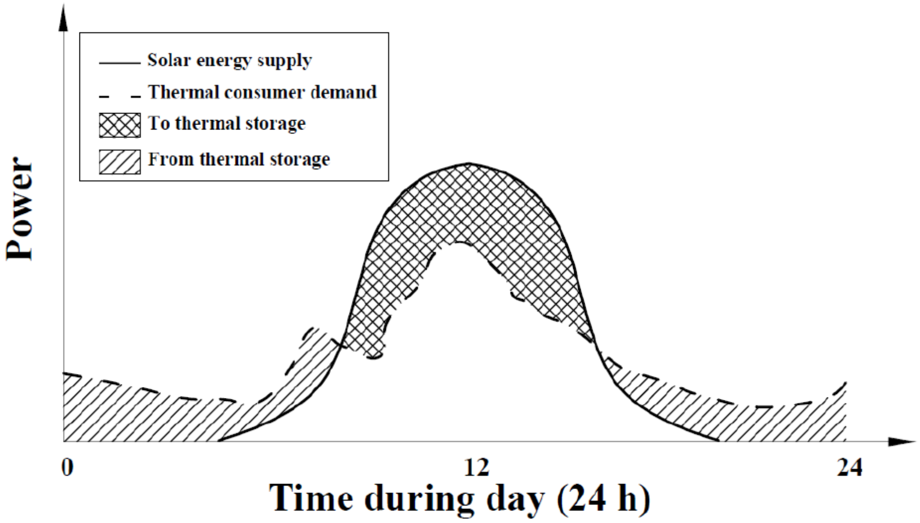

Figure 2-1: Hypothetical power supply and demand curves showing a scenario where thermal storage is beneficial for solar collectors (Nakhla et al., 2015)

Another example of an application for which thermal storage can solve the issue of a time delay between production and demand for thermal energy is waste heat recovery systems. Waste heat recovery systems are ones that harvest thermal energy that would otherwise be rejected from a system to the atmosphere as a result of thermodynamic inefficiencies. These inefficiencies exist even in ideal systems due to the second law of thermodynamics. For example, in a Rankine cycle, thermal energy must always be rejected from the cycle in order for it to produce work; a waste heat recovery system attempts to capture. Once the waste heat recovery system has stored the energy it can be used at another time. Figure 2-2 illustrates the mismatch between waste heat production and thermal energy demand.

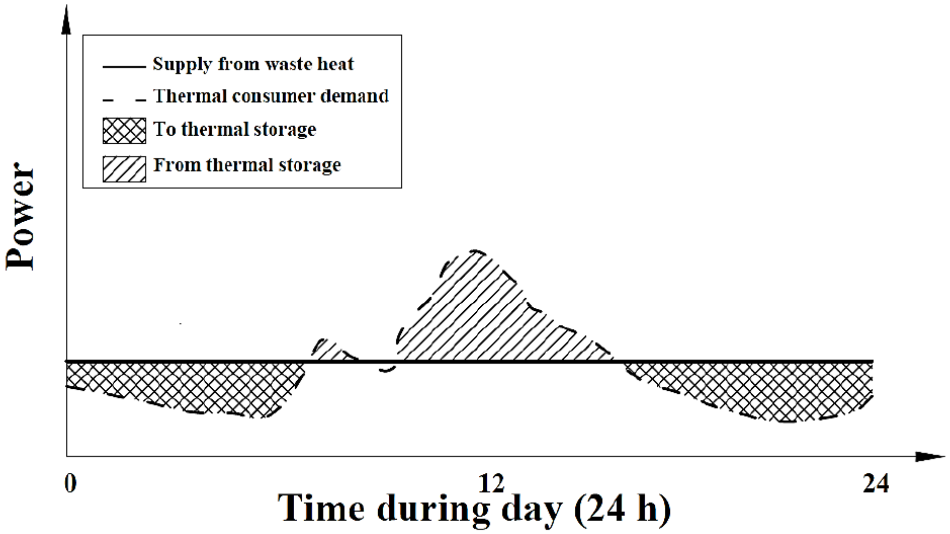

Figure 2-2: Hypothetical power supply and demand curves showing a scenario where thermal storage is beneficial for waste heat recovery (Nakhla et al., 2015)

A hospital would be an example of a system where the supply of thermal energy needs to be reliable. In the event of a power outage, a hospital must keep its equipment functioning. Thus, a thermal energy storage system allows for the thermal equipment to keep functioning in a power outage, by storing thermal energy when power is available and using the stored thermal energy during the power outage. An example of a system where thermal inertia is required is a heat pump. Heat pumps operate at their peak efficiency when they are operating between two steady temperatures. If the heat pump is operating in an environment where either the hot or cold side temperatures fluctuate, then it would be beneficial to add thermal inertia to the system. Adding thermal inertia will reduce the temperature fluctuations and result in a more uniform temperature because the larger thermal inertia requires more energy per degree of temperature change. By storing and releasing energy a thermal storage system provides thermal inertia which acts to stabilise the operating temperatures for the heat pump.

2.1.1 Type of thermal storage

All thermal storage systems act by taking energy from a source and storing it in some material; the material, that stores the energy, will be referred to as the storage material. There are three methods of storing thermal energy in thermal storage systems: sensible heat storage, latent heat storage and thermochemical heat storage.

2.1.1.1 Sensible energy thermal storage

A common form of thermal storage is sensible energy thermal storage systems. These systems include water tanks used in residential buildings and geothermal thermal storage systems. In all sensible energy thermal storage systems, energy is stored by increasing the temperature of a storage material. In water tanks the storage material would be water; in geothermal storage, it is the ground or rock. The amount of energy stored depends on the mass of the storage material, the specific heat of the storage material and the temperature increase of the storage material. The storage capacity can be seen in the Equation 2.1 for the energy stored. In Equation 2.1, E_{stored} represents the total energy stored as sensible thermal energy, C_p is the specific heat of the material, m is the total mass of the material, T_h is the average temperature of the storage material and T_0 is the ambient temperature or the lowest temperature in the thermal cycle.

$$E_{stored} = C_p\, m\, (T_h - T_0) \qquad [2.1]$$

One of the benefits of using sensible energy thermal storage is that the working fluid of a thermal process can be used as the storage material. This ensures that the charging and discharging rate is high because energy does not have to be transferred between a secondary heat exchanger. The storage material for sensible energy thermal storage systems such as water and mineral oil are inexpensive compared to the materials used in phase change materials such as paraffin wax. Since the change in volume of sensible energy storage materials is small, there are not issues with voids or structural integrity associated with the large volume change of phase change materials.

One of the problems with sensible thermal energy storage is that when the temperature difference between the thermal process and the maximum storage temperature is small, very large systems are required. The reason for this is that, since the amount of energy stored is directly related to the temperature increase of the storage material, then the overall temperature change in the storage material is small. Thus only a small amount of energy can be stored if the temperature difference between the heat source and the storage material is same.

2.1.1.2 Latent Heat Thermal Storage

In latent heat thermal storage systems, commonly referred to as phase change material (PCM) systems the energy is stored by inducing a change of state in a storage material. Typically, this storage material undergoes a change of state from solid to liquid to store energy and from liquid to solid to discharge energy. However, liquid-gas and solid-solid phase transformations are also possible. For a material undergoing a change of state the energy stored is given by Equation 2.2. In Equation 2.2, m is the mass of the material that has changed state, H is the latent heat of fusion of the material and Δm is the mass that has changed phase. It is difficult to design a system where energy is only stored in latent heat, so the system will also store energy in sensible heat as well. For these systems the energy stored is given by Equation 2.3; in this equation, the first term on the right-hand side of the equation is the sensible energy stored in the solid, the second term is the energy stored in the latent form and the third term is the energy stored in the fluid in the sensible form.

$$E_{latent} = m\,H \qquad [2.2]$$

$$E_{stored} = m_s\,C_s\,(T_m - T_s) + \Delta m\,H + m_f\,C_f\,\left(T_f - T_m\right) \qquad [2.3]$$

One benefit of latent heat thermal storage systems is the high energy storage density for relatively small temperature differences associated with these systems. Since the latent heat of fusion is evolved from the storage material over a narrow temperature range, the storage capacity of a latent heat thermal storage system can be many times larger than a sensible energy thermal storage system over the same temperature difference. Figure 2-3, shows a comparison between the energy stored in octadecane and water per unit mass. The figure assumes that the ambient temperature is 20℃. Initially, the water is able to store more energy than the octadecane, due to the large specific heat of water. The energy stored in the octadecane system jumps at the melting temperature of the material, which is 28℃. After this point the octadecane stores more energy than the water even up to 100℃ temperature, the analysis assumes that specific heat of the materials are constant. This means that the octadecane is able to store more energy per unit mass than water over most of the 80℃ temperature difference. The analysis was stopped at 100℃ because under standard conditions the water will begin to vaporise and the energy will no longer be stored in the sensible form. However, boiling can be avoided by increasing the pressure of the system. If the temperature range was extended the water would eventually store more energy than the octadecane.

Latent heat systems also typically have higher efficiencies than sensible energy storage systems, because the temperature difference between the working fluid and the storage material can be smaller. In addition, latent heat thermal storage systems can be used for temperature modulation. Latent energy of the storage material is added and removed in a very narrow temperature range, the storage material will transfer energy to the working fluid to keep its temperature close to the melting temperature of the storage material. In sensible energy systems, the energy is added and removed in a nearly linear manner over a temperature range.

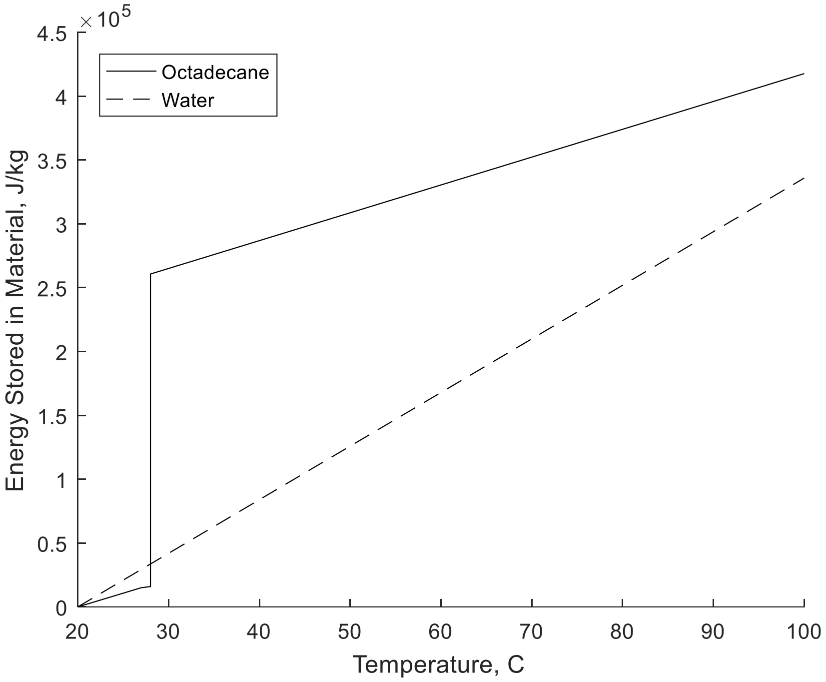

Figure 2-3: Comparison of Energy stored per unit mass of octadecane and water. Assuming the ambient temperature is 20℃. Using information from Ho (1982)

One of the primary problems with these latent heat thermal storage systems is that they store and discharge heat energy much slower than sensible energy thermal storage systems. This is because the thermal conductivity of the phase change materials used in these systems is typically very small. Thus, heat transfer enhancement techniques must be employed. However, these enhancement techniques typically require replacing some of the storage material with a highly conductive material. The highly conductive materials have lower storage densities that the storage material and thus the overall storage density of the system is decreased.

Another issue with latent heat thermal storage systems is that the volume change associated with a change of state can complicate the design of the storage container. For liquid-gas phase change systems, the volume change can be significant; therefore the storage container must be designed to accommodate large volume changes. For solid-liquid systems, the density change is much lower. For example, solid paraffin wax expands by 15% when it melts.

Abhat defines two classifications of solid-liquid latent heat phase change materials organic and inorganic, shown in Figure 2-4. Zalba et al. (2003), explains that the advantages of organic phase change materials are they are not corrosive, they have low or no risk of undercooling and they are chemically and thermally stable. However, compared to inorganic phase change materials, organic phase change materials have a low enthalpy of fusion, low thermal conductivity and are flammable. Zalba et al. (2003) further explains that an advantage of inorganics materials is the larger latent heat of fusion. The disadvantages of inorganic materials are that they tend to undercool, they are corrosive, and there is a risk of phase separation and phase segregation. (Zalba et al. 2003) These advantages and disadvantages are summarised in Table 2-1.

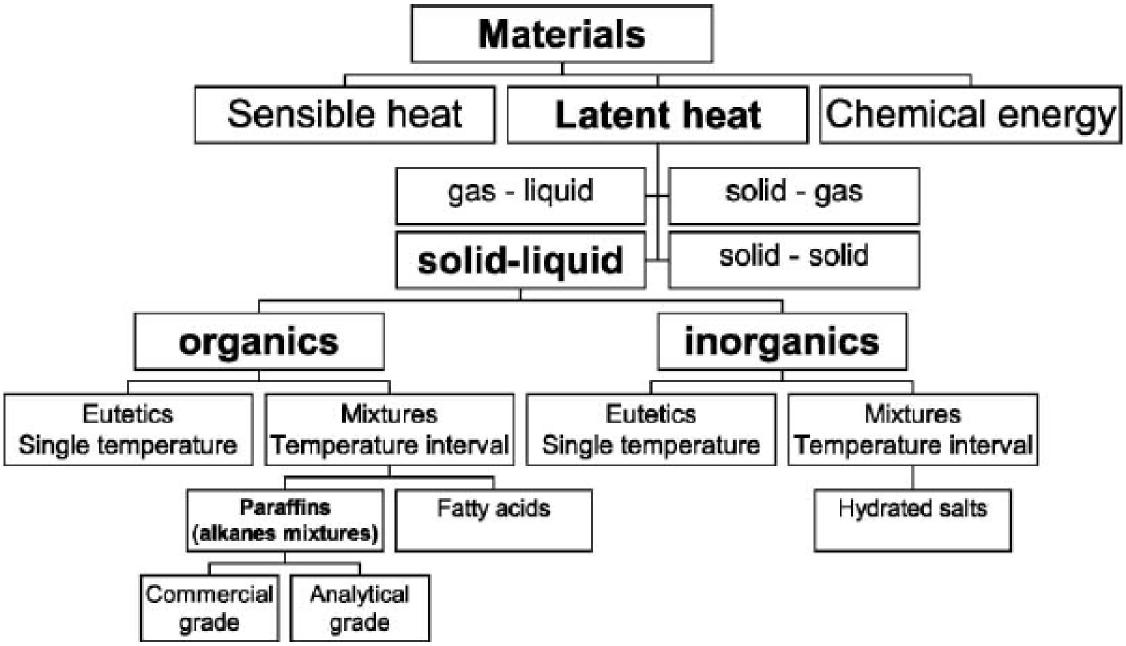

Figure 2-4: Classification of energy storage materials. (Abhat, 1983)

Table 2-1: Comparison of organic and inorganic phase change materials from Zalba (2003)

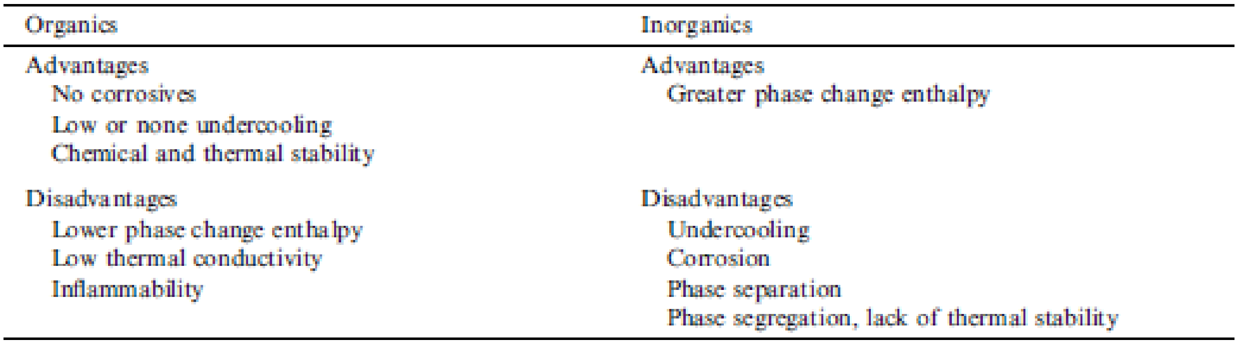

Organics	Inorganics
Advantages	Advantages
No corrosives	Greater phase change enthalpy
Low or none undercooling	
Chemical and thermal stability	
Disadvantages	Disadvantages
Lower phase change enthalpy	Undercooling
Low thermal conductivity	Corrosion
Inflammability	Phase separation
	Phase segregation, lack of thermal stability

2.1.1.3 Chemical Energy Thermal Storage

Chemical energy thermal storage systems are designed to store energy by causing a chemical reaction to occur in the direction that requires heat energy; these systems extract the energy by reversing the chemical reaction. These systems tend to have very high storage densities, in many cases higher than that of latent heat systems. These systems all work on the basic principle of causing some chemical or combination of chemicals to undergo a reaction that creates a new chemical(s) by adding heat to the systems. The ideal reaction would be one that requires a large amount of heat and one that is completely reversible by removing heat. Equation 2.4 shows the general form of a thermochemical reaction that this method relies on, in this equation two reactants on the left-hand side of the equation are combined in an endothermic reaction to create two products on the right-hand side. The letters used in Equation 2.4 to denote the products and reactants are arbitrary. Thermal energy is stored in these thermochemical reactions, by combining heat with one or more reactants to produce one or more products. When the energy needs to be extracted the product(s) are cooled and the will undergo a chemical reaction to transform back into the original reactants and release the stored thermal energy. One problem with these systems is that chemical compatibility between the reacting materials and the container can be an issue for certain chemicals.

$$A + B + heat \leftrightarrows C + D \qquad [2.4]$$

Abedin and Rosen (2011) compiled a list of potential thermochemical energy storage materials and presented their energy storage density and reaction temperatures. This data is presented in Table 2-2. The materials presented show very large energy storage densities, however, the reaction temperatures are fairly high.

Table 2-2: Potential Thermochemical Energy Storage Materials (Abedin and Rosen, 2011)

Thermochemical Material	Solid Reactant	Working Fluid	Energy Storage Density (GJ/m^3)	Charging Reaction Temperature(℃)
$MgSO_4 \cdot 7H_2O$	$MgSO_4$	$7H_2O$	2.8	122
$FeCO_2$	FeO	CO_2	2.6	180
$Ca(OH)_2$	CaO	H_2O	1.9	479
$Fe(OH)_2$	FeO	H_2O	2.2	150
$CaCO_2$	CaO	CO_2	3.3	837
$CaSO_4 \cdot 2H_2O$	$CaSO_4$	$2H_2O$	1.4	89

2.1.2 Comparison of the types of thermal storage

A direct comparison between each of the methods is difficult without knowledge of the application. Each type of thermal storage has advantages over the other in certain application. Table 2-3 shows the general ranges of the capacity power and efficiency of the types of thermal storage systems. Table 2-4 shows the storage densities of the three energy storage methods mentioned.

Latent heat thermal storage systems typically have higher thermal storage densities than sensible energy thermal storage systems for small temperature differences. Since the change in the sensible energy of a material depends on what the temperature change is, for small changes in temperature only a small amount of sensible energy can be stored. This allows for latent heat storage systems to have a higher energy density. When large changes in temperature are allowable, then the benefit of using latent heat thermal storage is reduced. One of the major problems with latent heat thermal storage systems is that low thermal conductivity of the material will results in latent heat thermal storage systems having slower charging and discharging rates compared to sensible energy systems. Latent heat thermal storage systems typically have smaller thermal storage density than thermochemical storage systems. However, the thermochemical storage systems can be much more difficult to implement than a latent heat thermal storage system. Thermochemical systems require that there is a chemical reaction that is reversible, that the temperature that the chemical reaction is reversible at is in the desired temperature range of the system and that the kinetics of the chemical reaction allows for a fast charging and discharging rate. If all of these constraints are met, then a thermochemical system may be viable. For some thermochemical reactions to meet these constraints pressurization is required. Beyond these basic constraints, other aspects must be considered such as chemical compatibility with the container it will be stored in, safety in terms of flammability and toxicity or risks and cost compared to the other storage methods. Due to all of these constraints, there are situations where latent heat thermal storage system are preferable to thermochemical systems, even if latent heat thermal storage systems have a lower storage density.

Table 2-3: Ranges of values for important design considerations for thermal storage system. Internal Energy Agency and International Renewable Energy Agency. (2013)

Thermal storage system	Capacity (kWh/t)	Power (MW)	Efficiency (%)	Storage period(hour/day/month)	Cost(€/kWh)
Sensible (water)	10-50	0.001-10	50-90	d/m	0.1-10
Latent	50-150	0.001-1	75-90	h/m	10-50
Chemical	120-250	0.01-1	75-100	h/d	8-100

Table 2-4: Typical storage densities of the storage techniques (Cengel,2010) (Mehling and Cabeza, 2008) (Abedin and Rosen, 2011)

Type of storage	Storage material	Storage density, kJ/kg	Temperature, ℃
Sensible energy storage (Cengel,2010)	Water	84	20-40
	Mineral oil	36	20-40
	Concrete	18	20-40
Latent heat storage	Water - ice	330	0
	Paraffins – solid liquid	200	30-120
	Salt hydrides – solid liquid	280	30-100
Thermochemical	$MgSO_4 \cdot 7H_2O$	10000	120

2.2 State of the art of phase change thermal storage heat transfer enhancement

One of the primary issues with latent heat thermal storage systems is that the low rates of charging and discharging of thermal energy. Thus, there is a need to increase the rate of heat transfer from and to these systems. Methods for increasing the rate of heat transfer in latent heat thermal storage systems can be categorised as either passive enhancement techniques or active enhancement techniques. Passive enhancement techniques are those where no external energy is added to the system to enhance heat transfer. Alternatively, active enhancement techniques require some energy to be added to the system to enhance heat transfer.

It is helpful to consider the two-phase Stefan problem when trying to understand the methods of enhancing heat transfer during phase change. A depiction of the Stefan problem is given in Figure 2-5. In this one-dimensional problem, there is a material that is initially fully solid (or liquid) at t=0 a wall temperature is imposed that is above (or below) the melting temperature of the material. As the material begins to melt (or solidify), it is assumed that melting occurs at a single temperature. To determine the rate at which the material grows, an energy balance can be performed, which is presented in Equations 2.5 and 2.6. In Equation 2.5, $\dot{E}_{Stored}$ is the rate that energy is stored in the material, ρ is the mass density of the material, H is the latent heat of fusion, A is the area of the interface perpendicular to the wall, S is the thickness of the solid, $Q_{interface\ to\ wall}$ is the heat transferred from the interface in the direction of the wall and $Q_{solid\ to\ interface}$ is the heat transferred to the interface from the solid side. In Equation 2.6, $\dot{E}_{discharged}$ is the rate that energy is discharged from the system and $Q_{fluid\ to\ interface}$ is the rate of heat transfer to the interface from the liquid material and all other symbols are the same as in Equation 2.5. From these equations, it can be seen that in order to increase the energy growth rate of the solid then either the rate that heat is transferred from interface to the wall must be increased or the rate that heat is transferred from the second phase to the interface must be decreased. Which is seen on the right-hand side of Equation 2.5 and Equation 2.6. The only practical way to reduce the heat transferred from the second phase to the interface is to bring the initial temperature of the material closer to the melting temperature. Equation 2.7 – the heat conduction equation – provides insight into how to increase the rate of heat transferred from the interface to the wall. In Equation 2.7, k is the thermal conductivity of the material between the interface and the wall, T is the temperature of the material and x is the distance in the direction perpendicular to the wall. Increasing the thermal conductivity of the material will result in an increased rate of heat transfer. The heat transfer area can also be increased to enhance the rate of heat transfer. The final way to increase the rate of heat transfer is to increase the temperature gradient between the wall and the interface.

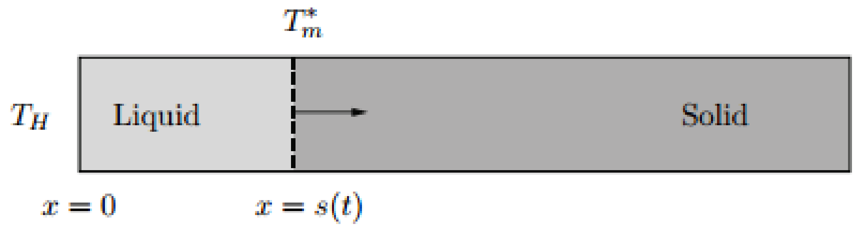

Figure 2-5: Illustration of a stefan problem for melting, the solid material is at the melting temperature (Martinez, 2014)

$$\dot{E}_{Stored} = \rho HA\frac{\partial s}{\partial t} = Q_{interface\ to\ wall} - Q_{solid\ to\ interface} \quad [2.5]$$

$$\dot{E}_{discharged} = \rho HA\frac{\partial s}{\partial t} = Q_{interface\ to\ wall} - Q_{fluid\ to\ interface} \quad [2.6]$$

$$Q_{interface\ to\ wall} = kA\frac{\partial T}{\partial x} \quad [2.7]$$

2.2.1 Passive enhancement Techniques

The following section will review the state of the art in increasing heat transfer and the amount of energy stored in a latent heat thermal storage system using passive techniques. Passive techniques are those that do not require an input of external energy to create the improved heat transfer. These passive enhancement techniques work by increasing either the thermal conductivity of the material, increasing the area of heat transfer or by trying to make a larger thermal gradient at the heat transfer surface. Passive enhancement techniques can be categorised into four sections:

1. Increasing heat transfer area using fins
2. Enhancing the bulk thermal conductivity by adding a highly conductive matrix
3. Enhancing the bulk thermal conductivity by adding nanoparticles
4. Micro-encapsulation

2.2.1.1 Increasing heat transfer area using fins

An experimental and numerical investigation on the effect of adding fins to improve heat transfer in latent heat thermal storage systems was performed by Henze and Humphrey (1981). They developed a theoretical model to account for the enhanced rate of heat conduction for a fin geometry that spans the lateral distance of the phase change material's container. The model used in the numerical study is shown in Figure 2-6. Figure 2-6 shows a rectangular cavity filled with phase change material, on the top surface there is a metal fin, the thickness of this fin is varied in the analysis but the total container thickness, including the fin and phase change material, is not changed. The wall on the left-hand side is set at a temperature above the melting temperature of the material. In the analysis, they varied the fin thickness, denoted by Lm, from 0 mm to 3.175mm. The total thickness of the container L_F is 25.4mm. Thus, the maximum volume fraction the fins occupied was roughly 13%. They compared the numerical model to experimental results. The model showed that adding lateral fins increased the rate of melting significantly; for example with 3.175mm fins the melt fraction was roughly 3.5 times greater than for the no finned case at the end of the test. Their results are shown in Figure 2-7, in this figure, TAU is a dimensionless time variable, and the melt fraction is the ratio of the volume of phase change material that has been melted to the total volume. Figure 2-7 shows that as the fin size is increased then the fraction of liquid at any time is increased. Furthermore, comparing the finned cases, where Lm>0, and the no fin case, where Lm=0, it is clear that the addition of fins greatly improves the amount of energy stored in the system over the given period of time. The finned cases had an improvement on the order of 400% compared to the no-fins case. However, the authors did not consider the fact that as the fin thickness is increased, the volume of the phase change material is reduced by the additional amount of volume that the fin now occupies. The results of this analysis are as expected, the higher thermal conductivity of the fin, allows energy to be transferred to the phase change material more rapidly. Henze and Humphrey (1981) also investigated the effect of the temperature difference between the phase change material's melting temperature and the wall temperature. The results showed that an increase in the temperature difference increased the rate at which energy was stored. This result is also expected because the higher wall temperature creates a larger temperature gradient between the solid front and the wall.

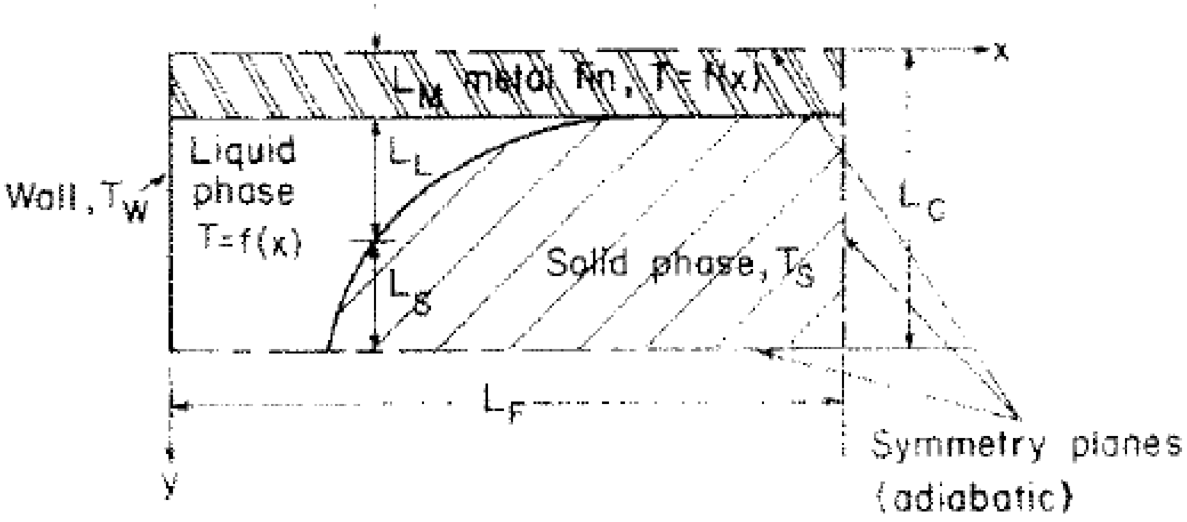

Figure 2-6: Domain used in the numerical analysis by Henze & Humphrey (1981). The domain consists of an initially solid phase change material that is melted by a constant temperature wall. There is one horizontal metal fin that is used to enhance the heat transfer which is represented by the double cross-hatched region.

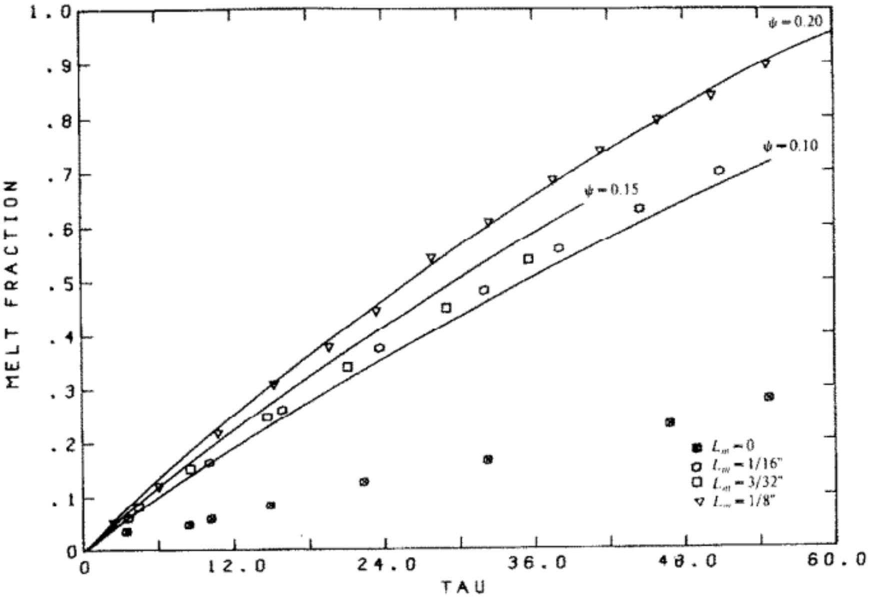

Figure 2-7: Results found by Henze & Humphrey (1981) for a ΔT of 10℃ between the heat exchanger and the melting temperature of the phase change material

Sparrow et al. (1981) performed an experimental study on outward solidification on a vertical longitudinal finned tube for conduction and natural convection controlled heat transfer. Paraffin was used as a phase change material, and it solidified on the outside of the tube. The energy was removed from the system, by cooling the tube with internally flowing water. It was found that the enhancement is less than the area ratio for conduction controlled heat transfer. The area ratio is the ratio of the outer surface of the finned and unfinned tube. For natural convection controlled heat transfer, it was found that the enhancement factor is nearly equal to the area ratio. For the conduction controlled case, the finding that the enhancement is less than the area ratio is expected because the solid layer that forms on the fins acts as a layer of insulation reducing their effectiveness. For convection controlled heat transfer, this insulating effect is still present; however, with fins, the metal is exposed to convection for longer than it would be without fins, so the enhancement is larger than the conduction controlled case. It was also found that the thickness of the frozen phase change material was increased as seen in Figure 2-8 and Figure 2-9. In Figure 7, Sparrow et al. (1981) compared the finned and unfinned design against each other at 15, 30 and 180 minutes after the start of the experiment. The thickness of the frozen layer is larger for the finned case than it is for the unfinned case. In Figure 2-9, the average frozen layer thickness, for the finned and unfinned cases, is plotted as a function of time. The curves in Figure 2-9 appear to level off, but in reality, the growth rate of the solid decreases as the solid gets thicker. So the solid is still growing, it is just growing at a slower rate. The study done by Sparrow et al. (1981) differs from that of Henze & Humphrey (1981) in the geometry used in the analysis, aside from that fact that Sparrow et al. (1981) used a cylindrical test section and Henze & Humphrey (1981) used a rectangular geometry. The fins used by Sparrow et al (1981) were much smaller than those used by Henze & Humphrey (1981); the volume fraction occupied by the fins in Henze & Humphrey (1981) was 13% whereas Sparrow et al. (1981) had a volume fraction of less than 1%. Despite this difference both authors saw a large improvement, which indicates that the design of the fin layout can be used to get large heat transfer improvements without sacrificing volume fraction. Specifically, a comparison of these studies indicates that a large amount of thin fins could offer a larger improvement than on thick fin.

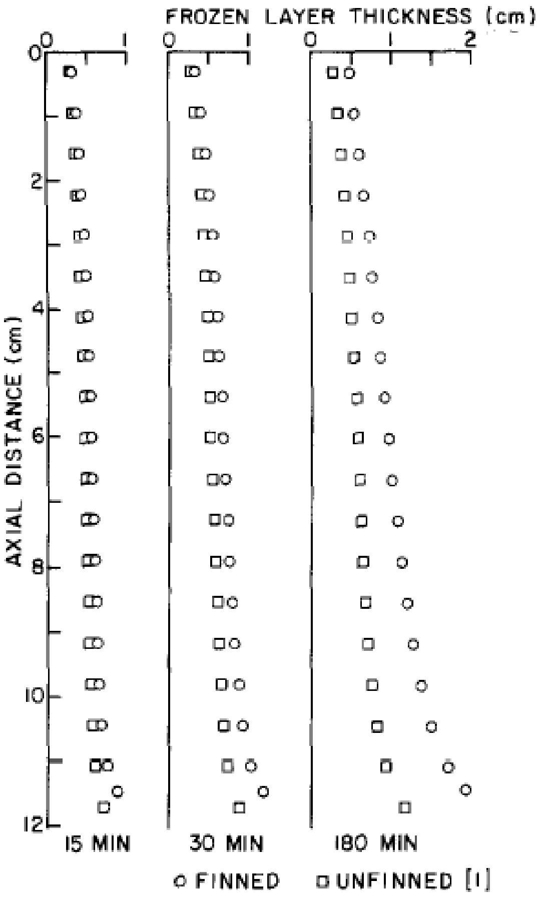

Figure 2-8: Comparison of the experimentally determined frozen layer thickness from Sparrow et al. (1981). The experiment consisted of a vertical, longitudinal finned tube, where the phase change material was solidified on the tube.

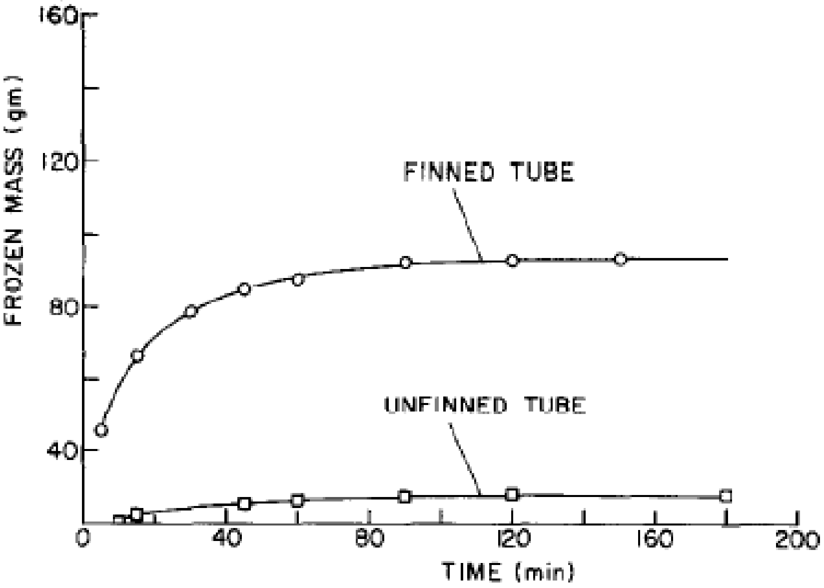

Figure 2-9: Comparison of finned and unfinned tube from Sparrow (1981) showing the solid mass as a function of time for the finned and unfinned tubes. . The experiment consisted of a vertical, longitudinal finned tube, where the phase change material was solidified on the tube.

Velraj and Seeniraj (1999) numerically studied solidification of a phase change material on an internally finned tube. The domain consisted of a tube submerged in a water bath, the tube was filled with the phase change material and had two internal fins cutting the tube into four sections. The domain used in the analysis is shown in Figure 2-10. The results showed that adding fins to this configuration reduced the time for solidification between 75 to 175% depending on the Biot number, which is a dimensionless quantity that represents the rate of heat transfer due to convection to the rate of heat transfer due to conduction, associated with the fins. The geometry proposed by Velraj & Seeniraj (1999) is the opposite of that used by Sparrow et al. (1981). Where Sparrow et al. (1981) used an externally finned tube, Velraj & Seeniraj (1999) used an internally finned tube. However, both of these designed showed an increase in the rate of heat transfer. However, it is difficult to compare the two devices because Velraj & Seeniraj (1999) did not report the volume fraction of their fins.

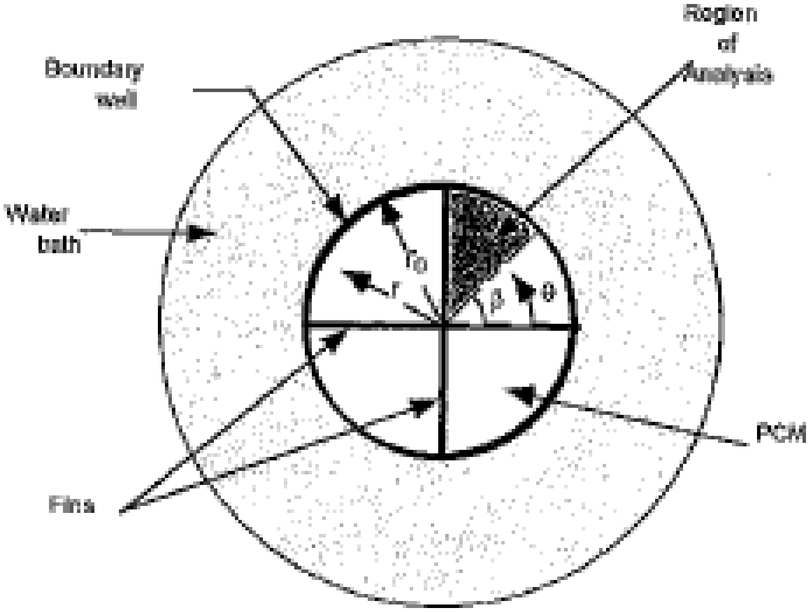

Figure 2-10: Image of the numerical domain used by Velraj and Seeniraj (1999). The apparatus consisted of a tube filled with phase change material that is surrounded by a water bath. The phase change material was initially melted and the water bath was at a temperature below the melting temperature of the phase change material.

Sciacovelli et al. (2016) performed a second law analysis to design a branched fin for a latent heat thermal storage system. The analysis was performed on a tube and shell heat exchanger, the phase change material was contained in the outer tube and was initially liquid. The heat exchanger is shown in Figure 2-11. The phase change material used was a paraffin wax with a melting temperature of 50-52 ℃. Then cold fluid is forced through the inner tube, such that solid begins to form on the heat exchanger surface. The solid front was then measured using digital images, by taking pictures through transparent walls. A numerical model was used to estimate the entropy generation, Sciacovelli et al. (2016) Equation 2.8 was used to calculate the entropy generation. Three designs were tested in the analysis. In the analysis, Design I consists of four straight fins spaced 90 degrees apart. The geometry of Design I and the local entropy generation are illustrated in Figure 2-12. Design II consists of four main fins each with two secondary fins with an angle of 30 degrees between the two secondary fins; the geometry of Design II and the local entropy generation are shown in Figure 2-13. Design III is similar to Design II but, the secondary fins are tilted in the axial direction by 8 degrees. Figure 2-14 shows the geometry and local entropy generation if Design III. The purpose of the tilt is to make the heat transfer more uniform in the axial direction. Design III reduces the space between the fins at the bottom of the test section, where the heat transfer will be lowest and increases the space at the top of the test section, where the heat transfer will be highest. The heat transfer highest at the top of the test section due to buoyancy effects carrying the hot liquid to the top of the test section and cold fluid to the bottom. The volume of the fins was kept the same in all the simulations. The results of the analysis showed that a design with uniform entropy generation also shows the fastest solidification rate as seen in Figure 2-15 and highest thermodynamic efficiency as seen in Figure 2-16. The analysis was conducted using a one-sixth axially symmetric model. The thermodynamic efficiency was defined by Equation 2.9, where $\dot{s}_{gen,global}$ is the global entropy generation and Ex_{in} is the rate of exergy released by the phase change material. The results of the analysis found that “Y” shaped fins provide the best performance. The results of this analysis show what was expected because by minimising entropy generation, the amount of superheating is essentially being minimised and thus energy is being added more uniformly. Henze & Humphrey (1981), Sparrow et al. (1981) and Velraj & Seeniraj (1999) all did not consider entropy generation when designing their test sections. However, in all the cases the author’s finned devices, in this case, device refers to the phase change material and the heat transfer surface, would result in a smaller entropy generation than the unfinned counterparts. This is because in designing the fins the authors were attempting to distribute the heat flow from the heat transfer surface throughout a larger area of the device. Since the same amount of heat transfer is taking place through a larger area for the finned devices the temperature gradient would be smaller and there from there should be less entropy generation.

$$\dot{s}_{gen}(x,t) = -\frac{\tau:\nabla\mathbf{v}}{T} + \frac{k(\nabla T)^2}{T^2} \quad [2.8]$$

$$\eta_{II} = 1 - \frac{T_0\,\dot{s}_{gen,global}}{Ex_{in}} \quad [2.9]$$

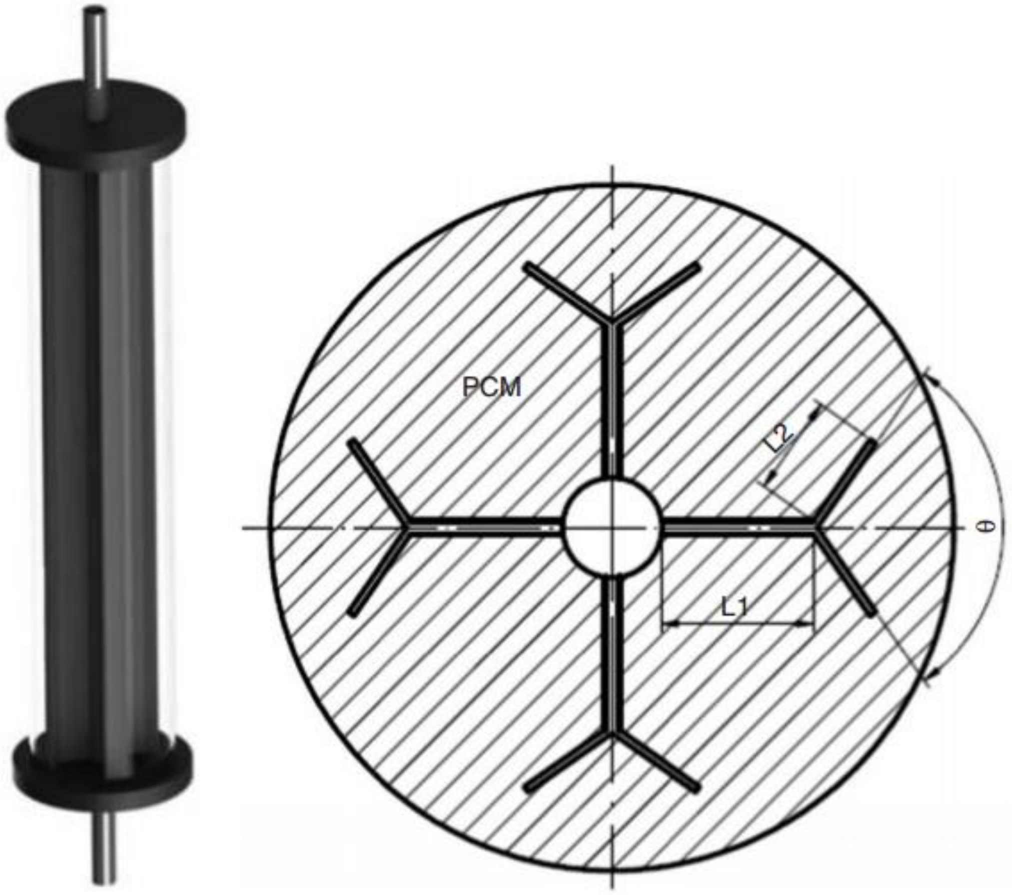

Figure 2-11: Branching heat exchanger used by Sciacovelli et al. (2016). The container consisted of a tube in tube heat exchanger that was used for thermal storage. Cold water was passed through the inner tube and the outer tube is filled with initially liquid phase change material. The analysis compared three different fin designs all of which were in the phase change material.

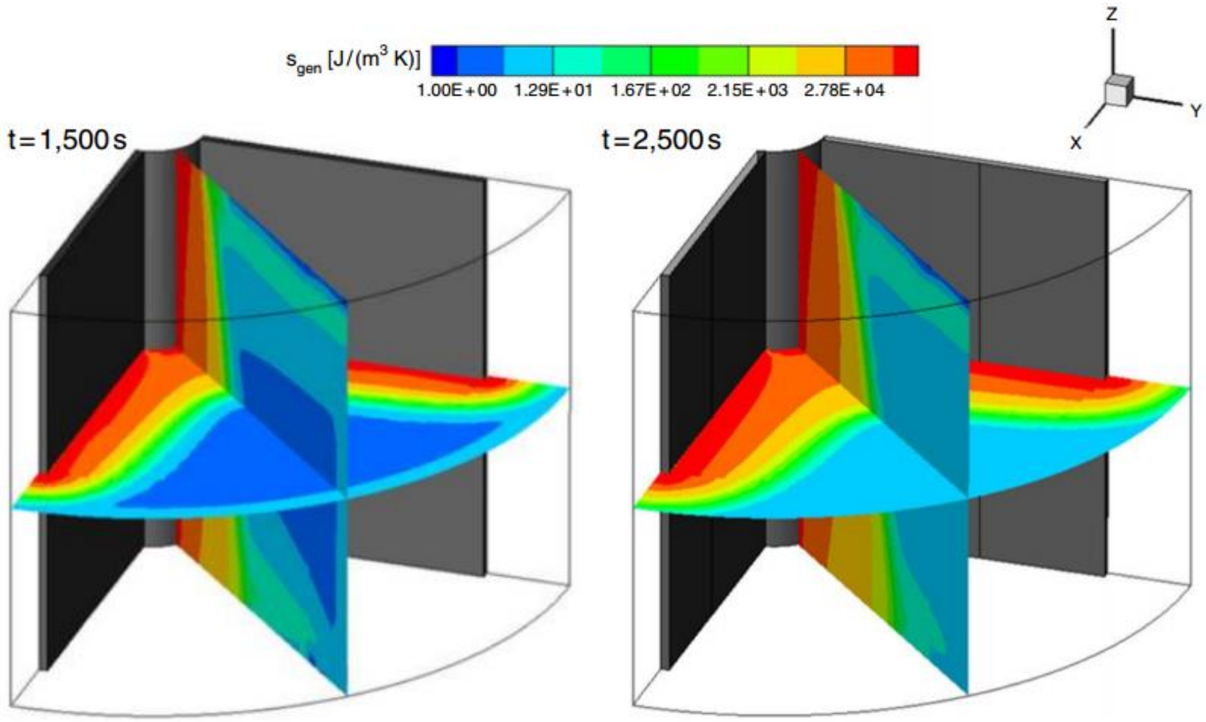

Figure 2-12: Local entropy generation for design I from Sciacovelli et al (2016).

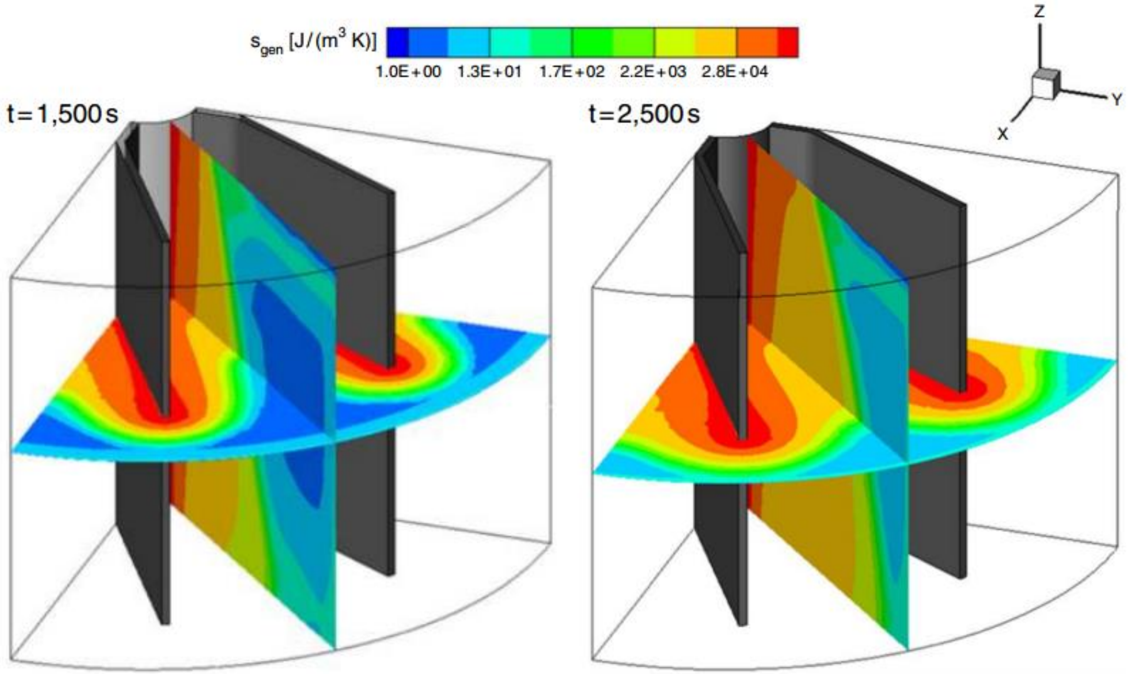

Figure 2-13: Local entropy generation for design II from Sciacovelli et al (2016).

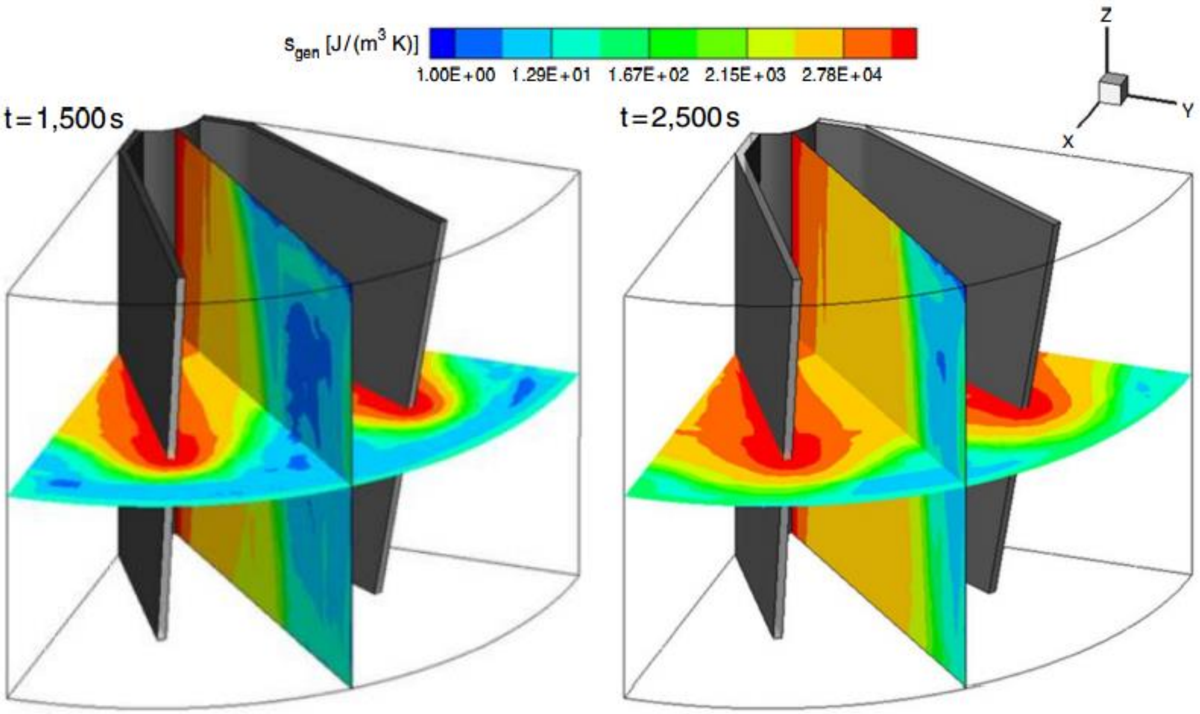

Figure 2-14: Local entropy generation for design III from Sciacovelli et al (2016).

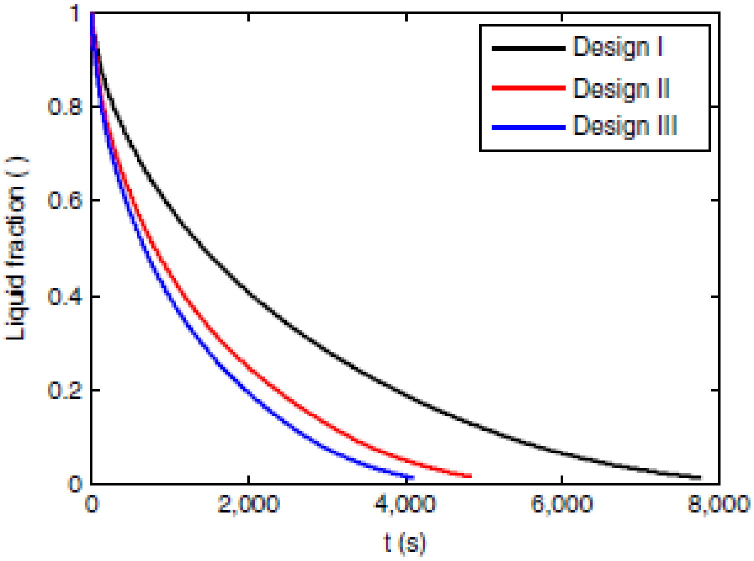

Figure 2-15: Liquid fraction from Sciacovelli et al (2016). The container consisted of a tube in tube heat exchanger that was used for thermal storage. Cold water was passed through the inner tube and the outer tube is filled with initially liquid phase change material. The analysis compared three different fin designs all of which were in the phase change material.

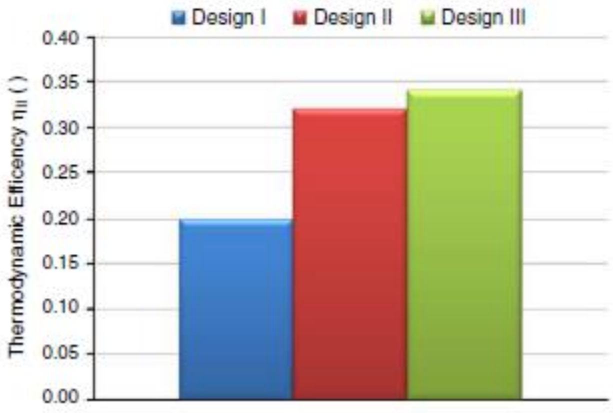

Figure 2-16: Second law efficiency from the analysis done by Sciacovelli et al (2016). The container consisted of a tube in tube heat exchanger that was used for thermal storage. Cold water was passed through the inner tube and the outer tube is filled with initially liquid phase change material. The analysis compared three different fin designs all of which were in the phase change material.

2.2.1.2 Enhancing the bulk thermal conductivity using a highly conductive matrix

Another method of increasing the rate of heat transfer in latent heat thermal storage systems is to add a matrix of highly conductive material to increase the bulk thermal conductivity of the system. Adding a conductive matrix increases the rate of heat transfer by increasing the thermal conductivity of the system. The trade-off is that the high conductivity matrix displaces phase change material inside the storage device. The result is a lower storage density.

Mesalhy et al. (2005) numerically studied the use of a high thermal conductivity porous matrix for increasing the rate of heat transfer while melting a phase change material. A tube in tube heat exchanger geometry was analysed with the inner tube set at a temperature above the melting point of the material and the outer tube wall being set as an adiabatic surface. The phase change material and highly conductive matrix filled the space between the two tubes. Mesalhy et al. (2005) found that for a porosity of 0.95, meaning that 95% of the volume is phase change material and the other 5% is the highly conductive matrix, the amount of heat absorbed into the phase change material is approximately 1.3 times greater than a case with no highly conductive matrix. The most extreme case tested was a porosity of 0.85 which absorbed 1.8

times the energy of the case with no highly conductive matrix. The design used by Mesalhy et al. (2005) is similar to the design used by Sparrow et al. (1981) where the heat is applied to the phase change material by an internal tube encapsulated in the phase change material. The high conductivity matrix allows for more high conductivity material for heat to transfer than the fins used in Sparrow et al. (1981). However, the trade-off is a larger volume fraction occupied.

Mills et al. (2006) used an expanded graphite matrix to increase the rate of heat transfer in latent heat thermal storage systems. It was shown that the effective thermal conductivity, or average the thermal conductivity of the graphite-phase change material mixture was increased significantly, between 20 to 130 times the thermal conductivity of the phase change material. The higher thermal conductivity will increase the rate of heat transfer from the latent heat thermal storage system. The authors also investigated if this phase change thermal storage system could be used to modulate the temperature of the electrical battery packs and found that the time for a battery pack to reach 85℃ was increased by 2.5 times when the phase change material was used. To implement the phase change for temperature modulation the phase change material was encapsulated in the composite matrix and place on the side of a battery.

2.2.1.3 Adding high conductivity particles

Another method of enhancing the rate of heat transfer in these systems is to add a high conductivity particles to the phase change material. The high thermal conductivity particles allow for another route for heat to conduct through, thus the thermal conductivity of the mixture has a high thermal conductivity than the phase change material. The thermal conductivity of the mixture is called the effective thermal conductivity. The highly conductive path enhances the effective thermal conductivity of the phase change material but reduces the storage density of the material.

Siegel (1977) studied the improvement in solidification rate in molten salt dispersed with high conductivity particles. He concluded that there was an improvement in the rate of heat transfer when the conductive particles are added. The study was analytical and considered three geometries. One geometry was a planar container where energy is added through one of the walls, another geometry is a tube where the phase change material is stored inside of a tube, where energy is added from the outside wall of the tube and a third geometry where the phase change material surrounds a tube where the energy is provided from inside the tube. It was found that for a concentration of 20% particles to 80% phase change material, assuming the particles have a thermal conductivity of 100 times that of the phase change material, the rate of heat removal can be increased by 10 – 20%. The results of this analysis illustrate that as the bulk thermal conductivity of the phase change material is increased so too does the rate that energy is discharged from the material. The heat transfer improvement of adding these particles is small relative to the volume occupied by the particles when compared to adding fins. For example, Velraj et al. (1999) implemented fins that occupied a volume fraction of 20%, which is the same volume fraction as Siegel (1977) used, and found a 500% increase in the rate of heat transfer.

Sanusi et al. (2011) experimentally studied using high thermal conductivity particles which were graphite nanofibers and using n-tricosane as the storage material. The geometry used in the analysis was a cubic container that was heated from the bottom using an electric heater. Adding graphite nanofibers significantly reduced solidification time of systems with aspect ratios equal to ½ and 2 compared to the non-enhanced case. Sansui et al (2011), found that the rate of heat transfer was increased by 70%. The improvement was greatest for small masses and less significant for larger masses. The volume fraction occupied by the particles was approximately 3%. Compared to Siegel (1977), Sanusi et al (2011) had a much larger enhancement for a much smaller volume fraction.

2.2.1.4 Microencapsulation

Another way to increase the rate of heat transfer for a latent heat thermal storage system is to use microencapsulation. Microencapsulation of phase change materials is when the phase change material is enclosed in a micro-size shell. Lots of these small containers are used in a full-scale system. The rate of heat transfer is increased because volume to area ratio of the phase change material is now very large compared to using a single block of phase change material. A drawback of microencapsulation is that the phase change material has a greater risk of supercooling. Supercooling is when a liquid material is in a meta-stable state below its melting temperature. The reason why supercooling is increased in microencapsulated is that microencapsulation is typically done using spherical containers with a small radius of curvature. These containers cause a solidifying material to undercool because when a material is solidifying a material will have a preferred growth direction. When a material solidifies on a flat surface, the preferred growth direction within a crystal will be parallel to each other, so the growth of one part of the crystal doesn't hinder the growth of any other part. However, molecules begin crystallizing on a curved surface their preferred growth directions will begin to overlap with that of their neighbouring molecules, which causes an additional energy barrier for crystal growth. In order to accommodate for the additional energy barrier, the equilibrium melting temperature decreases. Which causes the temperature difference between the melting temperature of the phase change material and the heat exchanger wall temperature to be lower. The lower melting temperature results in a smaller temperature gradient in the phase change material, thereby reducing the rate of heat transfer during discharge.

Regin et al. (2009) studied spherical PCM capsules numerically. The apparatus consisted of a cylindrical heat exchanger. The phase change material capsules filled the cylindrical heat exchanger and hot fluid flowed over the capsules. The apparatus is shown in Figure 2-17. They found that having a larger phase change temperature range increases the rate of melting of the phase change material. It was also shown that the charging rate was faster than the discharging rate due to the convection in the capsule during charging, the time to melt the capsule with a radius of 40mm was nearly decreased by 2 times. It was concluded that capsules of a smaller radius resulted in higher charging and discharging rates than capsules with a larger radius; this was due to the higher surface area to volume ratio. The fraction of space not occupied by the microcapsules was 40%, meaning that the volume fraction of this method of enhancement was more than 40%.

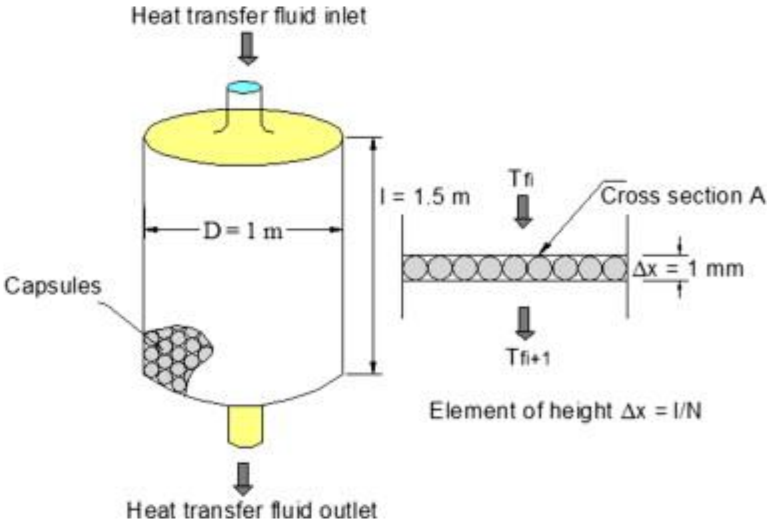

Figure 2-17: Layout and details of the storage system used for microencapsulation research by Regin et al. (2009)

An issue with microencapsulation is that some shell materials - the material used to encapsulate the phase change material - can react with phase change material. Werner (1987) observed that a phase change material of 90% myristic acid and 10% lauric acid, showed diffusion with polypropylene and polyethylene containers.

2.2.1.5 Comparison of Passive enhancement techniques

The four methods of passively increasing the rate of heat transfer in latent heat thermal storage systems. These methods are fins, a highly conductive matrix, adding nano-particles and microencapsulation. Fins, highly conductive matrix and adding nano-particles increase the rate of heat transfer by providing a material will a high thermal conductivity that allows heat to be transferred through the phase change material faster. Microencapsulation increases heat transfer by reducing the maximum solid front location, which limits the thermal resistance of the phase change. Table 2-5 provides a summary of authors that have used passive enhancement techniques to increase the rate of heat transfer from latent heat thermal storage systems. In Table 2-5, the enhancement found for fins are typically higher than the enhancement for the other methods. Highly conductive matrices and particles also show large improvements. Highly conductive particles have the benefit over fins and highly conductive matrices of having a higher volume fraction of phase change material; which allows them to have a higher storage density. One aspect that didn't receive much attention is a comparison of manufacturing costs between the methods. Each of these methods requires more complex manufacturing techniques than a latent heat thermal storage system without any enhancement.

Adding fins showed the largest increase in the rates of heat transfer compared to the other methods considered. However, fins also take up a comparatively small amount of volume than the other methods considered. For example, Saha et al. (2006) found that pin fins that take up 8% volume fraction provide the best heat transfer enhancement for the amount of volume displaced. Adding high conductivity particles also showed a high increase in the heat transfer rate, Siegel (1977) found the increased heat transfer by 70% and Mettawee and Assassa (2007) were able to increase the rate of heat transfer by 300%, but the particles used by Mettawee and Assassa (2007) occupied more than 14% of the container and Siegel's (1977) particles occupied a volume fraction of 20%. Based on these analyses, fins are the better choice than adding high conductivity particles. Fins also showed a higher heat transfer enhancement than the high conductivity matrix considered by Mesalhy et al. (2005) showed an 80% increase in the rate of heat transfer while occupying a volume fraction of 15%. Microencapsulation does show a very high heat transfer enhancement however, the storage density is greatly reduced because the spacing between each of the microcapsules doesn't store any energy. Thus, the conclusion of this analysis is that fins provide the best means of enhancing a latent heat thermal storage systems while also providing the best storage density of all the passive methods considered.

Table 2-5: Summary of the heat transfer enhancement achieved by various authors using Passive enhancement techniques for latent heat thermal storage systems

Author	Technique	Numerical / Experimental	Enhancement	Volume fraction of enhancement technique
Henze and Humphrey (1981)	Fins	Experimental and Numerical	400% higher heat transfer rate	13%
Sparrow (1981)	Fins	Experimental	350% higher heat transfer rate	<1%
Velraj et al. (1999)	Fins	Experimental	500% higher heat transfer rate	20%
Velraj and Seeniraj (1999)	Fins	Experimental	75% shorter solidification time	N/A
Siegel (1977)	High Conductivity Particles	Numerical	20% higher heat transfer rate	20%
Sanusi et al. (2011)	High Conductivity Particles	Experimental	70% higher heat transfer rate	3%
Mettawee and Assassa (2007)	High Conductivity Particles	Experimental and Numerical	300% higher heat transfer rate	14%
Mesalhy et al. (2005)	High Conductivity Matrix	Numerical	80% higher heat transfer rate	15%
Regin et al. (2009)	Microencapsulation	Numerical	50% shorter solidification time	40%

2.2.2 Active enhancement Techniques

Active enhancement techniques are those that use energy to create a heat transfer enhancement. In thermal storage systems, where the energy efficiency is important, it is only practical to use active techniques if the energy required for enhancement is very small compared to the energy stored in the system. Only a few studies on active techniques have been completed. The two methods that have been studied are ultrasonic vibration and electrohydrodynamic. The electrohydrodynamic method will be discussed in detail in Section 2.2.2.1. The ultrasonic vibration method is used to agitate the fluid to induce convection in the liquid phase.

The mechanism for ultrasonic heat transfer enhancement are acoustic cavitation and acoustic streaming (M. Legay et al. 2011). Acoustic streaming is a phenomenon where fluid convection is created by causing a gradient in momentum in the fluid. These gradients in momentum are caused by the dissipation of the acoustic energy in the fluid. Acoustic cavitation is a phenomenon where fluid convection is created by causing a non-uniform pressure field in the fluid. When the pressure at a point in the fluid drops below the vapour pressure of the fluid, an air bubble will form. This air bubble will grow and collapse rapidly, the growth and collapse of bubbles throughout the fluid causes convection. The power consumption of ultrasonic heat transfer enhancement can be on the order of 10 Watts (M. Legay et al. 2011). For latent heat thermal storage systems, this power consumption is large. For example, the apparatus for investigating electrohydrodynamics used in the current study, stores approximately 30 kJ and takes approximately 1-2 hours to discharge, depending on the experimental conditions. Using 10 Watts for 2 hours requires 72 kJ, which is more than double the amount of thermal energy stored. Thus, the large power requirements of this method limit its applicability in latent heat thermal storage systems. Typically, when used on a latent heat thermal storage system, a very low power ultrasonic device will be used.

Oh et al (2002) investigated applying ultrasonic vibrations to the melting of Octadecane, both experimentally and numerically. In the experiments, the energy was supplied by an electric heater. In the numerical analysis, this was modelled as a constant heat flux. The energy was only supplied at one vertical boundary, and all the other surfaces were adiabatic. The top surface of the container was a free surface exposed to air and the other boundary surfaces were walls. The apparatus used in the analysis is shown in Figure 2-18. It was found that applying ultrasonic vibrations improved the melting rate by 2.5 times in their best case. The results of the analysis are shown in Table 2-6. The numerical results showed that the ultrasonic vibrations induced fluid cells in the melted Octadecane.

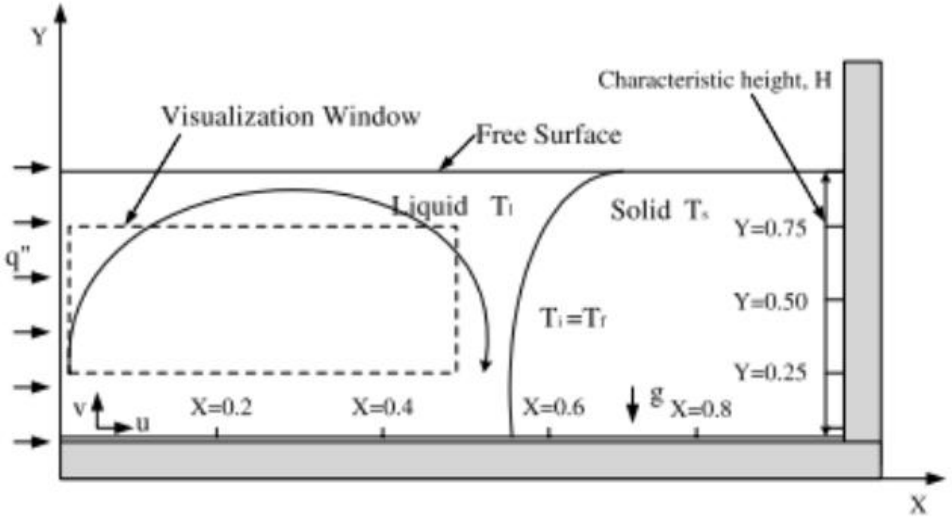

Figure 2-18: image of the domain used in the numerical analysis by Oh et al (2002). Heat was passed through one surface and the phase change material was initially solid.

Table 2-6: Comparison of the total consumed electricity for a melting process from Oh et al (2002)

Heat Flux (kcal/(hr· m^2)	Melting time (min)	Heater (Wh)	Ultrasonic vibration (yes or no)	Total consumed electricity (Wh)
9905.1	161	448.1	No	448.1
	76	211.5	Yes	445.9
5535.2	275	444.6	No	444.6
	94	152.0	Yes	441.8

2.2.2.1 Electrohydrodynamic enhancement of heat transfer:

Electrohydrodynamics is the study of fluid motion induced by an applied electric field. Electrohydrdyanmiccs can be used to enhance heat transfer by creating more vigorous convection in a fluid. This more vigorous convection increases mixing and increases the thermal gradient near a heat exchanging surface. In this chapter, the governing equations for electrohydrodynamics will be discussed, as well as a summary of the enhancement effects that electrohydrodynamics has on single-phase fluid heat transfer, two-phase fluid heat transfer and two-phase solid-liquid heat transfer. As all three mechanisms of enhancement have been shown to increase phase change thermal storage rates.

The general equations of electrohydrodynamics arise from the mass, moment and energy conservation equations of fluid mechanics and Maxwell's equations of electrostatics. The equation for conservation of mass is given by Equation 2.12. In Equation 2.12, ρ is the density, u is the vector field that describes the velocity of the fluid and t represent time. The Naiver-Stokes momentum equation for two-dimensional incompressible flow is given in Equation 2.13. In Equation 2.13, the force due to the electric charges and dipoles shows up as a source term, denoted by f_e, the electric body force. In Equation 2.13, u is the velocity in the x direction, v represents the velocity in the y direction, P describes the pressure field and μ is the kinematic viscosity. The term on the left-hand side of the equation describes the acceleration of the fluid in an Eulerian coordinate system, the first term on the right-hand side of the equation describes the force due to pressure acting on the fluid and the second term represents the viscous forces acting on the fluid. To determine the magnitude of the electric body force, Maxwell's equations are required. Maxwell's equations are given by Equations 2.14, 2.15, 2.16 and 2.17. In Equation 2.14, **E** is the electric field strength and **B** is the magnetic field flux. Equation 2.14 shows that the curl of the electric field strength is equal to the negative of the change in magnetic field flux. In Equation 2.15, **H** is the magnetic field strength, **D** is the electric displacement field strength and **J** is the electric current. In Equation 2.17 the value ρ_e represents the electric charge density of the material. Maxwell's equations allow the electric and magnetic states to be determined.

$$\frac{\partial \rho}{\partial t} = \nabla \cdot (\rho u) \qquad [2.12]$$

$$\frac{\partial u}{\partial t} + u\frac{\partial u}{\partial x} + v\frac{\partial u}{\partial y} = -\frac{1}{\rho}\frac{\partial P}{\partial x} + \frac{\mu}{\rho}\left(\frac{\partial^2 u}{\partial x^2} + \frac{\partial^2 u}{\partial y^2}\right) + f_e \qquad [2.13]$$

$$\nabla \times \mathbf{E} = -\frac{\partial \mathbf{B}}{\partial t} \qquad [2.14]$$

$$\nabla \times \mathbf{H} = \frac{\partial \mathbf{D}}{\partial t} + \mathbf{J} \qquad [2.15]$$

$$\nabla \cdot \mathbf{B} = 0 \qquad [2.16]$$

$$\nabla \cdot \mathbf{D} = \rho_e \qquad [2.17]$$

The governing equations for electrohydrodynamics were derived by Chu (1959), who showed that for fluids moving at speeds much less than the speed of light Equation 2.18 can be used to explain the electric force acting on a fluid cell. In Equation 2.18 and Equation 2.19, ρ_e is the electric charge density, **E** is the electric field strength vector field, **J** is the electric current **B** is the magnetic field strength, E is the magnitude of the electric field strength, ε is the electric permittivity, H is the magnitude of the magnetic field strength, μ_e is the magnetic permeability, ρ is the density of the material. The first term on the right-hand side of Equation 2.18 describes the forces acting on free charge carriers, the second term is the magnetic force acting on moving charges in the fluid. The third term in Equation 2.18 is a force that arises due to imbalances to in the electric force due to changes in the electric permittivity; the fourth term is a force that arises due to imbalances in the magnetic permeability in space. The final term represents the force that arises due to changes in density in the fluid, the change in density causes a change in permittivity and permeability. For dielectric fluids, the conductivity is very low. For the case where the conductivity of the medium is very low then the current and magnetic field strength becomes small thus, the electric body force can be rewritten as Equation 2.19.

$$f_e = \rho_e \mathbf{E} + \mathbf{J} \times \mathbf{B} - \frac{1}{2}E^2\nabla\varepsilon - \frac{1}{2}H^2\nabla\mu_e + \nabla[\frac{1}{2}\rho E^2\frac{\partial\varepsilon}{\partial\rho} + \frac{1}{2}\rho H^2\frac{\partial\mu}{\partial\rho}] \qquad [2.18]$$

$$f_e = \rho_e \mathbf{E} - \frac{1}{2}E^2\nabla\varepsilon + \frac{1}{2}\nabla\left(\rho E^2\frac{\partial\varepsilon}{\partial\rho}\right) \qquad [2.19]$$

The first term of Equation 2.19 is the electrophoretic force and represents the force that arises due to electric charges distributed throughout the medium. The last two terms in Equation 2.19 are referred to as the polarisation forces. The second term is the dielectrophoretic force, which arises either due to special change in permittivity or due to non-uniform electric fields. The third term is the electrostrictive force. This term is primarily driven by the non-uniform electric field. However, this term tends not to be significant in causing fluid motion and rather results in a change in the pressure field (Antonio, 2011). The polarisation forces that are usually significant in multiphase systems are often not significant in single phase systems except when there are large temperature gradients (Antonio, 2011). The dielectrophoretic force becomes an interfacial force in two phase systems. This interfacial force arises from the large gradient in the dielectric constant at the interface between two materials. Applying an electric field also adds a heat generation term in the energy equation, which is represented by Equation 2.20. In Equation 2.20, ρ is the mass density of the fluid, C_p is the specific heat, T is temperature, u is the velocity, k is the thermal conductivity and q_e''' is the heat generation per unit volume for the fluid. The two terms on the left-hand side of Equation 2.20 represent the increase in temperature of the fluid in an Eulerian coordinate system. The first term on the right-hand side represents the heat transfer due to conduction and the final term represents how much thermal energy is being generated per unit volume in the fluid. Chang et al. (1994) defined the heat generation term as Equation 2.21. In Equation 2.21, the symbols used are the same as those used in Equation 2.18.

$$\rho C_p \frac{\partial T}{\partial t} + \rho C_p \bar{u} \cdot \nabla T = k \nabla^2 T + q_e''' \qquad [2.20]$$

$$q_e''' = (\mathbf{J} - \rho_e \bar{\mu})(\mathbf{E} + \bar{u} \times \mathbf{B}) + \nabla \cdot [(\bar{E} + \bar{u} \times \bar{B})(\bar{H} - \bar{u} \times \bar{D})] + [\mathbf{E} \frac{d}{dt}\left(\frac{\boldsymbol{D}}{\rho}\right) + \mathbf{H} \frac{d}{dt}(\frac{\mathbf{B}}{\rho})] \qquad [2.21]$$

The first term on the right-hand side of Equation 2.21 is due to the flow of charged particles. The second term is the energy generation due to fluid polarisation. The final term is due to time varying electric and magnetic field; this is similar to the energy stored in inductors and capacitors. If the conductivity of the medium is very small and there are no charges in the medium than this equation can be simplified to the simple Joule heating relation, shown in Equation 2.22.

$$q_e''' = \sigma_e E^2 \qquad [2.22]$$

The body force term in Equation 2.13 is the source of the heat transfer enhancement effect of electrohydrodynamics. The first term on the right-hand side of Equation 2.19 is the electrophoretic force. The electrophoretic force acts on free charges and ions in a fluid, it acts to move the charges along the electric field lines. There are three sources of charges in a dielectric fluid which are dissociation of impurities, dissociation of the dielectric fluid and changes in the electric conductivity of the fluid (Castellanos, 1998). As the number of impurities in a system increases, the strength of the electrohydrodynamic forces also increases (Sheshakamal and Cross, 1989) (Jayaram and Cross, 1994). The impurities in the fluid affect the electrohydrodynamics force because the impurities can gain electric charges that build up on the electrodes.

Charge injection causes charges to be injected into the fluid by transferring an electric charge from an electrode to the dielectric fluid, which creates electric charges that are free to move within the fluid. Free charges can also build-up due to local changes in the electric conductivity and permittivity (Turnbull, 1968). In single phase fluids, changes in the electrical conductivity could be due to inhomogeneous impurity concentration or temperature gradients (Turnbull, 1968). In solid-liquid two-phase mixtures, there is an inherent difference in the electrical conductivity of the solid and the electrical conductivity of the liquid. This difference in the conductivities cause ion rejection from the solid into the liquid which generates charges in the liquid. This phenomenon is referred to as the thermodielectric effect (Gross, 1954) (Tomas and Novotny, 2015).

The second and third terms on the right-hand side of Equation 2.19 are primarily responsible for the heat transfer enhancement when there are large temperature gradients or in a two-phase fluid. The second term in the equation acts as a result of differences in the permittivity in space; in single phase fluids, this difference could be due to a non-uniform electric field. For two-phase fluids, this difference in permittivity can be due to inherent differences in the permittivity between the two phases. The permittivity can vary with density due to impurity concentration differences and temperature gradients in the fluid.

2.2.2.1.1 Electrohydrodynamic heat transfer enhancement in Single phase fluids

In single phase fluids, both the electrophoretic force and the polarisation forces, in Equation 2.19, can be used to create convection in the fluid. However, the electrophoretic force is typically much larger than the polarisation forces because the polarisation force depends on the gradient of the electric permittivity. In single phase fluids the gradient of the electric permittivity is small unless there are large temperature gradients, thus for most applications, the electrophoretic forces dominate. In this section, electrophoresis and corona wind will be discussed in regards to how electrohydrodynamics using the electrophoretic force can be used to enhance heat transfer. Enhancing heat transfer using the dielectrophoretic force will also be discussed.

Corona wind is created when charges are injected into the air from an electrode at high electric potential. The flow is created by the repulsive force acting on the ions in the air and the electrodes. The unionized fluid gets gains momentum from the ionized fluid due to viscous forces. These viscous forces cause the fluid to flow which can be used to enhance heat transfer. Although this method does increase heat transfer, the electric power consumption is higher than other electrohydrodynamic enhancement phenomena (Allen & Karayiannis, 1995). In latent heat thermal storage systems, power consumption is important. If the electric energy consumption is on the same order as the thermal energy stored in the system, then the cost of electricity could make the latent heat thermal storage system financially unviable.

Kalman and Sher (2001) experimentally studied using corona wind to provide air cooling. They found that when a negative electric potential was used, the velocity of the air was about 20% less than for a positive electrode; even though, the negative electrode drew a larger electric current. Thus, a positive corona is more effective than a negative one. However, other studies have found that this is not universally true, and depends on the dielectric material (Nangle-Smith, et al 2013). The experimental apparatus used by Kalman and Sher (2001) is shown in Figure 2-19. The corona wind was generated by a wire and two wings. Ions are injected into the air near the wire, an electric potential is applied to the wire, and the ions flow towards the grounded wings dragging the air with them. The air then flowed into an electrically heated plate. The heat transfer coefficient was measured by measuring the surface temperature of the plate, the temperature of the air and the electric heat flux. Kalman and Sher (2001) further found that the at the centre of the plate the heat transfer coefficient was increased by 2.5 times for an applied heat flux of 260 W/m^2 and 1.7 times for an applied heat flux of 580 W/m^2. The areas of the plate further away from the centre showed smaller enhancements. Figure 2-20 shows the enhancement; in this graph, Alpha signifies the angle between the plate and the wing.

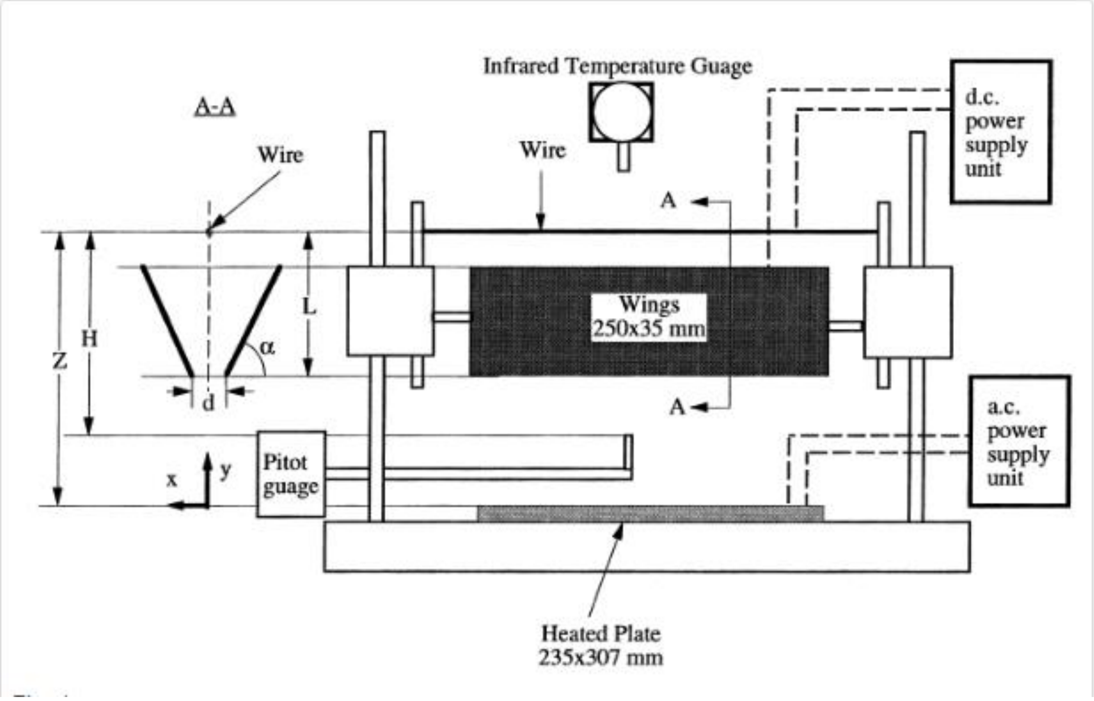

Figure 2-19: Experimental apparatus used by Kalman and Sher (2001). Image on left shows side view of image on the right. The device generates corona wind by applying an electric potential to the wire and grounding the wings. The corona wind then causes convection heat transfer on the heat plate.

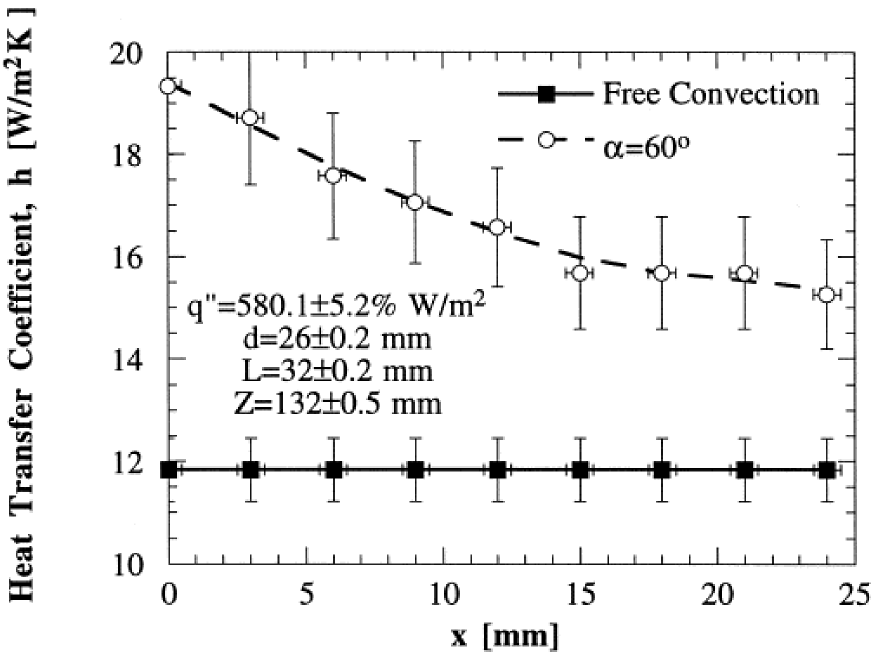

Figure 2-20: Heat transfer coefficient at different distances along the plate found in Kalman and Sher (2001)

Kasayapanand (2008) studied the enhancement of vertical fin arrays by applying electrohydrodynamics using computational fluid dynamics. The geometry used was a rectangular enclosure heated from the bottom and cooled from the top with vertical fins protruding from the bottom wall. The geometry and boundary conditions are shown in Figure 2-21. In the study, Kasayapanand (2008) found that the fluid flow and heat transfer are dependent on the number and location of the electrodes around the fins. It was also shown that the heat transfer coefficient is enhanced by applying electrohydrodynamics, as seen in Figure 2-22. Figure 2-22 shows that the Nusselt number can be increased by approximately 4 to 7 times. The source of the enhancement in heat transfer is greater fluid flow, as seen in Figure 2-23.

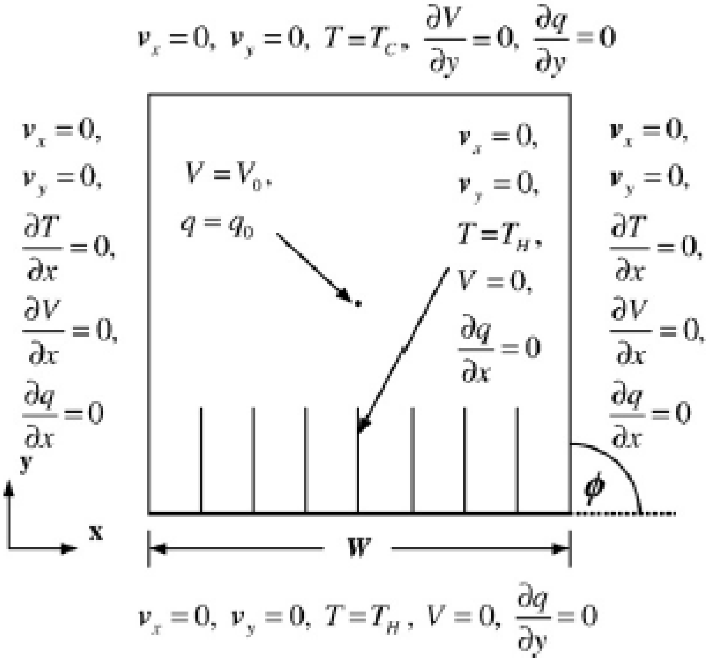

Figure 2-21: Domain and boundary conditions used by Kasayapanand (2008) in a numerical analysis. Bottom wall has a constant temperature boundary condition, top wall has a constant cold temperature boundary condition. Fluid is initially at rest and at the bottom wall temperature.

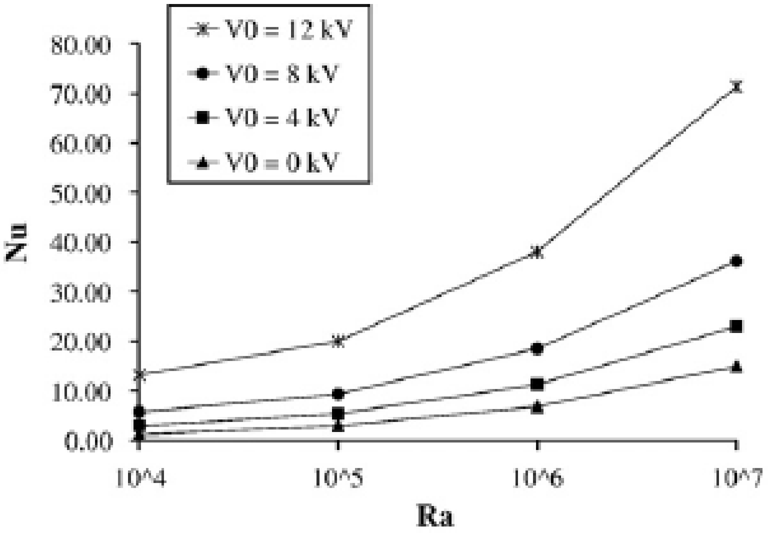

Figure 2-22: Nusselt number as a function of Rayleigh number from Kasayapanand (2008)

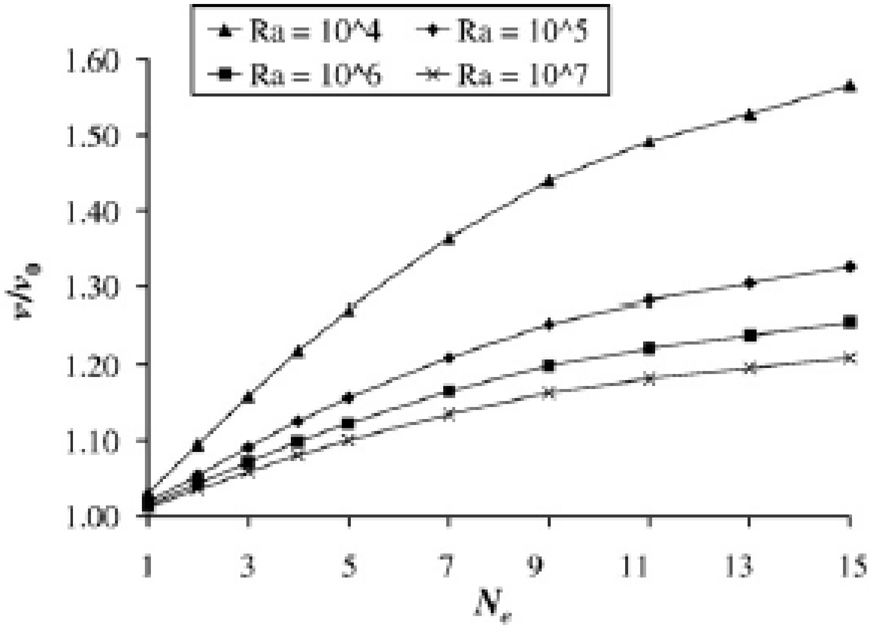

Figure 2-23: Dimensionless flow velocity as a function of electric Reynolds number from Kasayapanand (2008)

Yoshikawa (2013) studied fluid convection due to the dielectrophoretic force in an annular geometry under microgravity with a radial temperature gradient. Yoshikawa (2013) analysed the stability problem that arises due to the dielectrophoretic force, which was shown to be similar to the Rayleigh-Bénard instability seen in natural convection heat transfer. Yoshikawa found that the critical Rayleigh number depends on the ratio of the radii, the temperatures of the tube walls and the applied field. This stability problem was also studied by Turnbull (1969). Turnbull (1969) analytically studied a Bénard stability problem associated with electrohydrodynamics. The problem Turnbull (1969) analysed was a single phase fluid contained between two infinite plates, with gravity acting in the direction from the cold plate towards the hot plate. Only the dielectrophoretic force was studied in the analysis, to eliminate the effects of the electrophoretic force an alternating current was applied with a frequency above the relaxation time of the material. The study found that when an electric field is applied the critical Rayleigh number for the onset of convection was smaller when an electric field was applied. The critical Rayleigh number was decreased by 10 times between the case with no electric field and the case with the largest electric field. Turnbull (1969) did not investigate the effect that this convection had on heat transfer.

2.2.2.1.2 Electrohydrodynamic heat transfer enhancement in two-phase fluids

Studies have investigated the use of electrohydrodynamics to enhance heat transfer in two-phase fluids. Many investigations have studied the effect of electrohydrodynamics to a two-phase annular heat exchanger. These studies have found that when the electric potential is increased the amount of mixing in also increased; which results in a higher rate of heat transfer and a higher pressure drop as well. The flow pattern of the fluid is altered when the electric potential, which is heavily influenced by the interfacial force acting on the gas-liquid interface. Depending on the vapour quality – or the volume fraction of vapour – generating an electric field can decrease the rate of heat transfer. This decrease occurs when the liquid phase is drawn away from the heat transfer surface, which forces the heat to be transferred through the vapour phase, which typically has a lower thermal conductivity and density, thus reducing the rate heat transfer (Norris et al. 1999).

Singh (1995) and Cotton (2000) conducted research on the effect of electrohydrodynamic heat transfer improvement of internal convective boiling for different refrigerants. It was found that increasing the voltage will increase the level of heat transfer enhancement and flow mixing. However, there is also an increasing pressure drop penalty. Norris et al. (1999) found that applying a voltage can hinder heat transfer during boiling due to dry out on the heating surface.

Ng et al. (2010) performed an experimental investigation into transient phase redistributions of a two-phase flow in an annular channel with an electrode in the centre of the tube and with the outer wall as an electrode and heat transfer surface. It was found that as the duty cycle of the applied voltage was increased the heat transfer coefficient and pressure drop both increased. These increases were observed because as the duty cycle was increased different flow patterns were observed. The maximum increase in pressure drop was approximately 6 times the no-electrohydrodynamics case. The increase in the heat transfer rate was between 1.2 and 2.7 times the no-electrohydrodynamics case.

Nangle-Smith et al. (2013) investigated the effect of high voltage DC waveforms on two-phase flow redistribution. The study was conducted on an annular flow channel with an electrode at the centre of the channel, and an electrode at the outer surface; the inner and outer surfaces are shown in Figure 2-24. The investigation addressed the fact that reversing the polarity of the electrodes results in different flow structures and heat transfer characteristics. It was found that for negative voltages the electrophoretic force aids in repelling the liquid to the outer surface, whereas for positive voltages it hinders the repulsion. The reason for this is that the mobility of the negative charges on the electrode is greater than that of the positive charges, which allows for more negative charges to be injected into the fluid. Thus, when the electrode is negative these injected electric charges will be repealed from the negative electrode, whereas they would be attracted to a positive electrode. This repulsion increases wetting of the outer heat transfer surface and thus improves heat transfer. The maximum increase in the heat transfer coefficient observed by Nangle-Smith et al. (2013) was 3.3 times the no-electrohydrodynamics case. However, the pressure drop increased by more than 5 times. The geometry used by Ng et al (2010) and Nangle-Smith et al. (2013) were identical; thus, the improvement for condensation was between 1.2 and 2.7 times which on the same order as the 3.3 times seen by Nangle-Smith et al. (2013). The pressure drop increase was also similar. The geometry used by Fernandez and Poulter (1987) was the same as Nangle-Smith et al. (2013); the improvement seen by Fernandez and Poulter (1987) was 2000% whereas the improvement seen by Nangle-Smith et al. (2013) was 330%.

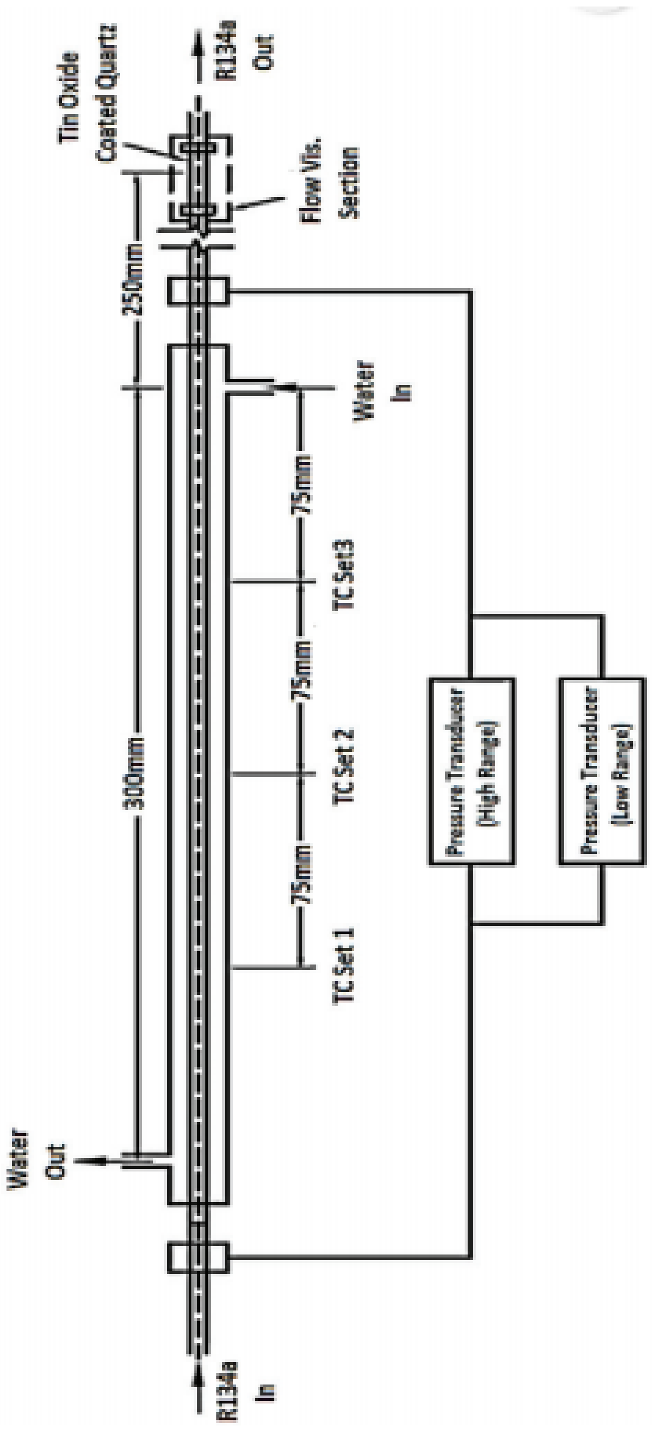

Figure 2-24: Experimental apparatus used by Nangle-Smith, (2013)

2.2.2.1.3 Electrohydrodynamic enhancement of heat transfer in two phase solid-liquids

The same mechanisms that caused enhancement in single phase and two-phase fluids will cause enhancement in the liquid phase of a two-phase solid-liquid system. However, in the solid phase, there will not be any electrohydrodyanmic enhancement because in the solid phase the material is strong enough to remain rigid when the electric forces are generated. Since there will be no convection in the material, there will be no change in the heat transfer rate in the solid phase. Thus, the amount of heat transfer enhancement is heavily dependent on whether the solid phase is interacting with the heat transfer surface or the fluid phase is interacting with the heat transfer surface. If the liquid phase is in contact with the heat transfer surface then there will be a heat transfer enhancement (Nakhla et al, 2015). The focus of the current investigation is to answer the question of what happens when the solid side is in contact with the heat transfer surface.

Two similar studies to the current investigation have been conducted in the past. One study was conducted by Dellorusso (1997) which experimentally investigated the effect of applying electrohydrodynamics to the solidification and melting of a phase change material. The other study was performed by Nakhla et al (2015) which experimentally investigated the enhancing melting of a phase change material using electrohydrodynamics when it is exposed to a constant heat flux. In addition to these studies, Dulikravich (1994) and Colaco et al (2004) studied solidification in the presence of electrohydrodynamics numerically.

Dellorusso (1997) conducted an investigation on enhancing the heat transfer performance of a latent heat thermal storage system using electrohydrodynamics. Dellorusso (1997) used paraffin wax with a 55℃ melting temperature as a phase change material and used air as the working fluid. The heat exchanger for the system was made out of aluminum with fins protruding into the wax. A schematic of the test section is shown in Figure 2-25. Air flows along the outer two walls in Figure 2-25, such that solidification and melting proceed on both of the aluminum walls. The electric field was induced by applying a 15 kV potential difference between the two opposing aluminum plates. Dellorusso (1997) performed experiments on both solidification and melting. For solidification, it was found that applying an electric field slowed down the rate of heat transfer, as seen in Figure 2-26. Dellorusso suggested that this was because during solidification conduction is the primary mode of heat transfer, however, this claim was not supported in any way. It was also suggested that the electrohydrodynamic forces slow down the nucleation and crystal growth rate during freezing. However, for the melting cycle, Dellorusso found that applying electrohydrodynamics had little effect on the melting rate of the paraffin wax, Figure 2-27.

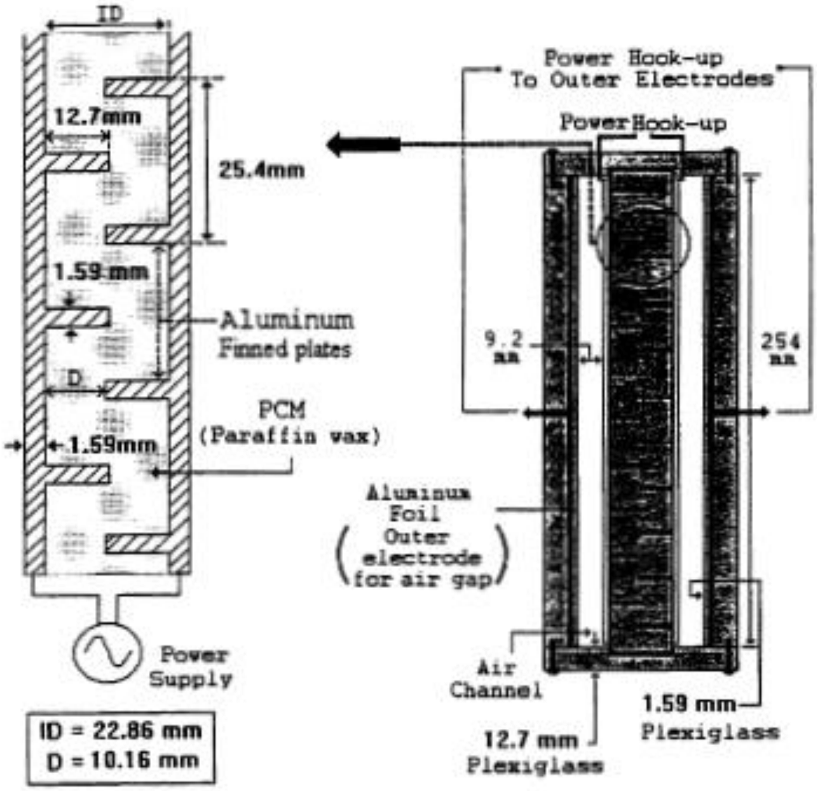

Figure 2-25, Experimental apparatus used by Delorusso (1994), in experiments investigating the effect of electrohydrodynamics on the charging and discharging rates of latent heat thermal storage systems. Phase change material fills the cavity between two aluminum finned plates.

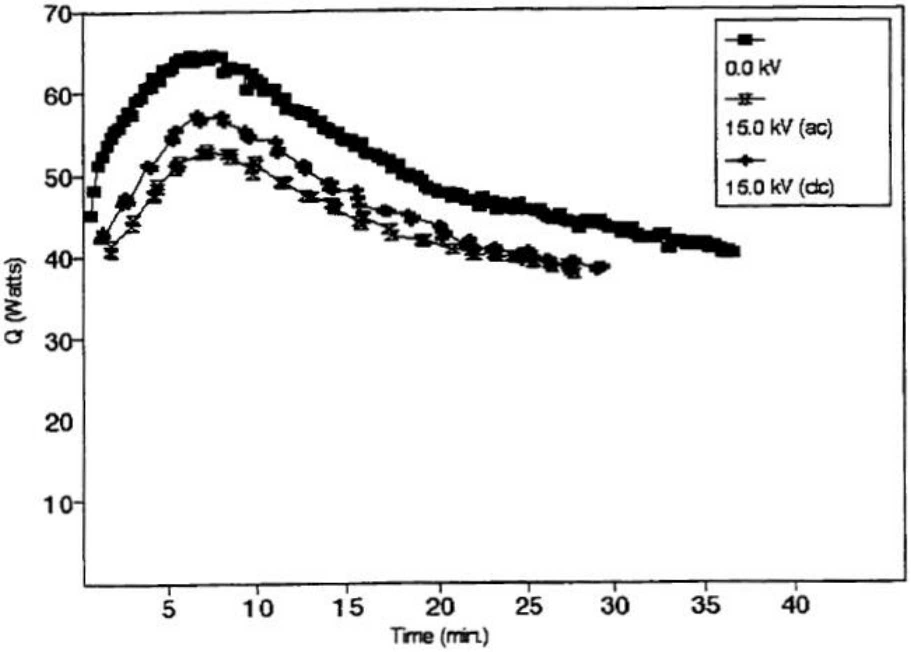

Figure 2-26: Dellorusso's (1997) results for the heat flow with an air Reynold's number of 2572 during freezing

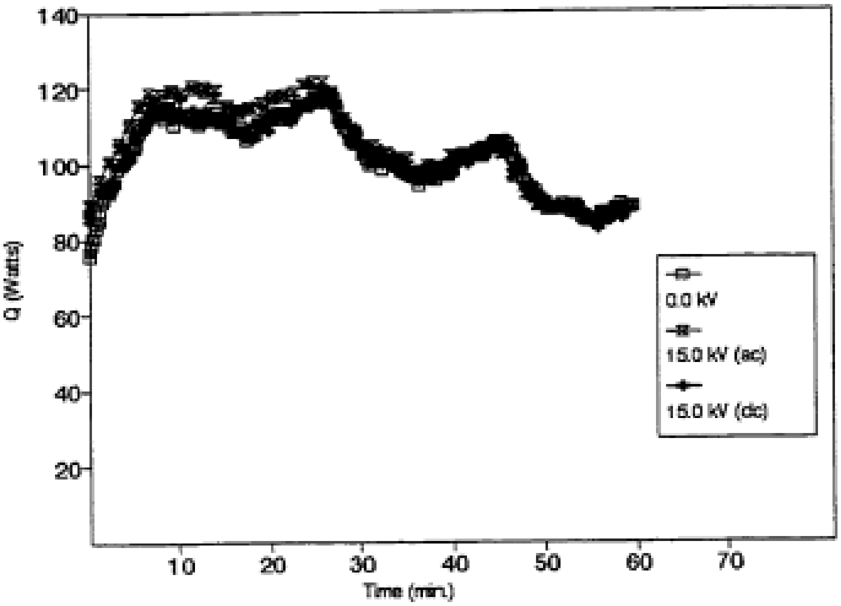

Figure 2-27: Dellorusso's results for the heat flow during the melting cycle for an air Reynolds number of 2259.

Nakhla et al (2015) conducted an experimental study on enhancing the heat transfer performance of a latent heat thermal storage system. The storage material used was paraffin wax and energy was added to the system using an electric heater. Circular steel electrodes were used as the electrical conductor, and a copper sheet attached to the electric heater was grounded to generate the electric field. A schematic of the test section used by Nakhla et al. (2015) is shown in Figure 2-28. In contrast to Dellorusso's (1997) results, Nakhla et al. (2015) found that applying an electric field increases the rate at which the paraffin wax was melted, which was quantified by measuring the melt thickness which is seen in Figure 2-29. Nakhla et al. (2015) reported an enhancement of approximately 40% in the melting time. The enhancement was attributed to two factors; one factor was electro-convection and the other factor was a phenomenon called solid extraction (Nakhla et al., 2015). Solid extraction is a process where solid particles from the solid phase change material are pulled into the liquid; solid extraction is analogous to liquid extraction seen in liquid-gas systems mentioned in Section 2.2.2.1.2. Nakhla et al. (2015) did not delineate the fraction of the enhancement due to electro-convection and the fraction of the enhancement due to solid extraction.

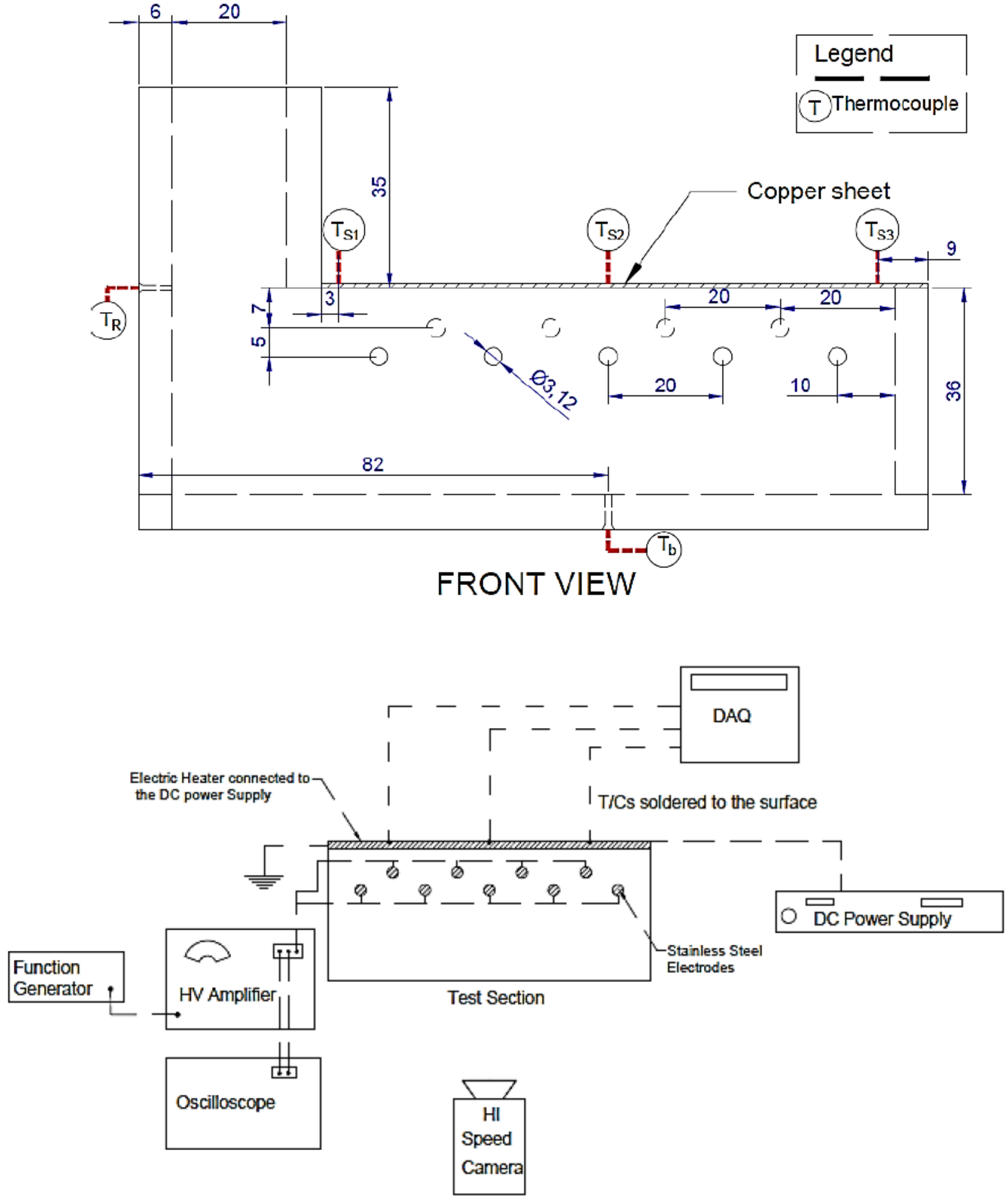

Figure 2-28: Image of test section used by Nakhla et al. (2015), image on top is side view showing the electrode positions, bottom image shows the electrical subsystems

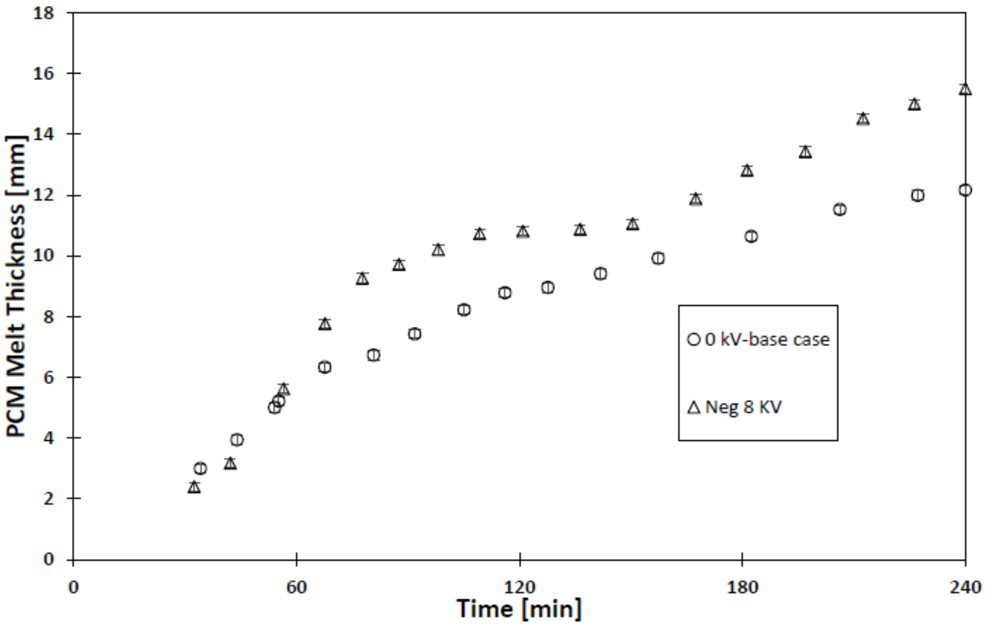

Figure 2-29: Melt front location with time for Q=10.4 W, with and without applied voltage (-8kV) Nakhla et al. (2015)

Dulikravich (1994) created a numerical code to model solidification and melting in the presence of electro-convection. The code was then used to analyse steady state cases where a rectangular geometry is cooled from the top and heated from the bottom. The cooling wall temperature is below the solidus temperature, and the heating wall is above the liquidus temperature of the fluid such that there is a solid, liquid and mushy zone in the enclosure. The results of the analysis showed that the electro-convection changes the temperature field and amount of solid on the cooling wall of the enclosure. With no electric field, 30% of the volume was solid, and with a 15 kV electric field generated between the heating and cooling wall, 27% of the volume was solid. This result indicates that the electro-convection increased the heat transfer between the hot wall and the solid-liquid interface. Colaco et al (2004) used a numerical hybrid optimising code to attempt to minimize natural convection in the rectangular geometry with a hot boundary condition on the bottom surface and a cold boundary condition on the top surface, and using the model made by Dulikravich (1994), which was done by changing the applied electric potential using several optimisation techniques. The results of the analysis showed that the hybrid optimisation could be used to optimise the electrode geometry to suppress natural convection.

2.2.2.1.4 Overview of Electrohydrodynamics Heat Transfer Enhancement

Electrohydrodynamics increases the rates of heat transfer by creating more vigorous convection in a fluid. This vigorous convection is created by one of the three force terms in Equation 2.18, the electrophoretic, dielectrophoretic and electrostrictive forces. The electrophoretic force is caused by free charge carriers in the fluid, the dielectrophoretic and electrostrictive forces are caused by changes in the electric permittivity in the fluid. An overview of the different enhancement in heat transfer when electrohydrodynamics is applied to various applications is presented in Table 2-7.

Table 2-7: Summary of Electrohydrodynamic Heat Transfer Enhancement

Author	Technique	Numerical / Experimental	Enhancement
Kalman and Sher (2001)	Single phase, electrophoretic	Experimental	160% increase in the rate of heat transfer
Fernandez and Poulter (1987)	Single phase, electrophoretic	Experimental	2000% increase in the rate of heat transfer
Kasayapanand (2008)	Single phase, electrophoretic	Experimental	400%-700% increase in heat transfer coefficient
Ng et al (2010)	Two phase fluid	Experimental	120-270% increase in heat transfer rate
Nangle-Smith et al. (2013)	Two phase fluid	Experimental	330% increase in heat transfer coefficient
Dellorusso (1997)	Two phase solid-liquid	Experimental	No effect in melting detrimental effect in solidification
Nakhla et al. (2015)	Two phase solid-liquid	Experimental	40% faster melting time

2.2.2.2 Comparion of Active Enhancement Techniques

Active enhancement techniques are techniques that require input energy to create an enhancement in heat transfer. The active heat transfer enhancement techniques that have been applied to latent heat thermal storage systems are ultrasonic vibrations and electrohydodynamics. Few studies in electrohydrodynamics have focused specifically on solidification; however, there have been many studies that have focused on single phase fluids and two phase fluids and two phase liquid-solid melting that provide some insight into the mechanisms that will affect solidification with electrohydrodynamics.

Table 2-8: Summary of active enhancement techniques

Author	Technique	Numerical / Experimental	Enhancement
Oh et al (2002)	Two phase solid-liquid, ultrasonic	Experimental	2.5 times faster melting time
Kalman and Sher (2001)	Single phase, electrohydrodynamic	Experimental	160% increase in the rate of heat transfer
Fernandez and Poulter (1987)	Single phase, electrohydrodynamic	Experimental	2000% increase in the rate of heat transfer
Kasayapanand (2008)	Single phase, electrohydrodynamic	Experimental	400%-700% increase in heat transfer coefficient
Ng et al (2010)	Two phase fluid, electrohydrodynamic	Experimental	120-270% increase in heat transfer rate
Nangle-Smith et al. (2013)	Two phase fluid, electrohydrodynamic	Experimental	330% increase in heat transfer coefficient
Dellorusso (1997)	Two phase solid-liquid	Experimental	No effect in melting detrimental effect in solidification
Nakhla et al. (2015)	Two phase solid-liquid	Experimental	40% faster melting time

2.2.3 Comparison of the methods of increase the rate of heat transfer in phase change thermal storage systems

There are two categories of heat transfer enhancement techniques: passive and active. Passive techniques are methods that do not require an input of energy to create the enhancement; fins, high conductivity matrices, high conductivity particles and microencapsulation are all examples of passive heat transfer enhancement techniques. Active techniques, alternatively, are methods of that do require an external energy input to generate the increased heat transfer. Ultrasonic vibrations and Electrohydrodynamics are examples of active enhancement techniques. For latent heat thermal storage systems, the passive techniques have shown to generate larger heat transfer enhancements than their active counterparts. For example, the heat transfer enhancements in Table 2-5, range from 20% - 500%, Nakhla et al.'s (2015) heat transfer enhancement was 40%. However, the benefit of active techniques is the opportunity for increasing heat transfer while not occupying a large volume fraction of the container. For example, Saha et al. (2006) found the optimum volume fraction of pin fins was 8%, whereas the volume fraction occupied by Nakhla et al.'s (2015) electrodes was less than 1%. Since the benefit of latent heat thermal storage systems over sensible thermal storage systems is storage density, the ability of active enhancement techniques to maintain a high storage density makes them attractive. However, the large increases in the rates of heat transfer that have been achieved using fins have not yet been achieved using electrohydrodynamics in these systems.

2.3 Literature Review of Solidification

This project focuses specifically on the solidification of phase change materials in latent heat thermal storage systems; thus, a detailed understanding of solidification will provide insight into the solidification process seen in the experiments. This section will describe the driving force of solidification, which is Gibbs free energy. Then, a detailed discussion regarding methods to control solidification.

2.3.1 Thermodynamics of Solidification

In order for a pure fluid to solidify, the Gibbs free energy of the solid must be lower than that of the liquid. The change in Gibbs free energy, ΔG, of a transformation of an initially liquid material to a solid at the melting temperature, T_m, is given by Equation 2.23. If this transformation takes place at a temperature, T, that is not the melting temperature Equation 2.24 is used. In these equations, ΔH is the latent heat of fusion and ΔS is the change in entropy of the phase change. If the temperature dependence of ΔH and ΔS and subtracting Equations 2.23 and 2.24, then equation 2.25 can be used to estimate the Gibbs free energy change as a function of the undercooling temperature $\Delta T = (T_m - T)$ (Flemings, 1974). This Gibbs free energy and by extension undercooling is the mechanism that drives solidification.

$$\Delta G = \Delta H - T_m \, \Delta S \quad [2.23]$$

$$\Delta G = \Delta H - T \, \Delta S \quad [2.24]$$

$$\Delta G = \frac{\Delta H \, \Delta T}{T_m} \quad [2.25]$$

The Gibbs free energy analysis can be used to provide perspective on micro encapsulation. Recall from Section 2.2.1.4, that one of the issues with microencapsulation is that materials tend to undercool more than they otherwise would. This means that the ΔT value in Equation 2.25 needs to be larger when a material is microencapsulated. Flemings presented a solution to the solidification of a material on a curved surface where the Gibbs free energy of solidification is given by Equation 2.26 and the Gibbs free energy change of melting is given by Equation 2.27. In these equations, S_S is the entropy of the material in the solid state, S_L is the entropy of the material in the liquid state, V_s is the volume of the solid, σ is the surface tension between the solid and the liquid phase and κ is the curvature of the surface. If the material is at equilibrium, then the undercooling due to curvature is given by Equation 2.28. In the Equation 2.28, if the curvature is increased then the undercooling will become more negative.

$$\Delta G_S = S_S \Delta T \quad [2.26]$$

$$\Delta G_L = S_L \Delta T + 2V_s \, \sigma \, \kappa \quad [2.27]$$

$$\Delta T = -\frac{2 \, V_s \, \sigma \, \kappa \, T_m}{\Delta \, H} \quad [2.28]$$

In non-pure materials, the concentration of each molecule present in the material will alter the melting temperature and the resulting solid that forms. The simplest impure material is a binary mixture, which is a mixture of only two elements or molecules. To analyse impure materials, a chemical potential of each element, μ_A, is used which is equal to the derivative of the free energy, G, with respect to the amount of that element in the material. Equation 2.29 shows the definition of the chemical potential of an element or molecule, n_A, which will be given the arbitrary name A. Using the Gibbs-Duhem equation with Equations 2.29, yields Equation 2.30 (Flemings, 1974). Following the same process for the element B yields Equation

2.31. In these equations, C is the mole fraction of B. Equation 2.30 and Equation 2.31 can be combined to yield Equation 2.32, which is an expression for the molar free energy based on the chemical potentials. Flemings (1974) provides the chemical potential for ideal solutions, which are given in Equation 2.33 and Equation 2.34. In these equations, term μ_0 is the chemical potential at some reference temperature, the ΔT term is the temperature difference between the reference temperature for μ_0 minus the actual temperature of the material, R is the gas constant and T is the temperature of the material. This solution is only for an ideal solution where there is no enthalpy associated with mixing the two elements together. Equation 2.33 and Equation 2.34 can be substituted into Equation 2.32, and the difference in Gibbs free energy between the solid and liquid phases can be calculated. For many materials, there is an enthalpy associated with this mixing which can be compensated for by adding an enthalpy of mixing term ΔH_m to Equation 2.32, which is seen in Equation 2.35 (Swalin, 1962). In Equation 2.35 the subscript S refers to the solid phase and the subscript B refers to the liquid phase. The phase diagram for a material that has a positive enthalpy of mixing is given in Figure 2-30. The next section will show that Paraffins have phase diagrams similar to that of Figure 2-30.

$$\mu_A = \left(\frac{\partial G}{\partial n_A}\right)_{T,P,n_B} \qquad [2.29]$$

$$\mu_A = G - C(\frac{\partial G}{\partial C}) \qquad [2.30]$$

$$\mu_B = G + (1 - C)(\frac{\partial G}{\partial C}) \qquad [2.31]$$

$$G = (1 - C)\mu^A + C\mu^B \qquad [2.32]$$

$$\mu^A = \mu_0^A + S^A \Delta T^A + RTln(1 - C) \qquad [2.33]$$

$$\mu^B = \mu_0^B + S^B \Delta T^B + RTln(1 - C) \qquad [2.34]$$

$$\Delta G = (1 - C_L)\mu_L^A + C_L\mu_L^B - (1 - C_S)\mu_S^A - C_S\mu_S^B + \Delta H_m \qquad [2.35]$$

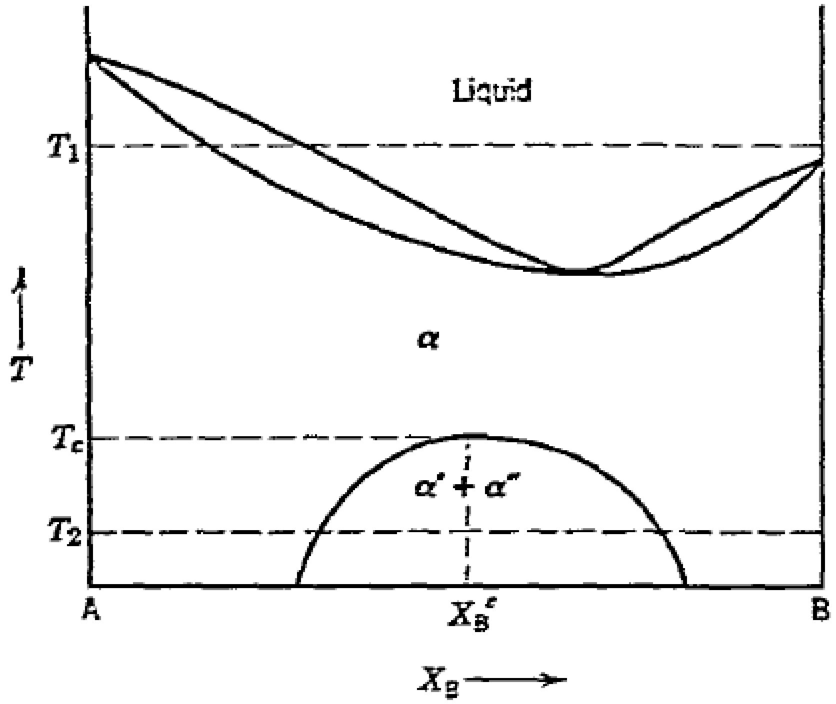

Figure 2-30: Phase diagram for an ideal solution with a positive enthalpy of mixing (Swalin, 1962)

2.3.2 Solidification of paraffins

The focus of the current investigation is to understand the effects of electrohydrodyanmics on the solidification of organic phase change materials. The specific type of organic phase change material that is being focused on is a paraffin, specifically Octadecane. Investigations into the phase diagrams of paraffin waxes will provide insight into the effect of impurities on melting temperature of the Octadecane being used in the experiments. He et al. (2003) analysed the phase diagram for a mixture, the resulting phase diagram is presented in Figure 2-31. The phase diagram in Figure 2-31 shows similarities to the phase diagram presented in Figure 2-30, implying that the enthalpy of mixing between two kinds of paraffin is positive. The phase diagram in Figure 2-31, shows that there is only one phase for the solid. Thus, if there are paraffin impurities in the Octadecane used in the current investigations, they will likely not form a different phase and should be soluble in the octadecane. In the current investigation the purity of the Octadecane in 99%, meaning these impurities should be of little importance anyway. Note that the phase diagram in Figure 2-31 is not made specifically for Octadecane, however no studies looking at the phase diagram for octadecane are available.

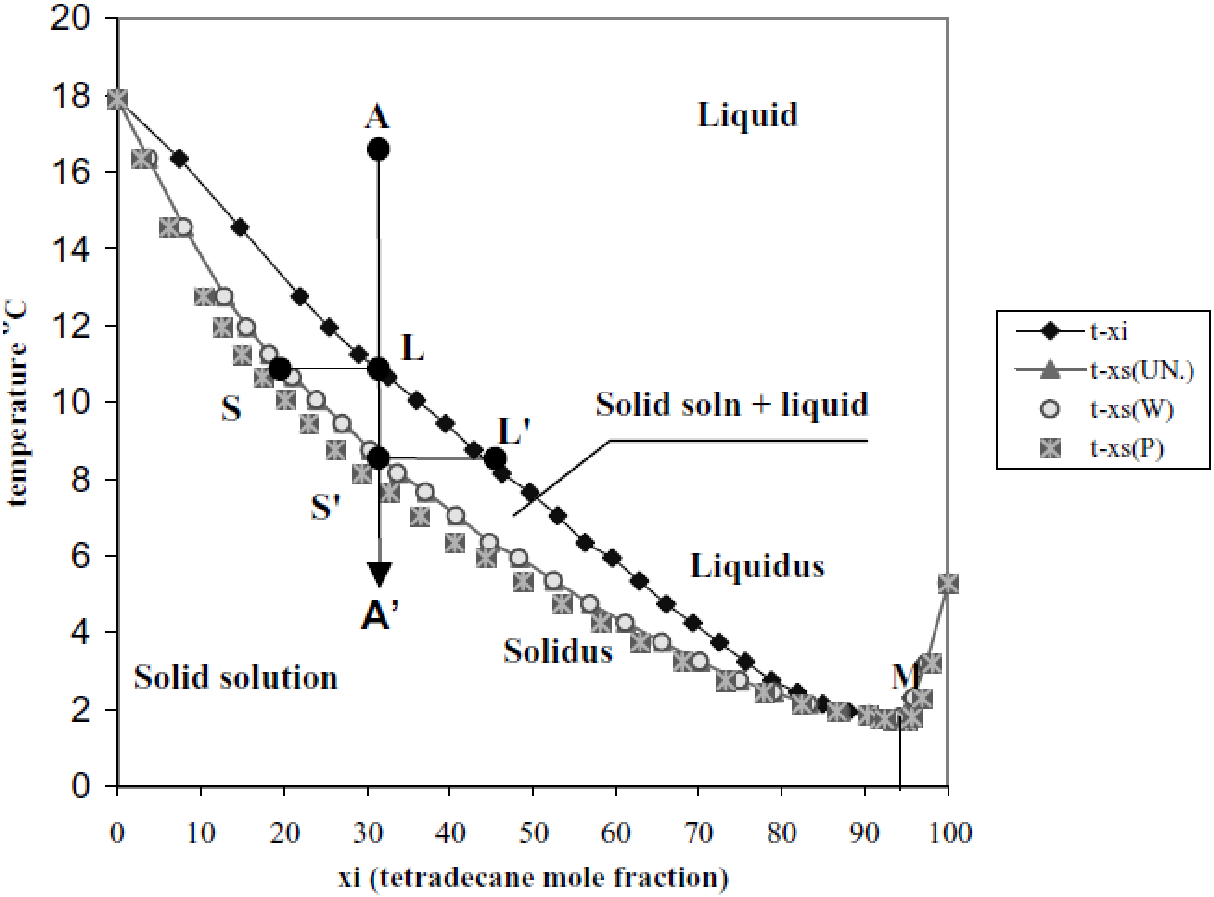

Figure 2-31: The liquid-solid phase diagram of binary mixture of tetradecnae and hexadecane from theoretical models used by He et al. (2003). In the legend three t-xi represents the liquidus, t-xs(UN.) represents the solidus calculated using a UNIFAC model, t-xs(W) represents the solid calculated using a model described by Won (1989) and t-xs(P) represents the solidus calculated using a model described by Pedersen and skovborg (1991)

A phenomenon known as the Thermodielectric Effect has been observed when paraffin wax solidifies (Tomas and Novotny, 2015) Gross (1954). The Thermodielectric Effect is when electric charges are released when a dielectric material changes state. Gross (1954) first observed this phenomenon when by measuring the electric potential that develops when liquid paraffin wax solidifies in a two phase capacitor. Gross (1954) defined two laws of the Thermodielectric Effect from these experiments. The first law, referred to as the law of intensities relates the electric current i, to the rate that mass transforms from liquid to solid $\frac{dm}{dt}$, through a constant of proportionality k_1. The first law is given in Equation 2.36. The second law is the integral of the first, which states that the total charge liberated from the liquid material Q, is proportional to the amount of mass that has changed from liquid to solid m through the constant of proportionality k_2. The second law is given in Equation 2.37. The source of these charges is a reduction-oxidation reaction that occurs when the paraffin wax changes state. When the liquid transforms into a solid an electron is liberated from the paraffin molecule (Tomas and Novotny, 2015). The Thermodielectric Effect is a potential source of free charge carriers in the liquid phase change material. These charge carriers will be acted on by the electrophoretic force in Equation 2.19. Thus, even if the octadecane is initially electrically neutral, charges can build-up in the liquid over the course of the experiment.

$$i = k_1 \frac{dm}{dt} \tag{2.36}$$

$$Q = k_2 m \tag{2.37}$$

2.3.3 Summey of solidification

The importance of Gibbs free energy in solidification and the relation between Gibbs free energy and melting temperature was discussed. The effect of curvature on the melting temperature, which was discussed in Section 2.2.1.4, was illustrated using Gibbs free energy. The effect of impurity concentration on solidification was also discussed. The solidification of hydrocarbons was also discussed. The thermodielectric effect and how it could result in free ions in the liquid phase change materials was discussed in detailed.

3 Experimental Apparatus

An experimental apparatus was constructed to study the effect of applying an electric field to the solidification processes of an organic, latent heat thermal storage system. This apparatus is designed to allow for optical tracking and high-speed imaging of the solid front. In this chapter, the experimental apparatus and the experimental procedure will be explained. Furthermore, the qualification of the measurements will be discussed.

3.1 Description of the device

A schematic of the experimental apparatus is shown in Figure 3-1 through Figure 3-4. The apparatus consists of the test section, the heat exchanger, the thermal bath, the high voltage power supply and the camera. The test section was designed such that the cavity for the phase change material was rectangular. Five of the cavity walls consists of 12 mm polycarbonate sheets. The bottom wall of the cavity is the heat exchanger which provides the cooling required for solidification. On the top wall of the cavity, there is a 12 mm polycarbonate sheet with a riser incorporated into the wall on the side of the cavity. The purpose of the riser is to compensate for the volume reduction that occurs due to the density difference between the solid and the liquid phase change materials. The phase change material that was used in these experiments was octadecane.

The dimensions of the test sections cavity are shown in Figure 3-2 and Figure 3-3. The electrodes are split into two rows. The centre of the first row of electrodes is 7 mm from the heat exchanger surface and the second row is 12 mm from the heat exchanger surface. Each of the electrodes within a row is spaced 20 mm apart and the first and second rows are staggered, such that an electrode in the second row is 10mm apart from an electrode in the first row. The electrodes are held in position by two acrylic plates, and a copper wire connects all the electrodes and runs through a cut-out in one of the plates. The electrodes are made out of brass. The electrode geometry was chosen as such to match the electrode geometry used by

Nakhla et al. (2015). Matching previous studies is important because it allows the results of this analysis to be used in conjunction with the results to provide approximate the performance of a system that uses electric fields to enhance both melting and solidification.

The heat exchanger removes heat from the phase change material to induce solidification. The heat exchanger is made from 6061 aluminum. Aluminum was chosen because of its high thermal diffusivity. Cooling water flows through the middle of the heat exchanger; this water is diverted around two baffles. The baffles are shown in Figure 3-4. The cooling surface of the heat exchanger is the surface which the phase change material first solidifies on. This cooling surface has cooling channels running 6mm below its surface. The heat exchanger is bolted onto the bottom of the container using a flange on the bottom of the heat exchanger. The bolts used to provide the clamping force were #8-32 nylon screws. The location of the heat exchanger surface was chosen to be on the bottom of the test section. This was done to ensure natural convection did not take place. The density of the fluid increases as the temperature is decreased. Since the cooling occurs on the bottom of the test section, the buoyancy force will act to suppress natural convection. The heat exchanger was designed to be on the bottom of the test section so that natural convection is suppressed. The purpose of this study is to understand how electrohydrodynamics affects the solidification of a phase change material. The convection effect of applying an electric field would have then depended on whether or not the electric field acted to promote convection or suppress it. Since modelling electrohydrodynamics requires parameters that have not yet been determined for octadecane, for example, the rate at which charges are injected into the fluid when the voltage is applied, it is difficult to determine whether or not an electric field will be beneficial for natural convection or whether it will suppress natural convection. Thus, to eliminate this uncertainty, the system was designed to suppress natural convection.

The power supply is a Glassman, Series EL, Power supply. The heat exchanger was grounded, and the electrodes were set at -8kV. A schematic of the electric circuit is shown in Figure 3-5. A thermal bath was used for the cooling circuit, the water flowed from the thermal bath through a pump, then into the heat exchanger. The inlet for the heat exchanger was in the bottom which can be seen in Figure 3-4. The water then flows out of the heat exchanger and back into the thermal bath. The thermal circuit is outlined in Figure 3-6.

The temperature of the cooling water is measured at the inlet and outlet of the heat exchanger. This measurement is taken to check the assumption that the temperature of the heat exchanger does not vary between the inlet and outlet. There are also thermocouples measuring the temperature of the heat exchanger to ensure that it is uniform. The thermocouple locations are shown in Figure 3-7. As mentioned earlier, the solid front location was measured optically. A Nikon D5200 camera was set-up outside the test section, and images were taken throughout the experiment to capture the solid-liquid interfaces progression with time. Figure 3-8 is a schematic of the optical measurement system.

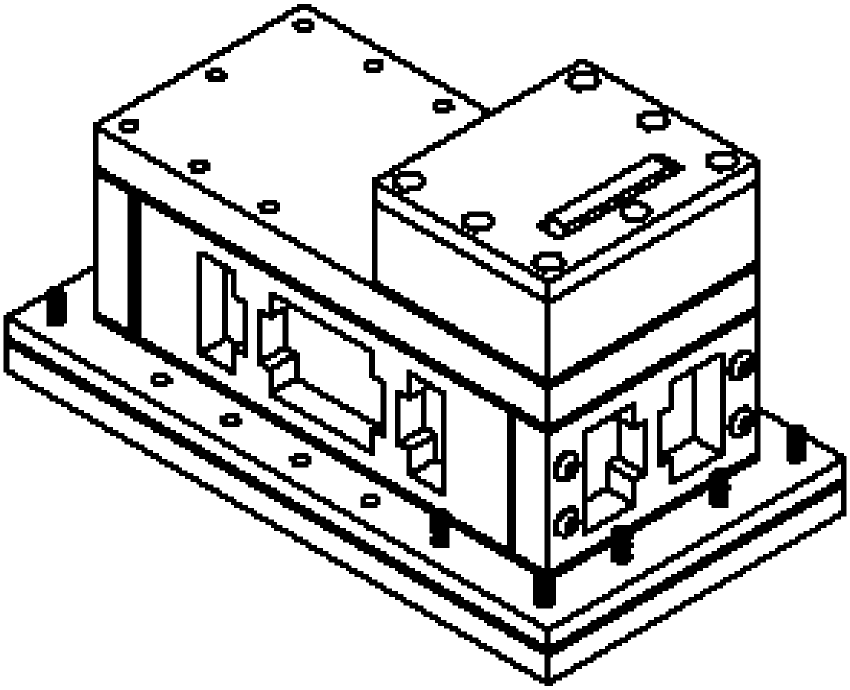

Figure 3-1: Isometric view of the test section

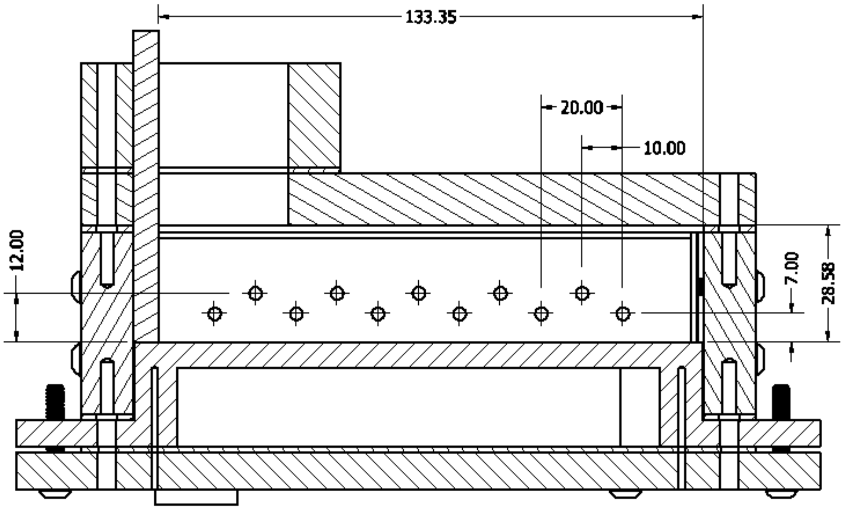

Figure 3-2: Section view showing length of test section

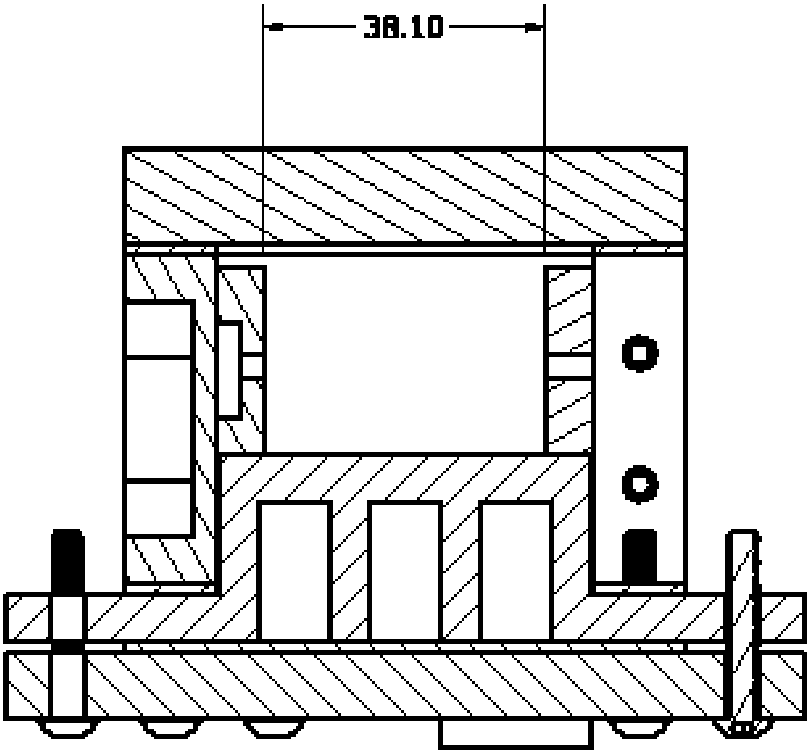

Figure 3-3: Section view showing width of test section and the electrode plates

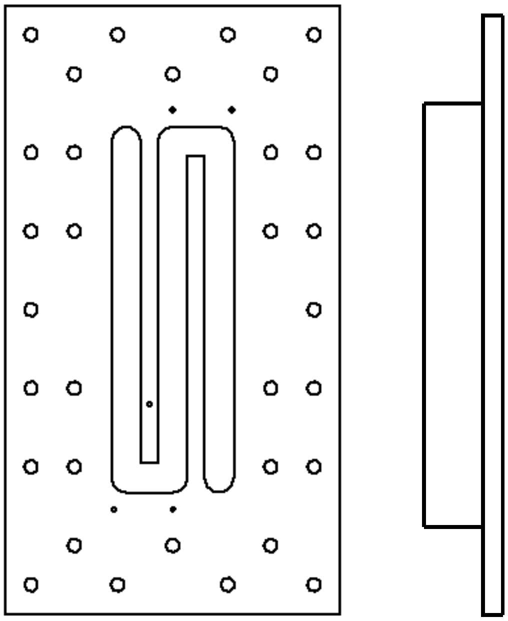

Figure 3-4: Orthonormal view of heat exchanger.

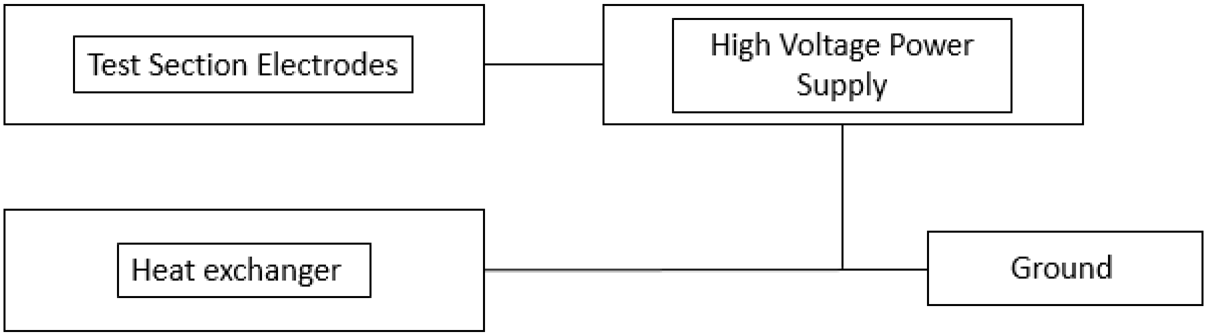

Figure 3-5: Block diagram showing how the electrical circuit used in the experiment was designed.

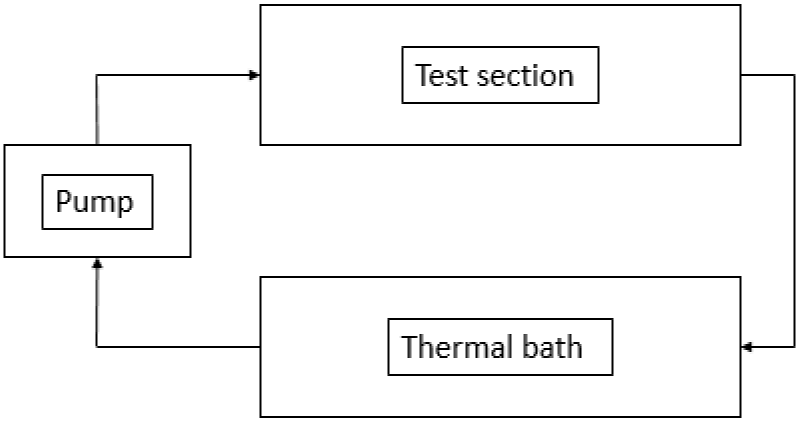

Figure 3-6: Block diagram showing how the hydraulic circuit used in the experiments worked. Arrows show the direction of flow

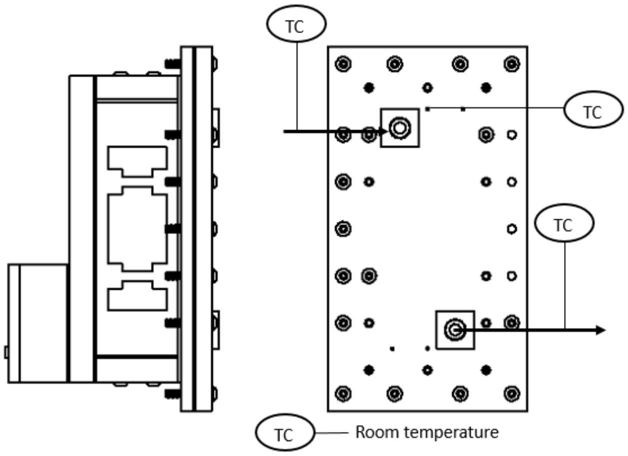

Figure 3-7: Schematic showing the measurement locations of the temperature sensors

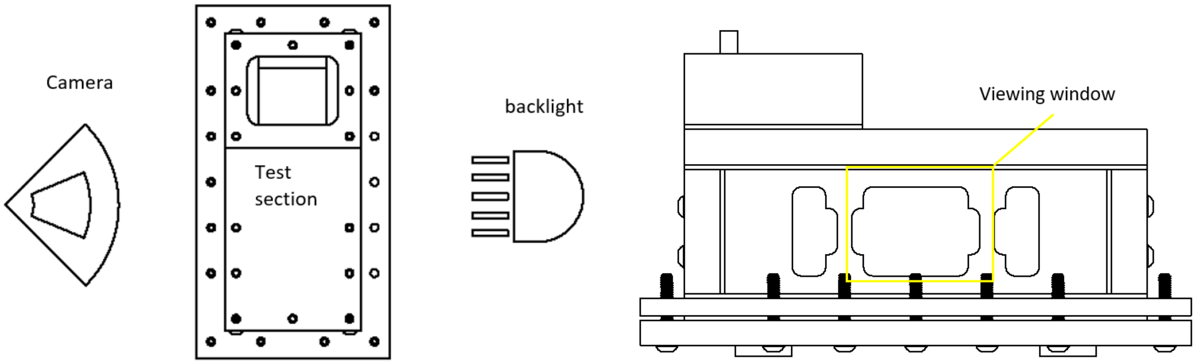

Figure 3-8: Schematic of optical system showing the test section, camera and backlight

3.2 Experimental procedure

The following procedure, in chronological order, was used to conduct the experiments:

1. The phase change material was melted by flowing 50℃ hot water through the heat exchanger
2. Once all the phase change material was melted, the water temperature was set to the initial temperature of the experiment.
3. The water was circulated until the phase change material reached the initial temperature for the experiment and stayed at this temperature for at least 30 minutes.
4. For the electrohydrodynamic, experiments the high voltage was then applied
5. The cooling water was turned on the exact second that the cooling water begins to flow is the time equal to zero on all of the graphs
6. Images of the solid front location were taken using the Nikon D5200 camera
7. The images were processed using Digimizer software

There were three variables that were being investigated in this study, which were the applied electric potential, the initial temperature of the phase change material and the heat exchanger wall temperature. The applied electric potential difference is important because the magnitude of the electric body forces depends on the applied electric potential. For these experiments, two potentials were used, there was 0kV and -8kV. These potentials were chosen because they match those of Nakhla et al. (2015). The -8 kV potential was also chosen because this was near the maximum voltage rating of the wires used in the experiments which was -12kV. Only the negative potential was chosen because it has been shown that negative electric potentials have stronger electrohydrodynamic forces than positive electric potentials (Fernadez and Poulter, 1987).

The purpose of investigating the initial temperature of the phase change material is that the dielectrophoretic force depends on the temperature gradient in the liquid phase change material; a high initial temperature means there will be a high-temperature gradient in the liquid. The liquid temperatures that were chosen are 30℃, 40℃ and 50℃. A 30℃ initial temperature is very close to the melting temperature, and so the sensible energy initially stored in the liquid will be very small. In Section 4, it will be shown that when the initial sensible energy in the liquid is small, the effect of convection will be small. Since the effect of convection is small, if there is any change in the solidification rate when the electric potential is applied, it must be due to a change in the nucleation kinetics as Dellorusso (1997) hypothesised. The 40℃ and 50℃ temperatures were tested because the dielectrophoretic force depends on the temperature gradient in the liquid phase change material, so testing these two points will provide two different temperature gradients to analyse. 50℃ was chosen as the maximum temperature because beyond this point octadecane begins to vaporise.

The heat exchanger temperature was investigated because the heat exchanger temperature directly impacts the growth rate of the solid phase change material. Recall Equation 2.6; the growth rate of the solid depends on the energy transferred from the solid-liquid interface to the wall – which depends on the wall temperature – and the energy being transferred from the liquid to the solid-liquid interface. Changing the growth rate also affects the solidification kinetics, the total time of the experiment and the time for the solid layer to reach the electrodes. The wall temperatures chosen are 8.5℃, 15.5℃ and 22.5℃. The wall temperature was controlled by flowing water through the heat exchanger at chosen are 8℃, 15℃ and 22℃, respectively.

3.3 Measurement of the latent energy discharged

The latent energy removed from the energy storage system can be directly related to the amount of solid in the container. The latent energy removed from the system can be found for a system using Equation 3.1. In Equation 3.1, E_{latent} is the energy stored in latent heat, ρ is the density of the material, H is the latent heat of fusion, S is the thickness of the solid and A is the area of the solid-liquid interface. Equation 3.1 is simply the mathematical statement that the energy stored in the latent form is equal to the amount of material that has undergone a change of state. To approximate this integral, a 5 point average was used over the 10 mm measurement window, which was between the fifth and sixth electrodes. An example of the measurement process is provided in Figure 3-9. If the solid front location is touching one of the electrodes, then the measurements are taken immediately beside the electrode, as seen in Figure 3-9. Otherwise, the measurement is taken from the middle of the first-row electrode to the middle of the second-row electrode.

$$E_{latent} = \int \rho \, H \, S \, dA \qquad [3.1]$$

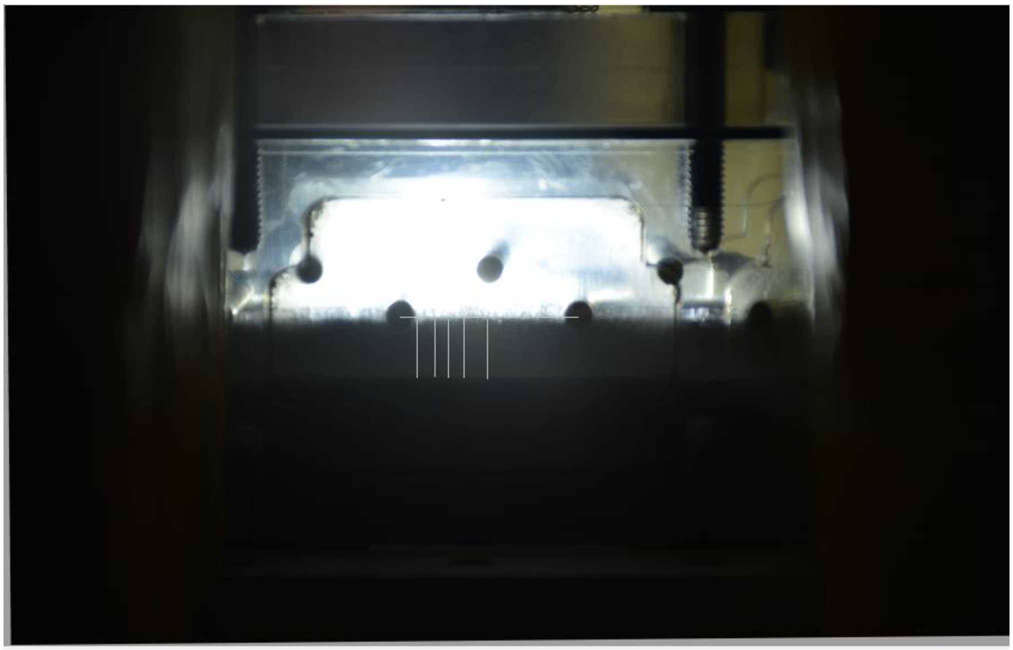

Figure 3-9: Images showing meaurement technique from Digimizer software

3.3.1 Vaidation of the meaurements

To validate the accuracy of these measurements, some of the known dimensions of the test section were measured. Four dimensions were measured, three of these dimensions are shown in Figure 3-10, the fourth is the height of the polycarbonate wall. Figure 3-11 shows the measurement of the four validation measurements in the Digimizer software. The distance between the two electrodes is 20mm, and this is used as a reference measurement. Table 3-1 shows the measurement and the error associated with each of the experiments conducted in this study. The maximum error in the validation measurements was approximately 3%; this was considered acceptable. This variation in the error is due to differences in the location of the camera set-up. The camera was supported on a tripod, which did not allow for fine adjustments of the camera location. As a result, the camera could sometimes be off centre from the test section. This issue was not identified until after the experiments were complete and in future studies, it is suggested that an alternative method of supporting the camera is used.

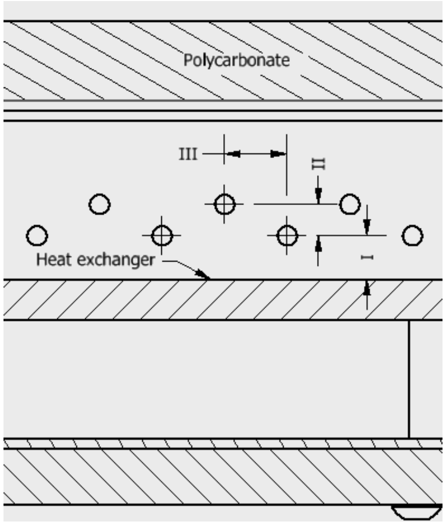

Figure 3-10: Schematic of three of the validation measurements

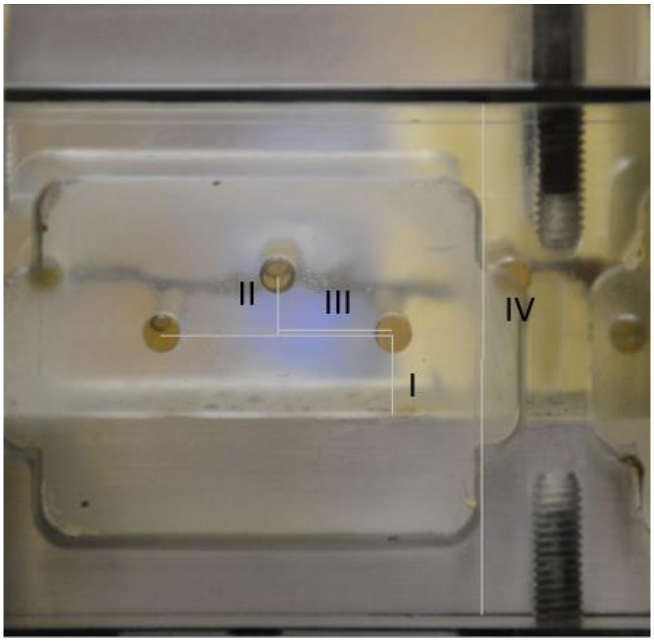

Figure 3-11: Image of the validation measurements from Digimizer software

Table 3-1: Validation of the optical measurements

Test	Measurements, mm				Error, mm				Error, %			
	I	II	III	IV	I	II	III	IV	I	II	III	IV
Nominal	7	5	10	43.69	N/A							
No Electric Field												
8°C, 30°C	6.96	5.00	9.91	44.10	0.036	0.00	0.09	0.42	0.51	0.00	0.89	0.96
8°C, 40°C	7.00	5.05	10.03	43.72	0.00	0.05	0.03	0.04	0.04	0.94	0.32	0.08
8°C, 40°C (2)	7.07	5.12	10.00	44.31	0.07	0.12	0	0.62	0.99	2.30	0.00	1.40
8°C,50°C	7.22	4.93	9.97	44.08	0.22	0.07	0.03	0.39	3.13	1.36	0.27	0.90
15°C, 30°C	6.87	5.01	10.25	43.69	0.13	0.01	0.25	0.00	1.81	0.28	2.53	0.00
15°C, 40°C	6.95	5.03	9.94	43.741	0.05	0.03	0.06	0.05	0.77	0.60	0.60	0.12
15°C, 50°C	6.97	4.99	10.03	43.789	0.03	0.01	0.03	0.10	0.41	0.26	0.27	0.23
22°C, 40°C	7.08	5.00	10.00	44.074	0.08	0.00	0.00	0.386	1.13	0.00	0.00	0.88
22°C, 30°C	6.989	4.95	10.05	43.952	0.01	0.05	0.05	0.26	0.16	1.08	0.54	0.60
-8 kV Electric Potential												
8°C, 30°C	6.88	5.18	10.00	44.00	0.12	0.18	0.00	0.32	1.74	3.70	0.00	0.72
8°C, 40°C	6.984	5.03	10.00	43.56	0.02	0.03	0.00	0.12	0.23	0.54	0.00	0.29
8°C, 50°C	7.06	5.06	10.00	43.98	0.06	0.06	0.00	0.29	0.80	1.12	0.00	0.67
15°C, 30°C	6.98	5.09	10.12	43.98	0.02	0.09	0.12	0.30	0.26	1.78	1.19	0.68
15°C, 40°C	6.96	4.95	9.95	43.84	0.04	0.05	0.05	0.15	0.63	1.08	0.54	0.36
15°C, 50°C	7.09	4.97	10.00	43.92	0.09	0.03	0.00	0.23	1.29	0.52	0.00	0.52
22°C, 30°C	7.18	5.07	9.97	44.07	0.18	0.07	0.03	0.38	2.56	1.44	0.28	0.86
22°C, 40°C	7.05	4.96	9.91	43.98	0.04	0.04	0.09	0.29	0.64	0.90	0.90	0.67

3.3.2 Selection of measurement method

Several alternatives for measuring the energy discharged from the systems were considered. These alternatives are listed below:

- Change in cooling water temperature
- Vernier Solid thickness measurement
- Capacitance measurement

One method for measuring the energy discharged from the phase change material is to measure the energy gained by the cooling water. The advantage of this method is that it captures both the latent energy as well as the sensible energy discharged from the system. This method works by considering an energy balance on the system, which is shown in Figure 3-12 and Equation 3.2. In this equation, Q_{Water} is the energy gained by the cooling water from the heat exchanger, $Q_{PCM\ to\ HX}$ is the energy transferred from the phase change material to the heat exchanger and $Q_{losses\ HX}$ is the energy transferred from the heat exchanger to the environment. If the heat exchanger is well insulated then the losses will be negligible and the heat transferred to the water will be the same as the heat transferred from the phase change material to the heat exchanger. The disadvantage of this method is that the temperature increase in the water is designed to be less than 0.5℃ for the majority of the experiment. The temperature rise is designed this way because the wall temperature must be kept as close to a uniform temperature as possible to compare the results against analytical solutions. If the water temperature did increase significantly, then this would cause a temperature distribution between the inlet of the heat exchanger and the outlet. In order to measure this temperature range accurately, an accuracy of 0.05℃ would be required. The instrumentation required to do this was not readily available and would be extremely expensive.

$$Q_{Water} = Q_{PCM\ to\ HX} - Q_{losses\ HX} \qquad [3.2]$$

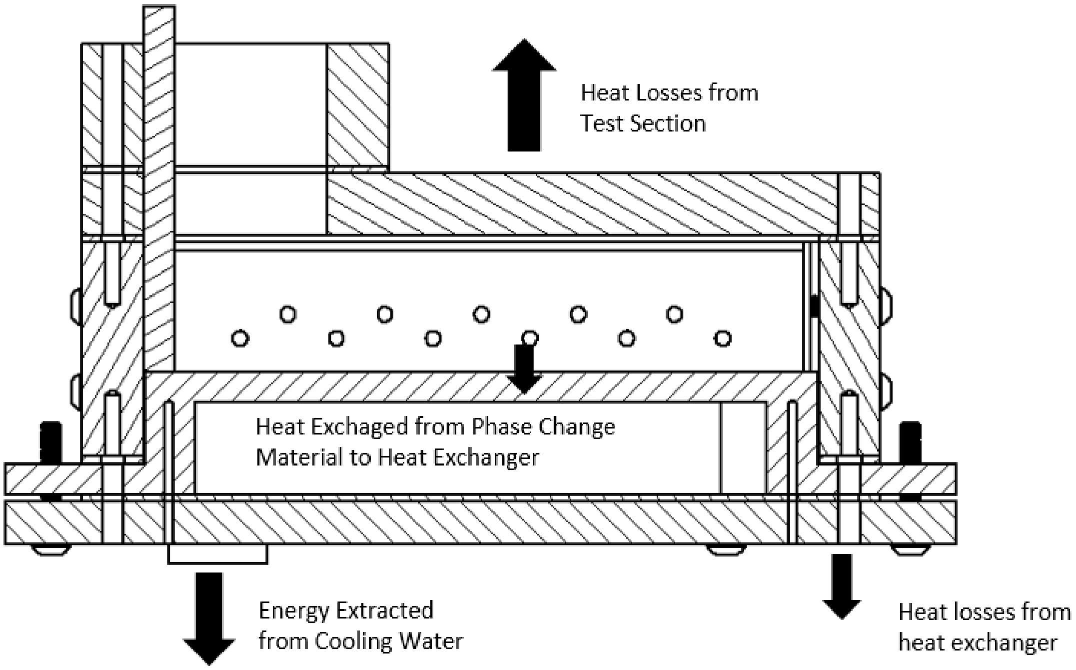

Figure 3-12: Energy flow diagram for the test section. Shows the paths that heat can flow through in the test section.

The technique of optically measuring solid front was chosen because it provided relatively accurate measurements compared to the other methods and there was no risk of contamination. However, the disadvantages of this method are that it measures the solid front location on the surface of the polycarbonate. At the walls there is energy being lost through the insulation to the environment; the result being that the optical measurement will tend to over-estimate the solid front location. To compensate for this, a backlight was used. The backlight will shine through the solid on the walls so that the measurement is more accurate than it otherwise would be.

3.4 Temperature measurement of the heat exchanger

3.4.1 Thermal response time

One assumption in the experiments is that the thermal response – in terms of how fast the temperature changes from the initial fluid temperature to the desired wall temperature – of the heat exchanger is fast enough that the instantaneously applied wall temperature assumption is valid. The temperature of the heat exchanger was recorded to ensure that this assumption is true. The thermal response is defined as the time required to reach 1℃ and 0.5℃ of the experiments average temperature; this is summarised in Table 3-2.

Table 3-2: Transient response of the heat exchanger or each of the test cases, the cases are described in Section 3.2. The no electrode case is a test without any electrodes in the test section, the Electrode cases are tests where the electrodes were in the test section, but no electric potential was applied and the electric field cases are tests where the electric potential was applied.

Case	Time to reach 1℃ of average temperature, s	Time to reach 0.5℃ of average temperature, s
No electrodes, 8℃, 40℃	74	107
No electrodes, 15℃, 30℃	144	200
No electrodes, 15℃, 40℃	76	102
No electrodes, 15℃, 40℃, repeat	72	40
No electrodes, 22℃, 40℃	108	119
Electrodes, 8℃, 30℃	97	138
Electrodes, 8℃, 30℃	121	181
Electrodes, 8℃, 40℃	215	270
Electrodes, 8℃, 40℃	217	270
Electrodes, 8℃, 50℃	230	323
Electrodes, 15℃, 30℃	54	73
Electrodes, 15℃, 40℃	101	138
Electrodes, 22℃, 30℃	34	44
Electrodes, 22℃, 30℃, repeat	81	114
Electrodes, 22℃, 40℃	92	125
Electric field, 8℃, 30℃	83	116
Electric field, 8℃, 40℃	123	178
Electric field, 8℃, 50℃	196	266
Electric field, 15℃, 30℃	179	238
Electric field, 15℃, 40℃	131	165
Electric field, 15℃, 40℃, repeat	109	148
Electric field, 15℃, 50℃	398	484
Electric field, 15℃, 50℃	180	232
Electric field, 22℃, 30℃	31	36
Electric field, 22℃, 30℃, repeat	32	41
Electric field, 22℃, 40℃	88	122

3.4.2 Thermal uniformity

Another important assumption is that the temperature of the heat exchanger is uniform. To ensure that this assumption is true in the experiments, thermocouples were installed in the heat exchanger to monitor the temperature of the heat exchanger’s surface. The temperature of two locations on the heat exchanger were measured in several experiments to ensure that the heat exchanger’s surface is uniform.

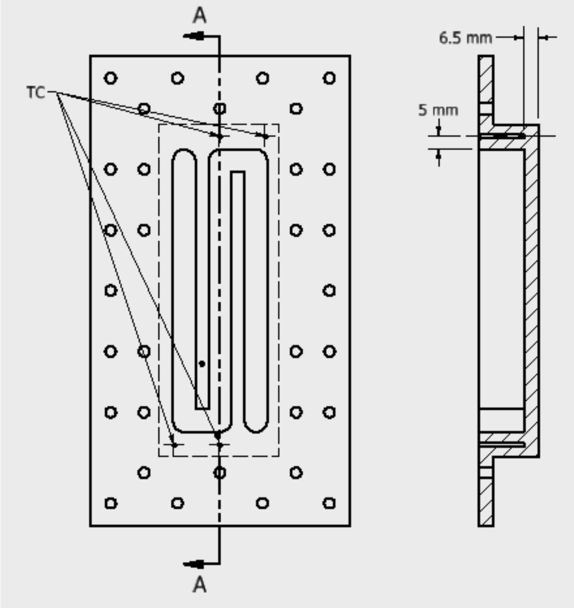

Figure 3-13: Heat exchanger thermocouple locations

3.4.3 Temperature measurement system selection

The data acquisition system used thermocouples to measure the temperature of the cooling water, the heat exchanger and the ambient temperature. The thermocouples used in the experiments are Omega Quick Disconnect Thermocouples that have an accuracy of ±0.2℃. In order to calibrate the device, a Neslab rte-10 thermal bath was used to provide a constant temperature, and an RTD with ±0.1℃ accuracy was used. According to the manufacturer's specification, the temperature of the thermal bath is uniform to within ±0.2℃. Therefore, the accuracy of the thermocouples would be ±0.5℃. A detailed error analysis is given in Appendix C.

To achieve a lower uncertainty an RTD could be used; however, the RTD would only reduce the uncertainty by ±0.1℃. The ±0.1℃ benefit of the RTD was not deemed significant compared to other sources of error in the system. This conclusion was made by using the Neumann solution for solidification. The Neumann solution is presented in Section 4.2, the details of the model used in this analysis are explained in depth in that section. To simulate the error in the temperature measurements, assume that the measured temperature is always the desired temperature, and the actual temperature is the desired temperature plus the maximum uncertainty of the measurement device. For example, if the desired temperature of the heat exchanger is 8.5℃ and the measurement error is 0.5℃, the actual heat exchanger temperature used in the analysis will be 9℃. Once that analysis was completed the results were compared to an analysis where the actual temperature was set to the desired temperature, such that there is no measurement error. In these experiments, the temperatures were 8.5℃, 15.5℃ and 22.5℃. Table 3-3 summarises this analysis; the RTD only provides a marginal benefit over the thermocouple. Since thermocouples were readily available for these experiments and RTD would have to be specifically ordered thermocouples provided a cost advantage over the RTD for a negligible performance trade-off. Thus, the thermocouple was chosen over the RTD. The analysis can be repeated, but instead of the actual temperature being the desired temperature plus the measurement error, the actual temperature can be the desired temperature minus the measurement error; but the error will always be greater when the actual temperature is set to the desired temperature plus the measurement error.

Table 3-3: Error due to temperature measurement

Condition	Error, %
Wall temperature 8.5℃, measured + 0.4℃	1.0
Wall temperature 8.5℃, measured + 0.5℃	1.3
Wall temperature 15.5℃, measured + 0.4℃	1.6
Wall temperature 15.5℃, measured + 0.5℃	2.0
Wall temperature 22.5℃, measured + 0.4℃	3.9
Wall temperature 22.5℃, measured + 0.5℃	5.0

3.5 Solid front location measurement validation

3.5.1 Repeatability of the solid front location measurement

To further examine the validity of the results of the experiments, the repeatability of the experiments was tested. The same experimental conditions were tested in two different experiments. As seen in Figure 3-14, Figure 3-15 and Figure 3-16, the results of all of the repeat tests fall within the experimental uncertainty. Therefore, the results of the tests are repeatable.

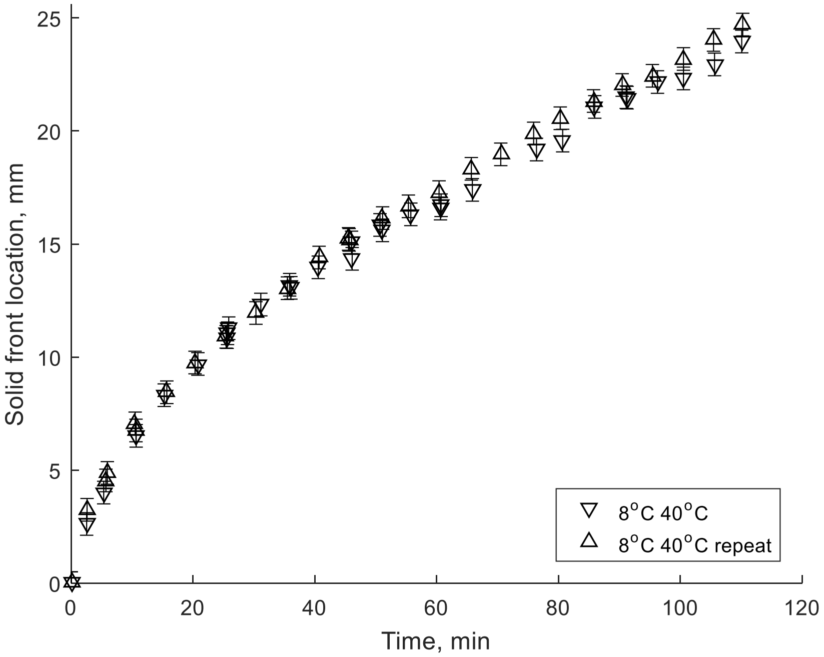

Figure 3-14: Solid front location as a function of time, repeatability study with wall temperature 8.5℃ and 40℃ initial temperature, no electrodes

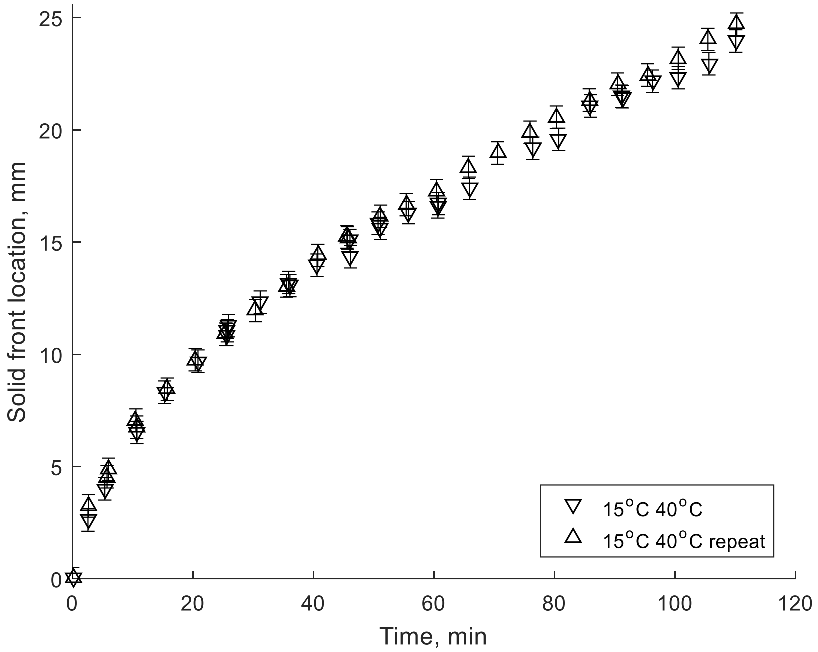

Figure 3-15: Solid front location as a function of time, repeatability study with wall temperature 15.5℃ and 40℃ initial temperature, no electric potential

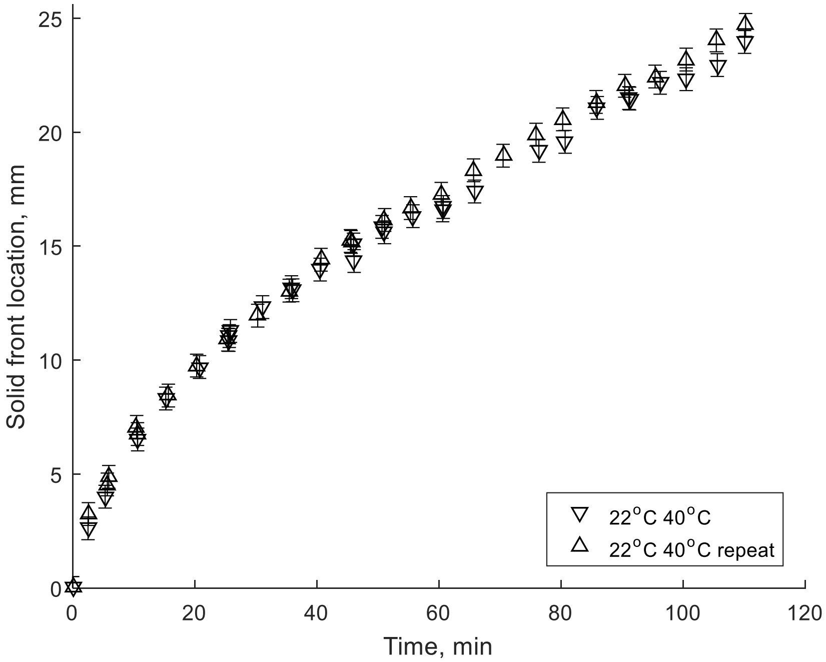

Figure 3-16: Solid front location as a function of time, repeatability study with wall temperature 22.5℃ and 40℃ initial temperature, no electric potential

3.5.2 Losses from system

To ensure that the results from the experiments agree with theory, validation experiments were performed. A numerical code was used to validate the experiments, it consisted of a 1-dimensional heat transfer. Since the model was 1-dimensional it did not model the electrodes. Thus, to ensure that the validation experiments were as close to the numerical solution as possible, these experiments were done without electrodes.

To account for the losses leaving the test section throughout the experiment, an analytical approximate of the losses was performed. The heat flow was assumed to be steady and solely due to heat conduction through the insulation. The insulation was Styrofoam with a thermal conductivity of 0.033 W/(m.K). Three inches of insulation was used. The walls of the test section are made of polycarbonate with a thermal conductivity of 0.19 W/(m.K). The thickness of the walls is 12 mm. A heat transfer coefficient was applied on the outer wall of the insulation to account for convection and radiation from the outer walls to the ambient air and surroundings. The inner wall of the polycarbonate was assumed to be at the initial temperature of the phase change material. This is conservative as the heat exchanger and the solid and liquid phase change materials will always be at or below this temperature

To estimate the heat transfer coefficient on the vertical walls of the test section Equation 3.3 was used (Churchill and Chu, 1975). In Equation 3.3, Nu is the Nusselt number, Ra is the Rayleigh number and Pr is the Prandtl number. For the horizontal sections equation when the Rayleigh number was less than 10^7 Equation 3.4 was used (Fujii and Imura, 1972). If the Rayleigh number was greater than 10^7 Equation 3.5 was used (Fujii and Imura, 1972). To account for radiation, the Stefan-Boltzmann law was used, which is given in Equation 3.6. In Equation 3.6, Q_{rad} is the heat transfer due to radiation assuming a view factor of 1, σ is the Stefan-Boltzmann constant, ε is the emissivity, A is the area of the emitting surface, $T_{insulation}$ is the temperature of the insulation and $T_{surrounding}$ is the temperature of the surroundings. The wall temperature was changed iteratively until the change in the heat flow between iterations was less than 0.1%.

$$Nu = (0.825 + \frac{0.387Ra^{1/6}}{(1+(\frac{0.492}{Pr})^{9/16})^{8/27}}) \quad [3.3]$$

$$Nu = 0.54Ra^{1/4} \quad [3.4]$$

$$Nu = 0.15Ra^{1/3} \quad [3.5]$$

$$Q_{rad} = \sigma \varepsilon A(T_{insulation}^4 - T_{surrounding}^4) \quad [3.6]$$

The total rate of heat loss from the test section based on the assumptions above is 0.5 W. To approximate the extra solid growth rate due to losses, the geometry of the test section and the thermal properties of the phase change material can be used, as seen in Equation 3.7. In Equation 3.7, S is the solid front location, t represents the time after the experiment began, Q_{losses} is the losses from the system, ρ is the mass density of the phase change material, H is the latent heat of fusion and A is the area of the solid-liquid interface, which should be the same as the area of the heat exchanger. The area of the heat exchanger is 0.006976 m^2. This area will be used in Figure 3-17 through Figure 3-21, which compares the experimental and the numerical results.

$$\frac{\partial S}{\partial t} = \frac{Q_{losses}}{A\, \rho\, H} \quad [3.7]$$

3.5.3 Experimental error

Another important factor that must be considered is that the boundary conditions in the experiments are not exactly known. The temperature of the heat exchanger is measured and the thermal response time of the heat exchanger was shown to be small. However, the certainty with which the temperature is known is limited by the uncertainty of the thermocouples that were used in the tests. Furthermore, the temperature of the thermal bath's cooling water is only uniform to within ± 0.2℃. The uncertainty in temperature results in differences in the solid front location because the growth rate of the solid is dependent on the cooling wall temperature. Thus, if the actual temperature of the heat exchanger is higher than the measured value, then the solid front location in the experiment will be less than that of the numerical simulation, and vice versa. Another source of error is from the camera measurements. As mentioned earlier, moving the camera to while setting up the experiments led to some minor inconsistencies in the results. These errors are taken into account by error bars on the experimental points, the error bars are determined from the error analysis in Appendix C.

3.5.4 Comparison

The experimental results and analytical results agree within the experimental uncertainty when the losses are taken into account. It is important to note that the experimental points tend to be higher than the theoretical curve. There are several possible explanations for the systematic discrepancy. One explanation is that due to the optical measurement system. The solid-liquid interface was measured using a camera one side of the test section and a light on the other. Since the solid is opaque and the liquid is transparent, the solid-liquid interface is measured by finding the first spot in the image where light is not transmitted through from the other side of the test section. However, since heat is lost through the wall that the measurement is taken from, the thickness of the solid layer near the wall will be larger than the thickness in the middle of the test section. The backlight is used to help reduce this issue, but it will not eliminate it completely. Another possible reason is that uncertainty in the properties and measurements could result in this difference. One property that would affect the results in the latent heat of fusion, if the measured value used in the analytical results is high that the latent heat of fusion for the octadecane that was used in the experiments, then this would result in the experimental solid front location being larger than the analytical. One measurement error that could have this effect is the heat exchanger temperature, if the temperature of the heat exchanger was consistently colder than the measured value, that the experimental solid front location will be larger than the analytical one.

To provide insight into the source of the losses, an analysis of the difference between the experimental and numerical results was performed. To start the analysis recall that the latent energy discharged from the system can be found using Equation 3.8. E is the energy stored in latent heat, ρ is the density of the material, H is the latent heat of fusion, S is the thickness of the solid and A is the area of the solid-liquid interface. The difference in the latent energy discharged is given by Equation 3.9. In Equation 3.9, the variables are the same as in Equation 3.8; this equation simply states that the difference in the experimental and numerical energy stored is proportional to the difference in the thicknesses multiplied by how many joules are stored per metre. Then the heat losses in the experimental case can be assessed using Equation 3.10. If the instantaneous losses are desired, then Equation 3.11 can be used. The results of this analysis are summarised in Figure 3-17 through Figure 3-21.

$$E = \rho\, H\, A\, S \tag{3.8}$$

$$E_{Experimental} - E_{Numerical} = \rho\, H\, A\, (S_{Experimental} - S_{Numerical}) \tag{3.9}$$

$$Q_{losses} = \frac{E_{Experimental} - E_{Numerical}}{\Delta t} \tag{3.10}$$

$$Q_{losses} = \rho\, H\, A\, \frac{\partial}{\partial t}(S_{Experimental} - S_{Numerical}) \tag{3.11}$$

To understand the difference between the experimental and numerical results, the difference between these results were calculated, and the heat losses in the experiments were estimated using Equation 3.11. The difference in the experimental and analytical, the derivative of the difference in the solid front locations with respect to time was approximated using a linear curve fit, shown in Figure 3-22 through Figure 3-27. The results of this analysis are summarised in Table 3-4. The highest average rate of heat losses are 1.1W which occurs in the 8.5℃ cases; the lowest average heat losses occurred for the 22.5℃, which were 0.64W. The curves in Figure 3-22 through Figure 3-27 and the results in Table 3-4 provide insight into the source of the losses. The curves in Figure 3-22 through Figure 3-27 show a trend where the losses are largest at small thicknesses, and lowest at large thicknesses; an explanation for this is that heat can be transferred through the polycarbonate walls of the container, which is not accounted for in the model. If the heat was being transferred through the polycarbonate walls, the losses would be highest when the thickness of the wax is small, because the thermal resistance of the wall will be smallest and the losses would be lowest when the thickness is large.

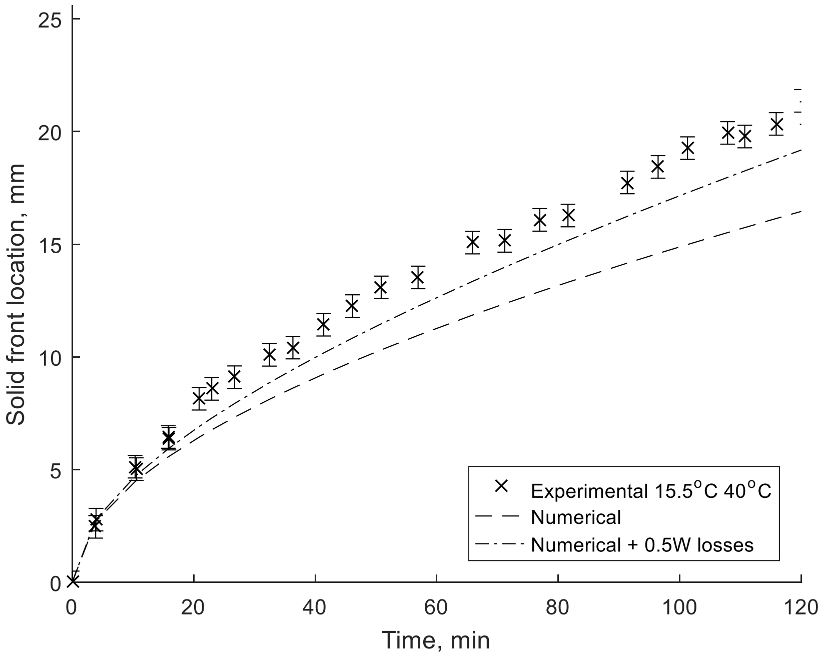

Figure 3-17: Validation case, solid front location as a function of time for wall temperature of 15.5℃ and initial temperature of 40℃

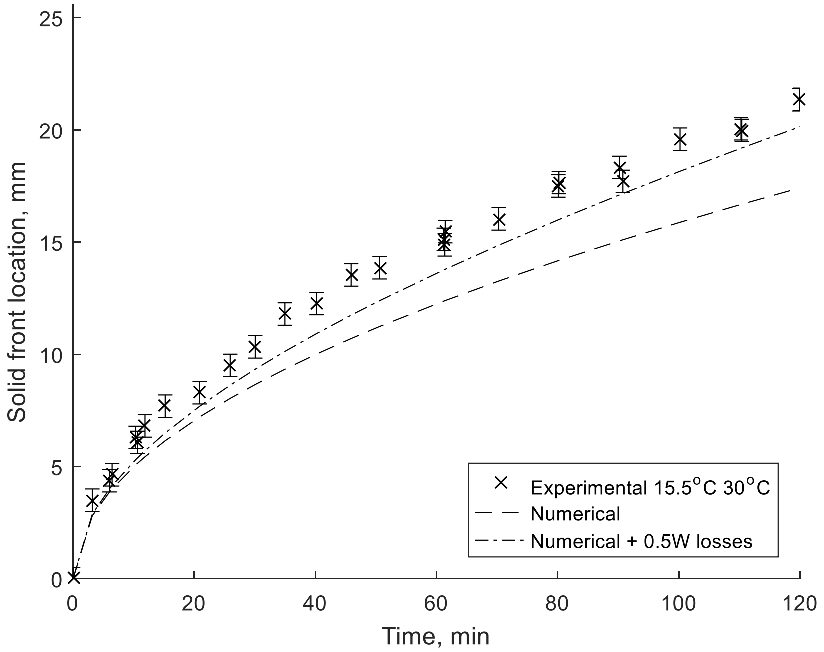

Figure 3-18: Validation case, solid front location as a function of time for wall temperature of 15.5℃ and initial temperature of 30℃

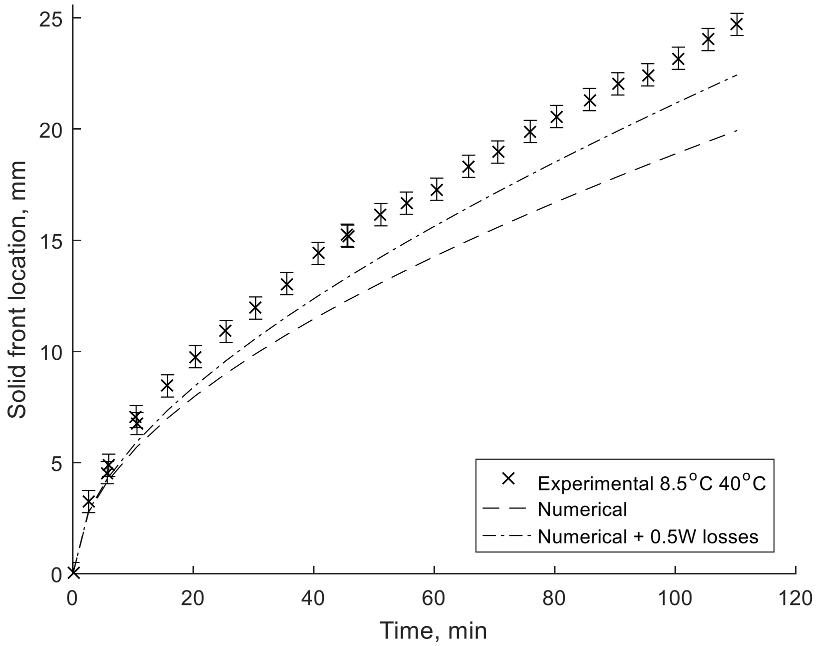

Figure 3-19: Validation case, solid front location as a function of time for wall temperature of 8.5℃ and initial temperature of 40℃

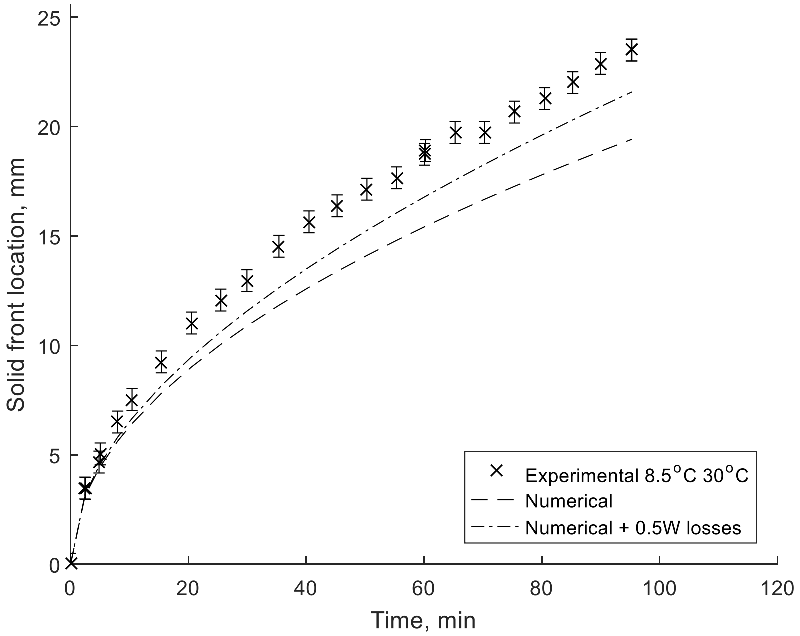

Figure 3-20: Validation case, solid front location as a function of time for wall temperature of 8.5℃ and initial temperature of 30℃

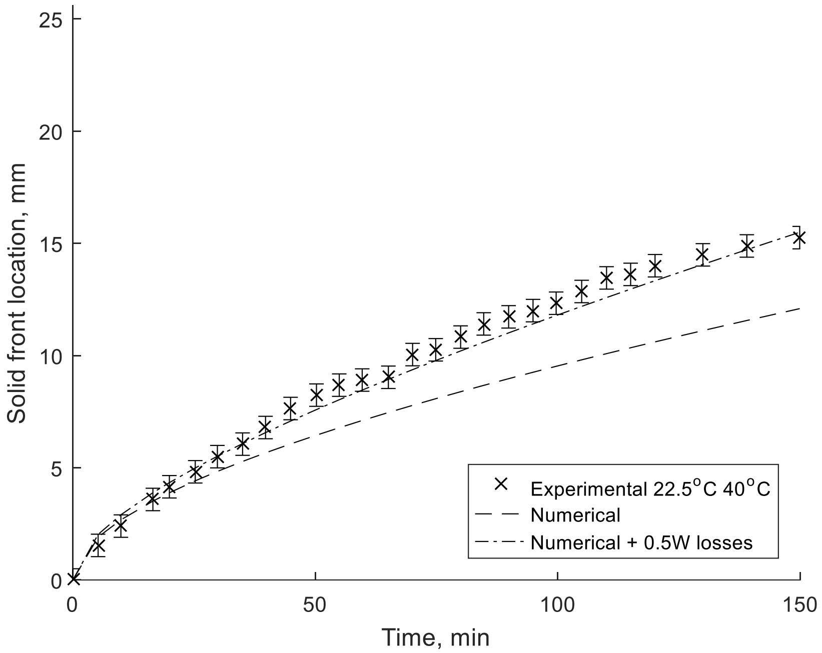

Figure 3-21: Validation case, solid front location as a function of time for wall temperature of 22.5℃ and initial temperature of 40℃

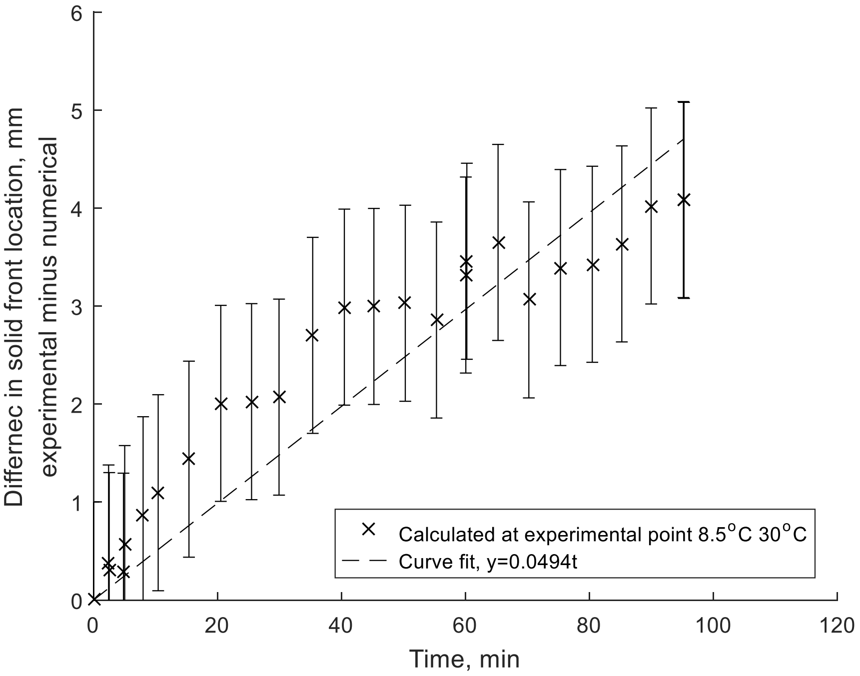

Figure 3-22: Difference in the experimental and numerical solid front locations and a linear curve fit for validation case with wall temperature 8.5℃ and initial temperature 30℃

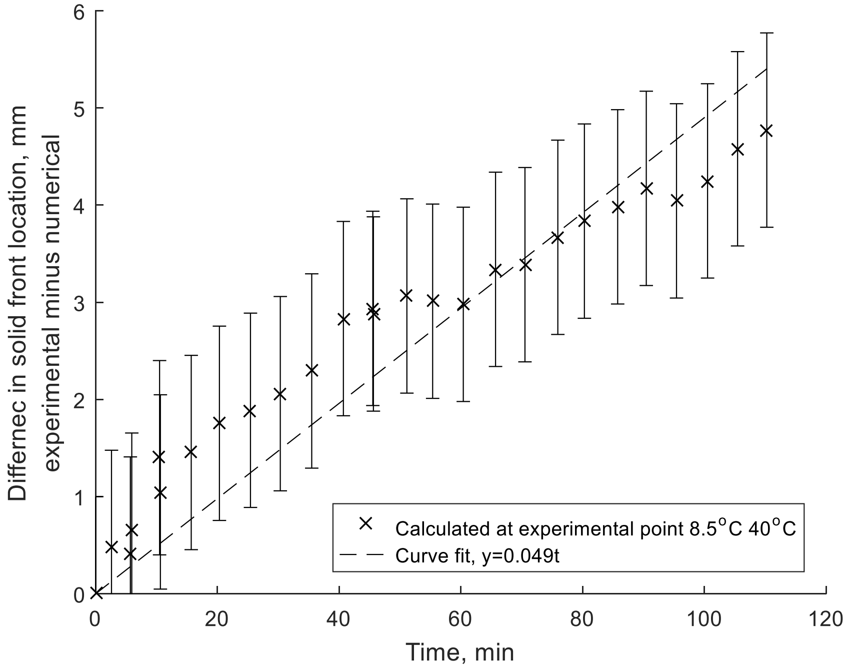

Figure 3-23: Difference in the experimental and numerical solid front locations and a linear curve fit for validation case with wall temperature 8.5℃ and initial temperature 40℃

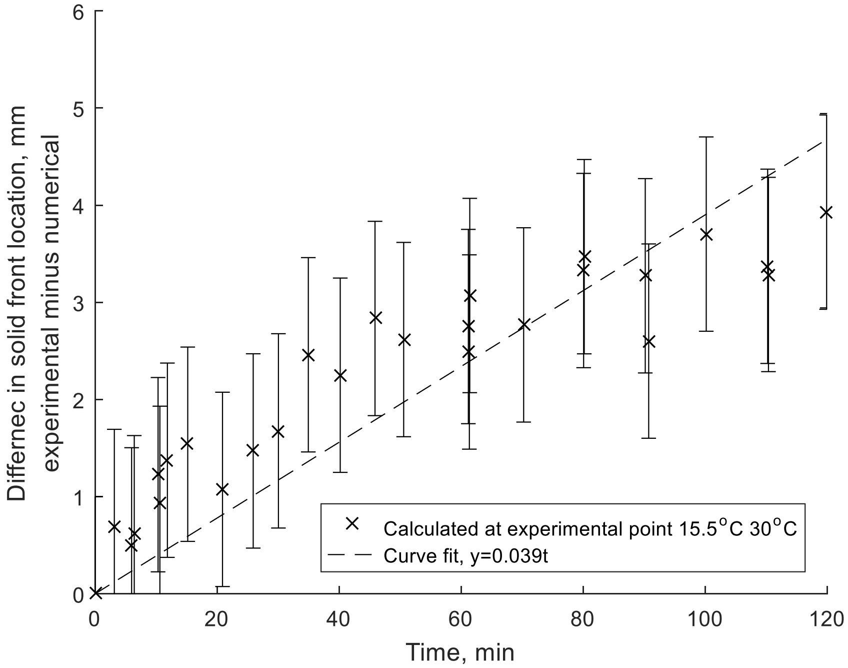

Figure 3-24: Difference in the experimental and numerical solid front locations and a linear curve fit for validation case with wall temperature 15.5℃ and initial temperature 30℃

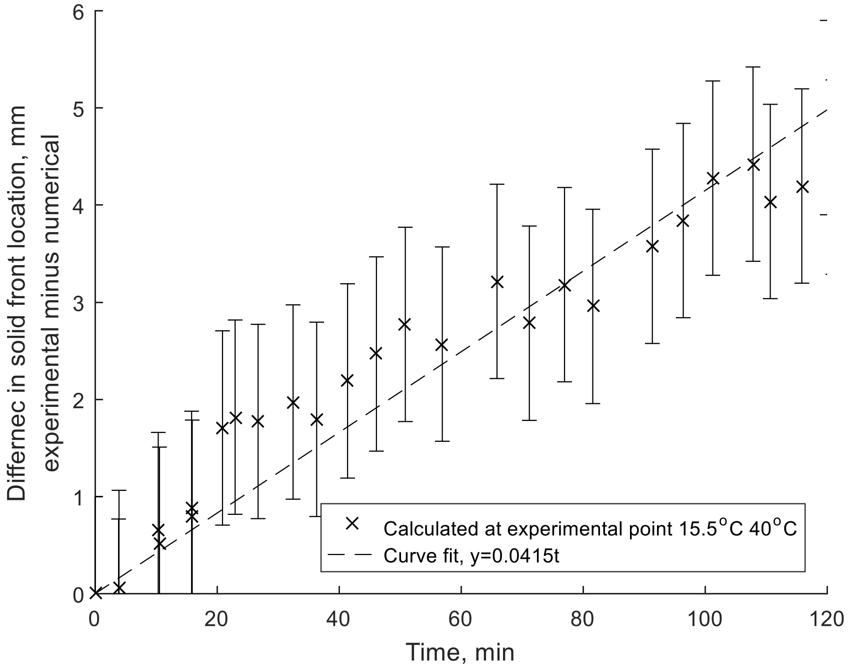

Figure 3-25: Difference in the experimental and numerical solid front locations and a linear curve fit for validation case with wall temperature 15.5℃ and initial temperature 40℃

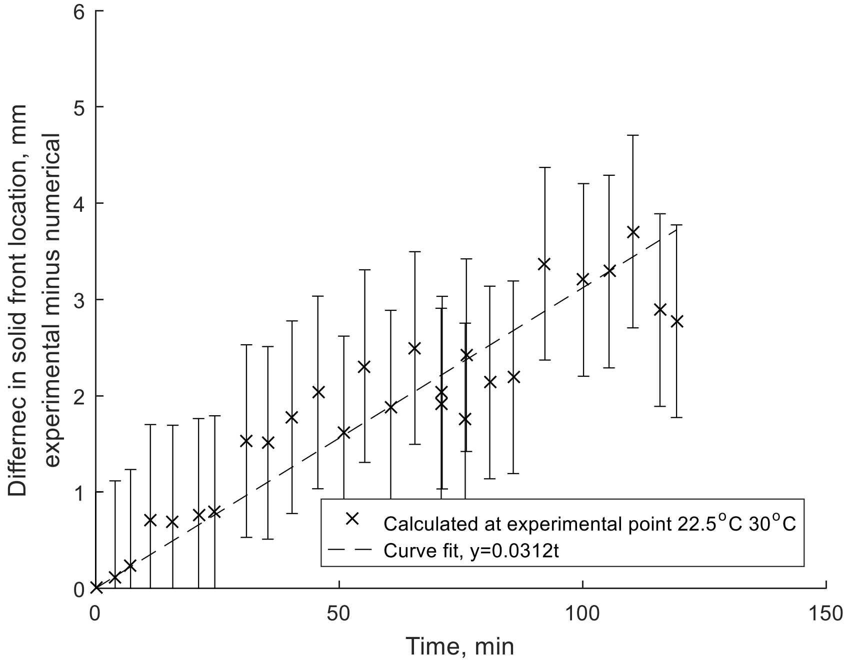

Figure 3-26: Difference in the experimental and numerical solid front locations and a linear curve fit for validation case with wall temperature 22.5℃ and initial temperature 30℃

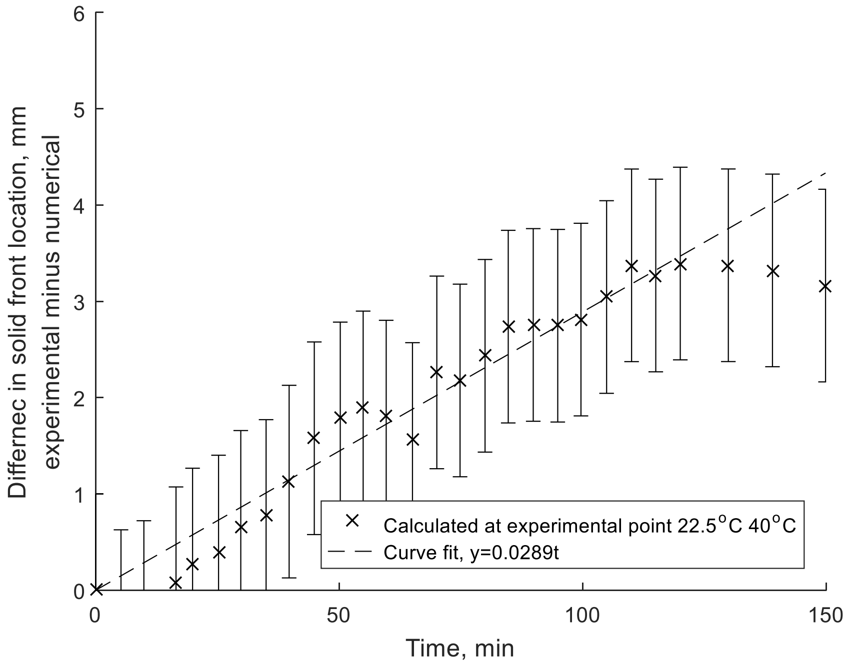

Figure 3-27: Difference in the experimental and numerical solid front locations and a linear curve fit for validation case with wall temperature 22.5℃ and initial temperature 40℃

Table 3-4: Summary of the estimated heat losses from the test section during the validation experiments

Case	Slope, mm/s	Average Losses, W
8.5℃, 30℃	0.049	1.1
8.5℃, 40℃	0.049	1.1
15.5℃, 30℃	0.039	0.86
15.5℃, 40℃	0.042	0.91
22.5℃, 30℃	0.031	0.69
22.5℃, 40℃	0.029	0.64

3.6 Measurement of solid extraction

The effect of solid extraction could have an impact on the results of the experiments. The extent of this impact will be addressed in Section 4.4. Thus, a measurement of the effect of solid extraction will provide useful information. To measure solid extraction two methods of measurement were used. One method was taking images of the area directly in of the electrodes during the experiments where the electric potential is applied. In Section 4.1, it will be shown that particles will be attracted to the front of the electrodes, so any solid particles should accumulate in this area. To compliment this method, experiments will be done with almost no superheat energy in the liquid phase change material, the initial temperature will be 30℃. Since the liquid phase change material is nearly at the melting temperature, the effect of convection on solidification should be negligible. Meaning any difference between the case where the electric field is applied and the case where it is not must be due to solid extraction. If solid extraction is having any effect on the results, then these methods will detect it. However, these methods will not be able to detect solid extraction if it is occurring at a rate so small that it does not affect the results.

Nakhla et al. (2015) measured solid extraction using a highly magnified high-speed camera to view the solid-liquid interface; this technique allowed solid extraction to be observed directly. Although this method allowed for solid extraction to be observed directly, the images didn’t have any scaling so the rate of solid extraction could not be estimated. High-speed camera measurements were not done in this investigation because a thin layer of solid was building up on the transparent walls of the test section. This thin layer of solid obstructed the view of the solid-liquid interface and did not permit the video of the high-speed camera to take clear images of the dendrites on the interface. As a result, the videos would not have been useful in identifying solid extraction, because the solid particles could not be clearly identified.

4 Analytical and Numerical Modelling

There are two effects of applying electric fields, one is the elecctrohydrodynamic effect and the other is the solid extraction effect. To theoretically understand the effect of applying an electric field, the two mechanisms will be modelled separately. One effect of applying electrohydrodynamics is the convection effect, which is caused by fluid motion induced by the electric field; whereas, solid extraction is when particles of the solid are pulled into the liquid phase. To better understand the source of convection and solid extractions the electric forces will be modelled in Section 4.1. The convection effect will be modelled by a two-phase Stefan solution in Section 4.2. In Section 4.3 the convection effect is modelled numerically, using a finite difference method. The effect of solid extraction is discussed in Section 4.4.

The fluid flow that would occur when the electric field is applied will not be modelled. The reason for this is that modelling the fluid flow requires material properties that are not currently available and not readily obtainable. Specifically, to model electrohydrodynamics, it is important to model the free charges in the fluid. However, electric charges will be injected into the fluid from the electrodes, but because of the low current that flows through the system, this could not be measured. As a result, only the heat transfer in the system will be modelled.

4.1 Analysis of electric field

An electrostatic analysis was done on the system to understand the electrostatic forces acting on the fluid. The electric field can be found using a numerical simulation. The charge density of the dielectric fluid is assumed to be zero, and the electric current through the material is assumed to be negligible. Thus the electric field is related to the electric potential through Equation 4.1. In Equation 4.1, E is the electric field strength and V is the electric potential energy. This equation shows that the electric field strength is the divergence of the electric potential energy. Equation 4.1 can be used in Gauss's law to find Equation 4.2. The numerical software used to calculate the electric field was Comsol; the software uses Equation 4.1 and

Equation 4.2 to determine the electric field distribution. In Equation 4.2, ρ_e is the electric charge density and ε is the electric permittivity.

$$E = -\nabla V \quad [4.1]$$

$$\nabla^2 V = \frac{\rho_e}{\varepsilon} = 0 \quad [4.2]$$

The electric field distribution changes as the solid layer grows. The reason is the dielectric constant of the solid and liquid are different. The difference in the dielectric constants of the materials changes the electric field because of the interface between the solid and liquid. The tangential component of the electric field stays the same, and the normal component varies according to the ratio of the dielectric constant, Equation 4.3 and Equation 4.4 show these relations (Stratton, 1941). In these equations, E is the electric field and ε is the electric permittivity. The positions of the interface that were tested are 0mm, 3mm, 5mm, 7mm, 9mm and 12mm.

$$E_{tangential,solid} = E_{tangential,liquid} \quad [4.3]$$

$$\varepsilon_{solid} E_{tangential,solid} = \varepsilon_{liquid} E_{tangential,liquid} \quad [4.4]$$

The dielectric constant of the solid and liquid phase change material is related to the density of the material through the Clausius-Mossotti relation, as shown in Equation 4.5. In this equation, ε_r is the dielectric constant of the material. N is the number of molecules per unit volume, α_p is the molecular polarizability. ε_0 is the permittivity of free space. The relation can be manipulated to include the mass density rather than the molecular number density, by adding the molecular mass, M. Assuming the polarizability of the molecules is not dependent on the phase of the material, then the equations for the solid and liquid materials can be combined to predict the change in dielectric constant when the material solidifies. Equation 4.6 is the relation between the solid density and dielectric constant to the liquid ones. In these equations, ε_r is the dielectric constant of the material, N is the number of dipoles per unit volume, α_p is the polarizability of the dipoles, ε_0 is the permittivity of free space and ρ is the density. The subscript s indicates the property is for solid and l indicates the property is for liquid. Using this relationship, if the density of the liquid is 770 kg/m^3, the density of the solid is 865kg/m^3 and the dielectric constant is 1.9 (Dhaidan et al. 2013) then the dielectric constant of solid is 2.05.

$$\frac{(\varepsilon_r-1)}{(\varepsilon_r+2)}=\frac{N\alpha_p}{3\varepsilon_0} \qquad [4.5]$$

$$\frac{(\varepsilon_s-1)}{\rho_s(\varepsilon_s+2)}=\frac{(\varepsilon_l-1)}{\rho_l(\varepsilon_l+2)} \qquad [4.6]$$

In a previous study, a phenomenon was discovered where solid particles were pulled from the solid phase into the liquid phase (Nakhla et al., 2015). The phenomenon was not observed in the experiments conducted for this thesis. The author explained these results using the interfacial force that arises at the boundary of two materials with different dielectric constants. The interfacial force is given by Stratton (1941) in Equation 4.7. In Equation 4.7, ε_0 is the permittivity of free space, $\varepsilon_{r,1}$ is the dielectric constant of one material and $\varepsilon_{r,2}$ is the dielectric constant of a different material. This equation is limited to use in fluids where the shear stresses are zero. However, this equation gives results that are physically nonsense. For example, the expected result is that the material with a higher dielectric constant will be pulled into the material with a smaller dielectric constant. This result has been validated experimentally (Cotton, et al. 2005) (Sadek, et al, 2010) (Ng, et al. 2011) (Nangle Smith, 2012). However, when Equation 4.7 is used with the dielectric constants for liquid and solid octadecane in the equation, the force acts to pull the fluid with the lower dielectric constant into the one with the higher dielectric constant. This is not a physical result, and thus this force must be derived again to get the correct result.

$$F_t=\frac{\varepsilon_0}{6}\left(\frac{1}{\varepsilon_{r,2}}\left(\varepsilon_{r,1}^2\varepsilon_{r,2}^2+4\varepsilon_{r,1}^2\varepsilon_{r,2}-6\varepsilon_{r,1}\varepsilon_{r,2}^2-3\varepsilon_{r,1}^2+2\varepsilon_{r,1}+2\right)E_{n,1}^2+\left(\varepsilon_{r,2}\left(\varepsilon_{r,2}-2\right)-\varepsilon_{r,1}(\varepsilon_{r,1}-2)\right)E_{t,1}^2\right) \qquad [4.7]$$

4.1.1 Derivation of the interfacial force

At an interface between two dielectric materials, a force imbalance will arise. This force imbalance is due to the difference in the internal stresses generated in the two materials when an electric field is applied. The material with the high dielectric strength will have a larger internal stress than the material with the smaller dielectric constant. This can be thought of physically as the forcing on the dipoles in the two materials, recall that the dielectric constant is a measure of the strength of dipoles generated in a material per unit volume. When an electric field is generated, dipoles near the positive and negative electrodes will be generated. The force on these dipoles will act to pull the material closer to the electrode, and a tensile stress will be generated in the dielectric material. At the interface, between two dielectric materials, the strength of the force acting on the dipoles changes abruptly. Since the force acting on the material with the higher dielectric constant is stronger than the force acting on the material with a lower dielectric constant, the material with the higher dielectric constant is pulled into the one with the lower dielectric constant. A general equation for the force per unit area at the interface, Equation 4.8, is given by Stratton (1941). In Equation 4.8, $\vec{E}$ is the electric field strength and $\vec{n}$ is the vector pointing orthogonal to the interface of the two materials. α_m and β_m in Equation 4.8 are constants that are defined in Equation 4.9 and Equation 4.10. The first two terms on the right-hand side of Equation 4.8 represent the force due to the elastic strain that runs parallel to the normal vector and the third and fourth terms represent the force due to elastic strains that run parallel to the interface. These constants are functions of the electric permittivity, and two material properties a_1 which defines the change in electric permittivity due to strain that is parallel to the electric field lines and $a_2$which defines the change in electric permittivity due to strain that is perpendicular to the electric field lines. Stratton (1941) defines these material properties by considering two fluids which follow Clausius-Mossotti law, which is given in Equation 4.11, where ε_r is the dielectric constant.

$$F_t = \left[\alpha_m \vec{E}(\vec{E}\cdot\vec{n})\right]_2 + \left[\alpha_m \vec{E}(\vec{E}\cdot\vec{n})\right]_1 - \left[\beta_m \vec{E}^2\vec{n}\right]_2 - \left[\beta_m \vec{E}^2\vec{n}\right]_1 \qquad [4.8]$$

$$\alpha_m = \varepsilon + \frac{a_2 - a_1}{2} \quad [4.9]$$

$$\beta_m = \frac{\varepsilon + a_2}{2} \quad [4.10]$$

$$a_1 = a_2 = -\frac{\varepsilon_0}{3}(\varepsilon_r - 1)(\varepsilon_r + 2) \quad [4.11]$$

The force that acts at the interface between two dielectric materials with different dielectric constants can be found using Equation 4.12. In Equation 4.12, ε_0 is the permittivity of free space, $E_{n,1}$ and $E_{t,1}$ are the electric field strength that is normal to the solid-liquid interface and tangential to it, respectively. The constants used in the equation can be found using Equation 4.13 and Equation 4.14. In these equations, $\varepsilon_{r,1}$ is the dielectric constant of one material and $\varepsilon_{r,2}$ is the dielectric constant of a different material. Using the dielectric constant for solid octadecane as material 1 and liquid octadecane as material 2, the traction force is given by Equation 4.15.

$$F_t = \frac{\varepsilon_0}{6}\left(C_1 E_{n,1}^2 + C_2 E_{t,1}^2\right) \quad [4.12]$$

$$C_1 = -2\frac{\varepsilon_{r,1}^2}{\varepsilon_{r,2}^2} + 4\frac{\varepsilon_{r,1}^2}{\varepsilon_{r,2}} - 4\varepsilon_{r,1} + 2 \quad [4.13]$$

$$C_2 = \varepsilon_{r,2}\left(\varepsilon_{r,2} - 2\right) - \varepsilon_{r,1}(\varepsilon_{r,1} - 2) \quad [4.14]$$

$$F_t = 4.71 \times 10^{-13} E_{n,1}^2 - 4.32 \times 10^{-13} E_{t,1}^2 \quad [4.15]$$

4.1.2 Geometry

A two-dimensional model of the test section was used to model the system. The geometries height spanned from the heat exchanger to the top of the heat exchanger. The width of the domain spanned from the centre of an electrode in the first row to the centre of an electrode in the second row. The geometry used in the analysis is given in Figure 4-1. The geometry consists of the polycarbonate wall on the top of the test section, a liquid portion of the phase change material and a solid portion of the phase change material. The high voltage and grounded boundary conditions are applied on the electrode and heat exchanger surfaces, respectively. The dielectric constant was assumed to be constant within the solid and liquid phases. The only spatial variation in dielectric constant is due to the material change.

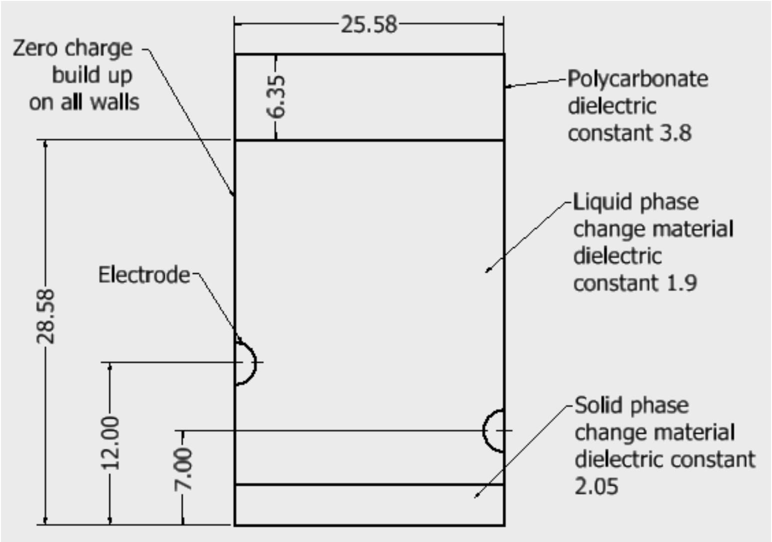

Figure 4-1: Geometry used in numerical simulation of electric field

4.1.3 Mesh sensitivity

To ensure that the results of the analysis are independent of the mesh size. A mesh density was chosen that resulted in less than a 1% change when the element size was halved. The mesh sensitivity was carried out for each of the conditions, and the results are shown in Figure 4-2 through Figure 4-7. In all the cases the results are overlapping. This means that the results of the analysis are independent of the mesh size and the mesh size is sufficiently small to yield accurate results.

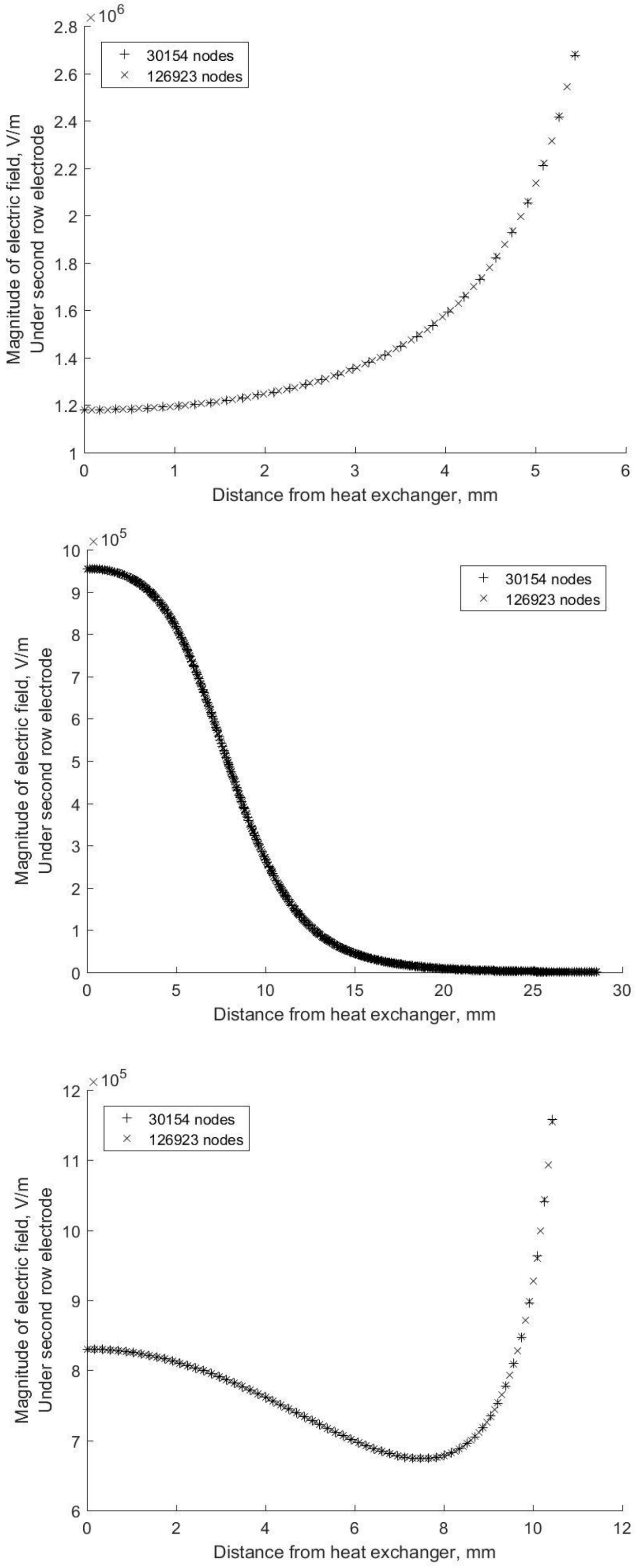

Figure 4-2: Magnitude of electric field, mesh sensitivity analysis for 0mm case

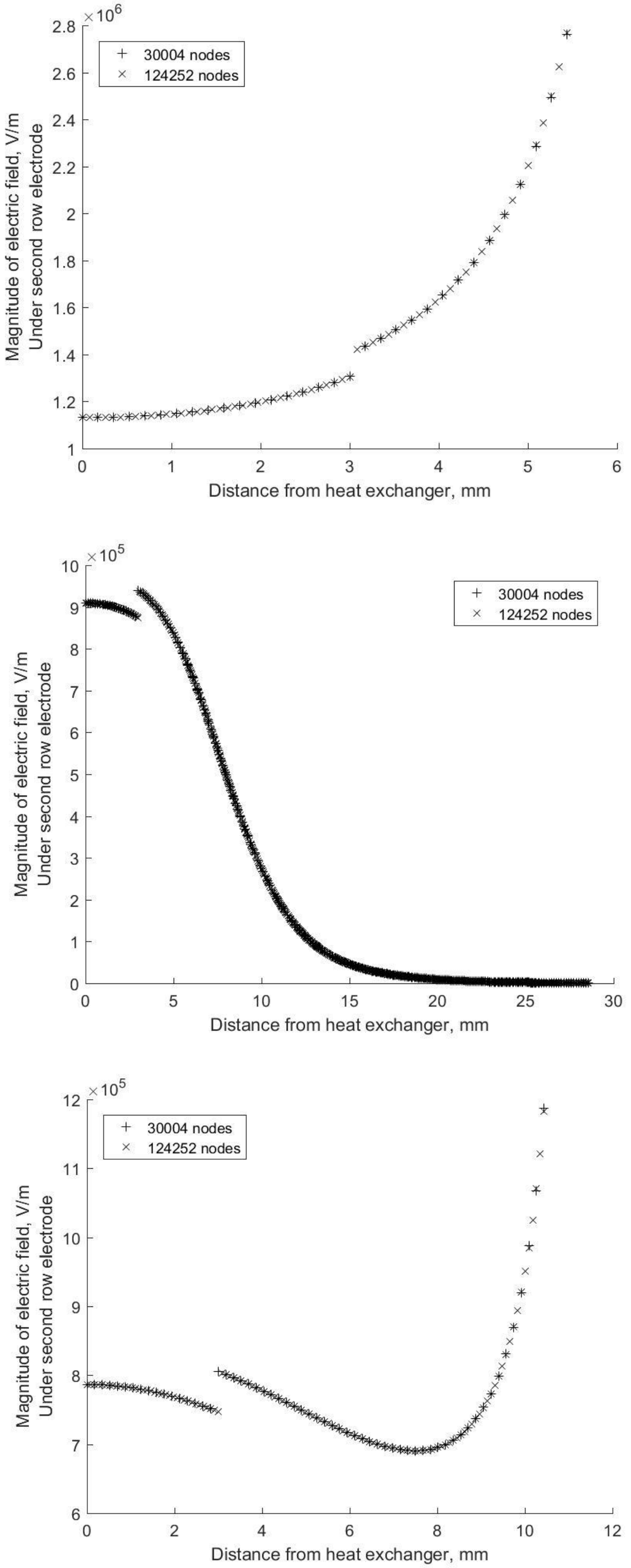

Figure 4-3: Magnitude of electric field, mesh sensitivity analysis for 3mm case

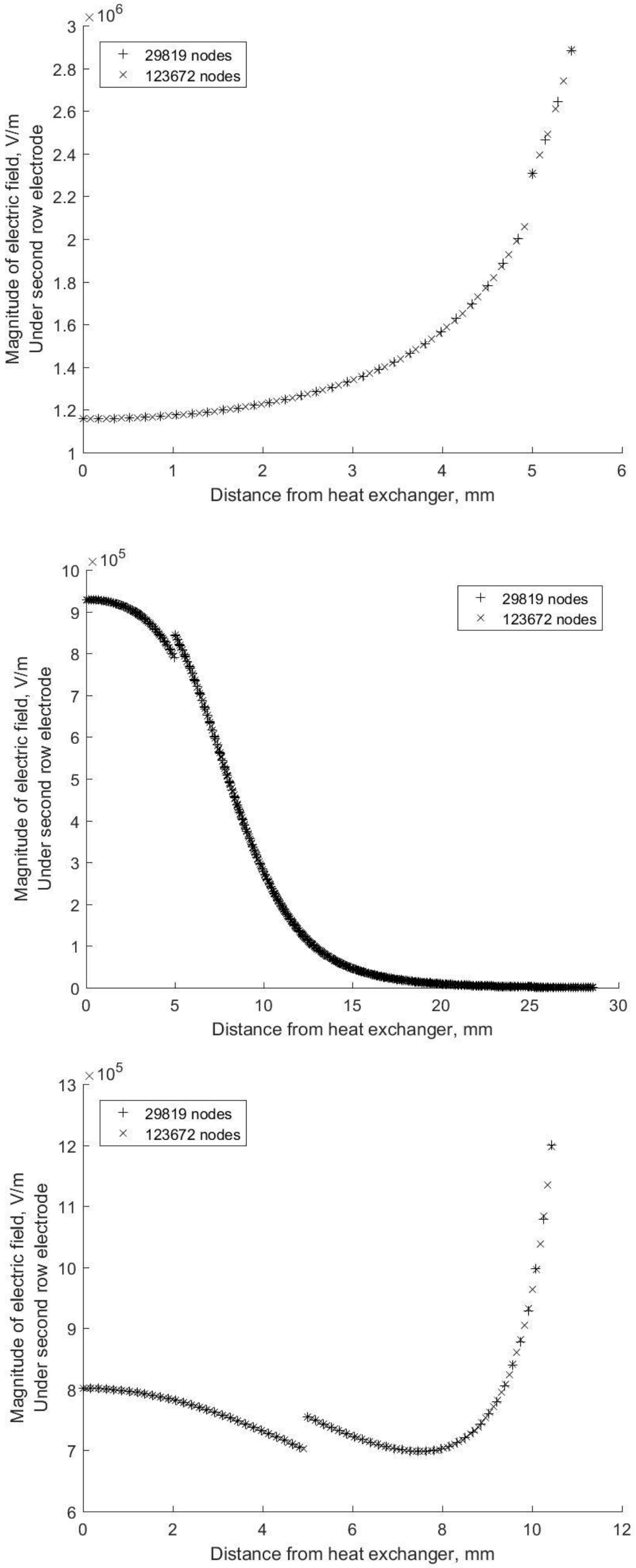

Figure 4-4: Magnitude of electric field, mesh sensitivity analysis for 5mm case

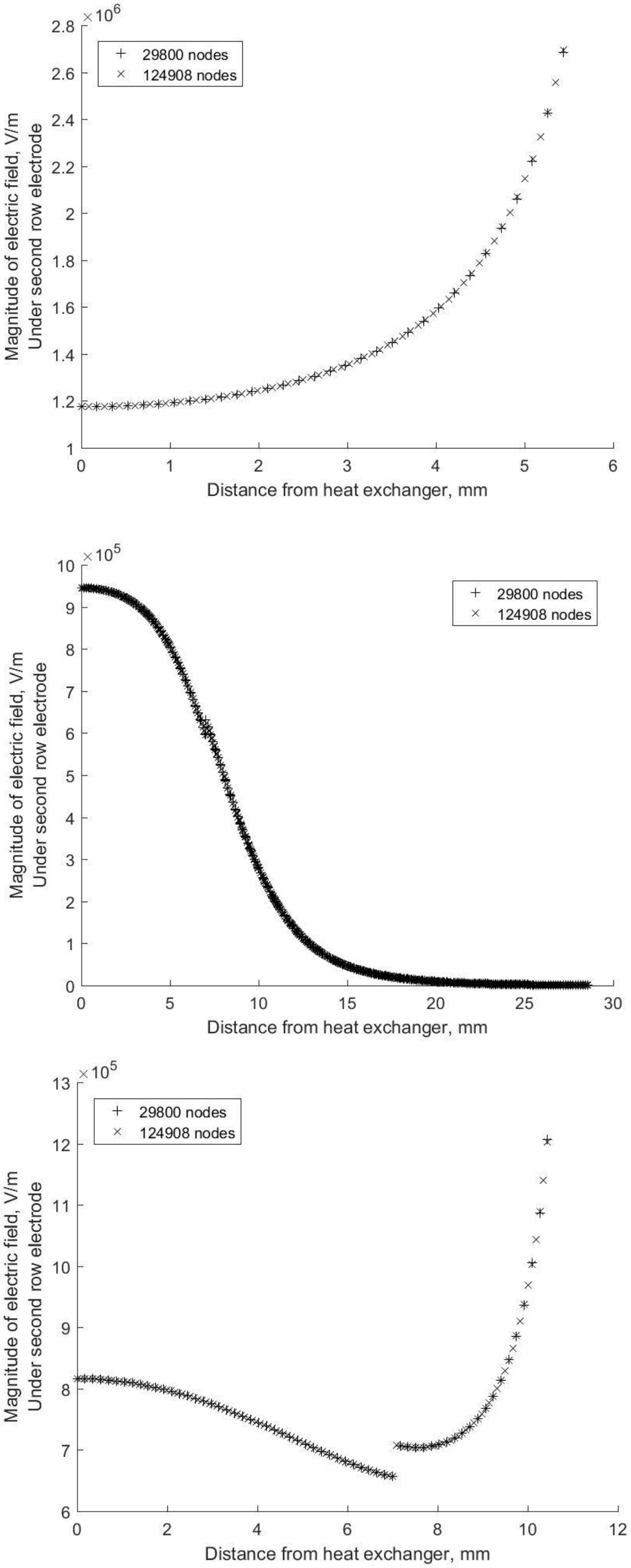

Figure 4-5: Magnitude of electric field, mesh sensitivity analysis for 7mm case

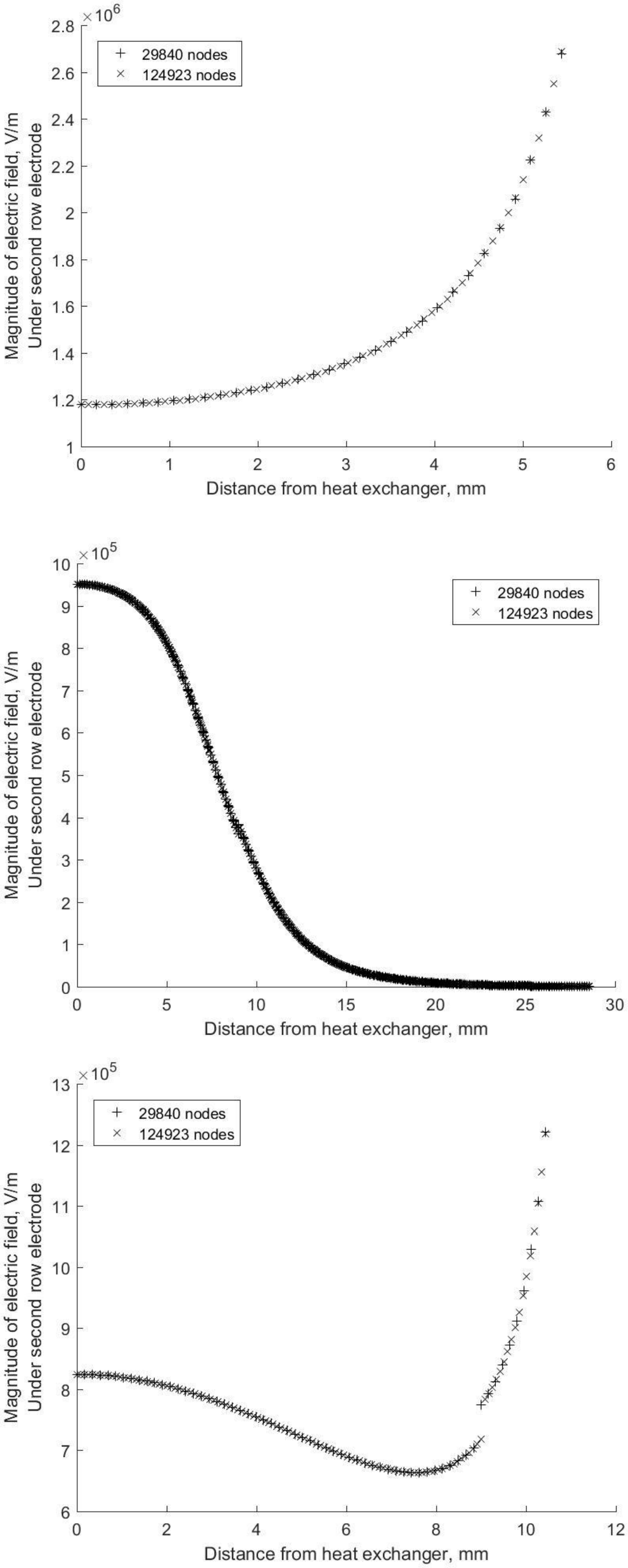

Figure 4-6: Magnitude of electric field, mesh sensitivity analysis for 9mm case

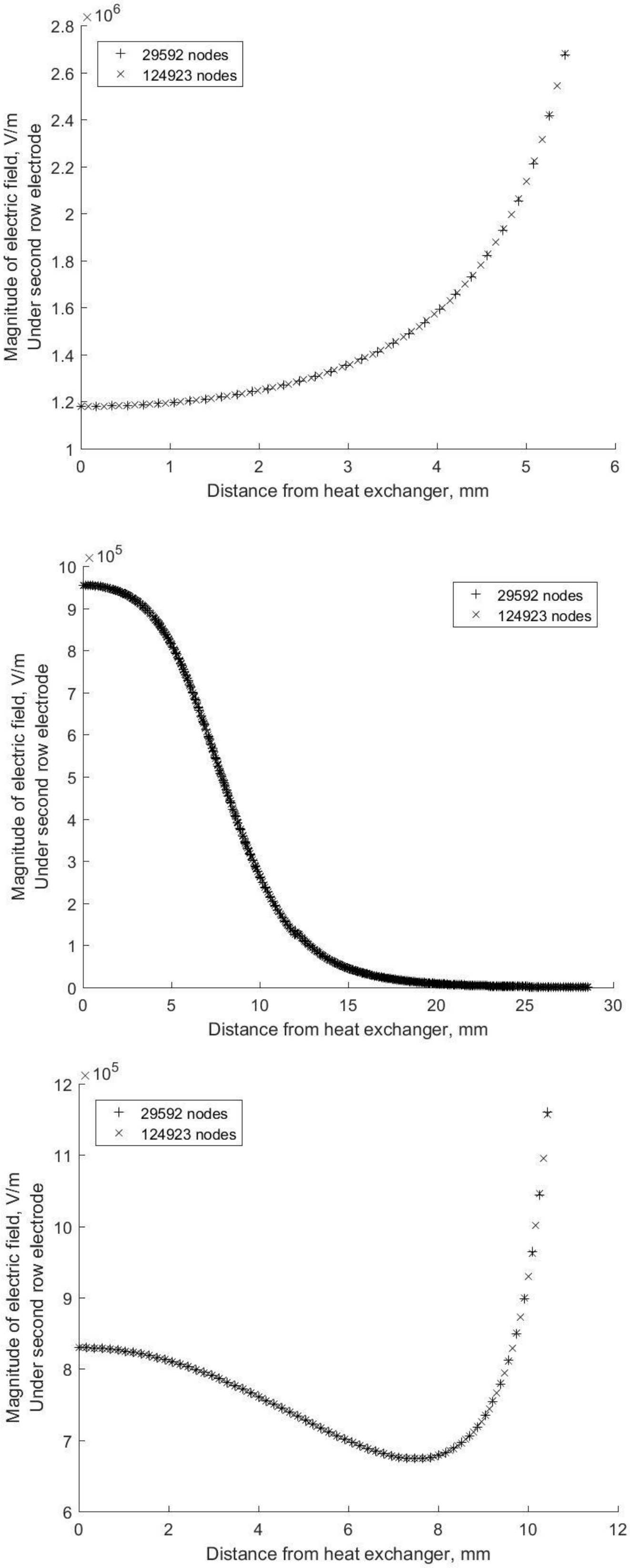

Figure 4-7: Magnitude of electric field, mesh sensitivity analysis for 12mm case

4.1.4 Results

The electric field distributions for each of the cases from the numerical analysis are shown in Figure 4-8. The results show a trend that was expected, the electric force is largest near the electrodes and quickly decreases further away from the electrodes. The electric force at locations between the electrodes is very small compared locations between the heat exchanger and the electrodes. The simulation gives a first order approximation of the forces on electric charges in the fluid.

The results of the interfacial force are shown in Figure 4-9. The analysis found smaller interfacial forces than the forces seen in the analysis done by Nakhla et al. (2015). The reason the forces were higher in Nakhla et al.'s study, is due to the larger change in the dielectric constant in Nakhla et al.'s analysis. The dielectric constant in Nakhla et al.'s work is 2.1 for the liquid and 2.5 for the solid, whereas the dielectric constant used in this study is 1.9 for the liquid and 2.05 for the solid. The smaller interface forces could explain why solid extraction was not seen in these experiments. However, no threshold for the onset of solid extraction exists, and the analysis requires an insight into the mechanisms of solid extraction which has yet to be developed. So it cannot be stated that the difference in the interface force is responsible for the lack of solid extraction in these experiments. The results show that the interfacial force is strongest when it is close to the electrodes.

This analysis indicates that the forces acting on particles on the solid liquid interface are smaller for the conditions tested in the current study than they are for the conditions tested in Nakhla et al. (2015). Therefore, it is expected that solid extraction will likely have a smaller impact on the results of the current study. Observations of solid extraction during the experiments will be discussed in Section 5.4. The calculation of the interface forces will show relevance in that discussion.

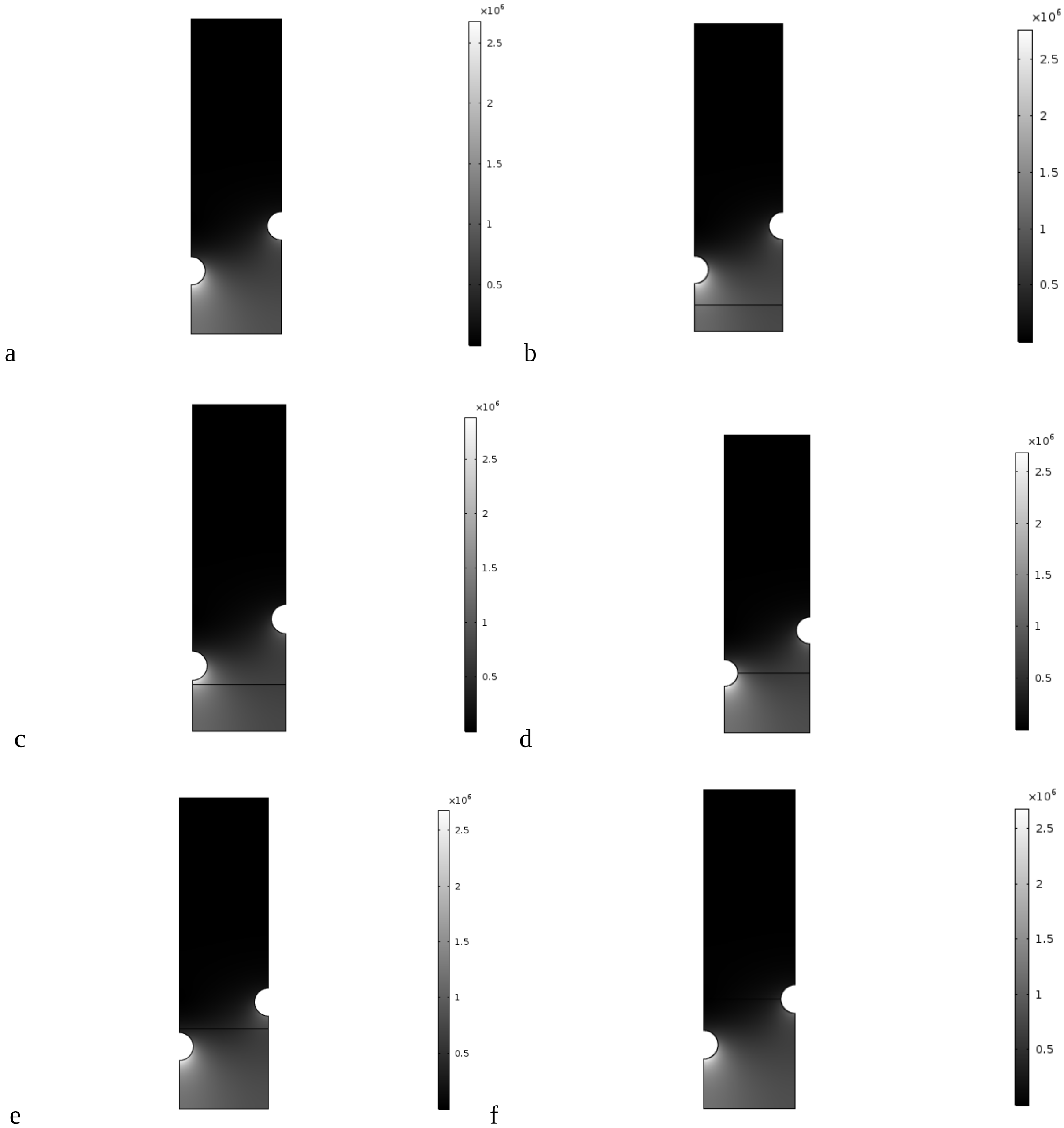

Figure 4-8: Electric field distribution in test section for various solid front locations. a) 0mm solid thickness b) 3mm solid thickness c) 5mm solid thickness d) 7mm solid thickness e) 9mm solid thickness f) 12mm solid thickness

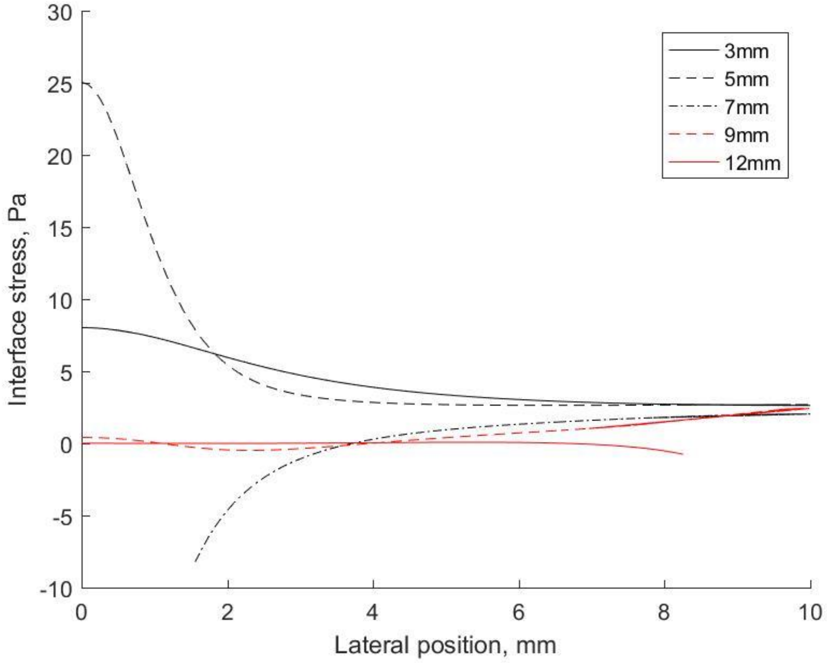

Figure 4-9: Interface stress along the interface. The center of the first row electrode is at a lateral position of zero and the center of the second row electrode is at a lateral position of 10mm.

4.2 Effect of Convection: Two-Phase Stefan Solution

A two-phase Stefan problem model will be used to estimate the maximum possible improvement that can be found by applying convection to a latent heat thermal storage system. This is a simple one-dimensional model that assumes constant wall temperature on one side of an enclosure, and the enclosure is infinite. The model assumes that a pure material, which melts at a single temperature is undergoing plane front solidification. The general expression for the model is given in Equation 4.16 (Alexiades and Solomon, 1993).

$$S(t) = 2\lambda\sqrt{\alpha_s t} \qquad [4.16]$$

To estimate the maximum possible improvement due to convection, assume that convection is so vigorous that all of the superheat is dissipated from the fluid in a negligible amount of time. Thus, the superheat term can be eliminated from the transcendental equation and Equation 4.17 can be used. The dimensionless numbers used in Equation 4.17 are described in Equations 4.18. γ is the ratio of the liquid density to the solid density, Equation 4.19 is used to find γ. In these equations, C_S and C_L are the specific heat for the solid and liquid respectively, T_f is the melting temperature of the material, T_w is the wall temperature of the material, T_0 is the initial temperature of the fluid, H is the latent heat of fusion, α_L is the thermal diffusivity of the liquid and α_S is the thermal diffusivity of the solid, λ and γ are two constants that are calculated using Equation 4.17 and Equation 4.19. Ste_S represents the ratio of sensible energy in the solid relative to the latent energy of the material and St_L represents the ratio of sensible energy in the liquid relative to the latent energy of the material. These four equations describe a model proposed by Alexiades and Solomon (1993) which estimates the solid front location as a function of time. Table 4-1 shows the properties used in the analysis. The analysis was conducted to estimate the maximum possible improvement, $\%improvement = \frac{S_{convection} - S_{conduction}}{S_{conduction}} \times 100\%$. The results of this analysis are presented in Table 4-2 and show that even for large superheated liquids the total improvement is still very small. For a 22.5℃ wall temperature and a 50℃ initial temperature, the maximum improvement is approximately 34%. All the other results are smaller than this. The problem with this analysis is that the enclosure holding the wax can be modelled as infinitely long which is only true when the solid front is very thin. The result of this assumption is that the effect of adding convection is exaggerated.

$$\frac{St_S}{\exp(\lambda^2)\mathrm{erf}(\lambda)} + \frac{St_L}{\nu\exp(\nu^2\lambda^2)\mathrm{erf}(\nu\,\lambda)} = \lambda\sqrt{\pi} \qquad [4.17]$$

$$Ste_S = \frac{C_S(T_f - T_w)}{H} \qquad St_L = \frac{C_L((T_0 - T_f))}{H} \qquad \nu = \sqrt{\frac{\alpha_L}{\alpha_S}} \qquad [4.18]$$

$$\frac{1}{Ste_S}\left(\frac{\lambda\,\gamma}{2}\right) = \sqrt{\frac{\alpha_S}{\pi}}\frac{\exp(-\gamma^2\,\lambda^2/(4\alpha_S))}{\mathrm{erf}(\lambda\,\gamma/\sqrt{4\alpha_S})} \qquad [4.19]$$

Table 4-1: Thermal properties of Octadecane (Ho, 1982)

Property	Value
Density solid, m^3/kg	778
Density liquid, m^3/kg	775
Specific heat solid, J/(kg.K)	2150
Specific heat liquid, J/(kg.K)	2180
Thermal conductivity solid, W/(m.K)	0.358
Thermal conductivity liquid, W/(m.K)	0.152
Melting temperature, ℃	27.4
Latent heat, J/kg	243500

Table 4-2: Maximum possible improvement in the thickness due to convection based on the two phase Stefan solution, improvement is defined by $\%improvement = \frac{S_{convection} - S_{conduction}}{S_{conduction}} \times 100\%$

Wall Temperature [$°C$]	Initial Temperature [$°C$]	Improvement from convection [%]
8.5	30	3
8.5	40	13
8.5	50	21
15.5	30	3.5
15.5	40	15
15.5	50	25
22.5	30	5
22.5	40	21
22.5	50	34

4.3 Effect of Convection: Numerical interface tracking method

4.3.1 Governing Equations

One issue with the analytical model is that the solution requires the problem to be modelled as semi-infinite. If the differential equations are solved numerically, then this assumption is no longer needed. The set of differential equations required for this analysis is summarised by Equation 4.20, which predicts the growth rate of the interface and Equation 4.21 governs the heat conduction in the two single phase regions. In Equation 4.20, ρ is the mass density of the material, H is the latent heat of fusion, A is the area of the solid-liquid interface, S is the solid front location, t is the time after the experiment began, Q_{solid} is the rate of heat transfer from the solid-liquid interface to the solid and Q_{liquid} is the rate of heat transfer from the liquid to the solid-liquid interface. Equation 4.20, is an energy balance on the solid-liquid interface that states the difference in energy leaving the interface into the solid and the energy entering the interface from the liquid, is equal to the amount of latent energy discharged from the material. In Equation 4.21, C_p is the specific heat of the material, $\boldsymbol{V}$ is the volume of the material cell being considered, T is the temperature of the material, t is the time after the experiment began, A is the area of the solid-liquid interface, k is the thermal conductivity and x is a coordinate that describes distance from the heat exchanger. In Equation 4.21, the first term is the energy stored in sensible form and the second term is the imbalance in the heat conduction entering the material.

$$\rho\, H\, A \frac{dS}{dt} = Q_{solid} - Q_{liquid} \qquad [4.20]$$

$$\rho\, C_p\, \boldsymbol{V}\, \frac{\partial T}{\partial t} = A\, k\, \frac{\partial^2 T}{\partial x^2} \qquad [4.21]$$

These equations were discretized using a first order, explicit finite difference discretization method. However, special care is required due to the moving interface. The variable, s, is used to track the solid-liquid interface location. This variable grows or shrinks based on the energy equation for the solid-liquid interface; however, the mesh stays fixed in space. A node is placed on the solid-liquid interface to accommodate for the moving interface. The node acts as a solid node and a liquid node in the two single phase regions. The set of discretized equations is given by the Equation set 4.22 through 4.27. Equation 4.22 is used for nodes in the single phase region. In Equation 4.22, T represents the temperature, the subscript represents the node index and the superscript represents temperatures taken in the previous time iteration, Δt is the time step used in the simulation, ρ is the mass density, c_p is the specific heat, x is the distance a point is from the heat exchanger and k is the thermal conductivity. This equation is used for all nodes up to the solid-liquid interface. For the interface, Equation 4.23 to Equation 4.27 are used; in these equations, j is used as an index for the node just before the solid-liquid interface. In these equations, S is the solid front location, T_m is the melting temperature of the material and H is the latent heat of fusion.

Equation 4.23 is used to calculate the temperature of the last node in the solid and Equation 4.24 is used to calculate the temperature of the first liquid node after the interface. Equation 4.25 is the energy being extracted from the interface to the cool wall, Equation 4.26 is the energy being transferred from the liquid to the interface. The boundary conditions are, a fixed temperature on the heat exchanger wall, a fixed temperature at the solid-liquid interface, which is set at the melting temperature and an insulated boundary at the wall opposite the heat exchanger. All surrounding nodes are set to be insulated as well. The set of equations were solved in Matlab.

If the distance between the solid front location and its closest node is too close, the solution will become unstable. So an additional criterion was set that if the solid front location and either one of the nodes were within 10% of the node to node spacing, then the closest node would be replaced with the next closest one. Increasing the node to node distance ensures that the solution will not become unstable.

$$T_i = T_i^o + \frac{2\,\Delta t}{\rho\, c_p\, (x_{i+1} - x_{i-1})} \left(\frac{k_{i+1}(T_{i+1}^o - T_i^o)}{x_{i+1} - x_i} - \frac{k_{i-1}(T_i^o - T_{i-1}^o)}{x_i - x_{i-1}} \right) \tag{4.22}$$

$$T_j = T_j^o + \frac{2\,\Delta t}{\rho\, c_p\, (s - x_{j-1})} \left(\frac{k_s(T_m - T_j^o)}{S - x_j} - \frac{k_{j-1}(T_j^o - T_{j-1}^o)}{x_j - x_{j-1}} \right) \tag{4.23}$$

$$T_{j+1} = T_{j+1}^o + \frac{2\,\Delta t}{\rho\, c_p\, (x_{j+1} - S)} \left(\frac{k_{j+1}(T_{j+2}^o - T_{j+1}^o)}{x_{j+2} - x_{j+1}} - \frac{k_{j-1}(T_j^o - T_m)}{x_{j+1} - s} \right) \tag{4.24}$$

$$Q_s = \frac{k_s\, (T_m - T_j^o)}{S - x_j} \tag{4.25}$$

$$Q_l = \frac{k_l\, (T_{j+1}^o - T_m)}{x_{j+1} - S} \tag{4.26}$$

$$S = S^o + \frac{\Delta t\, (Q_s - Q_l)}{\rho\, H} \tag{4.27}$$

4.3.2 Mesh sensitivity analysis

To ensure that the results of the analysis are independent of the mesh size and time step. The results of the mesh sensitivity analysis are given in Figure 4-10. The mesh sensitivity analysis showed that the results were independent of the mesh and timestep.

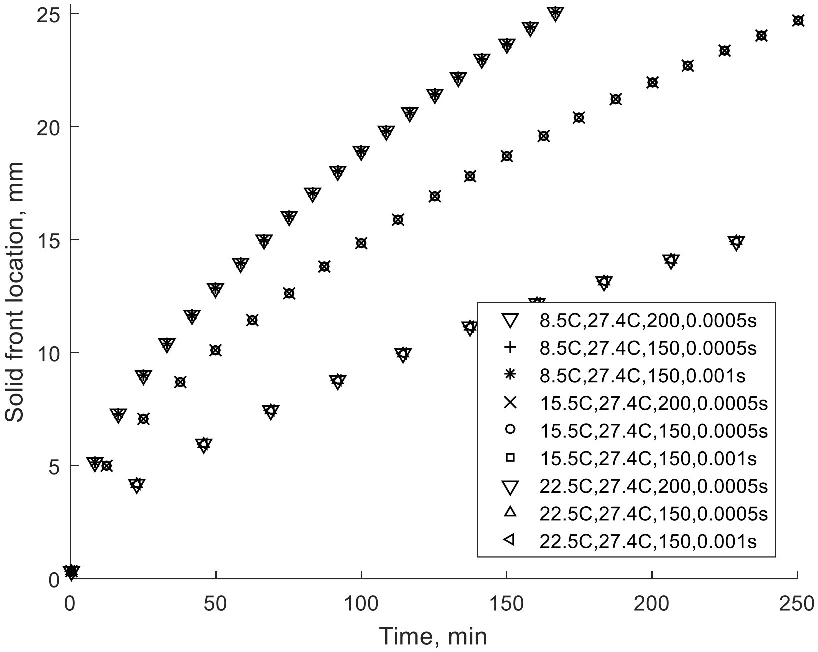

Figure 4-10: Results of a mesh sensitivity analysis for interface tracking method. Legend format [wall temperature, initial temperature, nodes, timestep]

4.3.3 Verification of code

The results of the code are compared to a one-phase Stefan solution from Alexiades and Solomon (1993) to ensure that the results of the code agree with the theory. The analysis was done for wall temperatures of 8.5℃, 15.5℃ and 22.5℃, and an initial temperature of 27.4℃. It was also assumed that the melting temperature is 27.4℃. The verification of the numerical code is shown in Figure 4-11. The numerical and analytical solutions overlap.

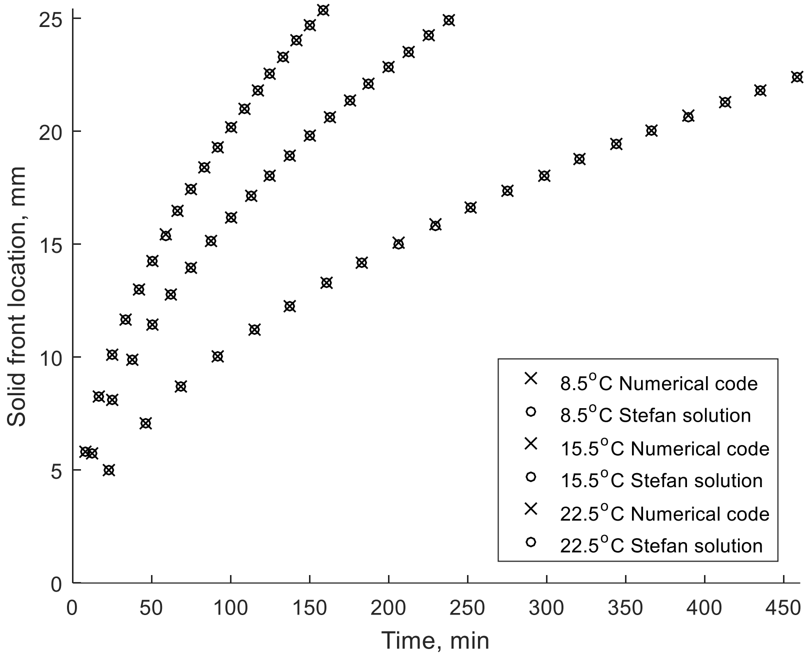

Figure 4-11: Verification of numerical code with various wall temperatures, initial temperature = melting temperature = 27.4℃ against the Stefan solution

4.3.4 Modelling the effect of electrohydrodynamic enhancement

4.3.4.1 Solid Front Location

The liquid phase thermal conductivity enhancement can be applied as a multiplication factor to the thermal conductivity. The method for applying the thermal conductivity factor used is to apply an additional term in the thermal conductivity. This factor is given in Equation 4.28, k_{eff} is the effective thermal conductivity, f is the multiplication factor and k_l is the thermal conductivity of the liquid. It is important to note that applying electrohydrodynamics does not change the thermal conductivity of the fluid. Rather, it induces advection which has the effect of increasing the rate of heat transfer and mixing in the fluid. Although the change in thermal conductivity is not physically accurate; however, it does result in a similar effect, and it doesn't require the calculation of fluid flow due to electro-convection. This effective thermal conductivity has been used in previous studies looking at enhancing latent heat thermal storage systems (O. Mesalhy et al. 2005) (Lingamneni et al. 2014).

$$k_{eff} = (1 + f)\, k_l \qquad [4.28]$$

Six conditions were tested, in the numerical code, three initial temperatures: 30℃, 40℃ and 50℃ were tested, and two wall temperatures were tested: 8.5℃ and 15.5℃. The results of these simulations are given in Figure 4-12, Figure 4-13 and Figure 4-14. The thermal properties of Octadecane used in the simulations are given in Table 4-1. The low superheat experiments shown in Figure 4-12 indicate that the improvement when the initial temperature of the fluid is close to the melting temperature is negligibly small. This conclusion theoretically makes sense, because by adding convection we enhance the rate at which sensible energy is removed from the liquid phase change material since the sensible energy in the liquid when it is near the melting temperature is negligibly small compared to the latent heat. The initial temperature of the liquid is 30℃; thus, the sensible energy stored in the liquid phase change material is 5,600 J/kg compared to the latent energy which is 243500 J/kg. The sensible energy was calculated using Equation 4.29, where $E_{sensible}$ is the initial sensible energy stored in the liquid, C_p is the specific heat, $T_{initial}$ is the initial temperature of the fluid and T_{melt} is the melting temperature of the material. When the sensible energy is increased by setting the initial temperature to 40℃, the enhancement due to convection increases, which is seen in Figure 4-13. This result also makes sense; because for the condition tested in Figure 4-13, the sensible energy in the liquid is 27,000 J/kg which is approximately 11% of the latent heat. However, the improvement that is seen in the numerical simulations is relatively small. If the sensible energy is further increased, the enhancement due to convection continues to increase. Figure 4-14, shows further improvements beyond that of Figure 4-13. The sensible energy in the liquid for these cases is 49,000 J/kg which is 20% of the latent heat. Even though the results in Figure 4-13 and Figure 4-14indicate a greater improvement compared to the lower superheat tests, the thickness of the enhanced condition is still only approximately 3% at times, near the end of solidification.

$$E_{sensible} = C_p(T_{initial} - T_{melt}) \qquad [4.29]$$

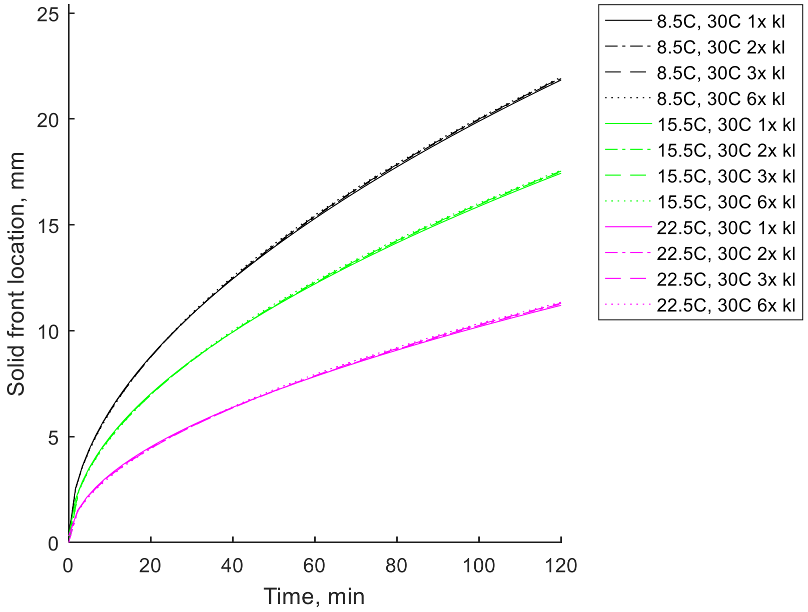

Figure 4-12: Solid front location as a function of time with and without enhancement with various wall temperatures and 30℃ initial temperature

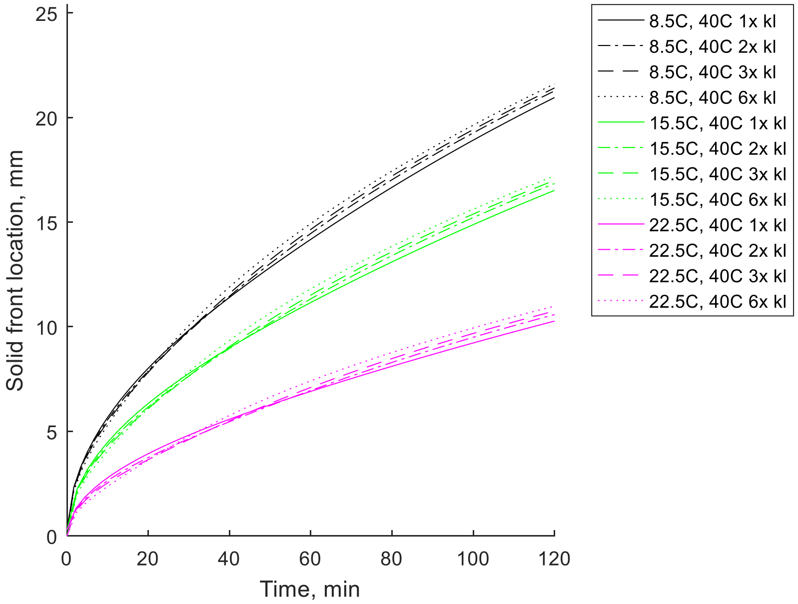

Figure 4-13: Solid front location as a function of time with and without enhancement with various wall temperatures and 40℃ initial temperature

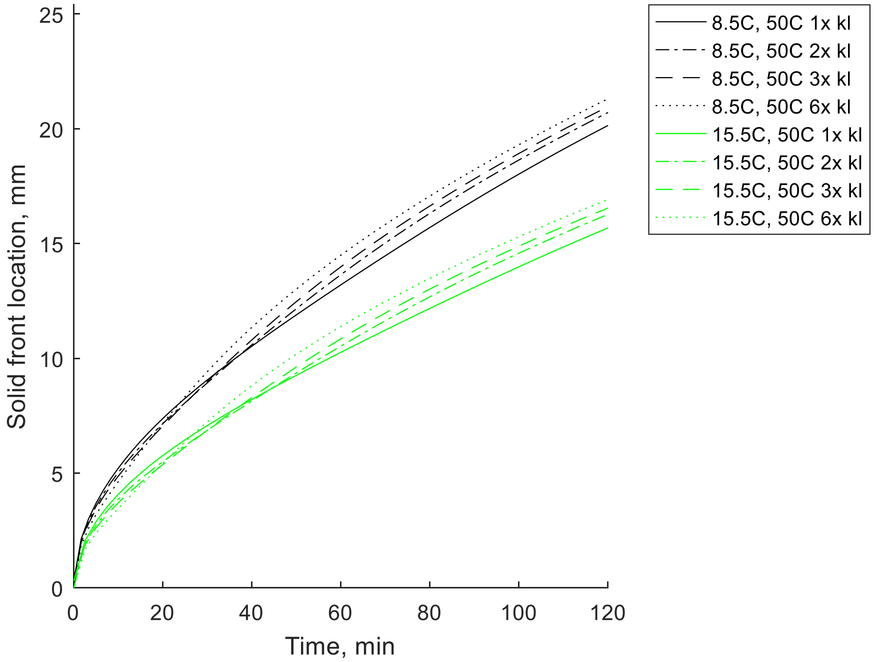

Figure 4-14: Solid front location as a function of time with and without enhancement with various wall temperatures and 50℃ initial temperature

4.3.4.2 Energy Extracted

The solid front location data only provides insight into the latent energy discharged from the system. The sensible energy removed from the system was calculated as well as the solid front location to model the total energy discharged from the system. The sensible energy was calculated using Equation 4.30. Equation 4.30, is comprised of three terms; the first term is the sensible energy removed from the liquid. The second term of Equation 4.30 is the sensible energy removed from the solid and the final term is the latent energy removed from the system, by converting the liquid phase change material to solid phase change material. In Equation 4.30, ρ is the mass density of the material, C_p is the specific heat of the material, A is the area of the heat exchanger, L is the length of the container, S is the solid front location, H is the latent heat of fusion, $T_{l,initial}$ is the initial liquid temperature, $T_{l,average}$ is the average temperature of the fluid at a certain time, T_m is the melting temperature and $T_{S,average}$ is the average temperature of the solid at a certain time. The results of the energy extracted from the system are given in Figure 4-15, Figure 4-16 and Figure 4-17.

$$E_{Discharged} = \rho C_p A(L-S)\left(T_{l,initial} - T_{l,average}\right) + \rho\, C_p\, A\, S\left(T_m - T_{S,average}\right) + \rho\, H\, A\, S \quad [4.30]$$

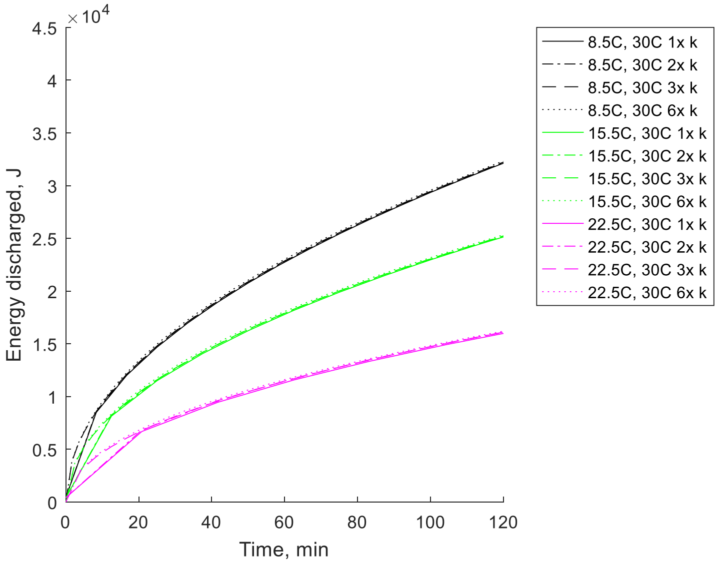

Figure 4-15: Energy discharged as a function of time with and without enhancement for various wall temperatures and 30℃ initial temperature

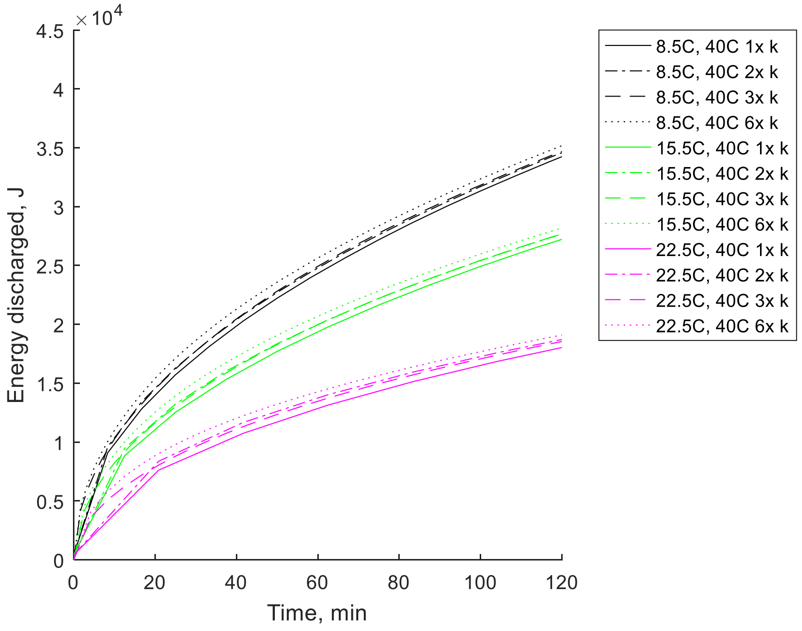

Figure 4-16: Energy discharged as a function of time with and without enhancement for various wall temperatures and 40℃ initial temperature

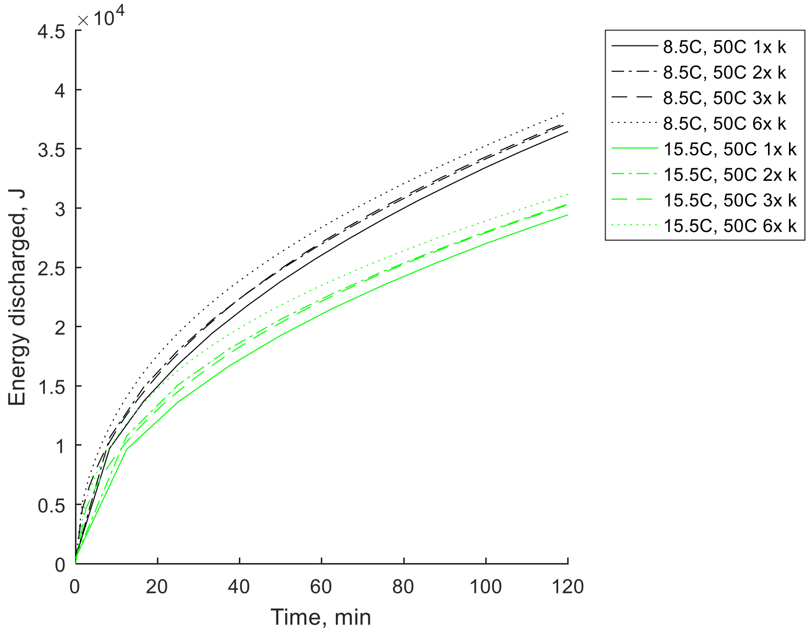

Figure 4-17: Energy discharged as a function of time with and without enhancement for various wall temperatures and 50℃ initial temperature, in the legend k refers to the thermal conductivity in the liquid.

4.3.5 Coupling between solid front location and energy extracted

To understand the effect that electrohydrodynamics has on the energy extracted it is important to understand how the solid front location grows. The energy extracted from the system can be approximated using the thickness of the solid and Equation 4.31. Equation 4.31, $Q_{extracted}$ is the rate of energy being extracted from the system, k is the thermal conductivity of the material, A is the area of the heat exchanger, T is temperature, x is a coordinate that describes the distance from the wall, T_m is the melting temperature, T_w is the wall temperature and S is the solid front location. Equation 4.31 simply states that the rate of energy extracted from the system is equal to the rate of heat conduction at the wall. Thus, understanding how the solid thickness is affected by electro-convection will provide an understanding of how the energy extracted will be affected. From Equation 4.31 it is clear that as the thickness of the solid becomes larger the rate of energy being discharged from the system increases. Figure 4-18 through Figure 4-21 shows the difference between the solid front location for the case where the liquid thermal conductivity is enhanced and the case with no liquid thermal conductivity enhancement.

$$Q_{extracted} = kA\,\frac{\partial T}{\partial x_{wall}} \sim kA\,\frac{(T_m - T_w)}{S} \qquad [4.31]$$

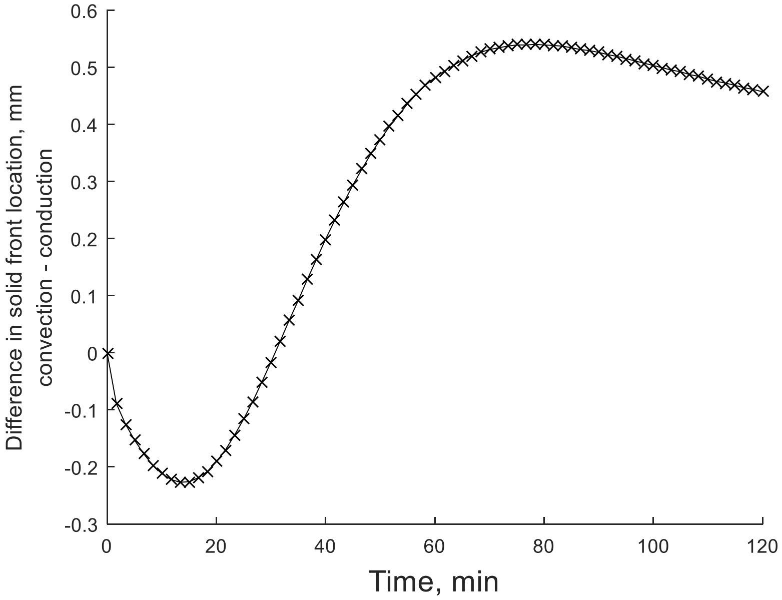

Figure 4-18: Difference between solid front location for the electro-convection and the conduction cases wall temperature of 8.5℃, initial temperature of 40℃

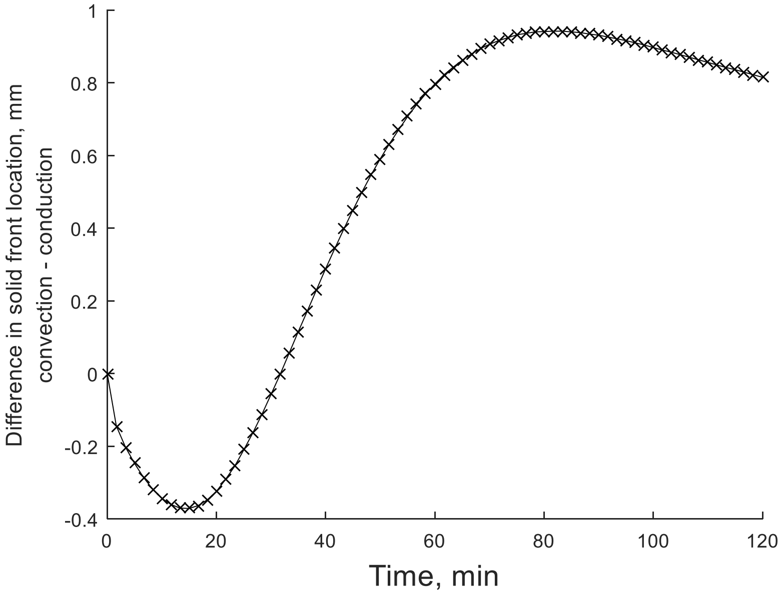

Figure 4-19: Difference between solid front location for the electro-convection and the conduction cases wall temperature of 8.5℃, initial temperature of 50℃

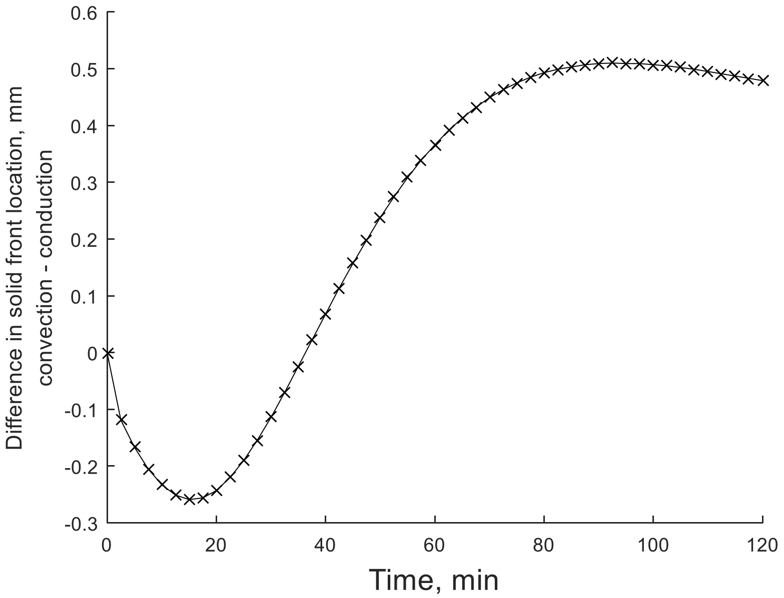

Figure 4-20: Difference between solid front location for the electro-convection and the conduction cases wall temperature of 15.5℃, initial temperature of 40℃

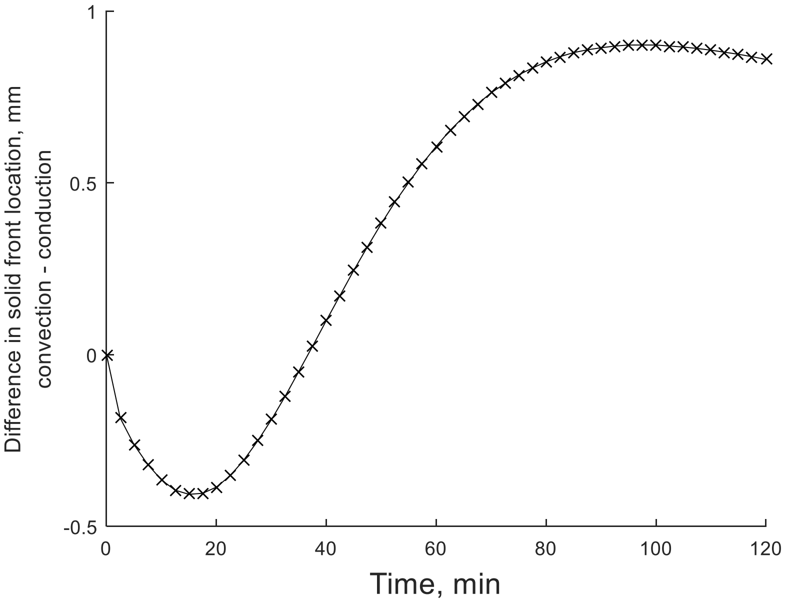

Figure 4-21: Difference between solid front location for the electro-convection and the conduction cases wall temperature of 15.5℃, initial temperature of 50℃

There are four distinct regions that are seen in the numerical results. To understand these regions, it is important to reconsider Equation 4.31, the energy balance on the solid-liquid interface. The first region is defined as the time from the instant the constant wall temperature is applied and the point where the curves, in Figure 4-21, reach a minimum. In the first region, the growth rate of the convection condition is slower than that of the conduction condition. The thickness of the solid for the convection condition is also smaller. The thinner solid layer implies the energy being removed from the interface is higher. However, the energy being removed from the liquid is much higher due to convection. In this region, the liquid temperature drops faster than the liquid temperature does for the pure conduction condition. This can be seen in Figure 4-21. The temperature of the liquid in the convection case is smaller than that of the conduction case, this is true for both of the wall temperature cases tested.

The temperature of the liquid falls faster in the convection case than the conduction case and the convection case is thinner than the conduction case. The decreasing temperature of the liquid is significant because this means that the liquid heat flow term in Equation 4.20 will decrease faster in the convection case; this has the effect of increasing the growth rate of the convection case relative to the conduction case. The fact that the solid layer in the convection case is thinner than it is in the conduction case means that the heat transfer from the solid-liquid interface is higher for the convection case. These two facts imply that the growth rate of the convection case will overtake the growth rate of the conduction case. When this happens, the minimum in the difference between the two thicknesses occurs, which is seen in Figure 4-21. This instant marks the start of region 2. Region 2 extends until the point where the two cases have the same thickness, which is seen in Figure 4-21, where the curve crosses the x-axis. In this region, the growth rate of the convection case is faster than that of the conduction case.

In region 2, the convection case is thinner than the conduction case. In this region, the higher rate of heat transfer leaving the interface and the lower rate of heat transfer entering the interface in the convection case, are responsible for the faster growth rate. However, once the convection case is thicker than the pure conduction case, the rate of heat leaving the solid is higher for the conduction case, and the rate of heat entering the interface is lower for the convection case. The difference in driving forces before and after the zero is responsible for the inflection point that occurs in Figure 4-21, and marks the start of region 3. Region 3 extends from the point where the two cases have an equal thickness to the maximum in the difference between the two cases. In this region, the convection case continues to grow faster than the conduction case and has a greater thickness.

As the temperature of the liquid gets close to the melting temperature, a maximum in the difference between the two cases occurs. The reason for this is the energy leaving the interface is high in the conduction case and the energy entering the interface is approaching zero for the conduction case, whereas in the convection case, the energy entering the interface is almost zero. This point marks the start of region 4 and after this point, the difference between the two cases continues to shrink until the end of solidification, which is seen in Figure 4-21.

From a high-level perspective, the reason why adding convection improves the rate energy is removed from a latent heat thermal storage system is that the sensible energy of the liquid is removed when the solid layer is thinner. The reason why the thickness is important is the thermal resistance of the solid layer increases linearly with thickness. Thus, the sensible energy of the liquid will have less of an effect when it is removed when the solid layer is thinner than when it is removed when the solid layer thicker.

4.3.6 Summary of the effect of convection

A numerical model was used to estimate the effect of convection on the rate of energy discharge from a latent heat thermal storage system. The numerical model simulated the effect of convection using an effective thermal conductivity. The results of the analysis show that in general applying convection increases the rate of heat transfer out of the system at early stages of solidification and decreases the rate at late stages of solidification. overall the total amount of energy extracted after any period of time will always be larger for the convection case compared to the conduction case, but this amount will only be a few percent at the end of solidification for a thermal conductivity improvement of 3 times.

4.4 Modelling the Effects of Solid Extraction

Solid extraction is a phenomenon where solid particles of phase change material are pulled into the liquid. The mechanism responsible for this phenomenon is the interfacial force that acts on the interface between the solid and liquid phase change material (Nakhla et al. 2015). The interfacial force was modelled in Section 4.1.4. Solid extraction affects the rates of heat transfer inside the latent heat thermal storage system in two ways. One way that solid extraction affects heat transfer is by removing the solid material from the heat exchanger surface; the solid material on the heat exchanger acts a layer of low thermal conductivity insulation, so removing increases the rate of heat transfer. The other way that solid extraction enhances heat transfer is by increasing the contact area between the solid and liquid phase change material. When the solid particles are removed from the solid material, it exposes more surface area to the liquid phase change material allowing them to melt faster. It is more a practical way to think of this enhancement as an increase in the heat transfer coefficient between the solid liquid interface and the liquid phase change material. This second method of enhancement only increases the rate that the sensible energy in the liquid will be removed. For the cases being analysed in this study, the sensible energy stored in the liquid is small, so only the effect of removing the solid from the heat exchanger will be analysed.

Solid extraction increases the rate of solidification by reducing the thermal resistance of the solid layer while keeping the total energy discharged the same or is greater. To understand the benefit of solid extraction consider two cases, one with solid extraction and one without extraction. For this analysis, the temperature profile in the solid will be assumed to be quasi-steady state, or completely linear. Since the temperature profile in the solid is assumed to be quasi-steady, in both cases the energy being extracted from the system is inversely proportional to the thickness of the solid thickness on the heat exchanger. The energy extracted is can be determined using Equation 4.32. In Equation 4.32, k is the thermal conductivity, A is the area of the heat exchanger, T_m is the melting temperature of the material, T_w is the wall temperature and S_1 is the thickness of the solid on the heat exchanger. In Figure 4-22 it is clear the thickness of the solid layer on the heat exchanger is smaller in the solid extraction case than in the non-solid extraction case, for the same total thickness. Thus, if the total thickness is the same, the rate of heat transfer is larger for a case with solid extraction than it is for the case without it. The ideal case would be one where the rate of solid extraction is so high that the solid layer stays negligibly thin. In reality, the temperature profile will not be exactly linear, as it is in the quasi-steady case, so the heat extracted will not necessarily be equal to Equation 4.32. However, the trend between the real case and quasi-steady will be the same.

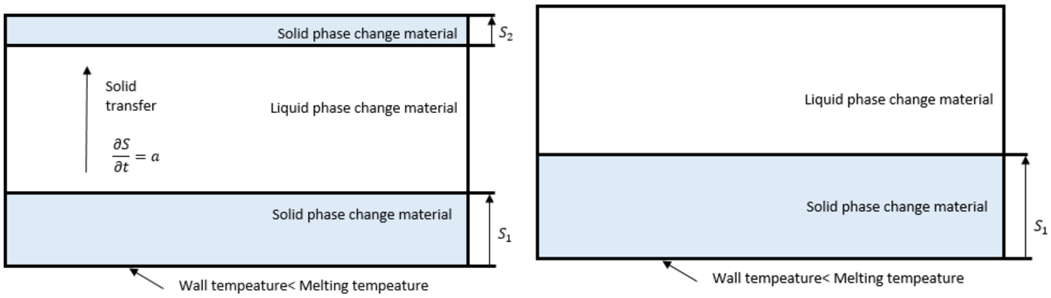

Figure 4-22: Comparison of the thickness of the solid layer on the heat exchanger for the cases with and without solid extraction

$$Q_{out} = kA\frac{T_m - T_w}{S_1} \qquad [4.32]$$

The effect of adding solid extraction can be modelled by applying a time varying function that removes material from the interface. In an ideal system, this solid will be transferred from the solid-liquid interface directly to the opposite side of the container. Calculating the rate at which particles are extracted from the interface requires knowledge about the mechanisms that cause solid extraction and how these mechanisms are affected by the electric field distribution and material properties. To provide an example of how solid extraction could affect the solidification rate consider a one-dimensional Stefan problem, where the rate of solid extraction is constant according to Equation 4.33. In this equation, S_2 is the thickness of the solid growing on the adiabatic side of the container and a is the rate that material is pulled from the solid-liquid interface. The domain used in the analysis is shown in Figure 4-23. To simplify the analysis and to gain insight into the problem, the quasi-steady-state analysis will be made, as depicted in Equation 4.34. In these equations, S_1 denotes the thickness of the solid layer on the heat exchanger, and S_2 denotes the thickness of the opposite side of the container. In this equation, ρ is the mass density, H is the latent heat of fusion of the material, A is the area of the heat exchanger, k is the thermal conductivity of the material. Equation 4.35 shows the integration of Equation 4.33 from 0 to a time, t, assuming that the initial thickness is zero. ρ is the mass density, H is the latent heat of fusion, T_m is the melting temperature and T_w is the wall temperature. Equation 4.36 shows the explicit discretized form of Equation 4.34 from 0 to a time t, assuming that the initial thickness is zero. In Equation 4.36 the superscript indicates whether the solid front using in the calculation is the solid front for the new timestep, represented by n, or the old timestep represented by o. A mesh sensitivity analysis was conducted to determine the time step required to get good results, resulting in a time step of 1s. The total thickness of the solid is considered to be the thickness of the solid on the heat exchanger plus the thickness of the solid on the opposite wall, seen in Equation 4.37.

$$\frac{\partial S_2}{\partial t} = a \qquad [4.33]$$

$$\rho\, H\, A\frac{\partial S_1}{\partial t} + a = kA\frac{T_m - T_w}{S_1} \qquad [4.34]$$

$$S_2 = a\, t \qquad [4.35]$$

$$S_1^n = \Delta t\left(\frac{k(T_m - T_w)}{\rho H S_1^o} - \frac{a}{\rho H A}\right) + S_1^o \qquad [4.36]$$

$$S = S_1 + S_2 \qquad [4.37]$$

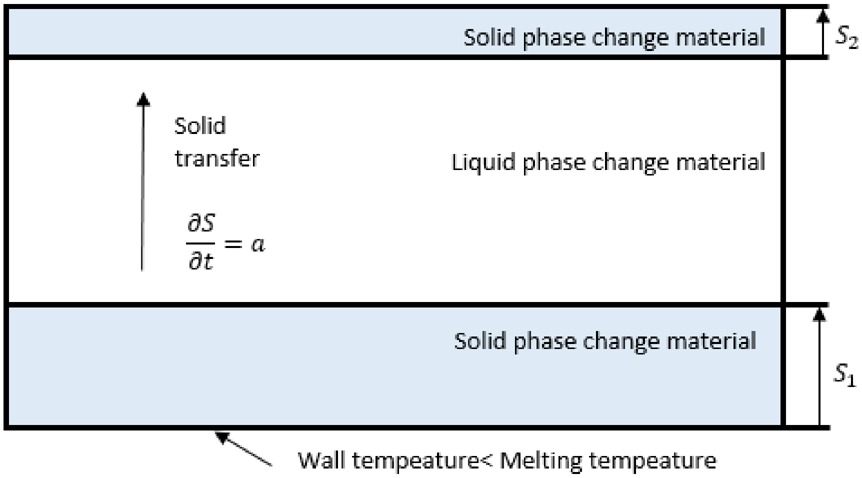

Figure 4-23: Illustration of the domain used in analysis of solid extraction

4.4.1 Validation

The code was compared to the analytical solution to validate the code. The analytical solution can be found by integrating Equation 4.38 to get Equation 4.39. In these equations, the variables are the same as those in Equations 4.33-4.37. Figure 4-24 shows a comparison between all of the cases. The cases show that the code and the analytical solution overlap.

$$\rho H A \frac{\partial S_1}{\partial t} = kA \frac{T_m - T_w}{S_1} \quad [4.38]$$

$$S_1 = \left(\frac{2k(T_m - T_w)}{\rho H}\right)^{1/2} \quad [4.39]$$

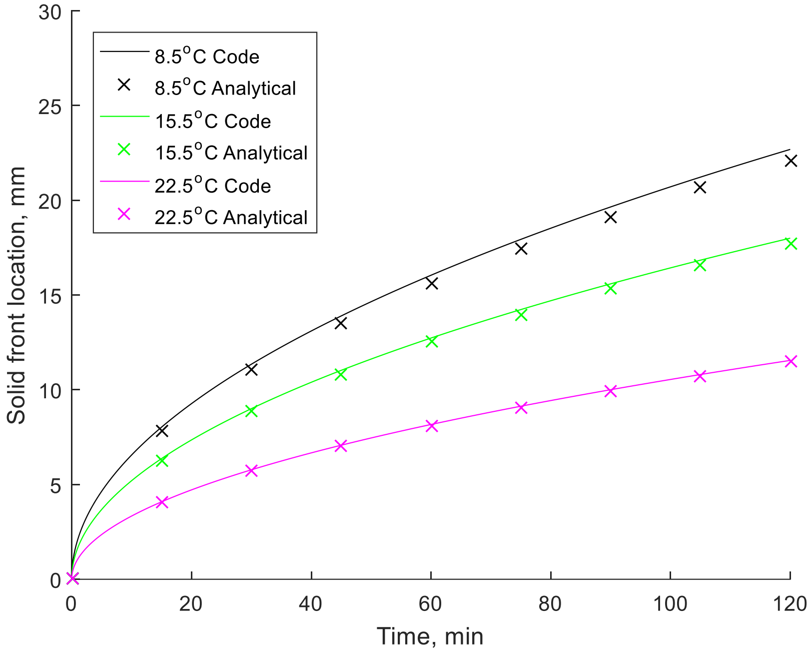

Figure 4-24: Validation of the solid extraction model against the one dimensional Stefan solution

4.4.2 Results of solid extraction model

The results of the analysis show that as the rate of solid extraction is increased the thickness of the solid increases. The increase is shown in Figure 4-25 through Figure 4-27. The results show that for extraction rates on the order of 0.1 $\frac{\mu m}{s}$ the solidification rate begins to deviate from the non-extraction case. Reconsidering the interfacial force found in Section 4.1.4 and presented in Figure 4-9 the largest stress acting on the solid-liquid interface is less than 25 Pa, which for most materials is well below the failure strength of the material. Therefore, an extraction rate with of 0.1 $\frac{\mu m}{s}$ is not expected.

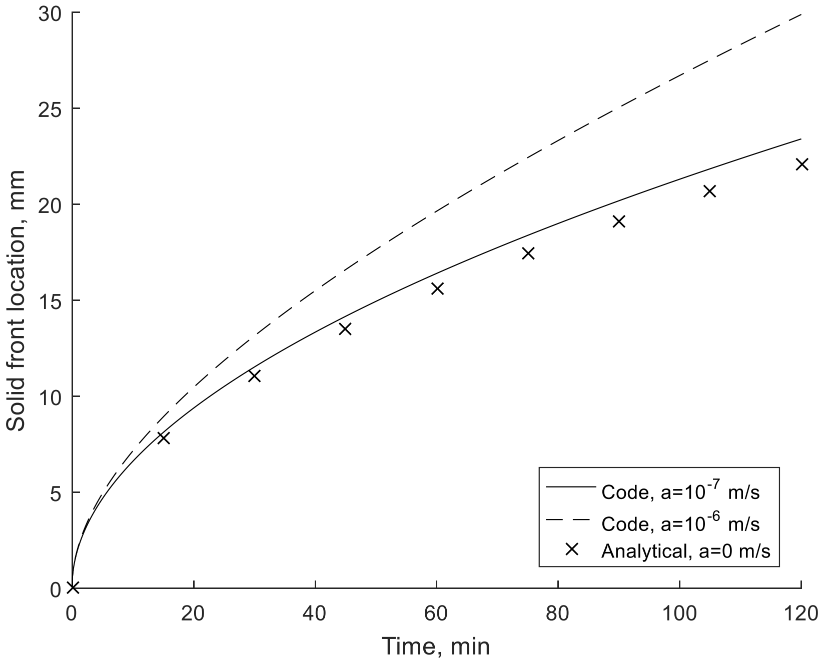

Figure 4-25: Numerical solution of solidification with solid extraction 8.5℃ wall temperature

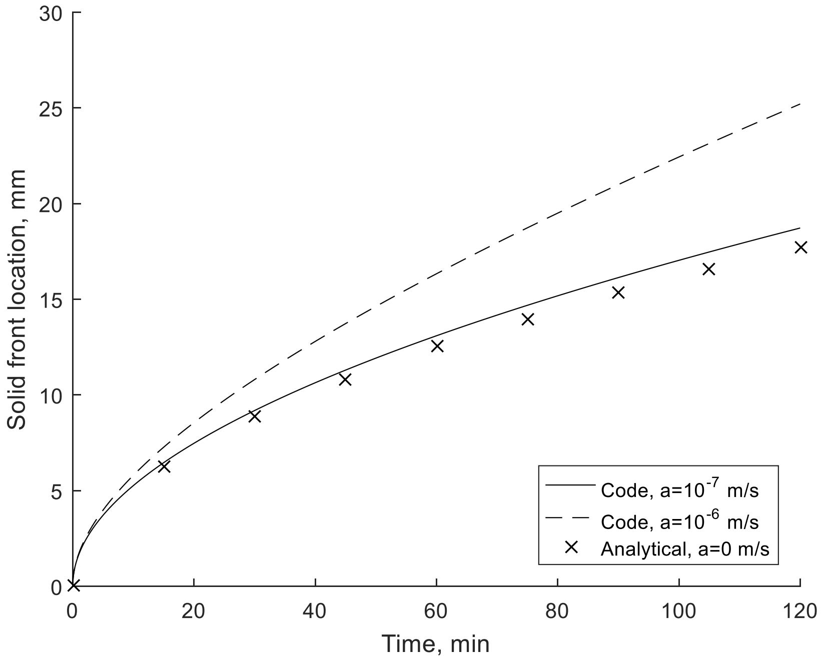

Figure 4-26: Numerical solution of solidification with solid extraction 15.5℃ wall temperature

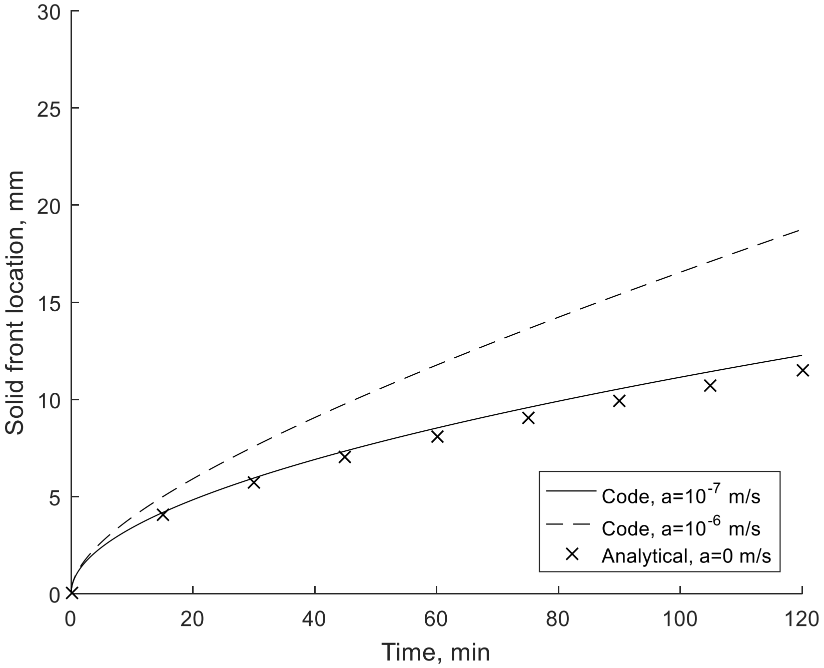

Figure 4-27: Numerical solution of solidification with solid extraction 22.5℃ wall temperature

4.5 Entropy analysis of the numerical interface tracking model

Sciacovelli et al. (2016) approached the design of a heat exchanger with fins by minimizing entropy analysis. A similar analysis will be conducted for the convection model to understand the role that entropy minimization can be used in designing the electrode geometry for electrohydrodynamic heat transfer enhancement techniques. The rate of local entropy generation is given by Equation 4.40 (Sciacovelli et al. 2016). In Equation 4.40, $\dot{S}'''_{gen}(x,t)$ is the local entropy generation per unit volume at a position x and time t, τ is the fluid stress tenors, ∇v is the gradient of the velocity field, T is the temperature and k is the thermal conductivity. The first term on the right-hand side of the equation is the entropy generation due to viscous dissipation in the fluid, the second term is the entropy generation due to heat transfer through a temperature gradient. For the one dimensional analysis in Section 4.3, the fluid motion was not calculated. Therefore for this entropy analysis, the viscous term will be removed. This method is not an accurate way to model the enhancement due to electrohydrodyanmics; however, it is the only way to perform the analysis without knowledge of the velocity field. Thus, Equation 4.41 will be used in this analysis. Equation 4.41 was then discretized, using a first order, explicit, finite difference discretization technique and Equation 4.42 was then used in the numerical model. In this equation, i, is an index representing each node. To get the total entropy generation per unit area Equation 4.42 was integrated over the time coordinate and the space coordinate, which is given in Equation 4.43. The results of the analysis are shown in Table 4-3. The results show that as the thermal conductivity is increased the rate of entropy generation is not affected. This result is expected because the overall change in the results at the end of solidification is only a few percent, so it's not surprising that the entropy generation is almost identical. It is expected that because as the thermal conductivity of the liquid increases the entropy generation will also increase, because more energy is discharged at the early stages of solidification when the temperature gradients are the largest. This result is contrary to the results of the analysis done by Sciacovelli et al. (2016), who found that decreasing entropy generation improved the heat transfer rate.

$$\dot{S}'''_{gen}(x,t) = -\frac{\tau:\nabla v}{T} + \frac{k(\nabla T)^2}{T^2} \qquad [4.40]$$

$$\dot{S}'''_{gen}(x,t) = \frac{k(\nabla T)^2}{T^2} \qquad [4.41]$$

$$\dot{S}'''_{gen}(i,t) = \frac{k(T_{i+1}-T_{i-1})^2}{T_i^2(x_{i+1}-x_{i-1})^2} \qquad [4.42]$$

$$\dot{S}_{gen} = \int\int \dot{S}'''_{gen}(i,t)\, dt\, dx \qquad [4.43]$$

Table 4-3: Results of entropy generation analysis

Test Condition	Thermal conductivity enhancement	Entropy generation, $\frac{J}{m^2}$
8.5℃ wall temperature, 50℃ initial temperature	$k_L = 1 \times k_L$	4.3×10^{11}
8.5℃ wall temperature, 50℃ initial temperature	$k_L = 2 \times k_L$	4.3×10^{11}
8.5℃ wall temperature, 50℃ initial temperature	$k_L = 3 \times k_L$	4.3×10^{11}
8.5℃ wall temperature, 50℃ initial temperature	$k_L = 6 \times k_L$	4.3×10^{11}
15.5℃ wall temperature, 50℃ initial temperature	$k_L = 1 \times k_L$	2.4×10^{11}
15.5℃ wall temperature, 50℃ initial temperature	$k_L = 2 \times k_L$	2.4×10^{11}
15.5℃ wall temperature, 50℃ initial temperature	$k_L = 3 \times k_L$	2.5×10^{11}
15.5℃ wall temperature, 50℃ initial temperature	$k_L = 6 \times k_L$	2.5×10^{11}
15.5℃ wall temperature, 40℃ initial temperature	$k_L = 1 \times k_L$	6.3×10^{10}
15.5℃ wall temperature, 40℃ initial temperature	$k_L = 2 \times k_L$	6.4×10^{10}
15.5℃ wall temperature, 40℃ initial temperature	$k_L = 3 \times k_L$	6.4×10^{10}
15.5℃ wall temperature, 40℃ initial temperature	$k_L = 6 \times k_L$	6.4×10^{10}

4.6 Summary of analytical modeling

Three analytical models have been used to attempt to understand the effect of electrohydrodynamics on the solidification of an organic phase change material. One of the models is an analysis of the electric field distribution and the resulting electric body forces and interfacial forces. This analysis showed that the convection cells should flow in the direction from the heat exchanger to the electrodes in the regions directly beneath the electrodes and in the direction from the electrodes to the heat exchanger in the regions between the electrodes. Another of the models focused on the effect of convection on the rate of solidification and the rate of energy discharged from the system. The model used an effective thermal conductivity to simulate convection. It was found that applying convection increases the rate of energy extraction at the early stages of solidification and reduces the rate of energy extraction at the late stages. Overall applying convection results in a small increase in the rate of energy extracted when the entire time period is considered. The third model predicts the effect of solid extraction on the solid front location; solid extraction was modelled as a constant rate of material removal at the solid-liquid interface. The analysis showed that applying solid extraction acts to increase the rate of solidification and the rate of energy discharge. An analysis of the entropy generation was also performed and the analysis found that changing the thermal conductivity of the liquid did not change the entropy generation.

5 Experimental Results

To understand the effect of electrohydrodynamics on the solidification of a phase change material in a latent heat thermal storage system, experiments were performed. The phase change material was initially liquid in these experiments and was solidified by running cold water through a heat exchanger, water temperature was kept constant throughout the experiments. Three initial temperature and three wall temperature were tested, the initial temperature being 30℃, 40℃ and 50℃ and the wall temperature were 8.5℃ 15.5℃ and 22.5℃. An electric field was generated in the phase change material by grounding the heat exchanger and applying an electric potential to electrodes which were dispersed through the phase change material, the applied electric potentials were 0 kV and -8kV. The goal of these experiments was to understand the effect of electrohydrodynamics on the rate of energy discharged from the system. The difference in the electrohydrodynamic cases and the pure conduction experiments was quantified using two enhancement factors, one called the solid thickness ratio improvement and one called the energy enhancement factor.

This study is one of a few studies investigating applying electrohydrodynamics to a material undergoing a solid-liquid phase change. This investigation sought to answer one specific question regarding this process of solid-liquid phase change in the presence of an electric field. There are still many other investigations that must be completed before this topic is well understood. A few of these investigation are:

- A model that accurately predicts the electro-convective currents when an electric field is applied.
- A model that describes solid extraction in terms of the stresses acting in the material and when the solid dendrites separate from the rest of the solid.
- A study of each of the individual electric body forces, electrophoretic, dielectrophoretic and electrostrictive and the relative magnitude of each of these forces. This study will provide an

understanding of when each of these forces becomes important and what the is contribution of each of the forces to the overall heat transfer enhancement.

- An investigation on the rate of solid extraction at the solid-liquid interface using high-speed imaging of the solid-liquid interface would be useful in providing an understanding of solid extraction.
- This investigation used Octadecane which is only one specific type of phase change material. The conclusions drawn with this material may not be applicable to other phase change materials. Octadecane is a non-polar, short chain length, non-branching hydrocarbon consisting of only carbon and hydrogen atoms. An understanding of the effect of polarity, chain length, side branches and variants on the basic monomer would be useful and required to generalize the results to other phase change materials.
- More engineering based investigations would be required as well, for example an investigation into how to design the electrodes to maximize heat transfer would be useful.
- Also an understanding of how electrohydrodynamics can be used with other enhancement techniques such as Nano-particles and Fins would provide a better understanding of how to enhance heat transfer using electrohydrodynamics.

5.1 Effect of electrohydrodynamics on the energy discharged

The experimental results show a similar trend to that of numerical results. The electro-convection case and the pure conduction case show comparable similar results. The difference between the two curves is within the experimental error for most points; however, the extreme points do show a deviation which supports the conclusions of the numerical results. This solid front location for the -8kV and the 0kV cases are illustrated as a function of time are illustrated in Figure 5-1, Figure 5-2 and Figure 5-3. It is seen that applying the electric field at low superheat has no effect on the growth rate, which is seen in Figure 5-1. This finding is in contrast to the results found by Dellorusso (1997) who concluded that the application of an electric field to the solidification of paraffin wax slows down the rate of solidification. The discrepancy between the two results is likely due to either microstructural changes in paraffin wax during solidification, which may not exist in the octadecane or it could be undercooling of the melt interface due to concentration or nucleation effects that the electric field brings about. These discrepancies can be deduced by considering Equation 2.7, in this equation there are only three ways to decrease the heat transfer either change the thermal conductivity (which requires a microstructural change), change the temperature gradient (which requires the melting temperature to change) or decrease area (which applying electrohydrodynamics will increases because the convection cells will induce a curved pattern on the interface) (Nakhla et al, 2015). It was also observed during the experiments that the fluid was being repelled from the electrode which indicates that the primary source of the convection was the electrophoretic force, since in this case, the dielectrophoretic force attracts the colder phase change material, as seen in Section 4.1.

$$Q_{interface\ to\ wall} = kA\frac{\partial T}{\partial x} \tag{2.7}$$

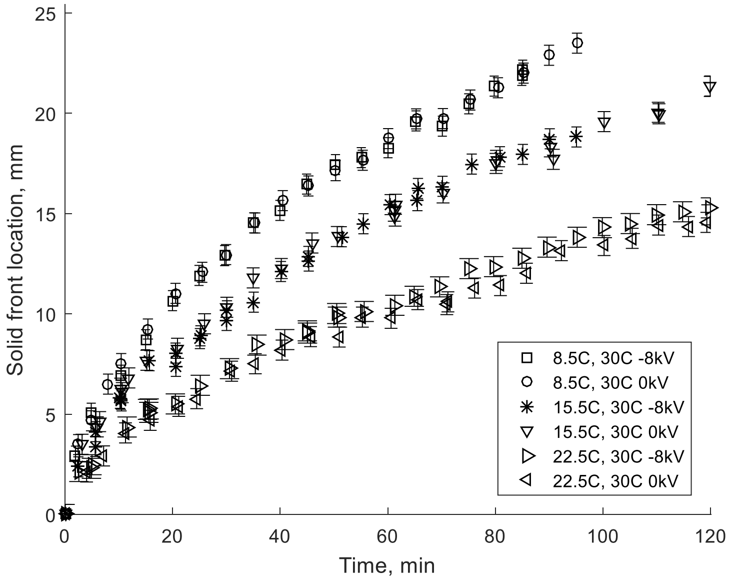

Figure 5-1: Experimentally measured solid front with 30℃ initial temperature, for various wall temperatures

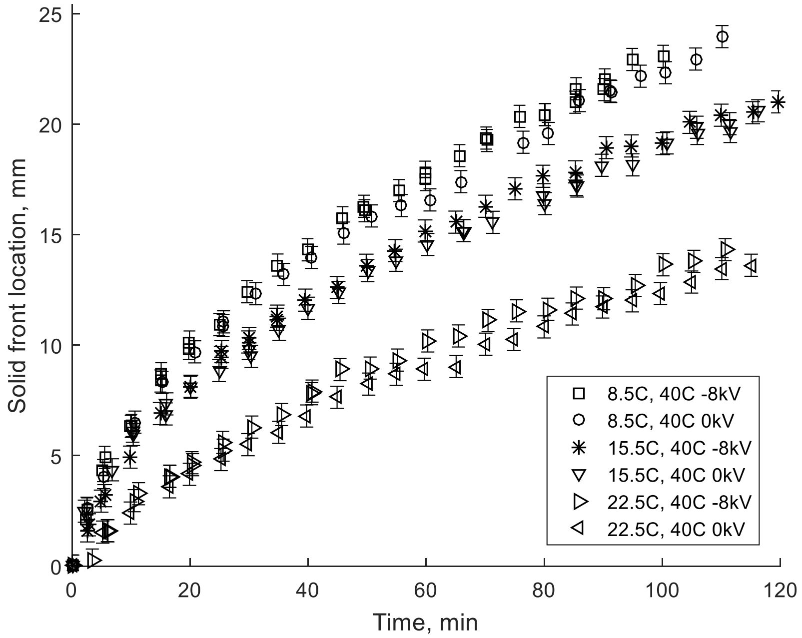

Figure 5-2: Experimentally measured solid front with 40℃ initial temperature, for various wall temperatures

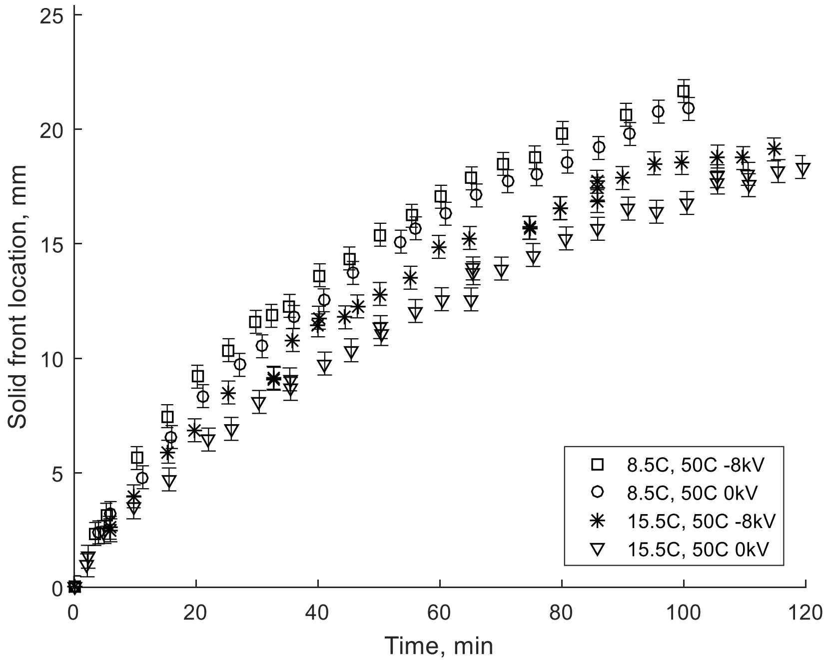

Figure 5-3: Experimentally measured solid front with 50℃ initial temperature, for various wall temperatures

The solid front location measurement can be used to approximate the energy extracted from the system. The latent energy extracted from the system can be determined using Equation 5.1, which simply takes the volume of the solid and multiplies it by the latent energy of fusion per unit volume. The sensible energy within solid phase change material can be found using Equation 5.2; the assumption that the temperature profile of the solid is linear was made. This assumption is supported by the numerical results, which show that the temperature profile in the solid is nearly linear. The sensible energy in the liquid is more difficult to account for as a function of distance. However, the results from the numerical analysis can be used to generate relationships between the solid front location and the average temperature of the liquid. Once this relationship is known Equation 5.3 can be used to determine the sensible energy of the liquid phase. Equations 5.1, 5.2 and 5.3 can be added to get the total energy in the system, given by Equation 5.4. In these equations, ρ is the mass density, A is the area of the heat exchanger, H is the latent heat of fusion, S is the solid front location, C_p is the specific heat, T_m is the melting temperature, T_s is the average solid temperature, T_w is the wall temperature, L is the length of the container, $T_{f,initial}$ is the initial temperature of the fluid, $T_{f,ave}$ is the average temperature of the fluid and T_m is the melting temperature of the fluid. Equation 5.1 is simply a statement that the latent energy discharged from the phase change material is equal to the mass of phase change material that has solidified. Equation 5.2 states that the sensible energy discharged from the solid is equal to the temperature decrease in the solid material, and Equation 5.3 states that the sensible energy discharged from the liquid is equal to the temperature decrease within the liquid. Equation 5.4 states that the total energy discharged from the system can be broken down in the amount of energy discharged from the system from the latent energy and the solid and liquid sensible energy. The average temperature of the liquid phase as a function of the solid front location is provided in Table 5-1. Using this information the energy extracted in each of the cases can be determined and compared, with the results being shown in Figure 5-4 through Figure 5-6. This is only a rough approximation of the energy discharged from the liquid. However, no measurements of the sensible energy in the liquid were taken, so using the numerical results provides a way of estimating this energy. To measure the sensible energy in the liquid several thermal couples would have needed to be placed throughout the liquid phase change material. In general, the energy extracted results show a similar trend to that of the solid front location. The result that the energy extracted and solid front location show similar trends is expected since a majority of the energy stored in the system is in the latent form. Furthermore, the sensible energy in the liquid will be nearly zero at times later in the solidification process, so the energy extracted at these times will be a linear function of the solid front location. The uncertainty associated with this can be found using Equation 5.5. In Equation 5.5, S_U is the uncertainty on the solid front location and $U_{E,total}$ is the uncertainty in the energy discharged.

$$E_{Latent} = \rho\ A\ H\ S \tag{5.1}$$

$$E_{Sensible,s} = \rho\ A\ C_p \int_0^S (T_m - T_s) ds \sim \rho\ A\ C_p\ S\ \frac{(T_m - T_w)}{2} \tag{5.2}$$

$$E_{Sensible,l} = \rho\ A\ C_p * [\ (L - S\ ) * \left(T_{f,initial} - T_{f,ave}\right) + S * \left(T_{f,initial} - T_m\right)] \tag{5.3}$$

$$E_{total} = E_{latent} + E_{sensible,s} + E_{sensible,l} \tag{5.4}$$

$$U_{E,total} = \ \rho\ A\ H\ S_U + \rho\ A\ C_p\ S_U\ \frac{(T_m - T_w)}{2} + \rho\ A\ C_p S_U \left(T_{f,i} - T_m\right) \tag{5.5}$$

Table 5-1: Curve fit relationships that describe the decrease in the fluid temperature as a function of the solid front location

Condition	Functional relationship for fluid temperature Tf[C], S[mm]	Bounds
8.5℃, 50℃, no electric field	$7.24 * 10^{-3}S^3 - 1.68 * 10^{-1}S^2 - 5.42 * 10^{-1}S + 50$	S<16mm
8.5℃, 40℃, no electric field	$3.62 * 10^{-3}S^3 - 9.14 * 10^{-2}S^2 - 2.24 * 10^{-1}S + 40$	S<16
8.5℃, 30℃, no electric field	$6.70 * 10^{-4}S^3 - 1.85 * 10^{-2}S^2 - 2.89 * 10^{-2}S + 30$	S<18
15.5℃, 50℃, no electric field	$8.75 * 10^{-3}S^3 - 1.56 * 10^{-1}S^2 - 1.12\, S + 50$	S<16
15.5℃, 40℃, no electric field	$4.69 * 10^{-3}S^3 - 9.41 * 10^{-2}S^2 - 4.77 * 10^{-1}\, S + 40$	S<16
15.5℃, 30℃, no electric field	$9.77 * 10^{-4}S^3 - 2.18 * 10^{-2}S^2 - 6.20 * 10^{-2}\, S + 30$	S<16
22.5℃, 40℃, no electric field	$1.21 * 10^{-2}S^3 - 1.43 * 10^{-1}S^2 - 0.998S + 40$	S<11
22.5℃, 30℃, no electric field	$2.13 * 10^{-3}S^3 - 3.03 * 10^{-2}S^2 - 0.155S + 30$	S<11
8.5℃, 50℃, electric field	$1.63 * 10^{-3}S^3 + 7.39 * 10^{-2}S^2 - 3.01S + 50$	S<12
8.5℃, 40℃, electric field	$1.75 * 10^{-3}S^3 + 1.11 * 10^{-2}S^2 - 1.42S + 40$	S<12
8.5℃, 30℃, electric field	$-1.15 * 10^{-4} + 4.72 * 10^{-3}S^3 - 5.19 * 10^{-2}S^2 - 6.9 * 10^{-2}S + 30$	S<14
15.5℃, 50℃, electric field	$-9.93 * 10^{-4} + 2.78 * 10^{-2}S^3 - 6.82 * 10^{-2}S^2 - 3.38S + 50$	S<16
15.5℃, 40℃, electric field	$1.38 * 10^{-2}S^3 - 1.37 * 10^{-1}S^2 - 1.25\, S + 40$	S<10
15.5℃, 30℃, electric field	$2.56 * 10^{-3}S^3 - 3.20 * 10^{-2}S^2 - 1.90 * 10^{-1}\, S + 30$	S<11
22.5℃, 40℃, electric field	$4.94 * 10^{-3}S^3 - 1.46 * 10^{-1}S^2 - 3.06S + 40$	
22.5℃, 30℃, electric field	$5.33 * 10^{-3}S^3 - 3.55 * 10^{-2}S^2 - 0.377S + 30$	S<8

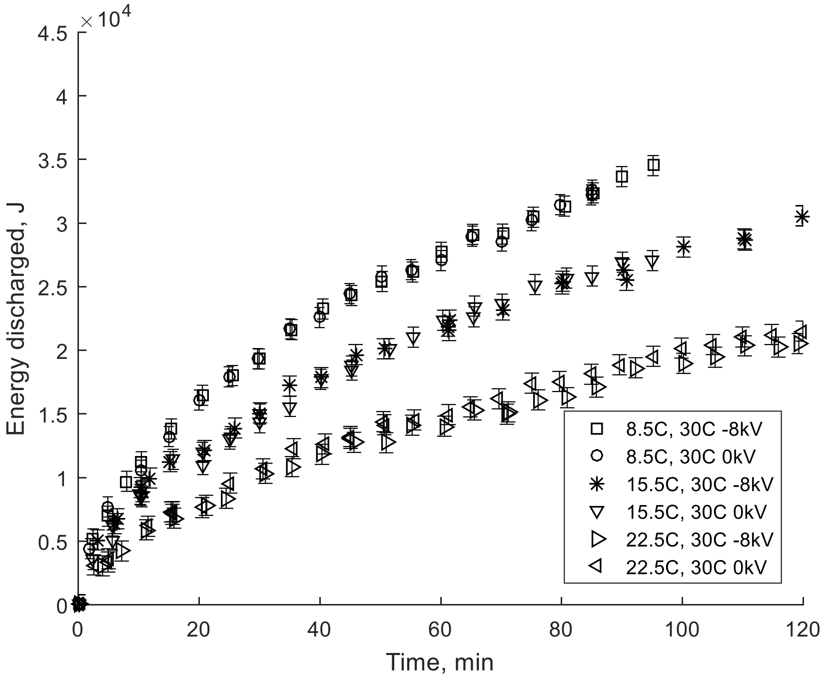

Figure 5-4: Estimated energy extracted from the system during the experiments with 30℃ initial temperature and various wall temperatures.

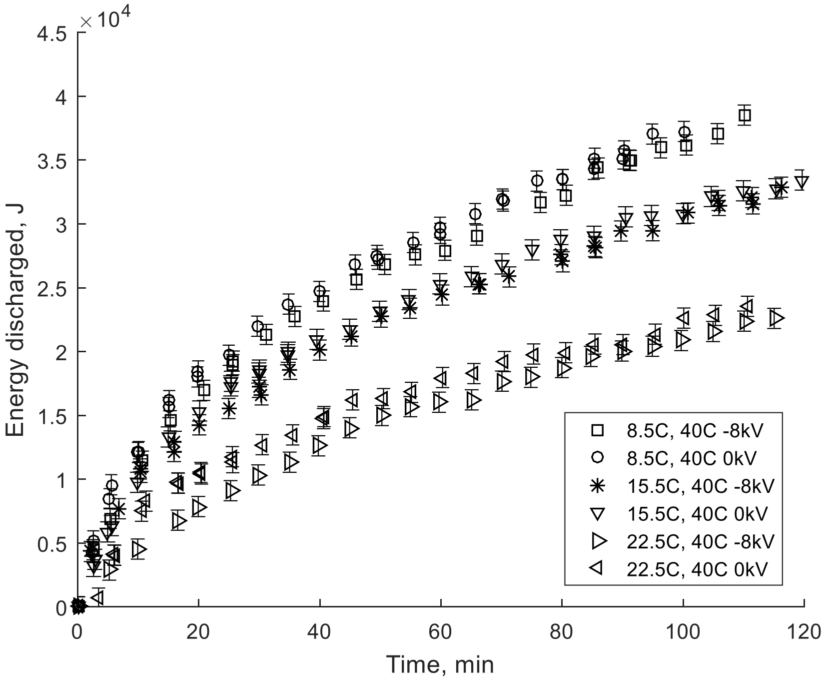

Figure 5-5: Estimated energy extracted from the system during the experiments with 40℃ initial temperature and various wall temperatures.

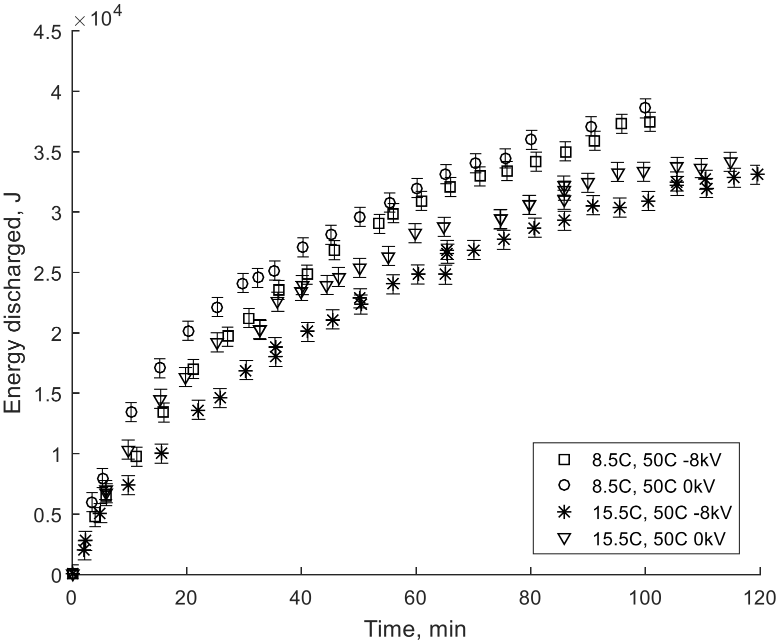

Figure 5-6: Estimated energy extracted from the system during the experiments with 50℃ initial temperature and various wall temperatures.

5.2 Solid thickness ratio improvement

To explain how much additional energy is stored in the phase change material when the electric field is generated, an enhancement factor will be used to quantify the effect. One factor that can be used to describe the extra amount of latent energy stored in the system is calculating the difference in the thickness of the solid with and without the electric field being generated, which will be referred to as the thickness enhancement factor. Equation 5.6 is an expression for the thickness enhancement factor. Equation 5.6 was used to calculate the thickness enhancement factor for both the numerical and experimental results. In Equation 5.6, TE is the thickness enhancement, S_{-8kV} is the solid front location for the case with -8 kV electric potential being applied and S_{0kV} is the solid front location for the case without an electric potential. Compute the thickness enhancement using Equation 5.6, the data first needed to be curve fit so that the results. The curves used to fit the data were found using Equation 5.7, the time to the one-half power is used because the analytical solution, presented in Section 4.2, relates the solid front location and time through a square root. In Equation 5.7, S is the solid front location t is the time coordinate and a, b, c, d, e and f are coefficients determined by minimizing the square of the residual. The results of the curve fitting process for most of the cases gives a good fit. However, the fit is not representative in areas where there is a large and sudden change in the growth rate of the solid front location.

$$TE = \frac{S_{-8kV} - S_{0kV}}{S_{0kV}} \times 100\% \tag{5.6}$$

$$S = a\, t^{1/2} + b\, t^4 + c\, t^3 + d\, t^2 + e\, t + f \tag{5.7}$$

The curve fitted experimental results and Equation 5.6 were used to determine the solid thickness ratio as a function of time. Figure 5-7 shows the solid thickness ratio for the 8.5℃ experiments. The general trend in Figure 5-7 agrees with the theory presented in Section 4.2 and Section 4.3, in that the higher the initial temperature of the liquid phase change material, the larger the solid thickness ratio and that the solid thickness ratio reaches a maximum early in the experiment and decays to a small positive number as the experiment progresses. It is also seen that the 50℃ initial temperature case has a higher solid thickness ratio than the 40℃ case and the 30℃ case shows almost no improvement. The shape of the curves in Figure 5-7 is generally not a perfect representation of the physical trend that is expected; the curves contain several inflexion points that should not physically exist. These inflexion points are likely due to the high power polynomial that is being used for curve fitting and the experimental error. The 15.5℃ experiments are presented in Figure 5-8. The trends seen in Figure 5-8 are the same as those in Figure 5-7. In general, experiment with the highest initial temperature showed the largest solid thickness ratio and the experiment with the lowest initial temperature showed the lowest solid thickness ratio. As in Figure 5-7, the curves show inflexion points that are not realistic. The 22.5℃ experiments are presented in Figure 5-9. In these experiments, the 40℃ initial temperature showed a larger solid thickness ratio than the 30℃ initial temperature. In Figure 5-9, both the initial temperatures show the solid thickness ratio decays with time. All of these, results show a very small improvement. The difference in solid thickness at the end of most of these experiments was only a few percent, and the largest solid thickness ratio at the end of an experiment was 10%. Considering that the improvement in heat transfer of some of the other methods of used in latent heat thermal storage systems, mentioned in Table 2-5 and Table 2-8, are between 500% and 20%, this method of enhancing heat transfer is not as effective as existing methods of enhancing heat transfer in latent heat thermal storage systems.

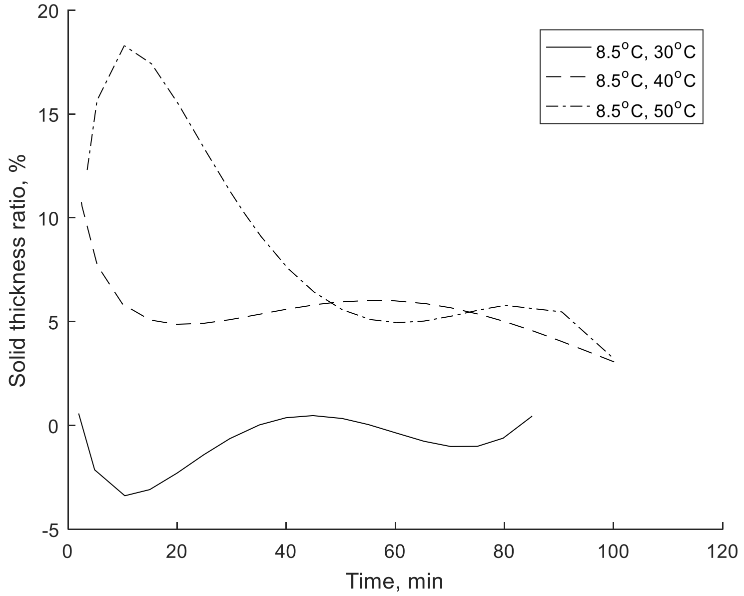

Figure 5-7: Solid thickness ratio based on curve fit experimental results for 8.5℃ wall temperature.

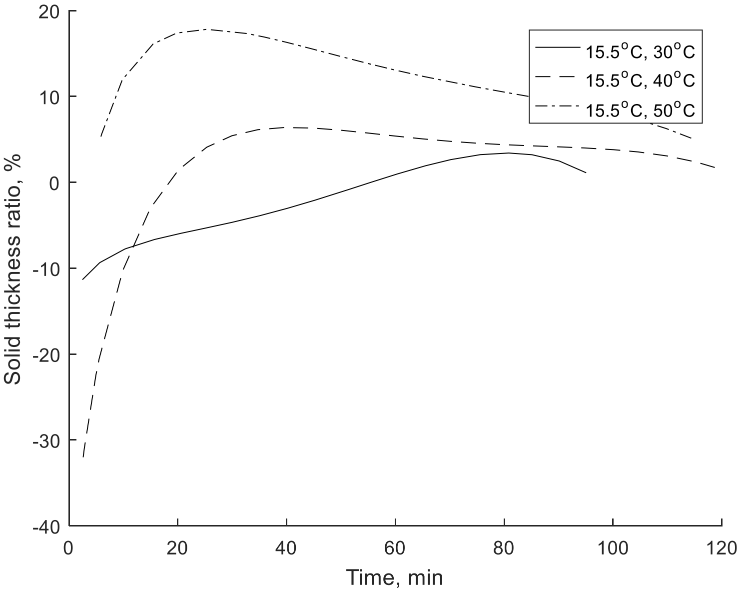

Figure 5-8: Solid thickness ratio based on curve fit experimental results for 15.5℃ wall temperature.

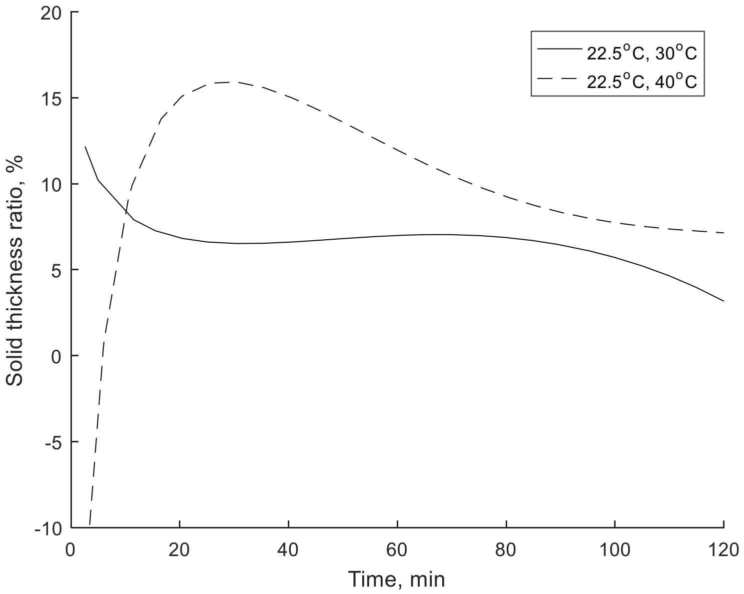

Figure 5-9: Solid thickness ratio based on curve fit experimental results for 22.5℃ wall temperature.

5.3 Energy enhancement factor

To quantify the effect of applying an electric field an enhancement factor based on the energy discharged was developed, as shown in Equation 5.8. In Equation 5.8, $E_{discharged,-8kV}$ is the energy discharged from the electro-convection case and $E_{discharged,0kV}$ is the energy discharged from the no-electro-convection case. This factor is defined the same way that the thickness enhancement factor is defined, it is the difference in the energy extracted from the electrohydrodynamic case and the pure conduction case divided by the pure conduction thickness. To observe the trends in the energy extracted results a fourth order polynomial with a square root of time term, similar to Equation 5.7, was curve fit to each of the data sets. In general the curves presented in this figures very accurately represent the experimental data they are fit to; however, the polynomial being fit to the data is a fourth order polynomial so it is not surprising that it follows the data well.

$$EF_{Energy} = \frac{E_{discharged,-8kV} - E_{discharged,0kV}}{E_{discharged,0kV}} \times 100\% \qquad [5.8]$$

The curve fitted experimental results and Equation 5.8 were used to determine the energy enhancement ratio as a function of time. Figure 5-10 shows the solid thickness ratio for the 8.5℃ experiments. Similar to the solid thickness ratio results, the general trend in Figure 5-10 agrees with the theory presented in Section 4.2 and Section 4.3, in that the higher the initial temperature of the liquid phase change material, the larger the energy enhancement ratio. The shape of the curves in Figure 5-10 are consistent, where the shapes of the curves for the solid thickness ratio are not. In general, the larger the initial temperature of the liquid phase change material the greater the enhancement. However, near the end of the experiments, all of the curves trended toward a small positive number. The curves with large initial temperatures showed large enhancements at the early stages of the experiment, indicating that the sensible energy is being removed during the early stages. This conclusion is expected because in the calculation of the energy extracted, the sensible energy transferred from the liquid to the solid-liquid interface was calculated using the numerical results from Section 4.3. Figure 5-11 shows the results of the 15.5℃ test. The solid enhancement factor for the 30℃ and 40℃ experiments is negative at the early stages of the test, which does not agree with the analysis in Section 4.3. This is likely due to experimental error, the trend corrects itself and at the late stages of the experiments all the curves are trending towards a small positive enhancement of a few percent. Figure 5-12 shows the energy enhancement factor for the 22.5℃ case. Similar to Figure 5-10, at early stages of the experiment, the high initial temperature experiment shows a large positive factor that decays toward a 5% factor by the end of the test. The no superheat scenario shows an almost constant 5% enhancement, which is likely due to experimental error. Considering that the improvement in heat transfer of some of the other methods of used in latent heat thermal storage systems, mentioned in Table 2-5 and Table 2-8, are between 500% and 20%, this method of enhancing heat transfer is not as effective as existing methods of enhancing heat transfer in latent heat thermal storage systems.

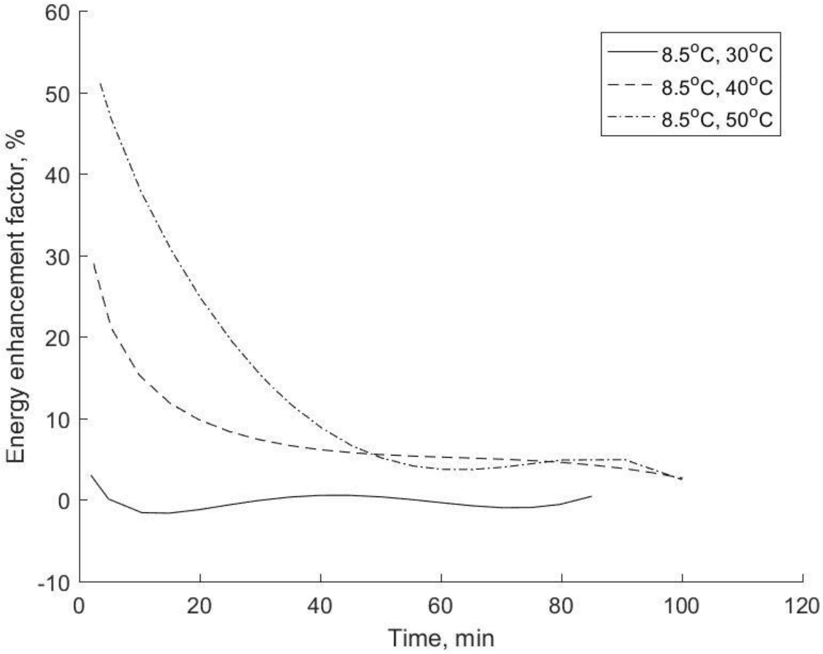

Figure 5-10: Energy enhancement factor based on curve fit experimental results for 8.5℃ wall temperature.

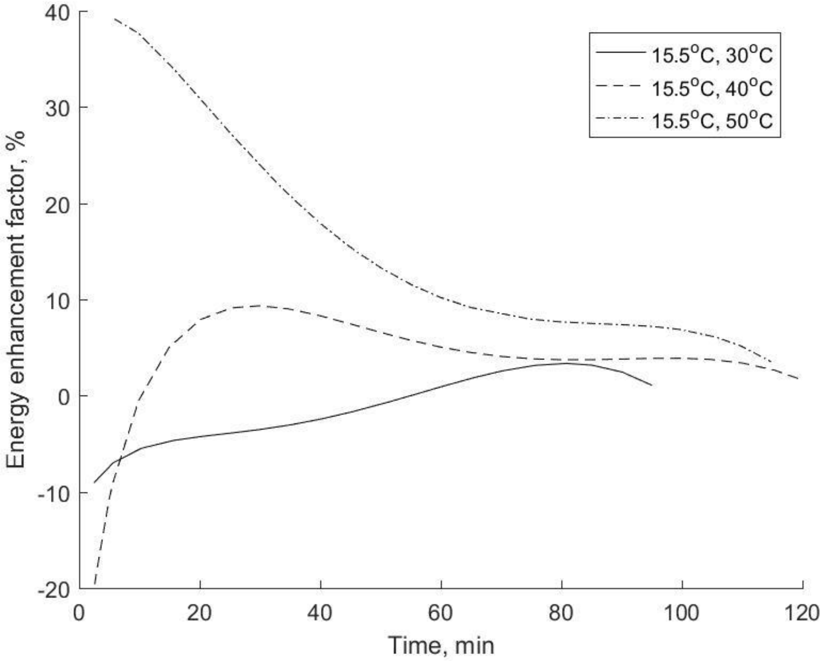

Figure 5-11: Energy enhancement factor based on curve fit experimental results for 15.5℃ wall temperature.

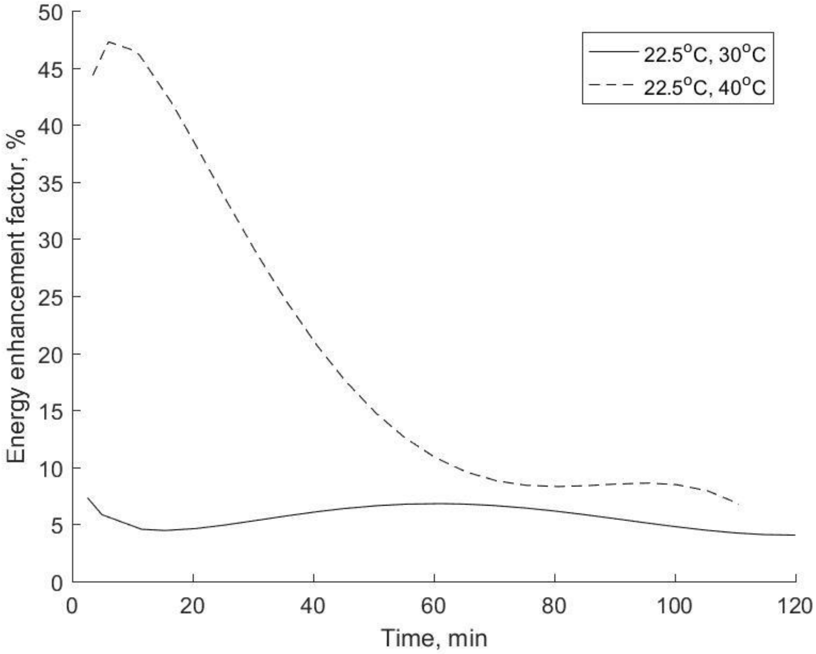

Figure 5-12: Energy enhancement factor based on curve fit experimental results for 22.5℃ wall temperature.

5.4 Measurement of solid extraction

The effect of solid extraction on the rate of energy discharged and the solid front location was analysed in Section 4.4. From the numerical models, it was shown that solid extraction will increase the solid thickness at all times. The force analysis in Figure 4-8 shows that solid particles will be pulled to the front of the electrodes. However, the force analysis in Section 4.1 also showed that the forces acting on the solid liquid interface are smaller than those seen by Nakhla et al. (2015). Thus, it is expected that the rate of solid extraction would be smaller. So if solid extraction was occurring to a significant degree, the solid particles would be visible on the front of the electrodes. However, none of the image taken in the experiments showed any solid on the front of the electrodes. Figure 5-13, Figure 5-14, Figure 5-15 and Figure 5-16 all show the electrodes during experiments where electrohydrodynamics. The solid in these images would accumulate in front of the two electrodes that are closest to the heat exchanger, which is the bottom surface in these images. This does not conclusively show that solid extraction did not occur in the experiments, but rather it indicates that if solid extraction did occur the macro effects of solid extraction were so small that it did not result in any solid build up on the electrodes.

The experiments that had a very small amount of superheat, where the initial temperature was 30℃, can be used to further analyse solid extraction. In these experiments, the effect of convection will be very small because the sensible energy in the liquid is small relative to the latent heat. Thus, if there was any difference in solid front location results it must be due to solid extraction. Figure 5-1 shows no difference between the can with an electric potential and the case with no electric potential. Thus, solid extraction did not have a significant impact on the results. Nakhla et al. (2015) measured solid extraction using a highly magnified high-speed camera to view the solid-liquid interface; this technique allowed solid extraction to be observed directly. Although this method allowed for solid extraction to be observed directly, the images didn’t have any scaling so the rate of solid extraction could not be estimated. A high-speed camera measurements were not done in this investigation because a thin layer of solid was building up on the transparent walls of the test section. This thin layer of solid obstructed the view of the solid-liquid interface and did not permit the video of the high-speed camera to take clear images of the dendrites on the interface. As a result, the videos would not have been useful in identifying solid extraction, because the solid particles could not be clearly identified. The fact that solid extraction was observed in Nakhla et al. (2015), and not this one, could be due to the higher extraction forces seen in the study. However, material strength could also be a factor. These extraction forces are discussed in Section 4.1.4.

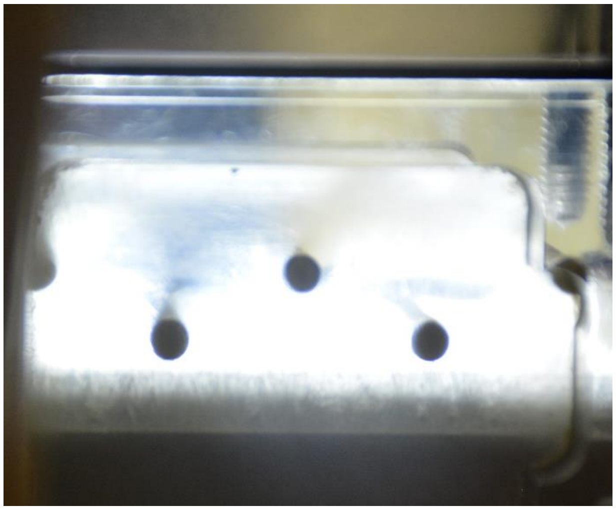

Figure 5-13: Image of the electrodes showing no solid build up in front of electrodes. -8kV electric potential applied to electrodes, 8.5℃ wall temperature 30℃ initial temperature. 2 minutes after cold wall bounda+ry condition was applied.

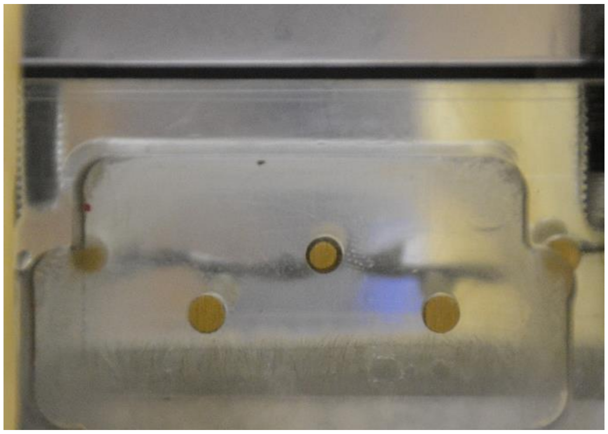

Figure 5-14: Image of the electrodes showing no solid build up in front of electrodes. -8kV electric potential applied to electrodes, 15.5℃ wall temperature 30℃ initial temperature. 2 minutes after cold wall boundary condition was applied. No backlight applied

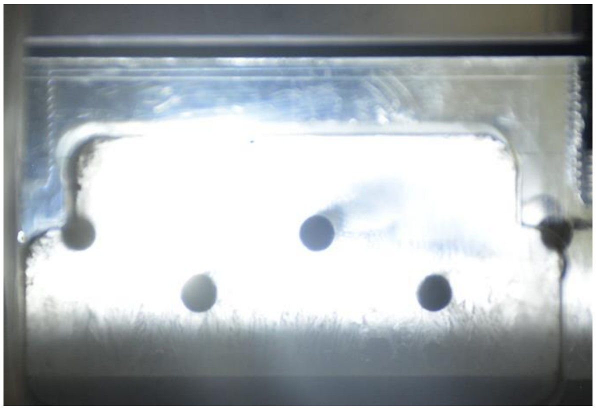

Figure 5-15: Image of the electrodes showing no solid build up in front of electrodes. -8kV electric potential applied to electrodes, 15.5°C wall temperature 30°C initial temperature. 5 minutes after cold wall boundary condition was applied.

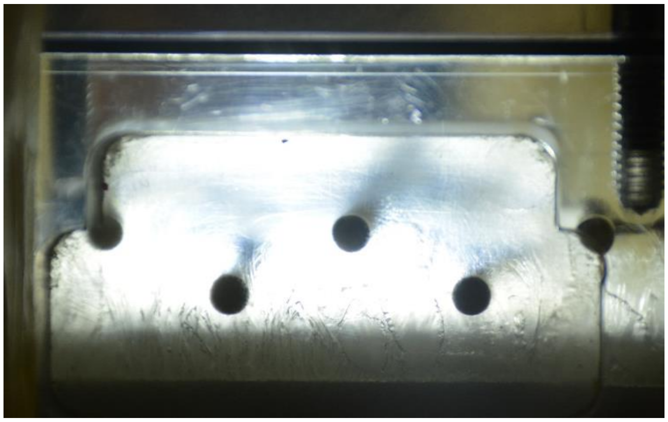

Figure 5-16: Image of the electrodes showing no solid build up in front of electrodes. -8kV electric potential applied to electrodes, 22.5°C wall temperature 30°C initial temperature. 12 minutes after cold wall boundary condition was applied.

5.5 Summary of experimental results

Experiments were conducted to understand the effect of electrohydrodynamics on the solidification of a phase change material in a latent heat thermal storage system. In the experiments, the phase change material was initially liquid and was solidified by running cold water through a heat exchanger, water temperature was kept constant throughout the experiments. Three initial temperature and three wall temperature were tested, the initial temperature being 30°C, 40°C and 50°C and the wall temperatures were 8.5°C 15.5°C and 22.5°C. Electrohydrodynamics was induced in the fluid by applying a voltage to electrodes and by grounding the heat exchanger, an electric potential of either 0kV or -8 kV was applied to the electrodes. The experiments found that the rate of energy discharge is increased at early stages of solidification and decreased at later stages. Over the entire time range considered, the enhancement was on the order of a few percent. It was also found that solid extraction did not contribute to the enhancement to a significant degree, which was seen from the experiments with an initial temperature of 30℃.

The results of these experiments can be compared to the results found for other methods of heat transfer enhancement presented in Table 2-5. All of the studies presented in that table show enhancement greater than or equal to 75% and all of these methods outperform the experiments conducted in this investigation. The results of the experiments show a smaller enhancement than that of Nakhla et al. (2015) conducted similar experiments for melting with the same electrode geometry as what was used in these tests and found which shows an enhancement of approximately 40%. The fact that electrohydrodynamics enhanced the rate of melting by a larger factor than it did for solidification is an expected result because the heat transfer enhancement only occurs in the liquid phase change material. When the phase change material is melting the liquid phase is in direct contact with the heat exchanger, resulting in a direct increase in the rate that energy is removed from the system. In solidification, the liquid phase change material is not in direct contact with the heat exchanger. Thus, the enhancement in heat transfer will not be as large in solidification because the liquid phase which experiences the heat transfer enhancement is not in contact with the heat exchanger. The results of these experiments contradict those of Dellorusso (1997) who found that the applying electrohydrodynamics slowed the rate of solidification. The results from Dellorusso (1997) do not agree with the theory presented in Section 4.2 and Section 4.3. However, Dellorusso's results could have been due to changes in the degree of undercooling of the solid-liquid interface, which is not accounted for in the theoretical models presented in Section 4.2 and Section 4.3.

Comparing the heat transfer enhancement of applying electrohydrodynamics to the solidification with the techniques explored in literature, show that the enhancement due to electrohydrodynamics is substantially smaller than that of the passive enhancement techniques in Table 2-5. The maximum enhancement using fins was 500% which was found by Velraj et al. (1999). The enhancement when using high conductivity particles was 300% which was presented in Mettawee and Assassa (2007) and the enhancement due to a high conductivity matrix was 80% which was presented in Mesalhy et al. (2005). By comparison, the maximum enhancement found using electrohydrodynamics and solidification at the end of the experiments was approximately 5%.

6 Conclusions

Organic phase change materials are used in latent heat thermal storage systems to store thermal energy. These materials have high storage densities, but relatively low thermal conductivities. The low thermal conductivity of these materials means that the rate of energy storage and discharge is very slow. Thus, these systems must be designed to accommodate this disadvantage. Organic phase change materials are typically dielectrics, and one way to enhance the energy storage rate in dielectric fluids is to apply electric fields. Applying electric fields causes the fluid to circulate and increase the rate of heat transfer. This is one way to accommodate the low thermal conductivity of organic phase change materials.

In this investigation, the enhancement of the energy discharge rate of latent heat thermal storage systems subject to electrohydrodynamics was investigated. The energy was removed from the system, using a heat exchanger kept at a temperature below the melting temperature of the phase change material. The test section was designed so that unidirectional solidification occurs, the section was also designed so that natural convection was suppressed. Natural convection was suppressed to isolate the fluid motion due to the electric field from other factors. The phase change material used in the investigation was octadecane with a melting temperature of 28℃. Circular electrodes were used to generate the electric field, this electric field would cause fluid motion.

To make predictions for how the energy discharge rate will be increased, numerical models were constructed to predict the effect that electro-convection will have on solidification. The model used is a one dimensional, unidirectional, plane front solidification model. The electro-convection enhancement was modelled using an increased thermal conductivity of the liquid. An analysis was done for initial liquid temperatures of 30℃, 40℃ and 50℃. The results showed that the maximum overall enhancement over the entire time to solidification as on the order of a few percent, which was less than the experimental error.

The effect of applying the electric field was also measured experimentally. Three different wall temperatures were tested and three different initial fluid temperatures were tested. The results of the experiments agreed with the predictions seen in the numerical results. Only a modest enhancement was observed; the enhancement was less than the experimental uncertainty near the end of the experiments. The amount of energy discharged from the system was determined by measuring the thickness of the solid built-up on the heat exchanger surface. Using this measurement the latent energy and sensible energy of the solid removed from the system was determined. The results of the numerical analysis were used to approximate the amount of sensible energy of the liquid that was discharged in the experiments.

The rate of solidification also changed for the case when the electric field was applied. Initially, the rate of solidification slowed as more sensible energy flowed from the liquid phase change material to the solid phase change material for the case with an electric field. However, once the sensible energy in the liquid was removed solidification proceeded faster for the electric field case. The end result is a slightly shorter time required to solidify the material when an electric field is applied.

6.1 Future work

This study is one of a few studies investigating applying electrohydrodynamics to a material undergoing a solid-liquid phase change. This investigation sought to answer one specific question regarding this process of solid-liquid phase change in the presence of an electric field. There are still many other investigations that must be completed before this topic is well understood. A few of these investigations are:

- A model that accurately predicts the electro-convective currents when an electric field is applied.
- A model that describes solid extraction in terms of the stresses acting in the material and when the solid dendrites separate from the rest of the solid.
- A study of each of the individual electric body forces, electrophoretic, dielectrophoretic and electrostrictive and the relative magnitude of each of these forces. This study will provide an understanding of when each of these forces becomes important and what the is contribution of each of the forces to the overall heat transfer enhancement.

- An investigation on the rate of solid extraction at the solid-liquid interface using high-speed imaging of the solid-liquid interface would be useful in providing an understanding of solid extraction.
- This investigation used Octadecane which is only one specific type of phase change material. The conclusions drawn with this material may not be applicable to other phase change materials. Octadecane is a non-polar, short chain length, non-branching hydrocarbon consisting of only carbon and hydrogen atoms. An understanding of the effect of polarity, chain length, side branches and variants on the basic monomer would be useful and required to generalize the results to other phase change materials.
- More engineering based investigations would be required as well, for example an investigation into how to design the electrodes to maximize heat transfer would be useful.
- Also, an understanding of how electrohydrodynamics can be used with other enhancement techniques such as Nano-particles and Fins would provide a better understanding of how to enhance heat transfer using electrohydrodynamics.

7 References

Abedin A.H. and Rosen A. (2011) “A Critical Review of Thermochemical Energy Storage System.” The Open Renewable Energy Journal. Vol. 4 pp 42-46

Abhat A. (1983). “Low temperature latent heat thermal energy storage: heat storage materials.” Solar energy. Vol. 30 pp 313-332

Alexiades V. and Solomon A. (1993) “Mathematical Modeling of Melting and Freezing Processes.” Hemisphere publishing.

Allen P.H. and Karayiannis T.G. (1995). “Electrohydrodynamic enhancement of heat transfer and fluid flow.” *Heat Recovery Systems and CHP.* 15, No 5. pp. 389-423

Antonio R. (2011). Electrokinetics and Electrohydrodynamics in Mircosystems. Vienna: Springer

Cabeza L.F., Castell A., Barreneche C., De Gracia A. and Fernandez A.I. (2011) “Materials used a PCM in thermal energy storage in buildings: A review.” Renewable and Sustainable Energy Reviews. Vol. 15 No. 3. Pp. 1675-1695

Castellanos A. (1998). Basic concepts and equations in electrohydrodyncamics. In A. Castellanos, editor, Electrohydrodynamics. Springer-Verlag.

Cegel Y. and Ghajar A. (2010) “Heat and Mass transfer: Fundamentals and applications.” 4th edition, McGraw-Hill

Chu B.T. (1959). Thermodynamics of Electrically Conducting Fluids. Physics of Fluids, 2(5). Doi: 10.1063/1.1705937

Churchill S.W. and Chu H.H.S. (1975) “Correlating Equations for Laminar and Turbulent Free Convection from a Vertical Plate.” *International Journal of Heat Mass Transfer* Vol. 18 pp.1323

Colaco M.J., Dulikravich G.S. and Martin T.J. “Optimization of wall electrodes for electro-hydrodynamic control of natural convection during solidification.” *Materials and Manufacturing Processes 19, No. 4 pp. 719-736.*

Cotton J., Robinson A., Shoukri M. and Change, J. (2005). A two-phase flow pattern map for annular channels under a DC applied voltage and the application to electrohydodynamic convective boiling analysis. International Journal of heat and mass transfer, 48 (25-26), 5563-5579

Dellorusso P.R. (1997). Electrohydrodynamic Heat Transfer Enhancement for a Latent Heat Storage Heat Exhcanger. Technical University of Nova Scotia.

Dhaidan N., Khadadadi J.M., Al-Hattab, T.A. & Al-Mashat, S.M. (2013) “Experimental and numerical study of constrained melting of n-Octadecane with CuO nanoparticle dispersions in a horizontal cylindrical capsule subjected to a constant heat flux.” International journal of heat and mass transfer 67 pp. 523-534

Dulikravich, G.S., Ahuja, V. and Lee, S. (1994). “Modeling of dielectric fluid solidification with charged particles in electric fields and reduced gravity.” *Numerical Heat transfer, Part B, 25* pp. 357-373.

Fernandez. J. and Poulter. R. (1987). Radial mass flow in electrohydrodynamically enhanced forced heat transfer in tubes. *International journal of heat and mass transfer, 30, no 10*, 2125-2136.

Flemings M.C. (1974) "Solidification processing." McGraw-Hill.

Fujii T. and Imura H. (1972) "Natural Convection Heat Transfer from a Plate with Arbitrary Inclination." *International Journal of Heat Mass Transfer* Vol. 15 pp. 755

Gross B. (1954) "Theory of Thermodielectric Effect." Physical Review, Vol. 94 No. 6. Pp. 1545-1551

He B., Martin V. and Setterwall F. "liquid-Solid Phase Equilibrium Study of Tetradecane and Hexadecane Binary Mixtures as Phase Change Materials (PCMs) for Comfort Cooling Storage."

Henze R. and Humphrey J. (1981) "Enhanced Heat Conduction in Phase –Change Thermal Energy Storage Devices." International Journal of Heat and Mass Transfer. Vol 24 pp 459-474

Ho C. (1982) Solid-Liquid Phase Change Heat Transfer in Enclosures, Purdue University. http://www.osti.gov/scitech/biblio/6775101 (accessed January 23, 2015)

Internal Energy Agency and International Renewable Energy Agency. (2013) "Thermal Energy Storage." Technology Breif.

Jayaram S. and Cross J.D. (1994). Effects of Ionic Impurities on EHD Motion and Conduction in Nonpolar Liquids. IEEE Transactions on Dielectrics and Electrical Insulation. Vol. 1 No. 6,

Jegadheeswaran S., Pohekar S. "Performance enhancement in latent heat thermal storage system: A review." Renewable and Sustainable Energy Reviews. Vol 13. 2009. Pp. 2225-2244

Kalman H. and Sher E. (2001) "Enhancement of heat transfer by means of corona wind created by a wire electrode and confined wings assembly" Vol. 21, No 3, pp 265-282.

Kasayapanand N. (2008). Electrohydrodynamic enhancement of heat transfer in vertical fin array using computational fluid dynamics technique. *International communications in heat and mass transfer, 35, pp. 762-770*

Lafdi et al. (2015) "Merits of employing foam encapsulated phase change materials for pulsed power electronics cooling applications." Material Science Engineering. Vol. 87

Legay M., Gondrexon N., Person S., Boldo P. and Bontemps A. (2011) "Enhancement of Heat Transfer by Ultrasound: Review and Recent Advances." International journal of Chemical Engineering article ID: 670108.

Lingamneni S., Asheghi M. and Goodson K. (2014) "A Parametric Study of Microporous Metal Matrix-Phase Change Material Composite Heat Spreaders for Transient Thermal Applications." *IEEE Intersociety Conference on Thermal and Thermomechanical Phenomena in Electronic Systems*.

Martinez F. (2014) "Beyond the classical Stefan problem." Doctoral Thesis, Applied Mathematics, Facultat de Matematiques I Estadistica, Universitat Politecnica de Catalunya. Spain

Mehling H. and Cabeza L.F. (2008) "Heat and cold storage with PCM: An up to date introduction into basics and applications." Springer

Mesalhy O., Lafdi K., Elgafy A. and Bowman K. (2005) "Numerical Study for Enhancing the Thermal Conductivity of Phase Change Material (PCM) Storage Using High Thermal Conductivity Porous Matrix." Energy Conversion and Management Vol. 46 pp. 847-867

Mettawee E. B. and Assassa G. (2007) "Thermal conductivity enhancement in a latent heat storage system." Solar Energy. Vol. 81 pp 839-845

Mills A., Farid M., Selman J.R. and Al-Hallaj S. (2006) "Thermal Conductivity Enhancement of Phase Change Materials using a Graphite Matrix." *Applied Thermal Engineering* Vol. 26 No. 14-15 pp. 1652-1661

Nakhla D., Sadek H. and Cotton, J.S. (2015) "Melting performance enhancement in latent heat storage module using solid extraction electrohydrodynamics (EHD)." International Journal of Heat and Mass Transfer. 81, pp. 695-704

Nangle Smith S. (2012). The effect of high voltage electric fields on two phase flow pattern redistribution and heat exchanger performance. Hamilton, Ontario: McMaster University

Nangle-Smith. S., Sadek. H., and Cotton. J.S. (March 2013). "The influence of the electrophoretic and polarization forces on two phase flow redistribution in a horizontal annular tube." *International journal of plasma environmental science & technology*. Vol. 7, No. 1.

Ng. K, Ching, C.Y. and Cotton, J.S. (2011). Transient two-phase flow patterns by application of a high voltage pulse width modulated signal and the effect on condensation heat transfer. Journal of heat transfer 133, No. 9

Norris C., Cotton J., Shoukri M., Chang J. and Smith-Pollard T. (1999) "Electrohydrodynamic Effects on Flow Redistribution and Convective Boiling in Horizontal Concentric Tubes Under High Inlet Quality Conditions." ASHRAE transactions – American Society of Heating Refrigerating Airconditioning Engineering Vol. 105 No 1, pp. 222-236

Oh Y.K., Park S.H. and Cho Y.I. "A study of the effect of ultrasonic vibrations on phase change heat transfer." International Journal of Heat and Mass Transfer 45 (2002) 4631-4641

Paschkewitz, J.S. and Pratt D.M. (2000). "The influence of fluid properties on electrohydrodynamic heat transfer enhancement in liquids under viscous and electrically dominated flow conditions." *Experimental Thermal and Fluid Science, 21* pp. 187-197

Pedersen K.S. and Skovborg P. (1991) "Wax precipitation from North Sea Crude Oils." Energy & Fuel Vol. 5 pp. 924-932

Regin F., Solanki A., and Saini, J.S. (2009) "An analysis of a packed bed latent heat thermal energy storage system using PCM capsules: Numerical Investigation." Renewable Energy. Vol. 34. Pp 1765-1773.

Sadek H., Chimg C.Y. and Cotton, J. (2010) "The effect of pulsed electric fields on horizontal tube side convective condensation." International journal of heat and mass transfer 53, No 19, 3721-3732

Saha S.K., Srinivasan K. and Dutta P. (206) "Studies on Optimum Distribution of Fins in Heat Sinks Filled with Phase Change Material." Journal of Heat Transfer. Vol. 130 No. 3

Salehi, M., Ohadi, M. M. and Dessiatoun, S. (November 1997). EHD Enhanced Convective Boiling of R-134a in Grooved Channels – Application to Subcompact Heat Exchangers. *Journal of Heat Transfer*. Vol 119 No. 4 pp. 805-809

Sanusi O., Warzoha R., Fleischer A. S. (2011) “Energy storage and solidification of paraffin phase change material embedded with graphite nanofibers.” International Journal of Heat and Mass Transfer. Vol. 54, No. 19-20. Pp 4429-4436. DOI: 10.1016/j.ijheatmasstransfer.2011.04.046

Sciacovelli A. and Verda V. (2016) “Second-Law Design of a Latent Heat Thermal Energy Storage with Branched Fins.” International Journal of Numerical Methods for Heat and Fluid Flow. Vol. 26 No. 2 pp. 489-503.

Sheshakamal J. and Cross J.D. (Oct 1989). The influence of impurities on electrohydrodynamic motion in insulating oils. In Proc. IEEE conf. Electr. Insul. Dielectric Phenomena. Pp/ 338-345.

Siegel R. (1977) “Solidification of low conductivity material containing dispersed high conductivity particles.” International Journal of Heat and Mass Transfer. Vol. 20 pp. 1087-1089.

Singh A. O. (1995) “Electrohydrodynamic (EHD) enhancement of in-tube condensation heat transfer of alternative refrigerant R-134a in smooth and microfin tubes.” ASHARE Trans, 103(1) 813-823

Sparrow E.M., Larson E.D. and Ramsey J.W. (1981) “Freezing on a Finned Tube for Either Conduction Controlled or Natural Convection Controlled Heat Transfer.” International Journal of Heat and Mass Transfer Vol. 24 pp. 273-284.

Stratton J.A. (1941). Electromagnetic Theory. McGraw-Hill Book Co. New York, 508

Swalin R.A. (1962) “Thermodynamics of Solids.” John Wiley & Sons Inc. New York.

Tomas M. and Novotny P. (2015) The Thermodielectric Effect in Paraffin Wax. Brazilian journal of physics, Vol 45. No 1. pp 28-35. ISSN 0103-9733

Turnbull R. (1968). Electroconvective instability with a stabilizing temperature gradient. l. Theory, II. Experimental Results. The Physics of Fluids, Vol. 11, pp. 2588-2603.

Turnbull R. (1969) “Effect of Dielectrophoretic Forces on the Bénard Instability.” *The physics of Fluids* Vol. 12 No. 9 pp. 1809-1815

Ukrainczyk N., Kurajica S. and Sipusie, J. (2010) “Thermophysical Comparison of Five Commercial Paraffin Waxes as Latent Heat Storage Materials.” Chemical Biochemical Engineering Vol. 24 No. 2 Pp. 129-137

Velraj R. and Seeniraj R.V. (1999) “Heat transfer studies during solidification of PCM inside an internally finned tube.” Journal of Heat Transfer. Vol. 121 No. 2 pp. 493-497

Velraj R., Seeniraj R.V., Hafner B.,Faber C., and Schwarzer K. (1999) “Heat transfer enhancement in a latent heat storage system.” Solar energy, Vol. 65 No. 3, 171-180

Wei J., Kawaguchi Y., Hirano S. and Takeuchi H. (2005) “Study on a PCM heat storage system for rapid heat supply.” Aplied Thermal Engineering Vol. 25. Pp 2903-2920

Werner, R. (1987) “Compatibility of organic latent heat storage materials and plastic container materials.” Heat Recovery Systems and CHP, Vol. 7. No 4. Pp 383-388

Won K.W. (1989) Fluid Phase Equilib. Vol. 53 pp. 376-377

Yoshikawa H., Crumeyrool O. and Mutabazi I. (2013) “Dielectrophoretic force driven thermal convection in annular geometry” *physics of Fluids* Vol 25.

Zalba B., Marin, J., Cabeza L. and Mehling H. (2003) “Review on Thermal Energy Storage with Phase Change: Materials, Heat Transfer Analysis and Applications.” Applied Thermal Engineering. Vol 23 pp. 251-283.

Zhang C., Wu L. 3and Chen Y. (2015) “Study on Solidification of Phase Change Material in Fractal Porous Metal Foam.” Fractals Vol. 23 No. 1.

Appendix A: Temperature data

For all of the experiments, thermocouples measured the temperature of the heat exchanger, water inlet and outlet temperatures and the ambient temperature. However, some of the temperature data was not saved properly, so not all of the data is available. The temperature data is available in Figure A-1 through Figure A-20. The temperature data shows that the heat exchanger temperature is approximately 0.5℃ higher than the inlet water temperature. In general the heat exchanger temperatures converge quickly on the set-point, as discussed in the experimental apparatus – validation section.

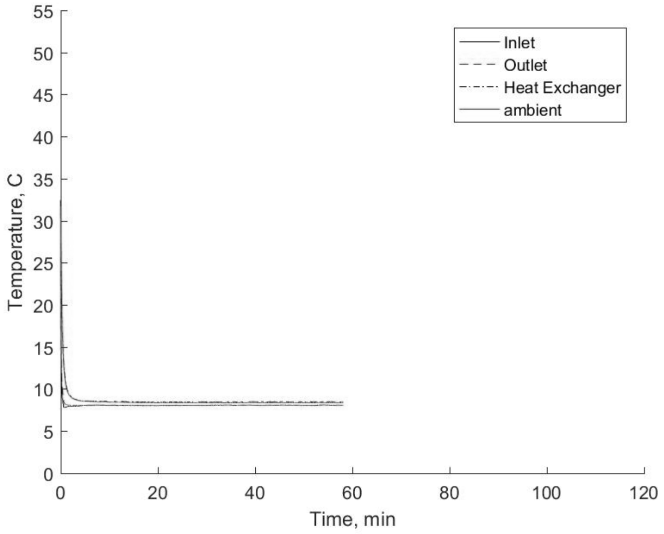

a)

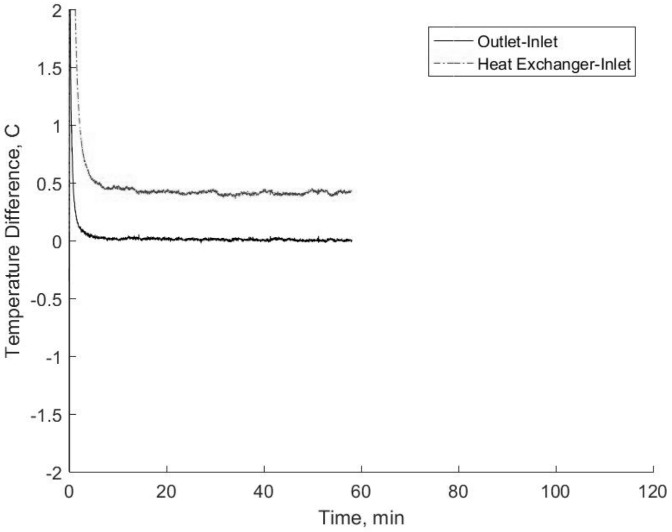

b)

Figure A-1: Temperature data for 8.5℃ wall temperature and 40℃ initial temperature, with no electrodes. a) The absolute temperature recordings of the thermocouples, b) The temperature difference between the thermocouples

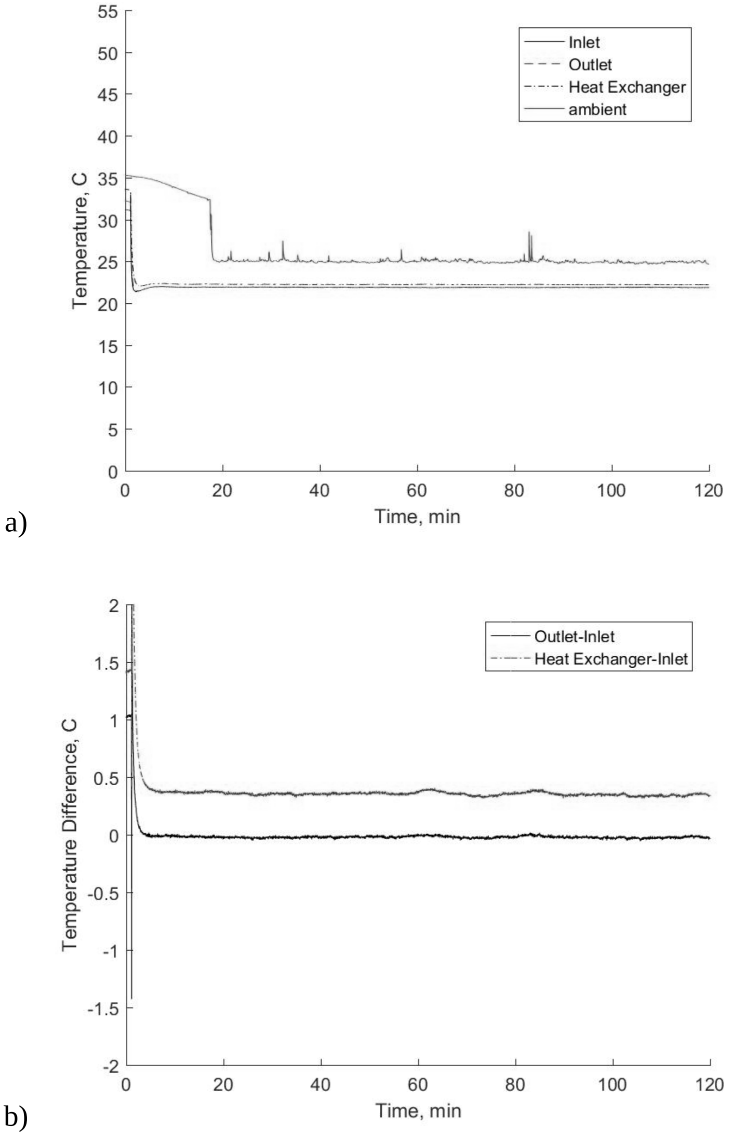

Figure A-2: Temperature data for 8.5℃ wall temperature and 40℃ initial temperature, with no electrodes. a) The absolute temperature recordings of the thermocouples, b) The temperature difference between the thermocouples

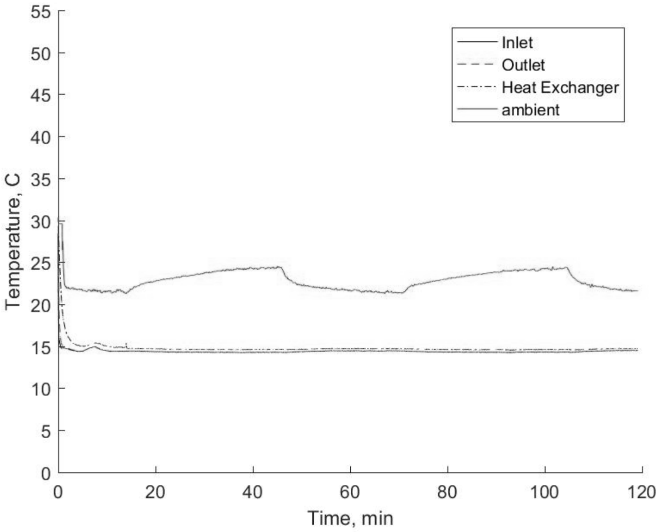

a)

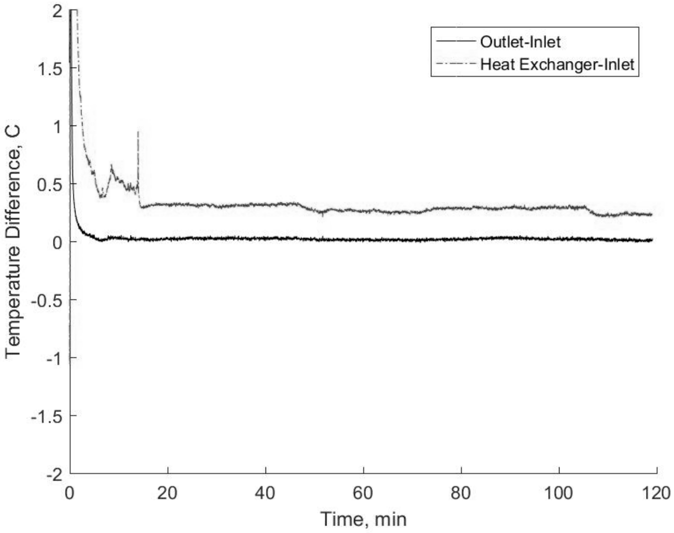

b)

Figure A-3: Temperature data for 15.5℃ wall temperature and 30℃ initial temperature, with no electrodes. a) The absolute temperature recordings of the thermocouples, b) The temperature difference between the thermocouples

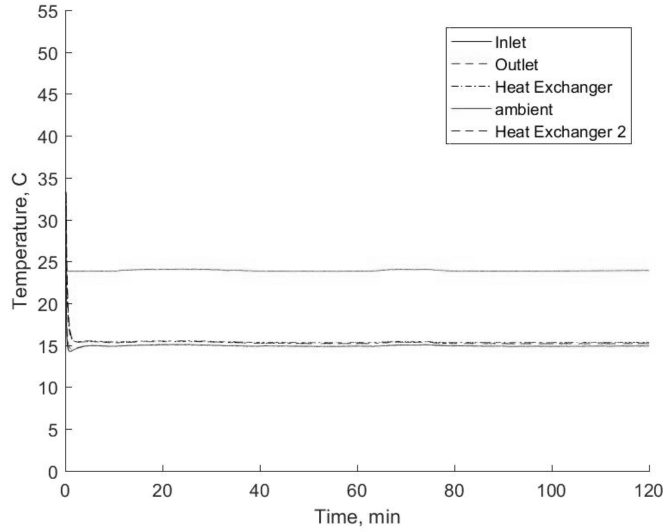

a)

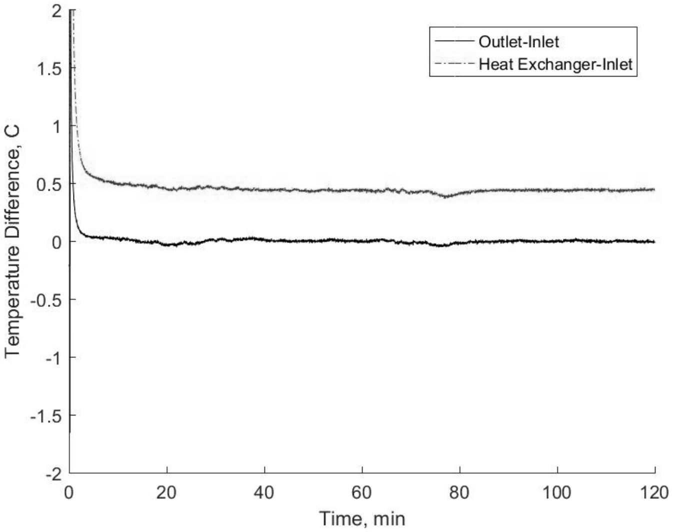

b)

Figure A-4: Temperature data for 15.5℃ wall temperature and 40℃ initial temperature, repeat, with no electrodes. a) The absolute temperature recordings of the thermocouples, b) The temperature difference between the thermocouples

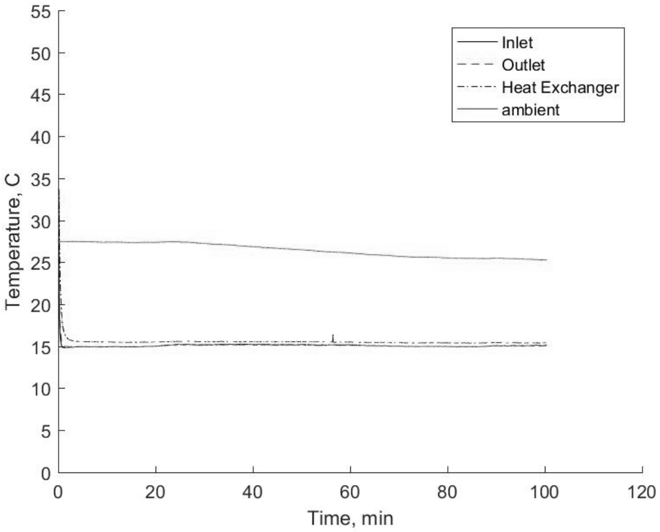

a)

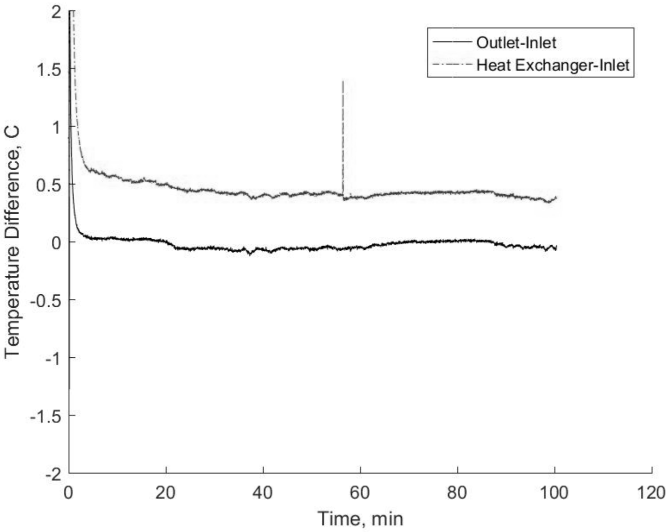

b)

Figure A-5: Temperature data for 15.5℃ wall temperature and 40℃ initial temperature, with no electrodes. a) The absolute temperature recordings of the thermocouples, b) The temperature difference between the thermocouples

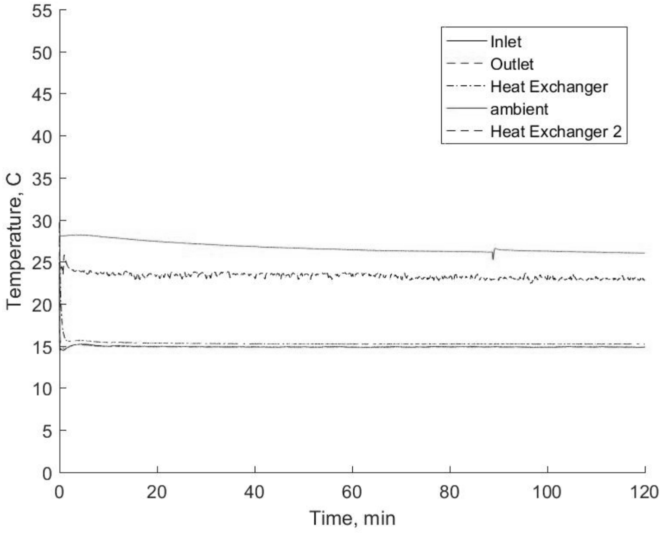

a)

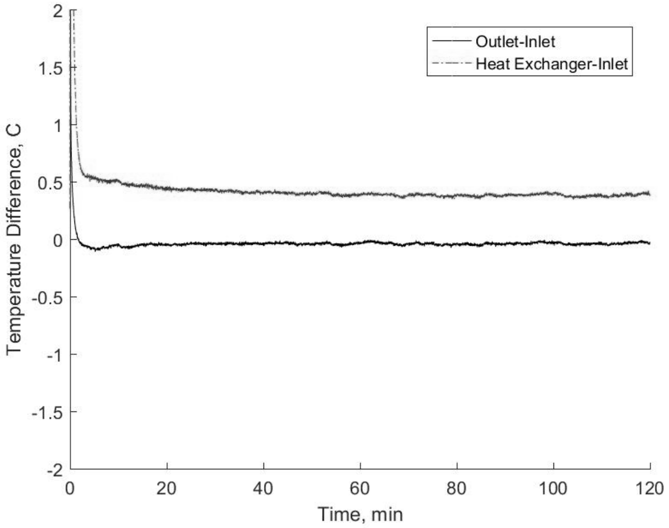

b)

Figure A-6: Temperature data for 15.5℃ wall temperature and 30℃ initial temperature, with electrodes and no electric field. a) The absolute temperature recordings of the thermocouples, b) The temperature difference between the thermocouples

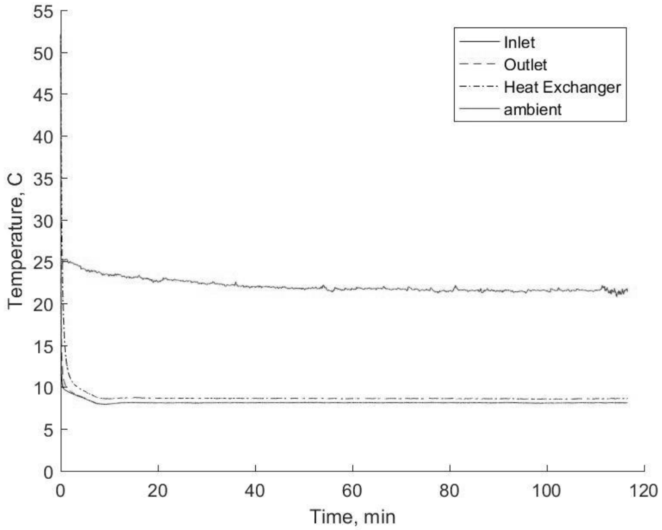

a)

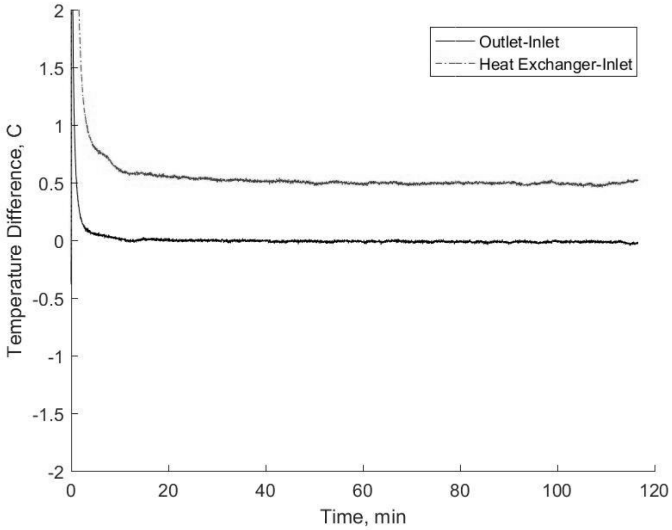

b)

Figure A-7: Temperature data for 8.5℃ wall temperature and 50℃ initial temperature, with electrodes and no electric field. a) The absolute temperature recordings of the thermocouples, b) The temperature difference between the thermocouples

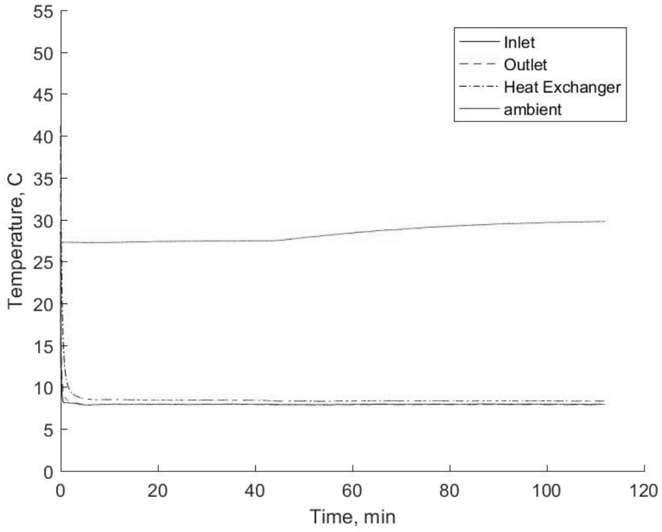

a)

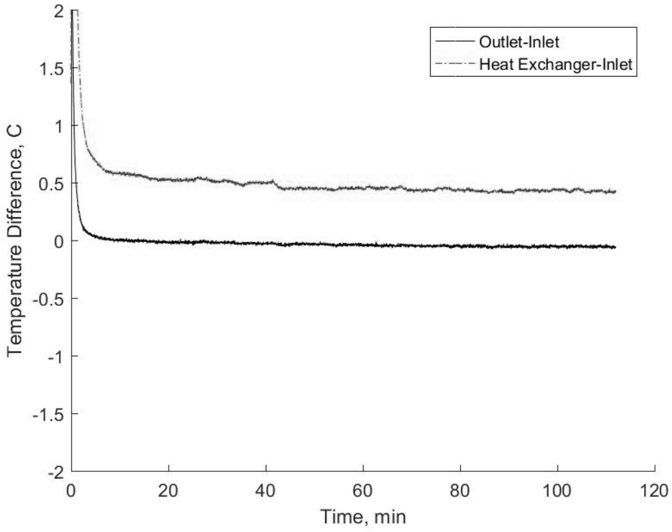

b)

Figure A-8: Temperature data for 8.5℃ wall temperature and 50℃ initial temperature, with electrodes and no electric field. a) The absolute temperature recordings of the thermocouples, b) The temperature difference between the thermocouples

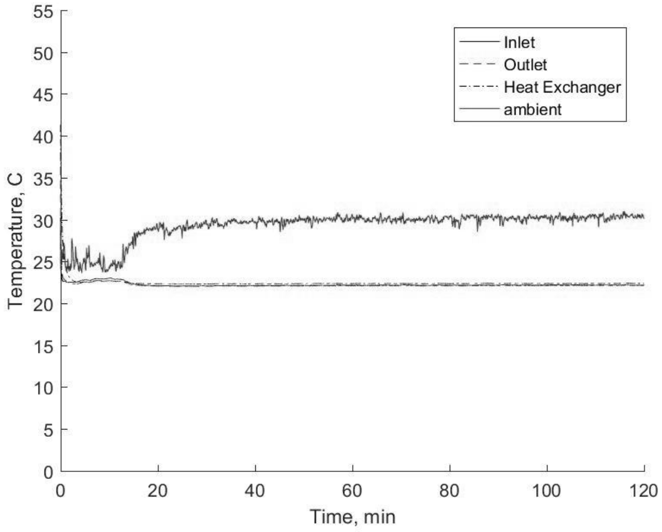

a)

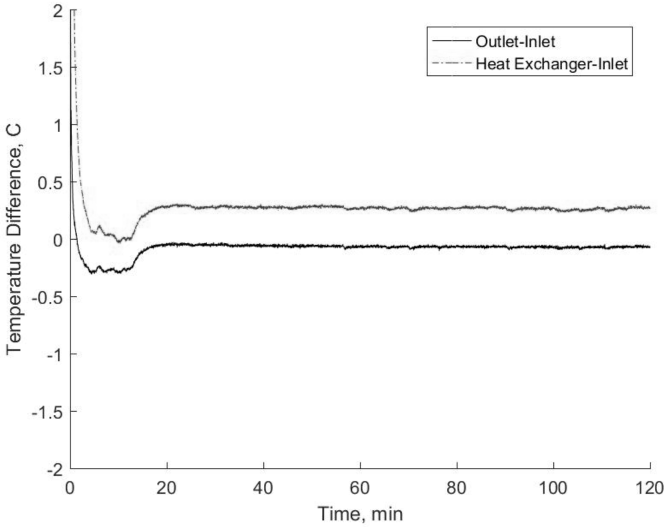

b)

Figure A-9: Temperature data for 22.5℃ wall temperature and 40℃ initial temperature, with electrodes and no electric field. a) The absolute temperature recordings of the thermocouples, b) The temperature difference between the thermocouples

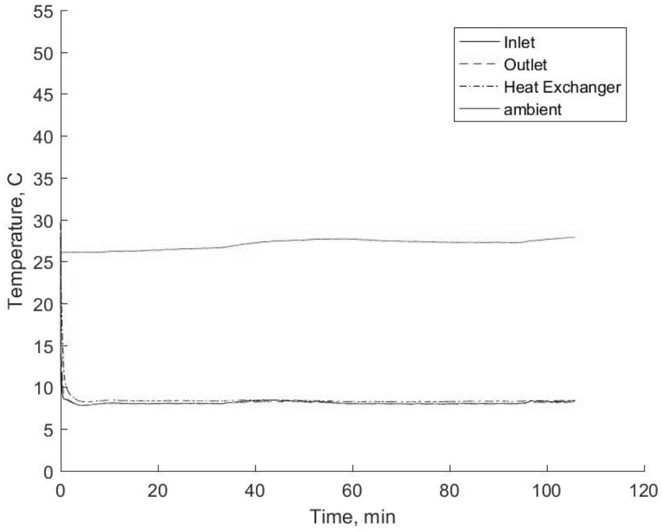

a)

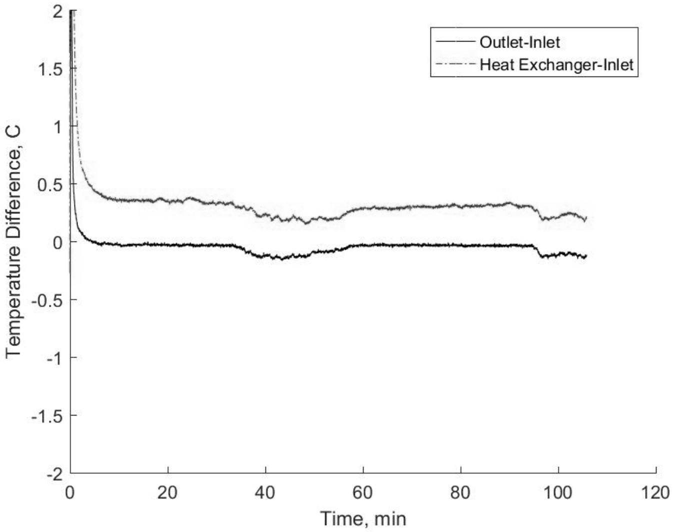

b)

Figure A-10: Temperature data for 8.5℃ wall temperature and 30℃ initial temperature, with electrodes and no electric field, repeat. a) The absolute temperature recordings of the thermocouples, b) The temperature difference between the thermocouples

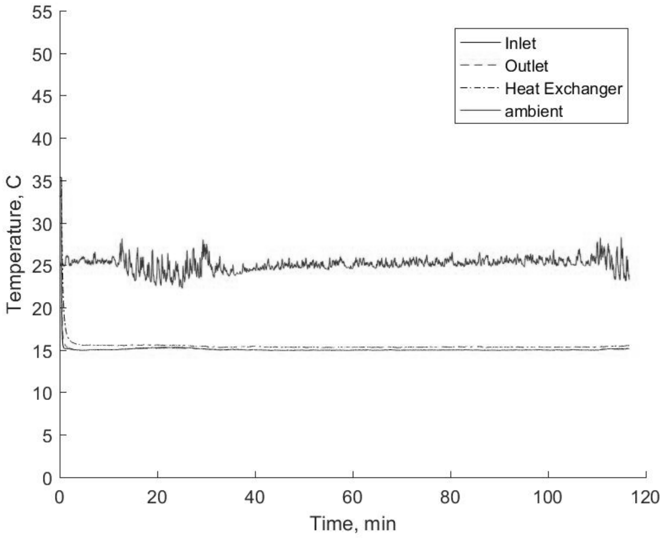

a)

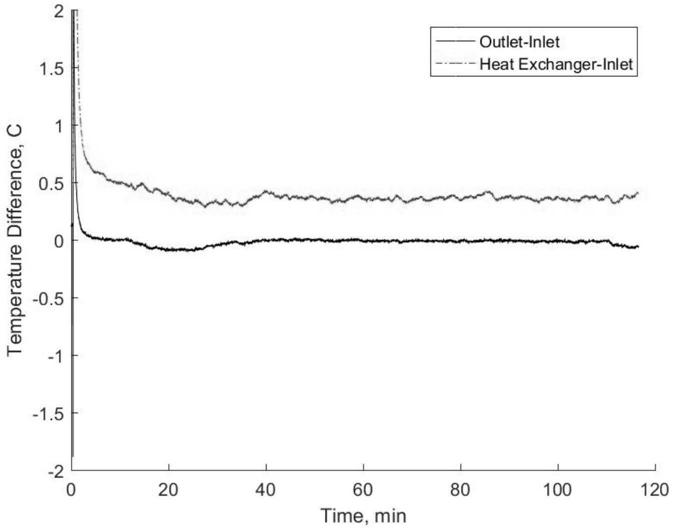

b)

Figure A-11: Temperature data for 15.5℃ wall temperature and 40℃ initial temperature, with electrodes and no electric field. a) The absolute temperature recordings of the thermocouples, b) The temperature difference between the thermocouples

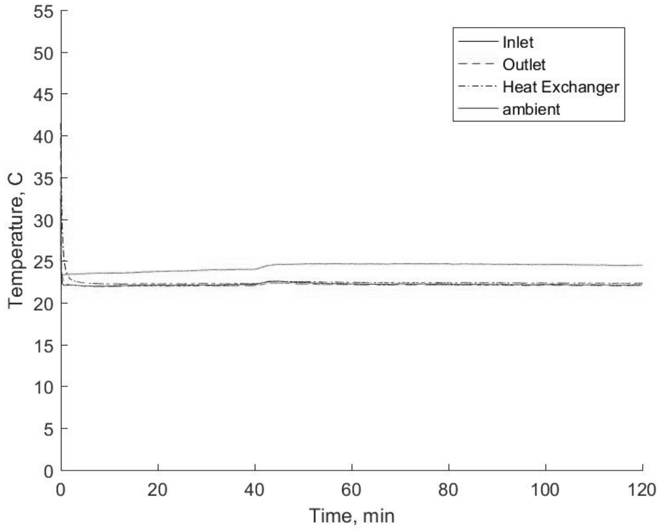

a)

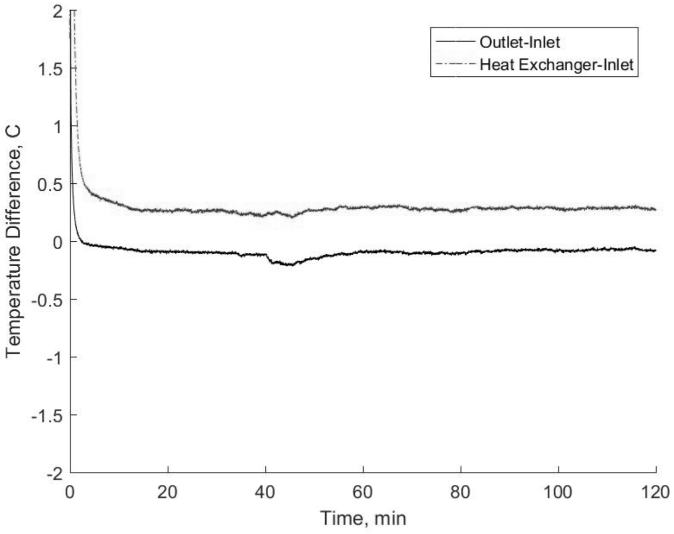

b)

Figure A-12: Temperature data for 22.5℃ wall temperature and 30℃ initial temperature, with electrodes and no electric field. a) The absolute temperature recordings of the thermocouples, b) The temperature difference between the thermocouples

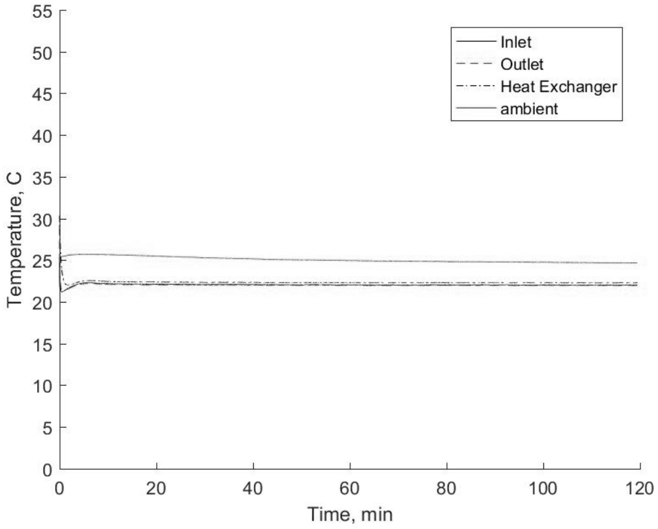

a)

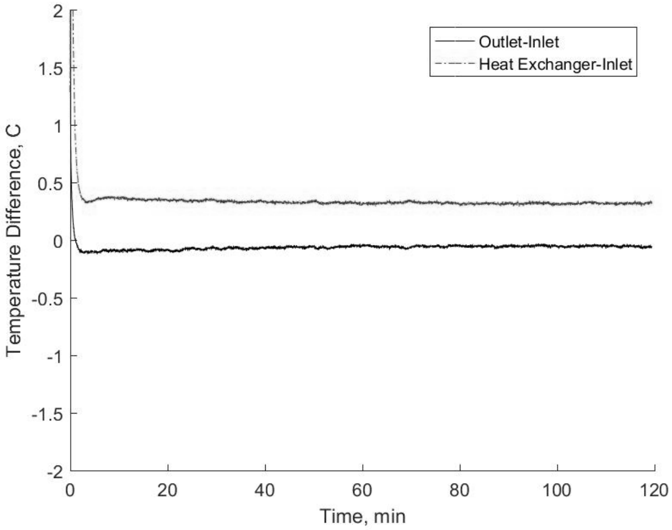

b)

Figure A-13: Temperature data for 22.5℃ wall temperature and 30℃ initial temperature, with electrodes and no electric field, repeat. a) The absolute temperature recordings of the thermocouples, b) The temperature difference between the thermocouples

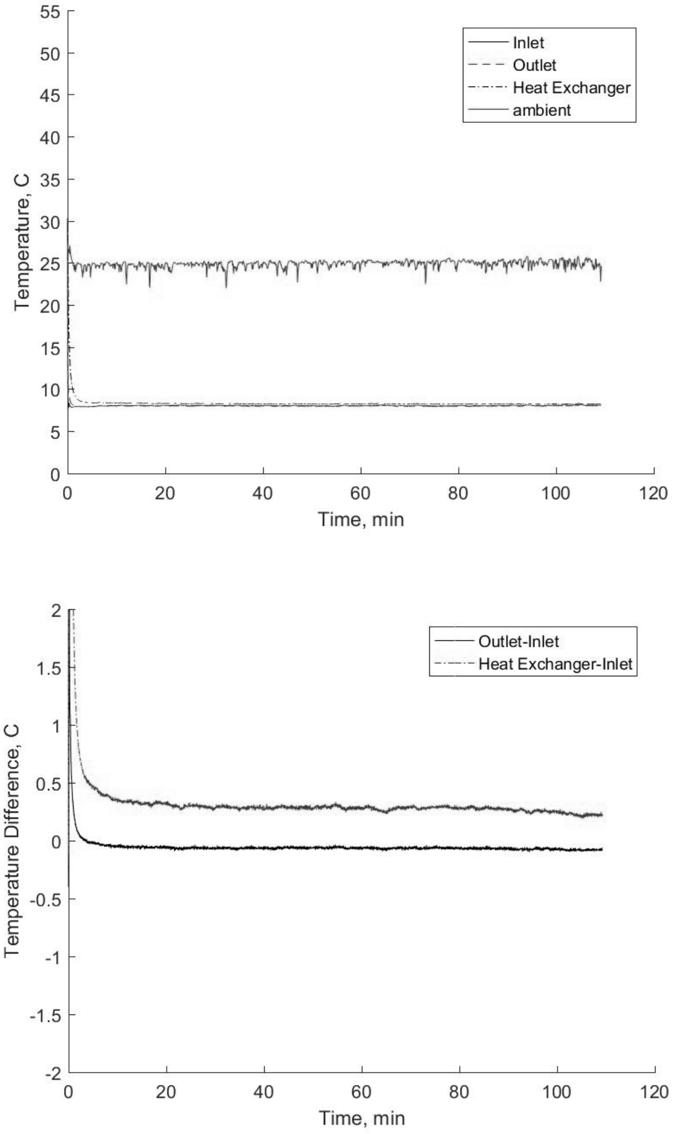

Figure A-14: Temperature data for 8.5℃ wall temperature and 30℃ initial temperature, with electrodes and electric field. a) The absolute temperature recordings of the thermocouples, b) The temperature difference between the thermocouples

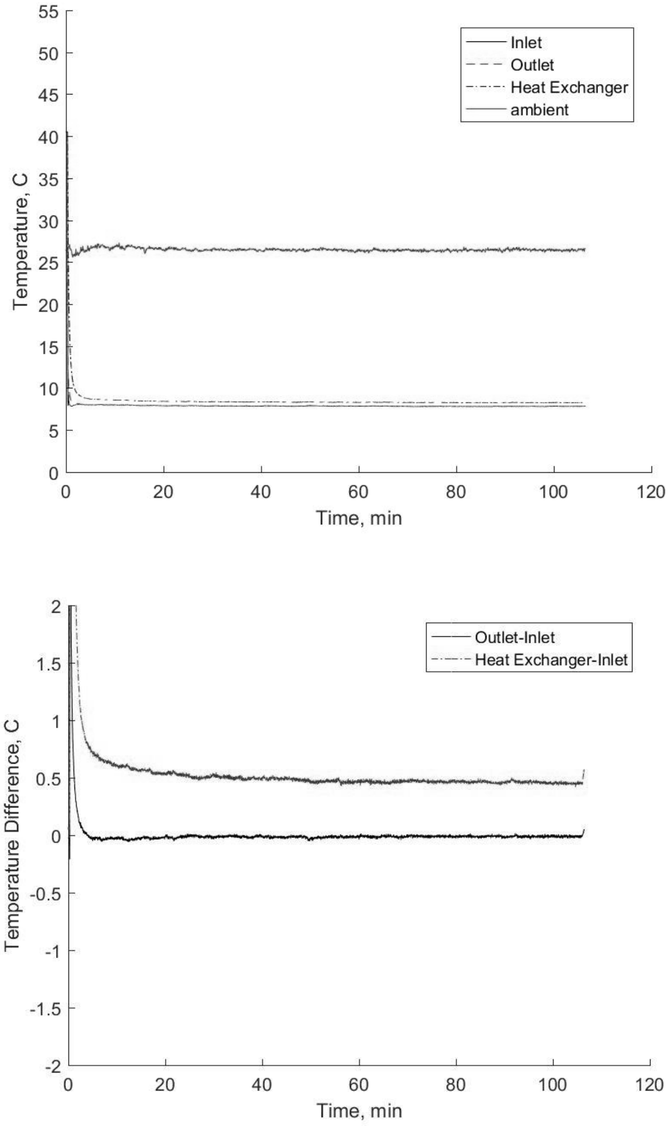

a)

b)

Figure A-15: Temperature data for 8.5℃ wall temperature and 40℃ initial temperature, with electrodes and electric field. a) The absolute temperature recordings of the thermocouples, b) The temperature difference between the thermocouples

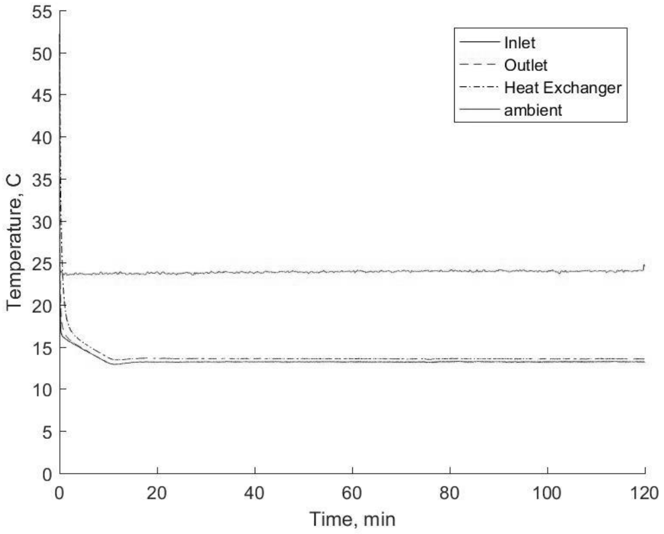

a)

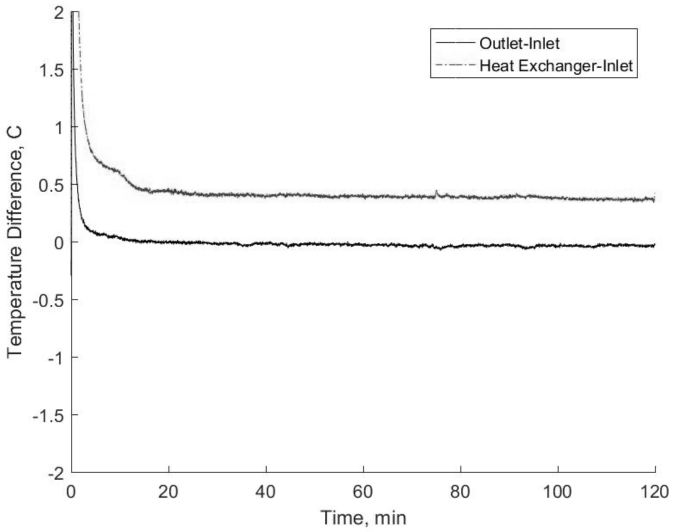

b)

Figure A-16: Temperature data for 15.5℃ wall temperature and 50℃ initial temperature, with electrodes and electric field. a) The absolute temperature recordings of the thermocouples, b) The temperature difference between the thermocouples

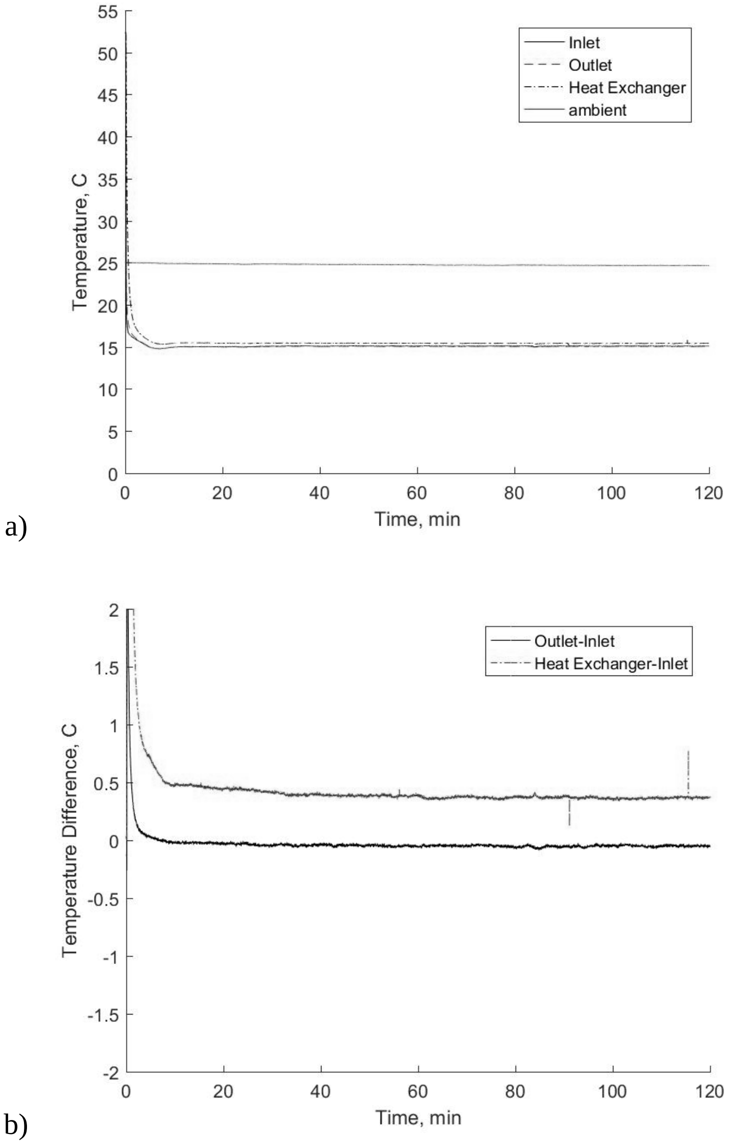

Figure A-17: Temperature data for 15.5℃ wall temperature and 40℃ initial temperature, with electrodes and electric field. a) The absolute temperature recordings of the thermocouples, b) The temperature difference between the thermocouples

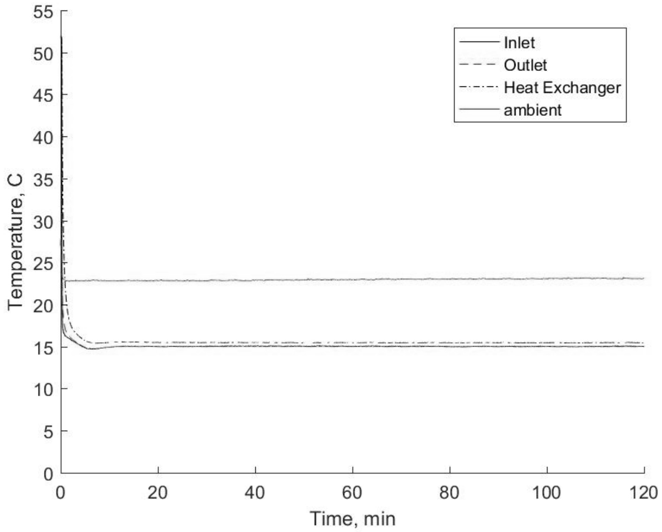

a)

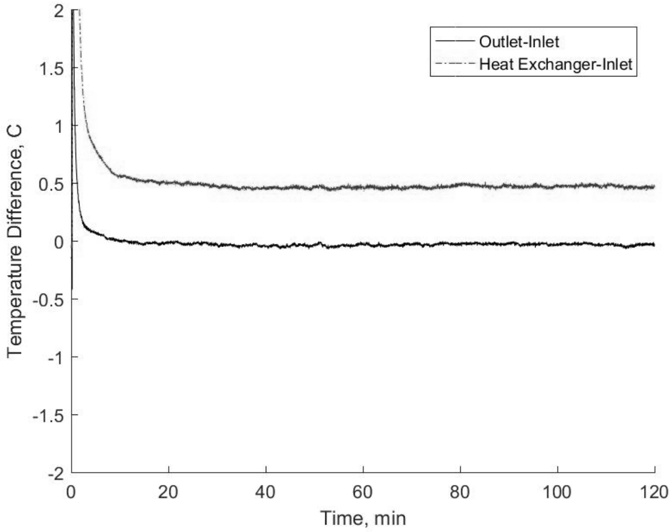

b)

Figure A-18: Temperature data for 15.5℃ wall temperature and 50℃ initial temperature, with electrodes and electric field. a) The absolute temperature recordings of the thermocouples, b) The temperature difference between the thermocouples

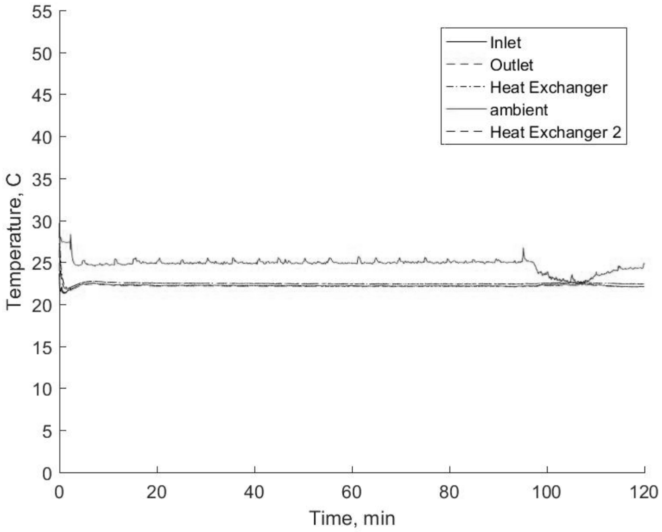

a)

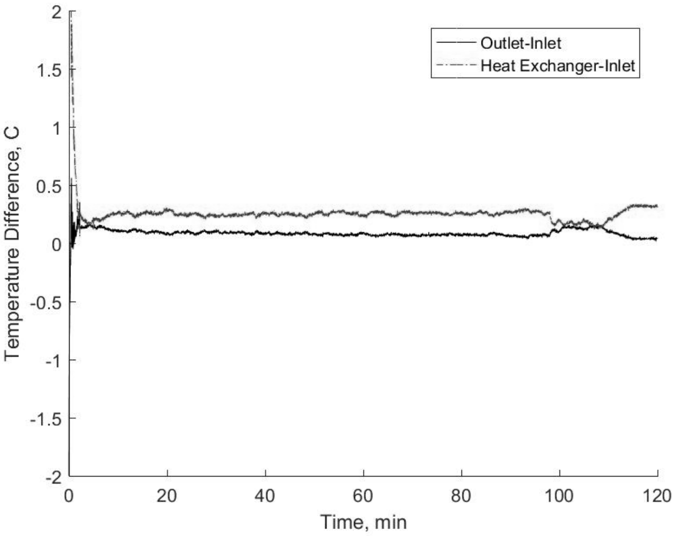

b)

Figure A-19: Temperature data for 22.5℃ wall temperature and 30℃ initial temperature, with electrodes and electric field. a) The absolute temperature recordings of the thermocouples, b) The temperature difference between the thermocouples

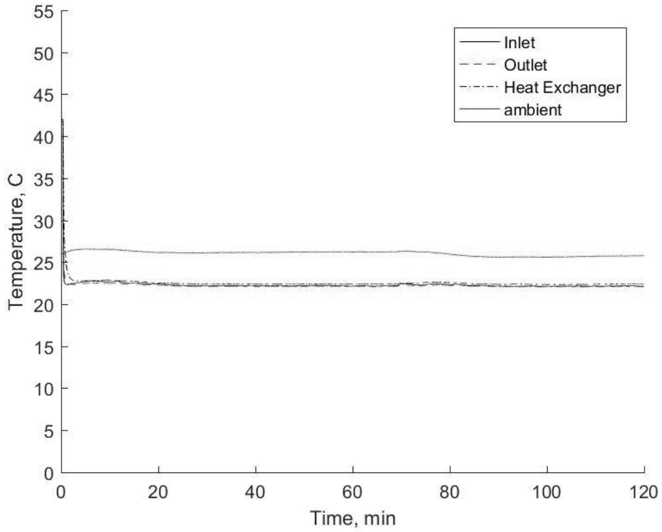

a)

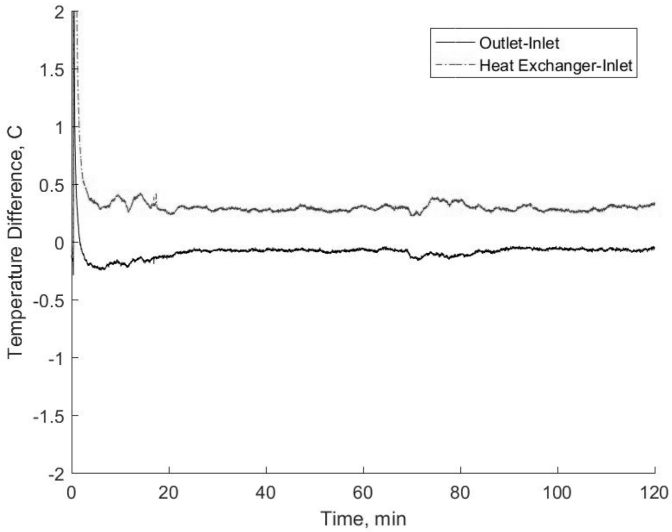

b)

Figure A-20: Temperature data for 22.5℃ wall temperature and 40℃ initial temperature, with electrodes and electric field. a) The absolute temperature recordings of the thermocouples, b) The temperature difference between the thermocouples

Appendix B: Experimental results in Dimensionless form

Non-dimensional plots were created to make the results of the experiments more general. The experimental results have already been discussed in the dimensional form, so the detailed discussion will not be replicated here for the non-dimensional results. To make the results non-dimensional Equation B.1, Equation B.2, Equation B.3 and Equation B.4 were used. In these equations, t^* is dimensionless time, α_s is the thermal diffusivity, S^* is the dimensionless solid thickness, Ste_l is the liquid Stefan number, Ste_S is the solid Stefan number, $C_{p,l}$ is the specific heat of the liquid and $C_{p,s}$ is the specific heat of the solid.

$$t^* = \frac{\alpha_s t}{L^2} \qquad \text{[B.1]}$$

$$S^* = \frac{S}{L} \qquad \text{[B.2]}$$

$$Ste_l = \frac{C_{p,l}(T_{i,f} - T_m)}{H} \qquad \text{[B.3]}$$

$$Ste_S = \frac{C_{p,s}(T_m - T_w)}{H} \qquad \text{[B.4]}$$

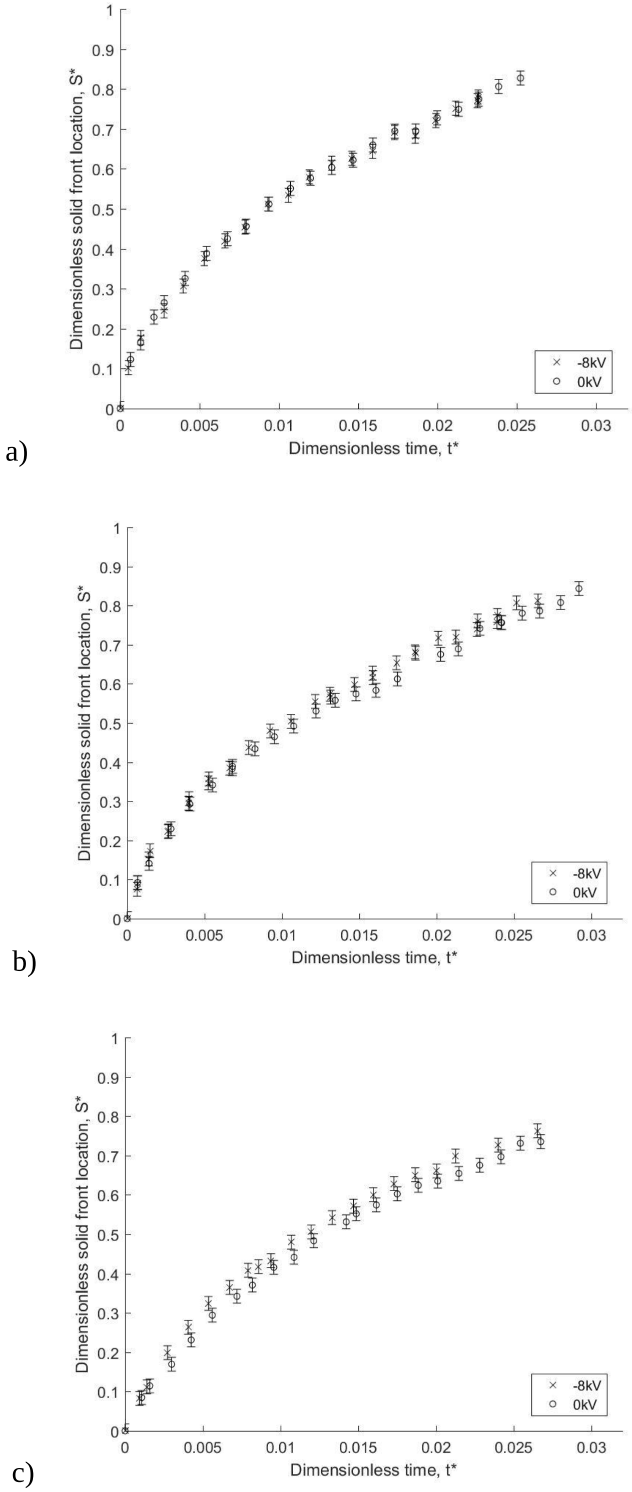

Figure B-1: Experimentally measured dimensionless solid front location a) 8.5℃ wall temperature. 30℃ temperature/Ste_s=0.17, Ste_l=0.02 b) 8.5℃ wall temperature, 40℃ initial temperature/Ste_s=0.17, Ste_l=0.11 c) 8.5℃ wall temperature and 50℃ initial temperature/Ste_s=0.17, Ste_l=0.20

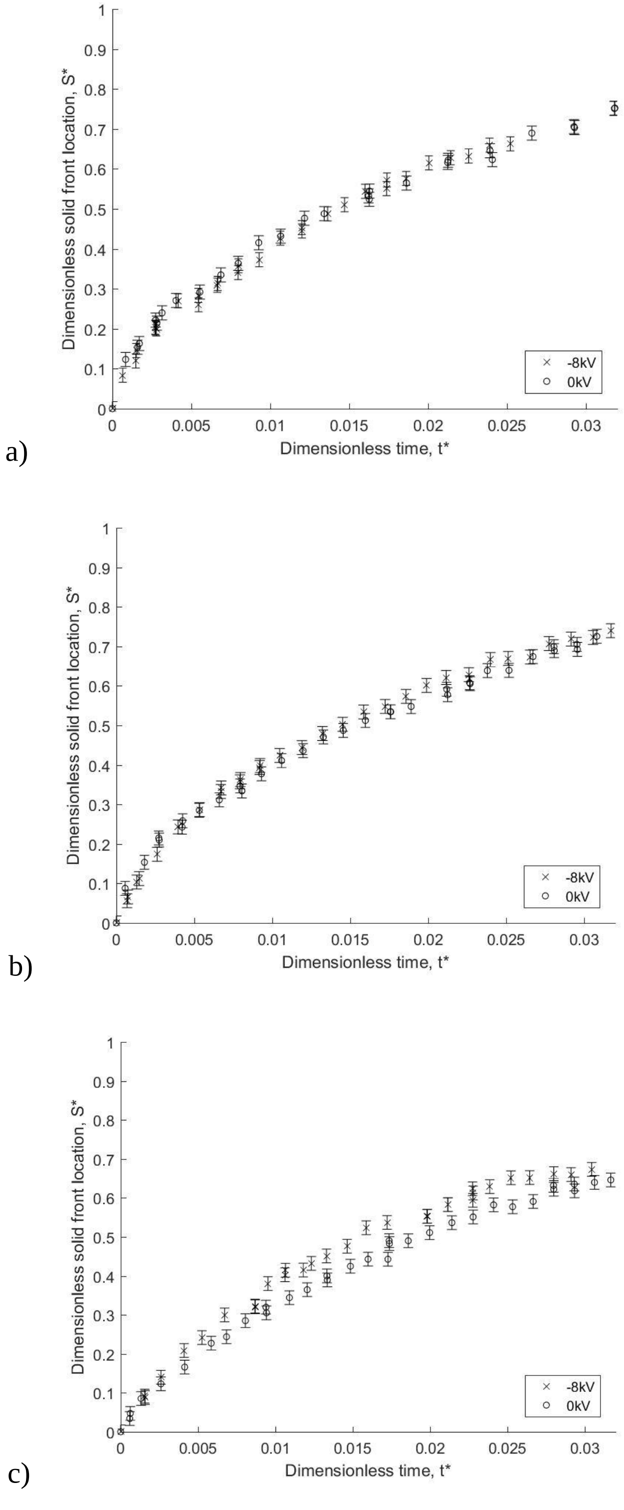

Figure B-2: Experimentally measured dimensionless solid front location a) 15.5℃ wall temperature. 30℃ temperature/Ste_s=0.11, Ste_l=0.02 b) 15.5℃ wall temperature, 40℃ initial temperature/Ste_s=0.11, Ste_l=0.11 c) 15.5℃ wall temperature and 50℃ initial temperature/Ste_s=0.11, Ste_l=0.20

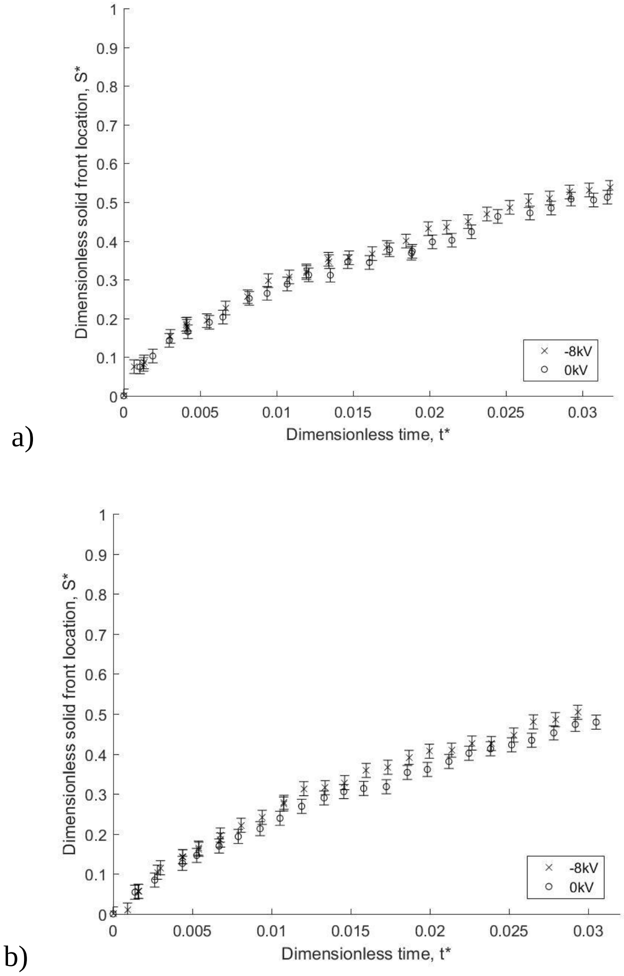

Figure B- 3: Experimentally measured dimensionless solid front location a) 22.5℃ wall temperature. 30℃ temperature/Ste_s=0.04, Ste_l=0.02 b) 22.5℃ wall temperature, 40℃ initial temperature/Ste_s=0.04, Ste_l=0.11

Non-dimensional plots were created to make the results of the experiments more general. The experimental results have already been discussed in the dimensional form, so the detailed discussion will not be replicated here for the non-dimensional results. Equation B.1, Equation B.3, Equation B.4 and Equation B.5 were used to make the results non-dimensional. The total energy in Equation B.5 can be found using Equation B.11. In these equations, the variables are the same as those in Equations 5.1 – 5.4.

$$E^* = \frac{E}{E_{tot}} \qquad [B.5]$$

$$E_{tot} = \rho_l \, A \, L \, C_{p,l}\left(T_{i,f} - T_m\right) + \rho_s \, H \, A \, L + \rho_s \, A \, L \, (T_m - T_w) \qquad [B.6]$$

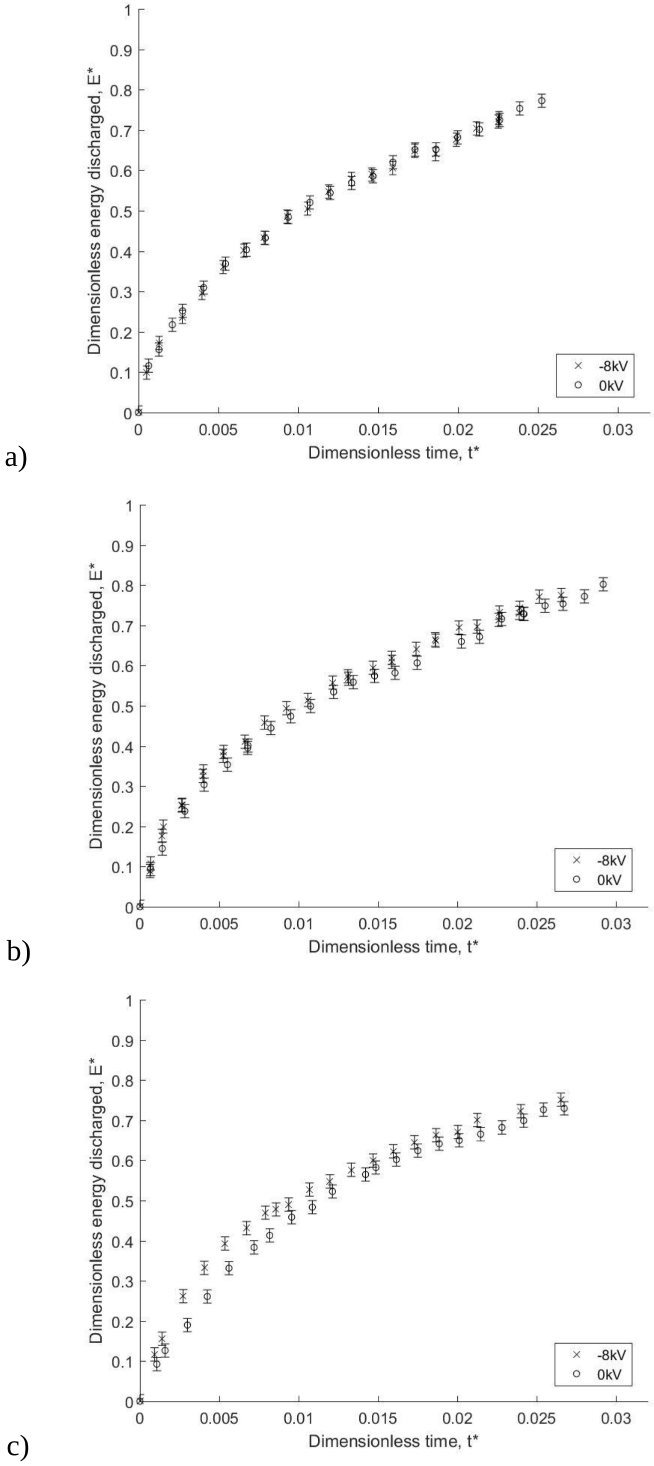

Figure B-4: Experimentally measured dimensionless energy extracted a) 8.5℃ wall temperature. 30℃ temperature/Ste_s=0.17, Ste_l=0.02 b) 8.5℃ wall temperature, 40℃ initial temperature/Ste_s=0.17, Ste_l=0.11 c) 8.5℃ wall temperature and 50℃ initial temperature/Ste_s=0.17, Ste_l=0.20

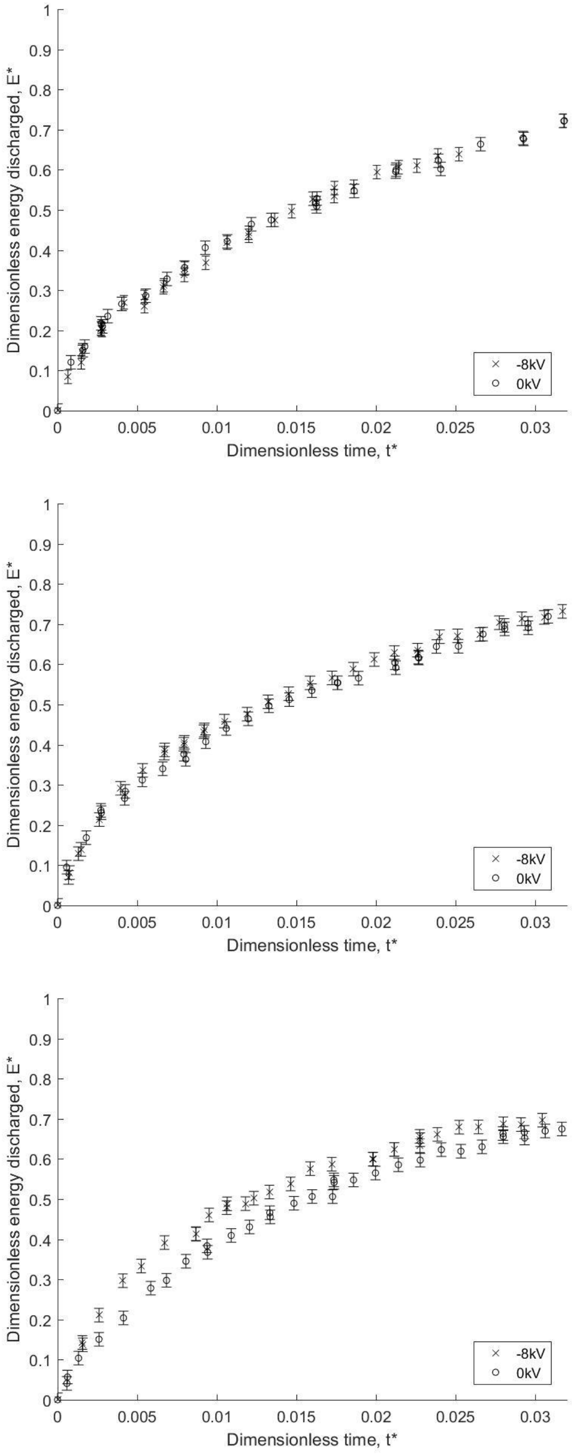

a)

b)

c)

Figure B-5: Experimentally measured dimensionless energy extracted a) 15.5℃ wall temperature. 30℃ temperature/Ste_s=0.11, Ste_l=0.02 b) 15.5℃ wall temperature, 40℃ initial temperature/Ste_s=0.11, Ste_l=0.11 c) 15.5℃ wall temperature and 50℃ initial temperature/Ste_s=0.11, Ste_l=0.20

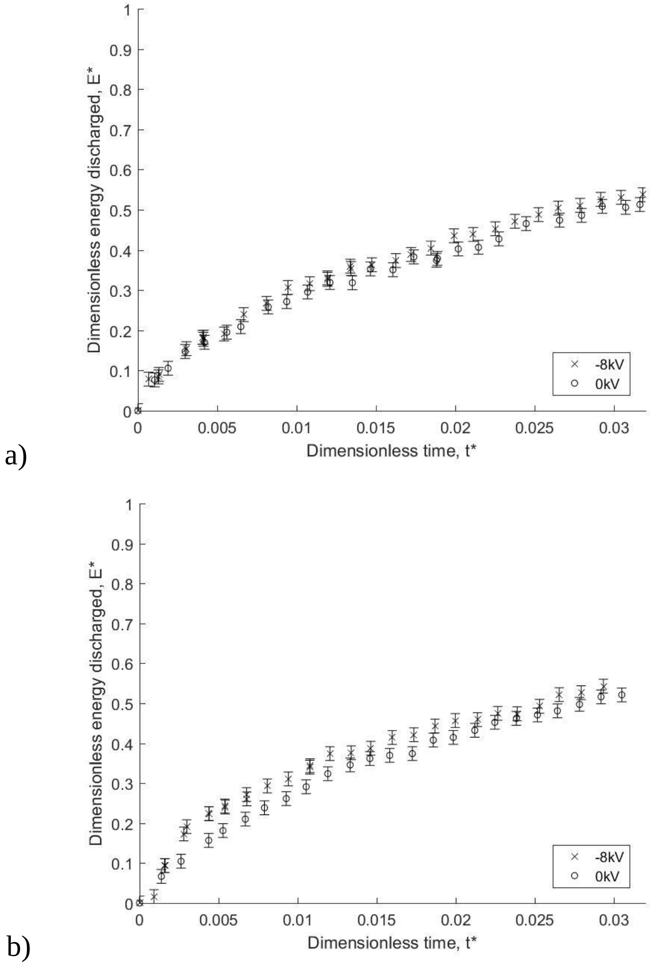

Figure B-6: Experimentally measured dimensionless energy extracted a) 22.5℃ wall temperature. 30℃ temperature/Ste_s=0.04, Ste_l=0.02 b) 22.5℃ wall temperature, 40℃ initial temperature/Ste_s=0.04, Ste_l=0.11

Appendix C: Uncertainty analysis

C.1 Solid front location uncertainty due to temperature uncertainty:

The uncertainty of the solid front location is partially due to the uncertainty in the heat exchanger temperature. The accuracy of the thermocouples used to measure the heat exchanger's temperature is ±0.5℃. The temperature uniformity of the thermal bath is ±0.2℃. To temperature uncertainty convert this to a solid front location uncertainty, the Stefan solution was used. This uncertainty was estimated by applying the ±0.7℃ to the wall temperature in the two-phase Stefan solution. In addition, the initial temperature of the fluid was measured using a thermocouple with a ±0.5℃ accuracy and the experiment was not started unless the fluid showed a temperature uniformity within ±0.5℃ of the desired temperature. Thus a ±1.0℃ was applied to the initial temperature. The results are given in the Table C-1. The results of this table indicate that error is small for low wall temperature and larger for high wall temperatures. This uncertainty predicts the actual temperatures to the real temperature. Thus, they can be used to compare the experimental results to analytical results.

Table C-1: Uncertainty due to the temperature of the heat exchange, if the exact temperature is required

Wall Temperature (℃)/ initial temperature(℃)	Wall Temperature +0.7℃/ initial temperature + 1℃ Error, %	Wall Temperature -0.7℃ Error/ initial temperature - 1℃, %
8/40	-3.0	2.9
15/40	-4.5	4.1
22/40	-9.6	7.8

Using the uncertainty analysis above greatly over predicts the error between two experiments using the same condition. For this purpose the repeatability of the thermocouples is the true source of the uncertainty. The repeatability of the thermocouples is 0.2℃. A similar analysis to the one above was conducted, and the results are shown in Table C-2.

Table C-2: Uncertainty due to the temperature of the heat exchange, if the relative temperature is required

Wall Temperature (℃)/ initial temperature(℃)	Wall Temperature +0.4℃/ initial temperature + 0.8℃ Error, %	Wall Temperature -0.4℃ Error/ initial temperature – 0.8℃, %
8/40	-2.0	1.9
15/40	-2.8	2.7
22/40	-5.7	5.0

C.2 Solid front location uncertainty due to camera measurements

There is also uncertainty in the camera measurements. To determine this uncertainty due to the position of the camera, two pictures in the experiments were taken in rapid succession. The difference of the solid front location between the images was then found, this was done for 13 different tests, seen in Table C-3. The tests were taken over different experimental conditions and times. Of these tests the maximum difference between any two pictures was found to be 0.4mm and the root mean square value of all the differences was 0.05mm. Thus, to estimate the uncertainty in the camera measurements the value of ±0.5 mm is used. This value was chosen because the maximum value of the difference was 0.404, but this level of precision, implies a level of accuracy that is greater than the accuracy of the measurements in the experiments, thus this value was rounded up to the nearest single decimal value.

Table C-3: Uncertainty due to the temperature of the heat exchange, if the relative temperature is required

Wall temperature, Initial temperature /solid front location, mm	Difference between 2 successive images	Percentage difference between 2 successive images
15℃, 30℃ / 4.4mm	0.265mm	6.0%
15℃, 30℃ / 6.3mm	0.222mm	3.5%
15℃, 30℃ / 15.1 mm	0.245mm	1.6%
15℃, 30℃ / 17.5 mm	0.152 mm	0.87%
15℃,30℃ / 18.4 mm	0.262 mm	1.4%
15℃, 30℃/ 20mm	0.09115 mm	0.46%
15℃, 30℃ / 20.4 mm	0.074 mm	0.36%
15℃, 40℃ / 5.1 mm	0.107 mm	2.1%
15℃, 40℃ / 6.4 mm	0.0729mm	1.1%
22℃, 40℃ / 3.5 mm	0.026 mm	0.74%
22℃, 40℃ / 4.8 mm	0.168 mm	3.5%
22℃, 40℃ / 5mm	0.404 mm	8.1%
22℃, 40℃ / 6 mm	0.081 mm	1.4%
22℃, 40℃ / 6.5 mm	0.0484 mm	0.74%
Maximum	0.40 mm	8.1%
Root Mean Square	0.09 mm	0.8%